Therapeutic drug monitoring, clinical metabolomics and pharmacometabolomics via solid phase microextraction (SPME): The first step towards an alternative rapid diagnostic tool

by

Nikita Looby

A thesis

presented to the University of Waterloo

in fulfilment of the

thesis requirement for the degree of

Doctor of Philosophy

in

Chemistry

Waterloo, Ontario, Canada, 2020

Examining Committee Membership

The following served on the Examining Committee for this thesis. The decision of the Examining Committee is by majority vote.

External Examiner	Prof. Maria del Coral Barbas Arribas Professor of Analytical Chemistry at Pharmacy Faculty Universidad CEU San Pablo, Madrid. Director for the "Centre for Metabolomics and Bioanalysis" (CEMBIO) at this Faculty.
Supervisor(s)	Prof. Janusz Pawliszyn University Professor, Canada Research Chair and NSERC Industrial Research Chair Department of Chemistry, University of Waterloo
Internal Member	Professor Michael Palmer Associate Professor Department of Chemistry, University of Waterloo
Internal Member	Professor Terrence McMahon University Professor Department of Chemistry, University of Waterloo
Internal-external Member	Professor Andrew Doxey Associate Professor Department of Biology, University of Waterloo

Author's Declaration

This thesis consists of material all of which I authored or co-authored: see Statement of Contributions included in the thesis. This is a true copy of the thesis, including any required final revisions, as accepted by my examiners.

I understand that my thesis may be made electronically available to the public.

Statement of Contributions

The results from Chapter 2 of this thesis were used by clinicians to develop a pharmacokinetic profile for tranexamic acid, which enabled dosing to be scheduled more effectively in patients with chronic renal dysfunction. This work was published in *Anesthesia and Analgesia* (**2018**, 127(6),1323-1332) under the title of "Tranexamic acid dosing for cardiac surgical patients with chronic renal dysfunction", and was authored by A. Jerath, Q. J. Yang, S.K. Pang, N. Looby (the author of this thesis), N. Reyes-Garcés, T. Vasiljevic, B. Bojko, J. Pawliszyn, D. Wijeysundera, W. S. Beattie, T. M. Yau, and M. Wasowicz. In addition, the results presented in Chapter 2 have also been formatted for submission to *Talanta*. All of the writing for this submission was done by the author of this thesis. Collaboration initiation and experimental design were executed by B.Bojko, J. Pawlisyzn, A. Jerath, and M. Wasowisz. For plasma analysis, experimental design, experimental planning and execution, sample preparation, and data analysis were carried out by N. Reyes-Garcés, T. Vasiljevic, and the author of this thesis. Finally, for urine analysis, experimental design, method development planning and execution, sample preparation, instrumental analysis, data processing, and data interpretation were all conducted mainly by the author of this thesis with help from A. Roszkowska.

Chapter 3 of this thesis has been formatted for submission to the journal, *Metabolomics*, with all writing having been done by the author of this thesis. Collaboration was initiated by J. Pawliszyn, V. Chandran, and V. Kulasingam, with experimental design being conducted by J. Pawliszyn, V. Chandran, V. Kulasingam, N. Reyes-Garcés, and the author of this thesis. Experimental planning was carried out by the author of this thesis, N. Reyes-Garcés, and A. Roszkowska, while device preparation (experimental execution) and sample preparation were performed by the author of this thesis and A. Roszkowska. The author of this thesis conducted instrumental analysis with help from I. Batruch and data processing, statistical analysis, and data interpretation with assistance from N. Reyes-Garcés.

Chapter 4 of this thesis has not yet been published. Collaboration on the work presented in this chapter was initiated by B. Bojko, J. Pawlisyzn, A. Roszkowska, and M. Cypel, who were also responsible for the initial experimental design. The tasks of further modifying the experimental design, preparing the devices used, sampling at the hospital, sample processing, instrumental analysis, data processing, statistical analysis, data interpretation, and writing were equally shared by the author of this thesis and A. Roszkowska.

Chapter 5 of this thesis has yet to be published. Collaboration on the research presented in this chapter was initiated by B. Bojko, J. Pawliszyn, and M. Cypel, who were also primarily responsible for the initial experimental design. Modifications to the experimental design for the untargeted analysis portion of this work were overseen by G.A. Gomez-Rios, while experimental execution, sampling at the hospital, sample processing, and instrumental analysis for untargeted data analysis were carried out by the author of this thesis and G.A. Gomez-Rios. Untargeted data processing and chemometric analysis was carried out by the author of this thesis with assistance from Miao Yu in running the data processing software script. For the targeted data analysis namely—the development of the LC-MS/MS method and SPME method for FOLFOX quantitation in lung tissue—experimental design, experimental planning and execution, instrumental analysis, data processing, and data interpretation were all performed exclusively by the author of this thesis. Experimental design and instrumental analysis for stability testing, data processing, and all chemometric analysis for the untargeted analysis work related to stability testing were all carried out solely by the author of this thesis. Biochemical interpretation based on annotation and was completed by A. Roszkowska. All sections except a portion from *section 5.5.2 entitled "Untargeted pharmacometabolomic analysis"* (related to biochemical interpretation—written by A. Roszkowska), were written by the author of this thesis.

Chapter 6 of this thesis has been formatted for submission. B. Bojko, J. Pawliszyn, and M. Cypel were responsible for initiating the collaboration and the experimental design. Experimental execution, sampling at the hospital, sample processing for targeted and untargeted analysis, instrumental analysis for targeted

and untargeted analysis, and data processing for the targeted and untargeted analyses were completed mainly by the author of this thesis with assistance from G.A. Gomez-Rios and M. Tascon for the first clinical case, and from M. Olkowicz for the second clinical case. Statistical analysis was completed by, B. Bojko, B. Kupcewicz, and the author of this thesis and biochemical interpretation from annotation was conducted by B. Bojko, A. Roszkowska, and M. Olkowicz. The final formatted manuscript was equally written by B. Bojko, A. Roszkowska, Khaled Ramadan, and the author of this thesis.

Chapter 7 has already been published in *Analyst* (**2019**, 144(12), 3721-3728) under the title, "Solid-phase microextraction coupled to mass spectrometry via a microfluidic open interface for rapid therapeutic drug monitoring". This paper was coauthored with M. Tascon, V.R. Acquaro, N. Reyes-Garcés, T. Vasiljevic, G.A. Gomez-Rios, M. Wasowicz and J. Pawliszyn. Experimental planning and design were carried out by G.A Gomez-Rios, M. Tascon, and the author of this thesis, while experimental execution, data acquisition, and data analysis were completed by the author of this thesis and M. Tascon. Statistical analysis and statistical interpretation were completed by V.R. Acquaro. The manuscript produced from the work in this chapter was written entirely by the author of this thesis.

Abstract

Personalized medicine is a branch of medicine that focuses on how a prescribed therapeutic treatment affects a specific individual as opposed to its general effects for the broader population. The goal of personalized medicine is to improve patient care by enabling concentrations of a therapeutic drug to be monitored in various biological compartments, while also measuring their effects in relation to the administered dose via therapeutic drug monitoring (TDM). Metabolomics—the study of all small endogenous and exogenous molecules within a cell, tissue, or organism—has recently been proposed as a method for developing patient-based metabolic profiles, which could enable clinicians to more effectively predetermine suitable courses of treatment for a variety of patients. The probability of success or failure for a given treatment is determined in large part by metabolic phenotyping, which considers several patient-based influential factors, such as age, diet, environment, and medical history. This approach allows treatment to be tailored to the needs of each individual patient, thereby avoiding under- or over-dosing or wasting time with unnecessary treatment options, which often occurs as a result of the current "trial and error" approach to personalized therapy. In this thesis, solid phase microextraction (SPME) coupled with liquid chromatography-mass spectrometry (LC-MS) is proposed as an alternative sample preparation tool for use in the field of personalized medicine. To this end, the work in this thesis presents the development of various SPME-based methods for TDM, and it explores SPME-based clinical metabolomics and proof-of-concept pharmacometabolomics for a range of biological matrices typically encountered in clinical practice, such as whole blood, serum, plasma, urine, and lung tissue. Furthermore, SPME is proposed as a practical tool for rapid diagnostics, as it can be directly coupled to sensitive detection methods like MS. While a number of preliminary steps are required before important diagnostic markers can be monitored—including the validation of these potential respective candidate biomarkers, which is already a major inherent challenge in metabolomics—the use of SPME for real-time TDM and point-of-care analysis of important metabolic markers remains feasible. This thesis consists of a brief introduction and 6

experimental chapters, with each successive chapter exploring increasingly complex samples of interest and discussing the challenges and limitations associated with their analysis. Moreover, each subsequent chapter also addresses the difficulties associated with performing solely TDM or metabolomics separately and how, particularly *in vivo* SPME, can overcome these challenges and be used to achieve both goals (TDM and metabolomics) simultaneously under even more complicated and dynamic circumstances. Specifically, Chapter 2 focuses on the therapeutic drug monitoring of TXA in plasma and urine samples from patients with chronic renal dysfunction who are undergoing cardiac surgery, while Chapter 3 presents a metabolomics study entailing the profiling of serum samples from various psoriatic patients. Chapters 4, 5, and 6 illustrate how SPME can be used to enable simultaneous TDM and metabolomics under more complicated and dynamic circumstances by using *in vivo* SPME for specifically tissue analysis. Chapter 4 explores lung tissue and perfusate metabolomics using a pre-clinical porcine model undergoing normothermic *ex vivo* lung perfusion (NEVLP). In contrast, Chapters 5 and 6 assess the use of *in vivo* SPME for the TDM of chemotherapy drugs administered via *in vivo* lung perfusion (IVLP) in pre-clinical porcine model (Chapter 5) and clinical human trial settings (Chapter 6), followed by proof-of-concept pharmacometabolomics. Finally, the potential use of SPME as a rapid diagnostic tool is showcased in Chapter 7—which shows the rapid analysis of TXA from plasma—concluding the thesis by further demonstrating that the dual goals of TDM and point-of-care testing for metabolic markers can be achieved with rapid analysis via the direct coupling of SPME to MS.

Acknowledgements

I would like to thank Professor Pawliszyn for the opportunity to do my PhD under his supervision at the University of Waterloo. Under his guidance, I have obtained invaluable technical experience in the field of analytical chemistry, and I have drastically improved my presentation, critical analysis, and critical thinking skills. Equally importantly, I have developed more effective intra- and inter-personal skills, which have in turn improved by ability to resolve conflicts. Professor Pawliszyn's mentorship has better equipped me to deal with the challenges that will inevitably arise in both professional and personal settings, and it has taught me to appreciate the little triumphs as well as the great ones.

I would like to thank my committee members, Professor Michael Palmer, Professor Terrence McMahon, and Professor Andrew Doxey, as well as my external examiner, Professor Maria del Coral Barbas Arribas, for accepting the invitation to participate in the evaluation of my thesis, and for taking the time to read my thesis and provide me with constructive feedback. I would also like to extend special thanks to Professor Palmer, with whom I started this program, for his time during my initial presentation proposals (Masters and Doctorate), comprehensive exams, and committee meetings.

I would like to thank Professor Barbara Bojko, who acted as the main liaison between the Pawliszyn research team and our collaborators at Toronto General Hospital (TGH). The work presented in my thesis would not have been possible without her hard work in creating these networks and pioneering SPME-based research in the clinical field. Special thanks goes out to all of the individuals in the University Health Network with whom I collaborated on this work, namely: Professor Marcelo Cypel MD, Mauricio pipkin MD, and Aadil Ali from the Division Of Thoracic Surgery at TGH for all lung-related projects; Professor Vathany Kulasingam from TGH and Professor Vinod Chandran MD from the Department of Laboratory Medicine and Pathobiology at Toronto Western Hospital for the "omic" studies on psoriatic patients; and Professor Marcin Wasowicz and Professor Angela Jerath from the Department of Anesthesiology and Pain Management at TGH for therapeutic drug monitoring of TXA.

I would like to express my gratitude to our fantastic biostatistician/bioinformatician, Miao Yu PhD., as it simply would not have been possible to complete the sheer volume of research related to untargeted metabolomics without his help. The development of his script in RStudio single-handedly saved the majority of my projects by drastically reducing the data pre-processing time. I am indebted to him for the countless hours he spent training/teaching me how to use various bioinformatics tools, explaining biostatistical techniques, and helping me understand the code used in his script. His continued support, even after his departure from our group, was greatly appreciated.

I would like to give special thanks to Nathaly Reyes-Garces PhD. and German A. Gomez-Rios PhD. for their tremendous help and support during the first few years of my journey. Thank you both for taking me under your wings and training me. I learned a great deal from listening to your discussions about science and SPME fundamentals, from spending hours assisting me with perfecting presentations, and for all of your help while I was studying for my comprehensive exam. Truly, I would not have made it this far without your support and guidance.

Thank you to Professor Ezel Boyaci and Professor Marcos Tascon for being my personal encyclopedias, and for always being ready, willing, and available to share your wealth of knowledge and experience whenever in response to my questions and suppositions.

I would like the express my sincerest gratitude to Professor Emanuela Gionfriddo—a person who has earned my deepest respect, both professionally and personally—for always challenging me to rise above the self-doubt; for always encouraging me to continue to push my boundaries; and for leading by example and teaching me the importance of a strong work ethic. I am grateful for your enduring friendship through the good, the bad, and the ugly.

To Sofia Lendor and Tijana Vasiljevic, with whom I started this journey, your strength, independence, efficiency, and determination are qualities that I have long admired in you both. I am grateful to have the

opportunity to work alongside you wonderful ladies, from the sleepless nights, working weekends, and devastating “jim” sessions; we survived.

I would like to thank Mona Bishara and Tarif Rahman for being my personal cheerleaders, and for being available at any and all hours to remind that there are other aspects of life outside of the laboratory. Your constant support and willingness to involve me in extracurricular activities always helped me to focus better, and it is much appreciated.

To Jamall Brown, my “partner in lime,” thank you for always standing by my side, forever being on my side, and always fighting for us. You always reminded me to remain strong and true to myself. This journey would have been impossible without your constant companionship and laughter. I love you dearly.

Finally, I would like to send a very big thank you to my brother, Kurt Eccleston, and especially my mother, Ina Vincent, for her unwavering love, support, and encouragement throughout this journey. Thank you for helping me not lose sight of the bigger picture, and for constantly helping me re-focus on it whenever I started to lose faith. Thank you for always believing in me, inspiring me to continue to be great, providing me with advice, and rewarding me with trips all over the world. There aren’t enough words to express my gratitude and appreciation.

Dedication

This thesis is dedicated to my mother, Ina Vincent, and my grandmother, Martella Vincent, for their unwavering faith and belief in me; to my older brother, Kurt Eccleston, for all his patience, assistance, and guidance throughout the years; and to all my family and friends for their support and understanding.

Table of Contents

Examining Committee Membership ..... **ii**
Author's Declaration ..... **iii**
Statement of Contributions ..... **iv**
Abstract ..... **vii**
Acknowledgements ..... **ix**
Dedication ..... **xii**
List of Figures ..... **xix**
List of Tables ..... **xxv**
List of Abbreviations ..... **xxvii**
Chapter 1 : Review of current literature **1**
1.1 Pharmacokinetics 1
1.2 Personalized medicine 2
1.3 Therapeutic drug monitoring 2
1.4 Metabolomics 3
1.5 Rapid analysis 6
1.6 Typically encountered samples in clinical practice 7
1.6.1 Blood and blood compartments 8
1.6.2 Urine 9
1.6.3 Steen solution 10
1.6.4 Tissue 11
1.7 Current sample preparation methods 12
1.7.1 Centrifugation/ centrifugation ultrafiltration 13
1.7.2 Ultrafiltration (UF) 13
1.7.3 Equilibrium dialysis (ED) 14
1.7.4 Plasma protein precipitation (PPt) 14
1.7.5 Dried blood spot (DBS) 15
1.7.6 Liquid-liquid extraction (LLE) 16
1.7.7 Solid phase extraction (SPE) 17
1.7.8 Homogenization 17
1.7.9 Microdialysis (MD) 18

1.8 Solid phase microextraction (SPME) 19
1.8.1 Overview of the technique 20
1.8.2 *In vivo* SPME 22
1.8.3 Thin-film SPME 22
1.8.4 Biocompatible coatings 23
1.9 Instrumentation 25
1.10 Typical SPME workflow 26
1.11 Research objective 27
Chapter 2 : Therapeutic drug monitoring of tranexamic acid in plasma and urine of renally impaired patients using solid phase microextraction 30
2.1 Preamble 30
2.2 Introduction 30
2.3 Materials and Methods 32
2.3.1 Chemicals and materials 32
2.3.2 Working solutions and calibration curves 33
2.3.3 Instrumental analysis 33
2.3.4 Sampling procedure 34
2.3.5 Preparation of thin-film microextraction devices 35
2.3.6 Concept-96 for SPME automation 36
2.3.7 Automated SPME protocol for the analysis of TXA in plasma 37
2.3.8 Automated SPME protocol for analysis of TXA in urine 37
2.4 Results 38
2.4.1 Device coating 38
2.4.2 Extraction conditions 39
2.4.3 pH modification 40
2.4.4 Extraction time profile 41
2.4.5 Rinsing conditions 42
2.4.6 Desorption conditions and desorption time profile 44
2.4.7 Device cleaning optimization 46
2.4.8 Evaluation of matrix effects 49
2.4.9 Method validation 51
2.5 Discussion 52
2.5.1 Application of SPME method to clinical samples 52
2.6 Conclusion 54

Chapter 3 : Serum metabolic fingerprinting of psoriasis and psoriatic arthritis patients using solid phase microextraction – liquid chromatography – high-resolution mass spectrometry 56

3.1 Preamble 56

3.2 Introduction 56

3.3 Materials and Methods 58

3.3.1 Materials 58

3.3.2 Thin-film microextraction device preparation 59

3.3.3 Instrumental analysis: liquid chromatography coupled with high-resolution mass spectrometry 59

3.3.4 Patients 61

3.3.5 Sample preparation 63

3.3.6 Data pre-treatment and analysis 63

3.4 Results 65

3.4.1 Baseline converters vs. baseline non-converters 66

3.4.2 Healthy controls vs. psoriasis without psoriatic arthritis vs mild psoriatic arthritis 72

3.4.3 PsC vs PsA 72

3.4.4 PsA group 73

3.4.5 Statistically significant features across patient groups 77

3.5 Discussion 83

3.5.1 Baseline converters vs. baseline non-converters 83

3.5.2 Baseline converters vs. follow-up converters 83

3.5.3 Healthy controls vs. psoriasis without psoriatic arthritis vs psoriatic arthritis 84

3.5.4 PsC vs PsA 85

3.5.5 PsA group—Confounding factors 85

3.5.6 PsA group—Severity related to joint information 85

3.5.7 PsA group—Cluster deviants 85

3.5.8 Statistically significant features across patient groups 86

3.6 Conclusion and future direction for research 87

Chapter 4 : Metabolomic fingerprinting of porcine lung tissue during pre-clinical prolonged normothermic *ex vivo* lung perfusion (NEVLP) using *in vivo* solid phase microextraction 90

4.1 Preamble 90

4.2 Introduction 90

4.3 Materials and Methods 93

4.3.1 Animals and research ethical approval 93
4.3.2 Normothermic ex vivo lung perfusion (NEVLP) strategy 93
4.3.3 Chemicals and materials 94
4.3.4 SPME fiber coating methodology 94
4.3.5 TFME blade coating methodology 95
4.3.6 Lung and perfusate sampling with SPME fiber 95
4.3.7 Perfusate sampling with TFME 97
4.3.8 Instrumental analysis 98
4.3.9 Data pre-processing 99
4.3.10 Data pre-treatment, data processing and model validation 99
4.4 Results 101
4.4.1 Rationale and data analysis 101
4.4.2 Unsupervised multivariate analysis 102
4.4.3 Supervised multivariate analysis 104
4.4.4 Univariate analysis 107
4.5 Discussion 108
4.5.1 Statistically significant metabolites and their biochemical relevance 108
4.5.2 Metabolite stability 125
4.6 Conclusion 129
Chapter 5 : Therapeutic drug monitoring of FOLFOX and screening of drug metabolites followed by pharmacometabolomic fingerprinting of porcine lung tissue during pre-clinical *in vivo* lung perfusion (IVLP) using *in vivo* solid phase microextraction 131
5.1 Preamble 131
5.2 Introduction 131
5.3 Materials and Methods 138
5.3.1 Materials 138
5.3.2 Animals 138
5.3.3 IVLP procedure 138
5.3.4 IV procedure 139
5.3.5 Lung sampling protocol 139
5.3.6 Perfusate sampling protocol 141
5.3.7 Fiber coating procedure 141
5.3.8 Sample preparation and sample extracts 142
5.3.9 Mass spectrometric parameters and conditions 142

5.3.10 LC-MS/MS method for FOLFOX and metabolites screening 143
5.3.11 Calibration curve and quality control 145
5.3.12 LC-HRMS for untargeted analysis 146
5.3.13 Data pre-processing for untargeted analysis 146
5.4 Results 147
5.4.1 Chemometric analysis and model validation 147
5.4.2 LC method development 148
5.4.3 Selectivity and specificity of LC-MS/MS method 151
5.4.4 FOLFOX compounds and drug metabolites stability 153
5.4.5 Coating performance and absolute recoveries 153
5.4.6 Extraction time profile 157
5.4.7 Calibration under *in vivo* conditions 159
5.4.8 Standard solutions, calibration curves, method validation and quality control 161
5.4.9 Sterilization and preconditioning 164
5.5 Discussion 165
5.5.1 Application of the developed SPME-LC-MS/MS protocol on samples obtained from pre-clinical trials of FOLFOX chemotherapy using IVLP 165
5.5.2 Untargeted pharmacometabolomic analysis 169
5.5.3 Storage conditions and metabolite stability 173
5.6 Conclusion 176
Chapter 6 : *In vivo* solid phase microextraction chemical biopsy tool for monitoring doxorubicin residue in human lung tissue during clinical *in vivo* lung perfusion (IVLP) 193
6.1 Preamble 193
6.2 Introduction 194
6.3 Materials and methods 197
6.3.1 Study design 197
6.3.2 *In vivo* animal study 198
6.3.3 *In vivo* human study 198
6.3.4 Statistical analysis 199
6.4 Results 200
6.4.1 Determination and quantification of DOX during IVLP 200
6.5 Discussion 205
6.5.1 Screening of small molecules in lung tissue during IVLP-DOX administration 207
6.6 Conclusion 214

Chapter 7 : Solid phase microextraction coupled to mass spectrometry via a microfluidic open interface for rapid therapeutic drug monitoring..... 216
7.1 Preamble..... 216
7.2 Introduction..... 216
7.3 Methods and materials..... 218
7.3.1 Chemicals and materials..... 218
7.3.2 Human plasma samples..... 219
7.3.3 High throughput analysis with concept-96 unit..... 220
7.3.4 Sample preparation..... 220
7.3.5 Calibration and quality control samples..... 221
7.4 Instrumental analysis..... 222
7.4.1 SPME-LC-MS/MS..... 222
7.4.2 Bio-SPME-MOI-MS/MS..... 223
7.5 Results and discussion..... 225
7.5.1 SPME-MOI as a tool for rapid analysis of clinical samples..... 225
7.5.2 Statistical validation of the MOI methodology..... 229
7.5.3 MS-based POC technologies..... 231
7.6 Conclusions..... 232
Chapter 8 : Conclusion..... 234
References..... 237

List of Figures

Figure 1.1 The typical metabolomics workflow 5

Figure 1.2 Various types of biological samples investigated in this thesis 8

Figure 1.3 Some conventional sample preparation approaches used in the bioanalytical and clinical field such as (*from the left*) centrifugation, plasma protein precipitation (PPt), dried blood spots (DBS), solid phase extraction (SPE). Solid phase microextraction (SPME) is a novel technique that is explored in this thesis. 13

Figure 1.4 Typical SPME fiber geometry (*left*) popularly employed for two types of extraction modes – headspace and direct immersion (*middle*). Fundamental SPME extraction kinetics and thermodynamics principle (*right*) 20

Figure 1.5 Graphical representation of the general SPME workflow. 26

Figure 2.1 Preparation of thin film microextraction (TFME) devices from bare blades to TFME brush. A) Bare blade/comb. B) Coated comb. C) Brush Assembly of 8 coated combs. 36

Figure 2.2 Automated software-operated SPME Concept-96 system employed for high throughput analysis of TXA from plasma and urine samples collected from patients undergoing cardiac surgery. 37

Figure 2.3 A) Extraction time profile of tranexamic acid (TXA) in urine and phosphate buffered saline (PBS). B) Extraction time profile of TXA in plasma 42

Figure 2.4 Rinsing time and agitation conditions evaluated for solution consisting of a 9:1 water/methanol mixture. A) The amount of TXA recovered from the desorption solution after varying rinse conditions. B) The amount of TXA recovered from the rinse solution after varying rinse conditions. 43

Figure 2.5 A) Optimization of three desorption solvents: 1:1 acetonitrile/water, 1:1:2 acetonitrile/methanol/water, and 3:3:4 acetonitrile/methanol/water. B) Carryover test for each desorption solution 45

Figure 2.6 A) Reassessment of optimum desorption conditions with increased aqueous content: 2:2:1 acetonitrile/methanol/water, 3:3:4 acetonitrile/methanol/water, 1:1 acetonitrile/water, 6:2:2 water/acetonitrile/methanol, and 9:1 water/methanol and pure water. B) Desorption time optimization in solution consisting of a 9:1 water/methanol mixture. 46

Figure 2.7 Evaluation of three cleaning solutions: 45:45:10 isopropanol/acetonitrile/acetone, 45:45:10 isopropanol/methanol/acetone, and 2:1:1 methanol/isopropanol/acetonitrile (yellow columns). The red columns represent the solutions mixed with 50% water. 48

Figure 2.8 Assessment of the number of cleaning cycles required to effectively remove traces of TXA from the device coating. Evaluation of how the addition of formic acid impacts desorption and cleaning efficacy. Devices initially desorbed in optimized desorption solution containing formic acid (des w/ FA) were cleaned in a solution containing formic acid (PC w/ FA) and compared with devices cleaned in a solution containing no formic acid (PC w/o FA). These two cleaning conditions were also evaluated against devices that had been desorbed in optimized desorption solution with no formic acid (des w/o FA). 49

Figure 2.9 Assessment of relative matrix effects. A 7-point calibration curve was constructed in 8 lots of urine, producing an average slope of 0.024 within a 10% relative standard deviation (RSD) and a linearity (R^2) of 0.99 across the 8 volunteers. 51

Figure 2.10 TXA profiles in plasma and urine from patients with varying degrees of chronic renal dysfunction who underwent cardiac surgery. A) TXA profiles in plasma from 5 patients undergoing high-

risk cardiac surgery. B) Corresponding TXA profiles in urine from 5 patients undergoing high-risk cardiac surgery. C) TXA profiles in plasma from 5 patients undergoing low-risk cardiac surgery. D) Corresponding TXA profiles in urine from 5 patients undergoing low-risk cardiac surgery. 54

Figure 3.1 Scheme of patient categories and subcategories of samples collected for analysis. Serum samples were obtained from healthy volunteers serving as controls (Ctrl) and patients with psoriasis (PsD). Patients with psoriasis who may or may not have developed psoriatic arthritis are grouped as converters (PsC); psoriatic patients who have developed psoriatic arthritis are classified as converters, while psoriatic patients who have not developed psoriatic arthritis are classified as non-converters. Samples were collected at baseline from both baseline converters and baseline non-converters, and at a subsequent time from both follow-up converters and follow-up non-converters. Patients with psoriatic arthritis (PsA) were categorized based on the severity of their conditions: mild, moderate, or severe. From each group, n = 10 patients were sampled. 61

Figure 3.2 Principal component analysis (PCA - PC1:76.2%, PC2: 12.8%, PC3:2.6%) of the pooled QCs and the three patient groups under investigation: healthy volunteers (Ctrl); patients with varying degrees of psoriatic arthritis (PsA); and patients with psoriasis, but without psoriatic arthritis (PsC). The pooled QCs, Ctrls, PsA patients, and PsC patients are represented by green, red, dark blue, and turquoise, respectively. Data shown were obtained via negative mode acquisition and were similar to the results obtained via positive mode acquisition (data not shown). 65

Figure 3.3 PCA (PC1:45.2%, PC2: 19.3%, PC3: 9.6%) plot of patients with psoriasis who developed psoriatic arthritis prior to disease progression (baseline converters) and patients with psoriasis who had not developed psoriatic arthritis (baseline non-converters). Baseline converters and baseline non-converters are represented by red and green, respectively. Data were obtained via negative mode acquisition and were similar to the results obtained in positive mode acquisition (data not shown). 66

Figure 3.4 PCA (PC1: 42.8, PC2: 17.9%, PC3: 10.3%) plot of a paired analysis of converter (PsC) patients who had psoriasis without psoriatic arthritis at baseline (baseline converters), and developed psoriatic arthritis (follow-up converters). Baseline converters and follow-up converters are represented on the plot by red and green, respectively. Data were obtained via negative mode acquisition and were similar to the results obtained in positive mode acquisition (data not shown). 69

Figure 3.5 A) Principal component analysis (PC1: 65.2%, PC2: 14.1%, PC3: 5.9%) for the comparison of three groups – healthy controls, follow-up non-converters and follow-up converters represented by red, green and blue circles on the plot respectively. B) Principal component analysis (PC1: 50.3%, PC2: 16.9%, PC3: 4.0%) for the comparison of three patient groups – healthy volunteers, follow-up converters and mild psoriatic arthritis represented by red, green and blue on the plot respectively. 72

Figure 3.6 PCA (PC1: 76.9, PC2: 13%, PC3: 2.4%) plot of healthy volunteers (control; red) and patients with psoriasis prior to conversion or non-conversion (PsC; turquoise). The plot also distinguishes between PsA patients based on level of disease progression (mild PsA-green; moderate PsA-dark blue; severe PsA-magenta). Data were obtained via negative mode acquisition and were similar to the results obtained in positive mode (data not shown). Pooled QC's were removed. 73

Figure 3.7 PCA (PC1:25.4%, PC2:16.5%) plot of healthy individuals (Ctrls) and patients suffering from varying degrees of psoriatic arthritis (PsA). The control group is represented by red dots, while patients with mild, moderate, and severe PsA are represented by green, dark blue, and magenta dots, respectively. Data were obtained via positive mode acquisition. Data obtained via negative mode acquisition can be found in Online resource 9. 74

Figure 3.8 The box plots on the left are representative of a statistically significant feature across the PsA group – m/z 289.2 (exact m/z: 289.1659) at a retention time 761 seconds (12.68 min). On the right is the

extracted ion chromatogram of that feature. This was tentatively identified as dodecanedioic acid, and putatively identified as such with an annotation score of 2 using xMSAnnotator.....87

Figure 4.1 Graphical representation of overall experimental design. The SPME sampling protocol is demonstrated in the center under "SPME sampling protocol" whereby steps B), C) and D) represent the rinsing, wipe with Kimwipe and dry ice storage after *in vivo* SPME lung sampling events or on-site extraction of perfusate. Perfusate samples were split into three portions: the first portion was sampled on-site using SPME fibers (in parallel with lung sampling events); the second portion (collected during lung sampling events) was stored in dry ice and transported to the lab for in-laboratory sampling with SPME fibers; the third portion (collected hourly) was stored in dry ice and transported to the lab for in-laboratory sampling with TFME. 96

Figure 4.2 Prolonged normothermic ex vivo lung perfusion (NEVLP/ EVLP) conducted over 19 hours. A) Perfusate sampling schedule during NEVLP for samples prepared using thin-film microextraction (TFME). Perfusate samples were collected hourly for 7 pig lungs, with red stars denoting samples that were used for further analysis. The samples prepared via TFME were collected at 1h, 3h, 4h, 6h, 9h, 11 h, 13h 15h, 16h, 18 h, and 19h after the start of NEVLP; the organ had been pronounced non-viable by the last two sampling points. Time 1 to Time 5 illustrate the 3-to-4 hour blocking strategy used to group the collected samples for data processing. B) Lung sampling schedule during NEVLP. SPME fiber lung sampling were conducted for 2 pig lungs. The blue stars denote the time points at which SPME fiber lung sampling events took place. Lung were sampled before the start of EVLP and at 1h, 3h, 5h, 8h, 11 h, 12h and 13h after the start of NEVLP.....97

Figure 4.3 Principal Component Analysis (PCA). A) PCA (PC1: 38.1%; PC2: 25.1%) of the perfusate samples collected during NEVLP and prepared via TFME. Time 1, Time 2, Time 3, Time 4, and Time 5 are represented by green, blue, turquoise, pink, and yellow, respectively. Each time point is comprised of a progressive 3-hour *time* block throughout the NEVLP process. B) PCA (PC1: 70.7%, PC2:15.2%) of the lung sample*d* with SPME fibers. The seven time groups—cold ischemic time (CIT), EVLP t_0, EVLP t_1, EVLP t_2, EVLP t_3, EVLP t_5 and EVLP t_6—are represented by red, green, blue, turquoise, pink, yellow, and gray, respectively. Each time point represents lung samples collected prior to the start of NEVLP, and 1h, 3h, 5h, 8h, 11h, 12h, and 13 h after the start of NEVLP. The pooled QCs are represented by red and black on the plot for the perfusate and lung samples, respectively. 103

Figure 4.4 Cross validation (CV) of PLS-DA models via k-fold CV, *leave one out cross validation (*LOOCV*)*, and permutation. A) CV for perfusate samples. On the left side, the optimized number of latent variables for a 10-fold CV was found to be 4 (denoted by a red star) with quality parameters $R^2 = 0.82$ and $Q^2 = 0.69$. B) CV for lung samples. On the left side, 8 latent variables (denoted by red star) were found to be the optimum for a LOOCV with $R^2 = 0.96$ and $Q^2 = 0.64$. On the right side for both sets of data, the observed statistics for the original data set was $p < 0.0005$ and $p < 0.001$ for perfusate and lung samples, respectively (highlighted by the red arrows).....105

Figure 4.5 Univariate analysis via *a non-parametric* analysis of variance (ANOVA)–*Kruskal Wallis test*. A false discovery rate (FDR) adjusted p-value of 0.05 was used as the cut-off for the selection of statistically significant features. Statistically significant features are highlighted in red, while non-significant features are highlighted in blue. *On the* right, shows the patterns over time for a single statistically significant feature. 107

Figure 4.6 PCA (PC1:51.6%; PC2: 35%; PC3: 6.5%) plot of samples collected *in vivo* from lung (red), perfusate samples collected on-site in the operating room (green), and perfusate samples collected, snap-frozen and sampled *ex vivo* in the laboratory (blue). 126

Figure 4.7 Group averaged heat maps of samples collected *in vivo* from lung (red), perfusate samples collected on-site in the operating room (green), and perfusate samples collected, snap-frozen, and prepared

in the laboratory (blue). Dark red squares on the heat map indicate a very high abundance of that particular feature in a specific group of samples, while dark blue indicates a very low abundance. A) Heat map for samples collected after the first hour of perfusion (EVLP T_0). B) Heat map for samples collected after 3 hours of perfusion (EVLP T_1). C) Heat map for samples collected after 6 hours of perfusion (EVLP T_2). 128

Figure 5.1 Lung sampling schedule using SPME fibers during *in vivo* lung perfusion (IVLP) (top schedule) and intravenous (IV) FOLFOX administration (bottom schedule). 141

Figure 5.2 Distribution of FOLFOX compounds and their metabolites according to their mass-to-charge ratio (m/z) and physiochemical properties (LogP).....149

Figure 5.3 Evaluation of LC-MS/MS selectivity and specificity. Neat solvent blank and extracts obtained from blank (non-spiked) lung homogenate with the hydrophilic-lipophilic balance (HLB) and C8-SCX (MM) coatings were injected and monitored at the mass spectrometric transitions of the target analytes. The blank signal from the HLB coating is shown in turquoise, the signal from MM is shown in dark gray, and the signal from the neat solvent is shown in dark purple bolded. 152

Figure 5.4 Evaluation of coating performance based on extractions from PBS spiked at clinically expected concentrations. The HLB coating is shown in red, the C18-SCX is shown in blue, and the C8-SCX coating is shown in yellow. The relative recoveries are shown for each compound along with their log P values in parentheses. 155

Figure 5.5 Absolute recoveries of FOLFOX and its metabolites from PBS and homogenized lamb lung tissue spiked at clinically expected concentrations. The log(p) value for each compound is provided in parentheses. Results shown only for the C8-SCX coating. 155

Figure 5.6 Extraction time profile of FOLFOX from lamb lung homogenate. The following extraction times were tested: 1 min, 5 min, 10 min, 20 min, 30 min, 45 min, and 60 min. The HLB and C8-SCX coatings were evaluated using 5 replicates for each coating at each time point. 158

Figure 5.7 The assessment of *in vivo* conditions for appropriate calibration. The following weights of homogenized lamb lung were tested: 1g, 5g, 10g, and 15g. This test sought to find the conditions under which the amount of extracted F becomes independent of the sample weight. 160

Figure 5.8 Matrix-matched external calibration curve in lamb lung homogenate for FOL (A) and F (C). A linear dynamic range from 50 µg/g to 1000 µg/g with a linearity (R^2) of 0.99 was achieved for both compounds. Each calibration curve was correlated with the amount of extracted FOL (B) and F (D) in order to streamline the analytical process. Linear dynamic ranges corresponding to 295 ng to 3000 ng and 30 ng to 800 ng were achieved for FOL and F, respectively. 162

Figure 5.9 Evaluation of sterilization and preconditioning of C8-SCX-coated fibers for F (A), FOL (B), and OX (C). Sterilization by autoclave was tested against non-autoclaved fibers. For each category of steam sterilization, preconditioning solutions of 50:50 methanol/water, saline solution, pure water, and no solution were tested.....165

Figure 5.10 Application of *in vivo* SPME protocol and developed LC-MS/MS method for the quantification of F in pre-clinical IVLP samples. (A) Lung concentration of F throughout the IVLP procedure. (B) Absolute recovery of F obtained from perfusate samples collected during IVLP. 167

Figure 5.11 Application of *in vivo* SPME protocol and developed LC-MS/MS method for the quantification of FOL in preclinical IVLP samples. (A) Absolute recoveries of FOL from lung tissue during IVLP. (B) Absolute recoveries of FOL from lung tissue during IV administration of FOLFOX.....169

Figure 5.12 Principal component analysis (PCA) plots of the overall structure of the data for lung samples taken during IVLP and IV administration of FOLFOX. A) PCA (PC1:94.8%, PC2: 3.8%, PC3: 0.6%) plot

for lung sampling events over the course of IVLP. Samples taken before, during, and after IVLP (during reperfusion) are represented in green, blue, and red, respectively. Pooled QC's are represented in turquoise. B) PCA (PC1: 92.7%, PC2:2.7%; PC 3: 1.1%) plot of lung sampling events during IV administration. Samples collected at baseline and hourly for 5 hours after the start of infusion are shown in red, yellow, green, blue, turquoise, and pink, respectively. Pooled QC's are represented in purple. C) PCA (PC1: 41.2%, PC2: 16.4%, PC3: 12.6%) plot for samples shown in B) with pooled QCs removed to enable closer observation. 171

Figure 5.13 (A) Metabolite profile of pre-clinical IVLP samples obtained and analyzed via LC-HRMS in 2015. (B) Metabolite profile of the same pre-clinical IVLP samples upon re-analysis in 2017. Both sets of data were filtered in the same way. 174

Figure 5.14 Principal component analysis (PCA) of lung samples taken before the start of IVLP (IVLP Lung Blank, Time L0, Time L1), during IVLP (IVLP T1 to IVLP T3), and post IVLP during reperfusion (IVLP T4 and IVLP T5). Each group of samples is represented by green, red, and blue, respectively. A) PCA (PC1: 79.6%, PC2:4.9%, PC3:1.1%) of samples acquired in 2015. B) PCA (PC1: 97%, PC2: 1.1%, PC3: 1%) of the same samples in 2017. Each data set shows the clustering of the pooled QCs at the centre of the data (represented by turquoise). 175

Figure 6.1 Pre-operative lung computed tomography (CT) scan for 1st patient subjected to IVLP showing numerous bilateral pulmonary sarcoma metastases as denoted by arrows 194

Figure 6.2 Biocompatible solid phase microextraction (Bio-SPME) probe 196

Figure 6.3 *In vivo* sampling of pig lungs during IVLP with doxorubicin. (A): triplicate of Bio-SPME probes during sampling; (B): the same location of lung after removal of SPME probes. *(Reprinted with permission)*[128] 200

Figure 6.4 Concentration profile of DOX in lower lobe of the lung during IVLP (sampling points: 30, 90, 150, and 210 min). Red circles and blue squares – levels of DOX after administration with 150 and 225 mg/m2, respectively. 201

Figure 6.5 Concentration of doxorubicin measured by Bio-SPME-HPLC-MS/MS in lung tissue during first (A) and second (C) clinical IVLP. Time points include 1-hour pre-IVLP, 1, 2, 3 hours during IVLP, and 30 minutes post-IVLP during lung reperfusion. Red, blue, and green dots represent the three locations of the fiber in the lung during sampling. The red circle designates the upper section of the lung, the blue square designates a section between the upper and lower lobes (middle) of the lung, and the green triangle designates the lower section of the lung. Black diamonds show when hospital biopsies were taken. (B, D) Concentration of doxorubicin in perfusate as measured by Bio-SPME-HPLC-MS/MS and the standard approach (hospital assay - PPT-HPLC/FLD or PPT-LC/MS), during human IVLP, represented by the blue and red diamonds, respectively. 202

Figure 6.6 Floating bars presenting levels of doxorubicin and its key metabolites (doxorubicinol and doxorubicin aglycone) over the course of IVLP procedure. The detection range together with median values for each compound analyzed in relevant matrixes (lung tissue (A, B) or perfusate samples (C-E), respectively) have been denoted. As indicated above, the intact drug was a predominant one detected in investigated systems with some amounts of metabolites resulting from its biotransformation but contributing no more than 5% to the resultant pool of analyzed compounds. 205

Figure 6.7 Principal component analysis showing separation of the data obtained at subsequent time points for different sections of the lung; red denote baseline sampling, before IVLP; green, blue, and turquoise denote 1 hour and 2 hours after the start of IVLP and 30 minutes after the start of blood reperfusion (RMSEC = 0.462, RMSECV = 0.838), respectively. The biplot reflects the distribution of molecular

features (compounds), denoted as grey points, selected with LASSO with respect to subsequent data points. 208

Figure 6.8 3-dimensional PCA score plots comparing LC/MS metabolomic profiles among four (1st clinical case (A))/five (2nd clinical case (B)) conditions corresponding to 4/5 sampling time-points (pre-perfusion, 1st, 2nd and 3rd hour of IVLP, reperfusion). Colored dots represent individual samples collected during sampling of different sections of the lung. Excellent discrimination among studied conditions (pre-perfusion vs. IVLP vs. reperfusion) has been found. Baseline – samples collected at pre-perfusion, LP1 – samples collected at 1st hour of IVLP, LP2 – samples collected at 2nd hour of IVLP, LP3 – samples collected at 3rd hour of IVLP, reperfusion – samples collected 30 min post reperfusion 209

Figure 6.9 The biplot reflecting distribution of the molecular features (compounds) from Table 6.2 with respect to subsequent data points (RMSEC = 0.470, RMSECV = 1.008). 210

Figure 6.10 Scatter plots showing relative intensities of selected features/metabolites primarily dysregulated upon one-time chemotherapy treatment for an individual patient. Each dot in the scatter plots represents an individual metabolite in each sample. 212

Figure 7.1 Patient blood samples were collected during surgery - which is segmented into 3 periods. First, baseline samples were collected prior to Period 1. Samples were then collected at 5 min and 10 min during Period 1 whereby a 30 mg/kg bolus dose of tranexamic acid is administered over 15 minutes. During period 2 of intravenous infusion of 16 mg/kg/hr, samples were collected post-sternotomy (after chest opening), 5 min before and after the start of cardiopulmonary bypass (CPB), at 30 minutes intervals during CPB for up to 4 sampling points, post CPB and prior to chest closure. During period 3, the post operation period where intravenous infusion was ceased, samples were finally collected at 1 hr, 2 hr, 4 hr, 8 hr, 12 hr, 24 hr, 48 hr and 72 hr. 220

Figure 7.2 The Concept-96 is a software operated system that permits high throughput solid phase microextration (SPME) sample preparation of 96 samples simultaneously. It automatically performs each step of the SPME protocol – preconditioning, extraction, wash and desorption – with the help of a robotic arm that houses the brush format of the SPME configuration to be used (Bio-SPME fibers). This brush format is compatible with 96 well plates which are placed on their respective stations. 221

Figure 7.3 The Analytical workflow for Bio-SPME-MOI-MS/MS 224

Figure 7.4 The signal for a blank plasma sample prepared with biocompatible solid phase microextraction (Bio-SPME) fibers and analyzed via microfluidic open interface tandem mass spectrometry (MOI-MS/MS). 225

Figure 7.5 The signal for a blank plasma sample superimposed with a signal from patient sample prepared using biocompatible solid phase microextraction (Bio-SPME) fibers and analyzed via microfluidic open interface tandem mass spectrometry (MOI-MS/MS) 225

Figure 7.6 Patient profiles of 6 patients from two different risk groups. Figures 2A, 2B and 2C show profiles for patients who underwent low risk cardiac surgery with a dosing schedule as per institutional practice at the Toronto General Hospital. Figures 2D, 2E and 2F show profiles of patients who underwent high risk cardiac surgery with Blood Conservation Using Antifibrinolytics in a Randomized Trial (BART) dosing schedule. Results obtained via SPME-LC-MS/MS is represented by bars in dark blue while results obtained via SPME-MOI-MS/MS are represented by grey bars. 226

Figure 7.7 Passing-Bablock regression of data obtained from LC-MS/MS vs. MOI-MS/MS. 229

Figure 7.8 Bland-Altman plot of data pairs (n=63) of LC-MS/MS and MOI-MS/MS 230

List of Tables

Table 1.1 Summary of recently used biocompatible coatings, respective matrices and methods. Excerpted from Souza-Silva et al.[29] 23

Table 2.1 Chromatographic parameters for TXA and its internal standard using a Shimadzu 10ADvp series binary pump. 34

Table 2.2 MS/MS parameters for the analysis of TXA and its internal standard on an API 4000 (AB Sciex) triple quadruple. 34

Table 2.3 Testing the buffering capacity of phosphate-buffered saline (PBS) and varying concentrations of phosphate buffer for pH adjusted urine 40

Table 2.4 Testing the capacity of 0.5M phosphate buffer for correcting the pH and ionic strength of urine samples from 13 volunteers. 41

Table 2.5 Evaluation of absolute matrix effects (%) tested at 5 lower-level concentrations in 14 different volunteers. Outliers (values less than 80 % and greater than 120 %) are highlighted in bold font. Each volunteer at each concentration was evaluated with 3 replicates. The values presented for each volunteer at each concentration level had RSD's (n = 3) < 15%. 50

Table 3.1 Liquid chromatographic gradient used for separation in both positive and negative mode 60

Table 3.2 General information describing the distribution of various biochemical parameters for patients and volunteers involved in the study 62

Table 3.3 Information for patients with psoriasis defined as converters or non-converters, prior to conversion (at baseline) 67

Table 3.4 Patient information for individuals with psoriasis who develop psoriatic arthritis and patients with mild psoriasis. 70

Table 3.5 Patient information for individuals with varying degrees of PsA. 75

Table 3.6 Joint information for patients with varying degrees of psoriatic arthritis 76

Table 3.7 Tentatively annotated features showing statistically significant differences via univariate analysis between healthy controls and severe psoriatic arthritis patients for positive mode data. 77

Table 3.8 Tentatively annotated features showing statistically significant differences via univariate analysis across patients with varying degrees of psoriatic arthritis for negative mode data. 77

Table 3.9 Variables of importance isolated from validated O-PLS-DA model that differentiate baseline converters from severe psoriatic arthritis. Data obtained from positive mode acquisition. 79

Table 3.10 Variables of importance isolated from validated O-PLS-DA model that differentiate baseline converters from severe psoriatic arthritis. Data obtained from negative mode acquisition. 81

Table 4.1 VIPS > 1 obtained from validated PLS-DA model for perfusate samples collected during NEVLP. Shown are statistically significant features changing from Time 1 to Time 5, all time points inclusive. Data from positive mode analysis with a mass tolerance of less than 5 ppm. 106

Table 4.2 VIPS > 1 obtained from validated PLS-DA model for SPME fiber lung sampling events during NEVLP. Shown are statistically significant features changing from EVLP t_0 to EVLP t_5, all time points inclusive. Data from positive mode analysis 106

Table 4.3 A comparison of unique features annotated by HMDB with medium-to-high confidence matches obtained by lung sampling and on-site perfusate sampling during NEVLP 112

Table 4.4 A comparison of unique features annotated by HMDB with medium-to-high confidence matches obtained from perfusate samples prepared in laboratory with SPME fibers and TFME (blades) 116

Table 5.1 Mass spectrometric parameters and conditions used for tuning compounds and metabolites in positive and negative mode. 143

Table 5.2 LC gradient conditions used with the Sequant® Zic®-pHILIC column (100 x 2.1 mm, 5µm particle size) for OX, F, and F metabolites. 143

Table 5.3 MS conditions and observed chromatographic retention times for OX, F, and F metabolites. Negative mode ionization was employed. 144

Table 5.4 LC gradient conditions for the Discovery HS F5-3 (PFP) column (100 x 2.1 mm, 5µm particle size) used for FOL and its metabolites, 5-methylTHF, 5-methylTHF, and THF. 145

Table 5.5 MS conditions and observed chromatographic retention times for FOL and its metabolites, 5-methylTHF, 5-methylTHF, and THF. Positive ionization was employed. 145

Table 5.6 VIPs > 1 obtained from a validated PLS-DA model for lung sampling events performed during IVLP with FOLFOX. Shown are statistically significant features changing from IVLP T0 to IVLP T3. Data obtained from positive mode analysis 148

Table 5.7 High- and medium confidence annotated features changing over the course of IVLP (Lung blank until the end of reperfusion IVLP T5) with FOLFOX administration 178

Table 5.8 High- and medium confidence annotated features from perfusate samples sampled on-site with SPME fibers in the hospital during IVLP with FOLFOX administration 184

Table 5.9 High- and medium confidence annotated features from lungs sampled *in vivo* with SPME fibers in the hospital during IV administration with FOLFOX. 188

Table 6.1 Concentration of DOX in perfusate collected during 1st clinical IVLP and measured via Bio-SPME-HPLC-MS/MS for samples obtained on site and samples brought back to the laboratory for traditional analysis (denoted as UW). 204

Table 6.2 List of selected masses by Least Absolute Shrinkage and Selection Operator (LASSO) for endogenous low molecular weight compounds. Putative identifications are based on accurate mass vs. database and RT/log(p) relation/correlation. 210

List of Abbreviations

5,6-DHET	5,6-dihydroxy-8Z,11Z,14Z-eicosatrienoic acid
5FdUMP	fluorodeoxyuridine monophosphate
5FdUrd	fluorodeoxyuridine
5FdUTP	fluorodeoxyuridine triphosphate
5FUrd	fluorouridine
5FUTP	fluorouridine triphosphate
AB	Applied Biosystems
ACN	acetonitrile
AGC	automatic gain control
AJ	active joints
ANOVA	analysis of variance
API	atmospheric pressure ionization
AU	arbitrary units
BART	Blood Conservation using Antifibrinolytics in a Randomized Trial
C18	octadecyl
C18-SCX	octadecyl-strong-cation-exchange
CAD	collision gas
CapLC	capillary liquid chromatography
CBS	coated blade spray
CE	capillary electrophoresis
CE	collision energy
CIHR	Canadian Institutes of Health Research
CIT	cold ischemic time
CNS	central nervous system
COPD	chronic obstructive pulmonary diseases
CPB	cardiopulmonary bypass
CR	creatine riboside
CRD	chronic renal dysfunction
CU	chlorouracil
CV	cross validation
CXP	cell exit potential
DART	direct analysis in real-time
DBD	donation after brain death
DBS	dried blood spots
DCD	donation after cardiac death
DESI	desorption electrospray ionization
DI	direct immersion
Dmards	disease modifying anti-rheumatic drugs
DMF	N,N-dimethylformamide
DMSO	dimethylsulfoxide
DOX	doxorubicin
DP	declustering potential
DPD	dihydropyrimidine dehydrogenase
dTMP	deoxythymidine monophosphate
dTTP	deoxythymidine triphosphate
ED	equilibrium dialysis

EP	entrance potential
EP	paper electrophoresis
ESI	electrospray ionization
EVLP	same as NEVLP – normothermic *ex vivo* lung perfusion
FAPESP	São Paulo Research Foundation
FBAL	fluoro-beta-alanine
FDA	Food and Drug Administration
FDR	false discovery rate
FEV	forced expired volume
FLr/FLD	fluorescence spectroscopic detection
FOL	folinic acid
FOLFOX	folinic acid-5-fluorouracil-oxaliplatin
FT-ICR	fourier transform ion cyclotron resonance
FUH_2	dihydrofluorouracil
FUPA	fluroroureidopropionic acid
FVC	forced vital capacity
GC	gas chromatography
GFR	glomerular filtration rate
HESI-II	heated electrospray ionization
HIV	human immunodeficiency virus
HLB	hydrophilic-lipophilic balance
HMDB	human metabolome database
HPLC	high performance
HPLC-MS/MS	high performance liquid chromatography coupled to tandem mass spectrometry
HR	high risk
HRMS	high resolution mass spectrometry
ICU	intensive care unit
ID	identification
ILP	isolated lung perfusion
IPO	isotopologue parameter optimization
IRC	Industrial Research Chair
IS	internal standard
IV	intravenous administration
IVLP	*in vivo* lung perfusion
LA	left atrial appendage
LASSO	lease absolute shrinkage and selection operator
LC	liquid chromatography
LC-MS	liquid chromatography coupled to mass spectrometry
LLE	liquid-liquid extraction
LOA	limit of agreement
LOD	limit of detection
LOOCV	leave one out cross validation
LOQ	limit of quantitation
LR	low risk
MALDI	matrix-assisted laser desorption
MD	microdialysis
METLIN	metabolite and chemical entity database
MOI	microfluidic open interface
MRS	magnetic resonance spectroscopy
MS	mass spectrometry

MS/MS	tandem mass spectrometry
MTA	5-methylthioadenosine
MTX	methotrexate
MWCO	molecular weight cutoff
NEVLP	normothermic *ex vivo* lung perfusion
NMR	nuclear magnetic resonance
NSA	non-specific adsorption
NSAID	non-steroidal anti-inflammatory drugs
NSCLC	non-small cell lung cancer
NSERC	Natural sciences and Engineering Research Council of Canada
OPLS-DA	orthogonal projection to latent structures-discriminant analysis
OX	oxaliplatin
PA	pulmonary artery
PAN	polyacrylonitrile
PAS	professional analytical systems
PASI	psoriasis area and severity index
PBS	phosphate buffered saline
PCA	principal component analysis
PDMS	polydimethylsiloxane
PET	positron emission tomography
PFP	pentaflurophenyl
PGD	primary graft dysfunction
PK	pharmacokinetics
PLS-DA	partial lease squares-discriminant analysis
PMID	PubMed identification number
POC	point-of-care testing
POD	postoperative day
PPt	plasma protein precipitation
PPY	polypyrrole
PRM	parallel reaction monitoring
PS	paper spray
PsA	psoriatic arthritis
PsC	psoriatic converters (transition from psoriasis disease to psoriatic arthritis)
PsD	psoriatic disease
PS-DVB	polystyrene divinyl benzene
QC	quality control
QqQ	triple quadrupole
Q-ToF	quadrupole time of flight
Q-trap	ion trap
RMSEC	root mean squares error of calibration
ROS	reactive oxygen species
RSD	relative standard deviation
RT	retention time
SBSE	stir bar sorptive extraction
SD	standard deviation
SIMCA	soft independent modelling of class analogies
SJ	swollen joints
SLE	solid-liquid extraction
SPE	solid phase extraction
SPME	solid phase microextraction

TDM	therapeutic drug monitoring
TFME	thin film microextraction (same as TF-SPME)
TF-SPME	thin film solid phase microextraction
THF	tetrahydrofolate
TJ	tender joints
ToF	time-of-flight
TS	thymidylate synthase
TXA	tranexamic acid
UF	ultrafiltration
UHN	University Health Network
UMP	uridine monophosphate
UTP	uridine triphosphate
UV/Vis	ultraviolet/visible spectroscopic detection
UW	University of Waterloo
VIP	variables of importance
WAX	weak anion exchange
XCMS	bioinformatics software platform for statistical analysis of mass spectrometry data

Chapter 1: Review of current literature

1.1 Pharmacokinetics

Pharmacokinetics (PK) is an aspect of pharmacology that is described as "what the body does to a drug."[1] It assesses the relationship between an administered dose of a drug and its concentration either in blood or at the site of administration.[2] It is important to establish a pharmacokinetic profile during drug development because it provides information as to whether a drug reaches its target receptors as well as to the duration for which it remains at these target sites to evoke the desired physiochemical response.[1] The processes that influence the pharmacokinetics of a drug are absorption, distribution, metabolism and elimination.[1] Absorption explains the uptake of a drug from the area of administration into the blood. Metabolism describes the rate at which specific enzymes in the body change the administered form or parent drug producing effective and/or toxic metabolites. Distribution focusses on the drug equilibrium established between four types of compartments in the body which are the intravascular volume, interstitial volume, aqueous intracellular volume and body fat. Excretion or metabolic inactivation describes the ways in which the body eliminates the drug.[1,2]

Even distribution of a drug among compartments is a rare occurrence. This is due to factors such as the differences in rates of blood perfusion to organs in the body and the pharmacodynamics of the drug.[1] Metabolism has interpersonal variability because it is dependent on patient biology and as such, the rate of drug elimination or clearance is affected by this process.[1-3] Many drugs exhibit large differences in blood levels between individuals due to these interpersonal differences and therefore pose a significant threat. This is especially dangerous in the cases of drugs that possess low therapeutic indicies.[4] Because blood concentration is difficult to control once a dose is administered, pharmacokinetic profiling is thus essential in determining whether the effective therapeutic steady state concentration was achieved. A comprehensive profile can be obtained by monitoring drug concentration in both blood and urine. As previously mentioned, metabolism affects drug clearance. By monitoring these particular biological fluids (biofluids), with

emphasis on the rate of drug clearance and urine concentration, drug doses can be corrected or adjusted accordingly and safely. [1-2] This need for therapeutic drug monitoring formed the foundation for personalized medicine.[3-4]

1.2 Personalized medicine

Personalized medicine is a branch of medicine that acknowledges the influence of patient phenotype and genotype on the therapeutic effect of a drug.[3] It highlights the need for individualized therapy by comprehensively studying a patient's biological fluids and tissue samples to attain tailored disease prognosis or diagnosis.[3] It is important because it renounces approaches to treatment that assume a standard dose as effective for all persons. It is beneficial in that it allows for dose adjustments or recommends for other treatment alternatives that are patient specific thus increasing chances of recovery. Personalized medicine is used heavily in the field of chemotherapy as the causes and consequences of cancer are strictly individual since they are profoundly impacted by genetics, race, gender, age and various environmentally induced stressors.[5-6] Some other types of drugs that experience variable therapeutic responses include, antibiotic agents for the critically ill, antiviral medication for those suffering from HIV, and antidepressant therapies.[7-8] In the expanding field of personalized medicine, the aim is to avoid unnecessary prescription of ineffective therapeutics. Hence, there is an increasing need for rapid diagnostic tools as well as simple and quick sample preparation techniques.[9]

1.3 Therapeutic drug monitoring

In essence, therapeutic drug monitoring (TDM) is the application of pharmacokinetic profiling in a single patient. The field of TDM is concerned with finding the relationship between the administered dose of a drug, the concentrations of that drug in various biological compartments, and the resultant therapeutic effects specific to a single individual.[10] However, unlike PK—which focuses on drug behavior for the majority of the population and is generally employed for the study of new drugs on the pharmacological market—TDM is specifically employed for drugs that have narrow or unknown/unestablished therapeutic

ranges, and that present large inter- or intra-patient concentration variability with respect to their PK profiles.[10] TDM is an important tool for preventing the under- or over-dosing of these drugs, as it enables dose adjustments to be made over the course of treatment, thereby tailoring treatment for a specific individual. Given the wide range of samples investigated during TDM, it is important to consider sample preparation techniques/assays that are not only rapid, but that are also selective and specific to the complexity of the sample under analysis. Furthermore, these assays should be cost effective and amenable to high throughput, as TDM can often require the analysis of large numbers of samples. Some examples of classes of drugs that require TDM include antiepileptics, antibiotics, antiretrovirals[11], immunosuppressants[12], and many chemotherapeutics[10]. In this thesis, antifibrinolytics and anticancer agents are addressed and investigated.

1.4 Metabolomics

Metabolomics is the study of all small endogenous and exogenous molecules within a living system at a given time for the purpose of obtaining information about the biochemical state of that system. Metabolomics is an emerging field in systems biology (wherein genomics, transcriptomics, proteomics, epigenomics are quite established approaches) that falls at the bottom of the "omics" cascade, but upstream from external stimuli such as lifestyle, dietary, medical, and environmental conditions. As such, metabolomics facilitates an understanding of the interconnectedness and complex interactions between the genome and exposome (exogenous molecules related to various forms of external stimuli).[13,14] Since the metabolome contains a wide range of compounds, including lipids, fatty acids, amino acids, xenobiotics, and sugars, it can provide information on disease states as well as the mechanisms of disease pathophysiology.[14,15] Moreover, the use of metabolomics in personalized medicine to significantly improve patient care and outcomes can be further enhanced through the development and use of metabolic phenotyping, which involves using metabolomics to characterize an individual or biological system.[13–15] Metabolic phenotyping allows clinicians to predetermine a patient's susceptibility or response to a given treatment, thus avoiding the "trial and error" approach that is commonly used personalized care.

Furthermore, metabolomics is especially useful for improving personalized targeted therapies, as it measures and considers all potentially influential factors (patient age, gender, weight, diet, gut microbiome, medical history etc.), whereas traditional personalized strategies only tend to focus on a single target or factor at time.[13,14] Further from metabolic phenotyping having the potential to predetermine more efficacious treatment courses, pharmacometabolomics is a branch of clinical metabolomics that investigates how the metabolome responds to treatments using a particular/combination of pharmaceuticals.[13] This branch of metabolomics is often associated with drugs that require TDM, and drugs that have highly variable patient responses due to an intricate balance of factors, such as variations in the activity and concentration of certain enzymes and/or varying patient gut microbiome profiles, which is also known to influence metabolism and has been implicated in a number of disorders including but not limited to inflammatory bowel disorders and disorders of the immune system.[14] However, pharmacometabolomics is also especially useful for singular drugs that present multiple mechanisms of action, as well as for monitoring polytherapy.[13] Thus, pharmacometabolomics overcomes the univariate-based approach to TDM wherein a single assay is used for a single drug/target by permitting the efficient simultaneous monitoring of multiple drugs and their impact on the treated system. Metabolomics can: 1) be used to identify prognostic, diagnostic, predictive, and surrogate markers of diverse disease states; 2) allow for disease subclassification and patient stratification; 3) provide a correlation for monitoring response and disease recurrence ; 4) determine treatment response or rejection due to treatment toxicity; 5) inform underlying disease pathophysiology; and 6) explore pharmacometabolomics (phenotypical drug response)[14,15]. The final three items in this list are discussed in more detail in this thesis.

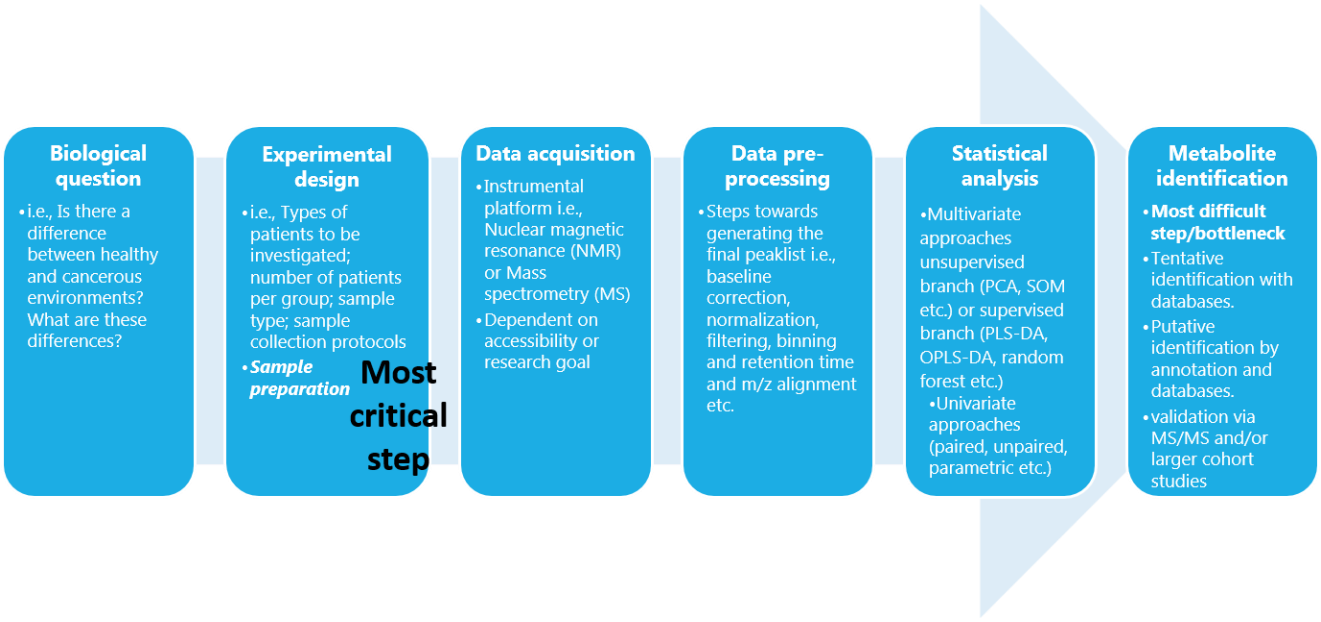

Figure 1.1 The typical metabolomics workflow

Despite the potential advantages of metabolomics, the field of "omics" research is not without numerous challenges. As shown in **Figure 1.1**, the metabolomics workflow consists of 7 steps: the biological question (i.e., what is the metabolic difference between healthy and cancerous samples?); the experimental design (i.e., how many of which kinds of samples from each group [healthy vs cancerous] will be investigated to answer the biological question?); sample collection, which follows stringent protocols for the collection of matrices such as blood, plasma, and urine in order to reduce experimental variation/errors; sample preparation, serves to simplify sample complexity and improving sample amenability for instrumental analysis; instrumental analysis, which involves selecting the metabolomics platform (nuclear magnetic resonance (NMR) or MS, the latter explored more in this thesis) to be used for separation and detection; data pre-processing, pre-treatment, and statistical analysis, which use one or a combination of several available software packages to convert and process the raw data obtained from instrumental acquisition, followed by the use of web-based or commercial software for chemometric analysis; and metabolite identification and validation which uses web-based databases or commercial packages/databases to tentatively/putatively identify metabolites of interest followed by validation via MS/MS and/or secondary

or tertiary cohort studies.[16–19] Since the compounds in the metabolome have a wide range of physicochemical properties (hydrophobic, hydrophilic, neutral, basic, acidic)[15] and the samples typically employed in metabolomic analysis (whole blood, plasma, serum, urine, stool, etc.) are generally rather complex, an initial step consisting of metabolism quenching (a method used to prevent metabolite degradation) followed by extensive sample cleanup is required in order to successfully isolate these metabolites from these biological matrices. Post quenching and sample cleanup, other non-specific sample-preparation measures are required for the global extraction of the constituent compounds of the metabolome. Thus, sample preparation is one of the most crucial steps in the metabolomics workflow, as it directly affects the outcome of the study.[16] Following data acquisition via the selected instrumentation and data preprocessing, the next major challenge is statistical analysis. The number of available data-processing platforms, including, but not limited to, SIMCA, Metaboanalyst, and XCMS Online, as well as the plethora of data pre-treatment and data processing options, can turn chemometric analysis into a very time-consuming process.[17] However, metabolite identification and validation remains the bottleneck in the metabolomics workflow. This bottlenecking occurs for a number of reasons, including the fact that: 1) only a fraction of metabolites in the metabolome are reported and recorded in databases; 2) there is no established protocol for performing untargeted analysis, which means that candidate biomarkers may be dependent on the sample preparation technique used; 3) metabolite identification/validation may be difficult and/or dependent on the detection method employed.[20] In the case of the latter, multiple larger cohort studies are required to the test robustness of candidate biomarkers before being used in official clinical settings, as mass spectrometry-based metabolomics is prone to in-source fragmentation, which can lead to misleading conclusions.

1.5 Rapid analysis

TDM and metabolomics utilize sophisticated instrumentation for separation and detection. However, the complexity of the samples involved precludes the direct injection of these untreated samples into these systems; thus, extensive sample preparation is required to ensure that the samples are compatible with the

instrumentation.[21] While the use of TDM and metabolomics is evidently advantageous in clinical and research facilities, these techniques face the common drawback of long analysis times due to involved sample preparation methods and long instrument run times. Fortunately, these limitations have been mitigated by the development of technologies that enable rapid analysis which allow for minimal sample preparation and direct detection without separation. As such, rapid-analysis technologies are able to decrease sample turnaround times, thereby enabling increased throughput and rapid information acquisition, all at a drastically reduced cost. Unlike the quantitative and semi-quantitative nature of TDM and metabolomics, respectively, rapid analysis is generally qualitative in nature and is most commonly associated with imaging techniques like magnetic resonance spectroscopy (MRS) positron emission tomography (PET). The instrumentation employed in this thesis – LC-MS and stand-alone MS – for TDM, metabolomics, and rapid analysis is discussed in more detail in *section 1.9 "Instrumentation"*.

1.6 Typically encountered samples in clinical practice

Biological fluids commonly investigated in PK studies, TDM, and metabolomics include whole blood, serum, plasma, urine, stool, cerebrospinal fluid, breast milk, sweat, saliva, and tears.[22-23] Among the array of available biofluids, blood, blood compartments, and urine are most commonly used in metabolomics, and especially TDM, with venous blood being the most extensively and frequently used.[22] The frequent and widespread use of venous blood is due to the fact that plasma or serum, usually show a good correlation between the concentration levels of a drug in the body and its therapeutic effect.[22] On the other hand, urine is more regularly studied when monitoring drug excretion patterns, drug bioavailability, and drug metabolites.[22] STEEN Solution™, commonly referred to as perfusate (discussed in more detail in *section 1.6.3 "Steen solution"*), is another fluid used in bioanalysis that is not typically encountered due to being specific to transplantation science or organ preservation strategies.[24] Since STEEN Solution is used either to flush an organ or is circulated through the organ before transplantation, it may contain valuable metabolite information that can shed light on why an organ was or was not rejected after transplantation. Additionally, there has been growing interest in TDM via tissue analysis, as plasma drug concentrations

may not accurately reflect drug concentrations in the tissue. This information is important because effective treatment (i.e., treatment of tumours) depends on accurate knowledge about the degree of penetration of a drug into the targeted organ.[25,26] Furthermore, in clinical metabolomics, site-specific metabolites found in tissue may be able to provide more insight about various other biochemical processes. However, these tissue-specific metabolites cannot be captured or accurately represented due to dilution effects in circulating blood.[27] For the purposes of this thesis, plasma, serum, urine, perfusate, and lung tissue (Figure 1.2) will be the biological matrices of interest, as they provide valuable and complementary information about drug concentration and distribution in addition to serving as important metabolite reservoirs

Figure 1.2 Various types of biological samples investigated in this thesis

1.6.1 Blood and blood compartments

Blood—which is 55% plasma in which red blood cells and macromolecules are suspended—remains one of the most useful matrices in bioanalysis, as well as one of the most challenging.[28] As a circulatory fluid perfusing throughout the entirety of an organism, blood contains rich and dense global information about the various biomolecules within that system including, but not limited to, metabolites (lipids, amino acids, organic and inorganic acids), proteins and peptides. To isolate plasma, the blood is first treated with anticoagulants before being subjected to centrifugation; in contrast, serum is extracted by centrifuging clotted blood. Centrifugation is discussed in more detail in *section 1.7.1 "Centrifugation/ centrifugation ultrafiltration"*. It is generally accepted that plasma and serum are roughly equivalent in terms of their

small-molecule profiles, but that their protein profiles differ significantly due to the reduction of proteins associated with blood clotting during serum processing; thus, there is a higher abundance of these proteins in plasma. One drawback to using whole blood as a sample is its poor stability under storage conditions (freezing) required for prolonged periods of time. This poor stability can result in erythrocyte hemolysis, which renders subsequent plasma and serum isolation—a step that generally simplifies the blood handling workflow—impossible. The limitations associated with using serum in metabolomics and TDM include potential changes in the metabolite profile or the possible loss of targeted/known analytes from erythrocyte-related biochemical degradation of drugs due to the length of time required for clotting. As such, plasma, which is obtained from collected blood on a much shorter time scale, is the preferred and more widely used blood compartment for analysis. However, it is important to note that the use of anticoagulants in plasma can cause interferences in TDM and metabolomics, which can be particularly harmful for the latter, as these interferences can overshadow potentially important low-abundance metabolites. Additionally, for metabolomics in particular, there are strict protocols regarding sample collection, as the blood metabolome reflects the circadian rhythm wherein certain metabolites concentrations naturally change over a 24-hour period, thus making it necessary to consider appropriate sample-collection times.[28]

1.6.2 Urine

A large proportion of drugs are excreted entirely or significantly via the kidneys as parent drugs or drug metabolites. The kidneys experience the highest rate of blood plasma perfusion per gram in comparison to other organs in the body and they are also responsible for the regulation and maintenance of a stable blood pH.[1] It is organized into units called nephrons, each of which contributes to urine processing. The sub processes occurring during renal elimination are glomerular filtration and tubular secretion and reuptake.[1] During urine processing, additional water is reabsorbed thus concentrating compounds in urine and resulting in the four-fold increase of osmolality in urine compared to blood.[1]

Urine is composed of more than 90% water and is thus classified as an aqueous biomatrix. It is important to stress that the complexities of urine make its use in analytical chemistry very difficult and as such, special considerations need to be made when dealing with this matrix.[29] Unlike blood wherein the average physiological pH is 7.4, urine pH can vary from 5-9.[1,30] This poses a significant challenge in isolating pH-dependent target compounds because their pKa values affect the type of species present in urine. This consequently influences the sensitivity and reproducibility of an analytical method for analyte isolation and in turn affects the quantification of substances from patient to patient.[29] Urine properties such as pH, ionic strength, inorganic salt content and the presence of exogenous and endogenous compounds can contribute to coelution and ion suppression or enhancement during analysis making identification and quantification of target compounds difficult.[31–33] These properties are further influenced by the age, gender, environmental exposure, metabolic behaviour (metabotype), medical history, gut microbiome and dietary and hydration habits of a patient.[29] These variables further emphasize the complications of urine analysis.

Unlike the stringent sample collection protocol in place for blood, urine is readily available in large quantities and can be easily and non-invasively collected.[22-29] The concentration of analytes is usually higher due to urine processing, there is an absence of proteins and time averaged information about a compound is available due to its storage in the bladder.[1,30] Besides TDM, metabolomics investigations can be conducted on urine due to the presence patient-dependent exogenous and endogenous compounds.

1.6.3 Steen solution

Steen Solution™, otherwise referred to as perfusate or perfusion fluid, is used as a general organ flush during the transplantation process, namely after explantation from the donor and prior to implantation in the recipient patient. It is also used during normothermic *ex vivo* lung perfusion (NEVLP or EVLP) and modified *in vivo* lung perfusion (IVLP) to help maintain the physiological integrity of the isolated organ throughout these procedures.[24] The NEVLP method used at Toronto General Hospital (the method used and described specifically in this thesis) uses a STEEN Solution™ that is acellular in nature in order to

prevent the occurrence of hemolysis during the procedure. STEEN Solution™ is a physiological salt solution that contains dextran 40, which is a polysaccharide and mild scavenger that helps to prevent thrombogenesis (clot formation) and excessive leukocyte interactions by coating and protecting the endothelium. The extracellular electrolyte content and low levels of potassium effectively decrease free radical formation, thus preventing vascular spasms under normothermic conditions. The use of human serum albumin in the perfusate regulates oncotic pressure in the lung, which reduces the formation of edema. Furthermore, STEEN Solution™ is thought to possess antioxidant properties, which help abate the ROS formation associated with ischemia-reperfusion-related lung injuries and improve the success rate of the NEVLP procedure.[24]

1.6.4 Tissue

The growing interest in tissue analysis raises the need for standardized sample preparation protocols for the various tissue types in order to ensure reproducible and reliable results. Compared to the analysis of systemic fluids in which the important metabolites would be otherwise diluted as a result of systemic circulation, tissue analysis is able to provide more information about both the site-specific interactions of therapeutics, and invaluable biochemical information about disease pathology.[25,27] While blood is a connective tissue, it falls into the category of biological fluids. Another category of tissue is delineated by the solid or semi-solid nature of biologically derived matter. Some examples of biological solids used in TDM and metabolomics include soft tissues, such as the liver, lung, spleen, and brain; hard tissues like bone, cartilage, hair, and skin; and tough tissues like muscle, heart, stomach, intestines, and arteries.[26] However, since the heterogeneity of tissue can lead to the non-uniform distribution of therapeutic drugs within an organ, the accurate quantitation of such drugs via tissue analysis can be rather difficult. Moreover, some metabolites are site specific, which means that they may occur in significantly higher or lower abundance in a particular region of the organ compared to the bulk organ or other areas of the organ. Therefore, careful, reproducible sampling procedures are necessary in order to ensure that the observed differences are representative of true changes rather than being the result of inappropriate sampling or

sample handling.[27] Unlike biological fluids such as blood or urine, tissue analysis requires much more involved sample-preparation methods. Tissue-related sample preparation practices are discussed in s*ection 1.7.8 "Homogenization"*.

1.7 Current sample preparation methods

In TDM, the measurement of free and total concentration is important in order to determine the relationship between dose and effect.[34] It remains a controversial issue as to whether total drug concentration in various biological compartments is more important than free concentration because the free concentration measurements are unnecessary if it is constant within and between individuals.[34] However, the free concentration within and between individuals, is dependent on the extent of enzymatic influences or protein binding of the drug.[1–3,34,35] Free concentration is then a function of pharmacokinetics as it is dependent on how an individual processes the drug. Sample preparation techniques were developed for the purposes of determining free drug concentration as the unbound fraction is bioavailable to partition into tissues, bind to receptors and induce a physiological or physiochemical response.[1,34,35] Some notable examples of such techniques specific for determining free drug concentration are ultrafiltration (UF) and equilibrium dialysis (ED), while other sample preparation methods that determine total drug concentration include plasma protein precipitation (PPt), dried blood spot (DBS), liquid-liquid extraction (LLE) and solid phase extraction (SPE). Other methods more suited for tissue sample preparation require an initial sample homogenization step followed by one or more of the above noted sample preparation methods (PPt or LLE) and/or centrifugation. Figure 1.3 graphically summarizes some of the conventional sample preparation techniques used for clinically-relevant samples analyzed via LC-MS specifically, the main instrumentation used in this thesis and discussed in more detail in *section 1.9 "Instrumentation"*.

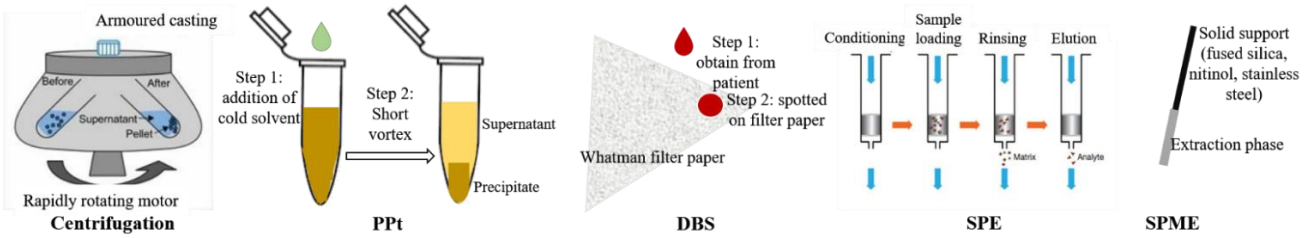

Figure 1.3 Some conventional sample preparation approaches used in the bioanalytical and clinical field such as (*from the left*) centrifugation, plasma protein precipitation (PPt), dried blood spots (DBS), solid phase extraction (SPE). Solid phase microextraction (SPME) is a novel technique that is explored in this thesis.

1.7.1 Centrifugation/ centrifugation ultrafiltration

Centrifugation is the most widely used sample-cleanup/sample-preparation technique. Briefly, centrifugation operates on the sedimentation principle wherein suspended particles such as blood cells in whole blood, proteins in plasma (after an initial precipitation from cold-solvent addition), or minerals in urine are separated as a result of centrifugal acceleration, with heavier, denser particles moving outward and downward towards the bottom and lighter particles moving to the center and settling based on density.[36] Centrifugation ultrafiltration operates under the same principle as centrifugation, but uses a semi-permeable membrane with a certain molecular weight cut off (MWCO) to prevent solutes above the MWCO from passing through.[37] Centrifugation is often used for a range of samples like blood and/or tissue after an initial homogenization step, while centrifugation ultrafiltration is more commonly used for the removal of proteins from plasma and serum. The respective concentrations of macromolecules and smaller molecules remaining in the sample after centrifugation or centrifugation ultrafiltration will vary depending on the type of solvent that is used, the ratio of solvent volume to sample volume, the centrifugal force applied, and the MWCO of the membrane being used.[37]

1.7.2 Ultrafiltration (UF)

UF is a method of separation involving sample centrifugation in the presence of a semipermeable membrane that has a molecular weight cut-off (MWCO) ranging from 3-50 kD.[34,35] The concentration gradient that

results from the filtration allows for the measurement of free drug concentration in the protein free ultrafiltrate.[34] The method's simplicity and speed make it the preferable choice for clinical applications.[34] Unfortunately, drugs are susceptible to nonspecific adsorption (NSA) to the UF devices, introducing potentially large errors in the quantification of free drug concentration.[34,35] Other issues include a change in temperature and pH at which centrifugation occurs which also contribute to analytical errors. It is believed however, that temperature and pH can be easily improved to better mimic physiological conditions while there are efforts being made to compensate for the problem of NSA.[34,35]

1.7.3 Equilibrium dialysis (ED)

Still considered the gold standard for monitoring free drug concentration, ED is a technique in which a semipermeable membrane separates two chambers, one of which contains plasma and the other contains a buffer that has a similar consistency as plasma.[34,35] After some time, through the process of diffusion, equilibrium is established between the chambers and the unbound fraction is determined as a ratio of the free drug fraction in the plasma chamber to that of the fraction in the buffer chamber.[35] Nonspecific adsorption and volume shifts due to osmosis are some method disadvantages pointed out by Musteata (2011)[34] but are considered negligible according to Nilsson (2013).[35] Other drawbacks include the disturbance in equilibrium which is proven by the consequent decrease in equilibrium concentration, the method is extremely labour intensive and time consuming, it requires long equilibration times, it is not ideal for water soluble compounds and artifacts are formed as a result of electrically charged proteins or drugs.[34,35]

1.7.4 Plasma protein precipitation (PPt)

Precipitation occurs as a result of protein insolubility due to either the presence of an organic modifier, a change in pH by the addition of an acid or base, or an increase in salt content.[38,39] Organic solvents such as methanol, ethanol or acetonitrile – the most effective organic solvent for precipitation according to Lee and Oh (2014)[38] – can be used.[38,39] Although basic conditions lead to protein precipitation, the addition of an

acid (trifluoroacetic acid or perchloric acid) creates a favorable environment for positively charged amino acids to become insoluble salts. These newly induced salts remove water molecules that saturate the proteins, thus causing precipitation.[38] The same mechanism applies with the simple addition of salt (ammonium sulfate) and is referred to as salt-induced precipitation.[39] Samples can be centrifuged following precipitation and the supernatant is used to quantify total drug concentration.[39] PPt is the longest and most widely used sample preparation method due to its low cost, speed and ease. It is still favoured in biological processing and in some cases produces higher recovery rates than other sample preparation techniques.[38] However, with bioanalysis using tandem mass spectrometry (MS/MS) subsequent to PPt, there can be significant matrix effects such as ion suppression or enhancement.[39]

1.7.5 Dried blood spot (DBS)

Blood is regularly used in pharmacokinetic and toxicokinetic studies because it circulates throughout the body and thus provides appropriate information on the distribution and concentration of drugs in the body.[22] DBS is the utilization of a filter paper that has a distinct pore size and thickness on which a small volume of pre-treated or untreated blood can be left to dry, incapacitating the growth of bacteria as a result of dried proteins and pathogens.[40] Requiring very small sample volumes, DBS is a suitable substitute for conventional blood collection approaches and is advantageous in therapeutic drug monitoring for neonates as well as pharmacokinetic studies involving small laboratory animals.[40] Traditional methods of serial blood collection was also a contributing factor to low volunteer recruitment in some studies but the development of DBS addressed this concern and became useful for other pharmacokinetic studies and *in vivo* concentration assessments because it is minimally invasive and non-painful.[40] DBS can be used on site in clinical studies, provides easy storage for transportation of samples, minimizes sample handling, and offers important qualitative and quantitative information. The filter paper can be studied directly through analytical, immunological and genomic detection with their respective instrumentation.[40] Given its benefits, DBS suffers from a plethora of limitations. It is insufficient to study sensitive and volatile analytes, as well as drugs that have minimal blood cell up take. The use of capillary blood for small volume sampling may

contain different information than venous blood, making this technique inadequate for pharmacokinetic assessment of certain drugs. It can only be coupled with highly sensitive analytical instruments due to the small volume used and it is not as receptive compared to other biofluids like plasma and serum to more commonly used analytical instruments such as high-performance liquid chromatography with ultraviolet-visible detection (HPLC-UV-Vis).[40]

1.7.6 Liquid-liquid extraction (LLE)

LLE is a conventional sample preparation method commonly used and was the first technique to be applied in analytical chemistry.[38,39,41] It has been used broadly in a range of fields including pharmaceutical, organic, inorganic and biochemical industries. There are four types of extraction modes and discontinuous extraction is the most traditionally used.[41] LLE exploits the incompatibility of water and water-immiscible organic solvents to extract organic analytes from aqueous media.[38] Separation occurs through the partitioning and equilibration of analytes from aqueous to organic phase based on various hydrophilic and hydrophobic properties and interactions.[38,41] Improvement in extraction efficiency can be achieved by making changes to the pH or the type of organic solvent used in order to convert hydrophilic analytes to hydrophobic compounds therefore, increasing analyte recovery. LLE is more effective than PPt for eliminating interferences in biomatrices by yielding more purified products, hence providing a higher sensitivity in terms of instrumental analysis.[38] Despite these advantages, the method suffers from the excessive use of organic solvents that lead to the generation of a large amount of waste.[41] Not only is LLE environmentally unfriendly, issues with emulsion and solvent evaporation during extraction lead to losses in analyte recovery, extensive clean up procedures are required for glassware and can cause sample cross-contamination, and labour intensive time consuming extractions result in poor repeatability and low throughput.[41]

1.7.7 Solid phase extraction (SPE)

SPE is an exhaustive sample preparation technique that aims to eliminate interfering species and increase analyte enrichment by loading a sample into a sorbent packed column and separating the desired analyte through a washing and elution step.[34,38,39,41,42] These steps are selective in that they are based on the partitioning of target and undesired compounds between the adsorbent packing and the organic liquid phase.[38,39,41,42] The method consists of the following four steps: conditioning, sample loading, washing and elution. Conditioning or preconditioning is done with water, a buffer or a diluted organic solvent. This step readies the adsorbent packing by activating the functional groups through solvation for the proper adsorbent mechanisms to take place.[38,39] Sample is then loaded by gravity, aspirated by vacuum or pumped.[39] The sample can be loaded in a solvent that has low elution power or strictly as a biofluid.[38] The wash step consists of flushing the column with an organic solvent that does not have the eluting power to affect the target analytes but rigorously removes a majority of matrix interferences. The final step is elution wherein a strong eluting organic solvent is used to remove the analytes of interest from the column.[38,39] SPE is applied for the quantification of trace organic materials in the environment, for food analysis and drugs in biofluids.[41] It is highly advantageous in its selectivity and ruggedness through newly developed polymeric sorbents, its ability for the complete extraction of analytes, its reduced solvent consumption and amenability for automation for high throughput leading to increased reproducibility. SPE's main weaknesses are that it is time consuming, more so than PP and LLE and the technique is limited for onsite or clinical applications that require quick analyte isolation.[41]

1.7.8 Homogenization

Sample preparation techniques for tissue range depending on the subcategory (soft, tough, hard) of the tissue of interest, as different tissue types have different water contents and degrees of vascularization.[25] Within the context of tissue-sample preparation, homogenization is a broad term that is used to refer to the complete and total disruption of the tissue structure by manual, physical, or mechanical means. Mechanical homogenization can sometimes be followed by enzyme digestion and is usually coupled with one or more

of the other sample preparation methods discussed earlier in this section (i.e., PPt, LLE, and SPE).[25,26] For soft tissue, physical or mechanical homogenization is most commonly performed via grinding, low-frequency rotating blades, bead beating, sonication/ultrasonication, or enzymatic digestion. Tough tissues are generally more fibrous, which means that more force is usually required to break them down; as such higher frequency mechanical energy and longer duration is needed. Thus, for tough tissues, high-speed rotating blades and high-frequency bead beating are often used with less emphasis on ultrasonication. Much more powerful homogenization methods are required for hard tissues, such as cryogenic pulverization (the grinding of initially frozen samples, which is especially useful for the analysis of thermally labile compounds), acidic treatment (usually employed for hair homogenization), and chemical treatment.[25–27] The majority of the outlined homogenization practices are suitable for TDM wherein extensive testing is completed at each stage of the sample preparation protocol to ensure maximum recovery, minimum carry over, and analyte stability. However, for metabolomics, wherein sample integrity is key for analysis, homogenization takes place under flash-frozen conditions or after quenching steps such as enzyme denaturing with acid.[27]

1.7.9 Microdialysis (MD)

Mircodialysis is a well-known and established method that is especially used for *in vivo* sampling. The microdialysis device consists of a probe approximately 200-600 μm in diameter, which is composed of tubing and a semi-permeable membrane that is placed in contact with the tissue of interest.[43,44] Extraction takes place when a constant flow of perfusion is pumped down through the center of the probe, flowing out of the bottom of the inner metal shaft and then upwards along the membrane between the inner shaft and the membrane, inducing solute exchange. The dialysate is then collected from the tubes outside the sampled site. The kinetics and dynamics of solute exchange during sampling vary depending on the flow rate of the perfusate (0.3–2 μL), the type of the semi-permeable membrane used and its MWCO, and the consistency of the perfusate (album addition to alleviate adsorption issues). Since microdialysis only samples free

concentrations of solutes in the interstitial/extracellular space, it has been instrumental in expanding our understanding of the distribution of unbound concentrations of drugs in tissue; however, it is also rather time consuming, advanced, and suffers from losses of lipophilic species via non-specific adsorption to the semi-permeable membrane. For these reasons, microdialysis has largely been employed for the quantitative measurement of hydrophilic compounds such as neurotransmitters within brain tissue.[43,44] While TDM is feasible with microdialysis, the device is inherently unsuitable; conversely, it is still used[45,46] for metabolomics due to its selectivity.

Solid phase microextraction (SPME), often confused as another form of SPE ("micro SPE"), is another analytical approach that can perform *in vivo* sampling. SPME confronts the challenges faced by the above mentioned techniques and thus was utilized in this research as the main method of analyses.[29,38,41] It has been proven to be a useful alternative approach for sample preparation and is advantageous in that it provides a balanced coverage of both polar and non-polar compounds, delivering solvent-less extraction of small molecules while minimizing the extraction of typical biological interferences (macromolecules).[41,42]

1.8 Solid phase microextraction (SPME)

SPME was developed some 25 years ago to address the issues of conventional sample preparation techniques by providing a means of rapid sample preparation to better facilitate on-site applications as well as increase laboratory efficiency.[41,42] This technique epitomizes the fundamentals of green chemistry in that it is sustainable in its reusability while eliminating or drastically minimizing the need for organic solvents. It achieves this goal by integrating sampling, sample preparation and analyte preconcentration into one step and therefore reduces the number of steps in the analytical process, decreases human intervention/sample handling and thereby reduces analytical error.[42] By enabling rapid sample preparation, time and cost per sample is also considerably reduced. Furthermore, automation of the technique in certain configurations enables its high-throughput capabilities.[47]

1.8.1 Overview of the technique

SPME is a non-exhaustive approach that applies fundamental thermodynamic and kinetic principles for method selectivity and increased extraction rate (Figure 1.4).[42] Of the two types of extraction, equilibrium and pre-equilibrium extraction, the former will be discussed in more detail since it is the more widely applied extraction technique in SPME, offering improved method sensitivity.[41] Of the two different modes of SPME extraction, headspace and direct immersion (DI), the latter is used extensively in this thesis.

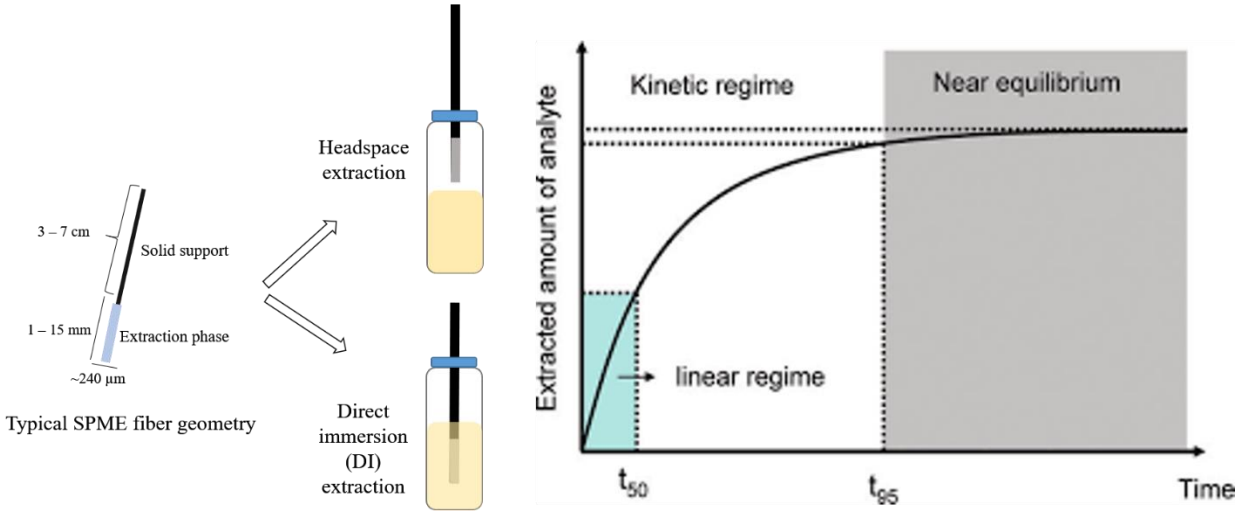

Figure 1.4 Typical SPME fiber geometry (*left*) popularly employed for two types of extraction modes – headspace and direct immersion (*middle*). Fundamental SPME extraction kinetics and thermodynamics principle (*right*)

Under equilibrium conditions, a small volume of extraction phase (a polymer coating), which is immobilized on a solid support (fiber), is exposed to a sample volume for a predetermined amount of time. Within this time, analytes migrate from the sample matrix to the coating and are either absorbed into or adsorbed onto the extraction phase (extraction mechanism depends on the type of coating, "liquid" vs solid coating). The sampling is completed when an equilibrium is established between the analytes in the coating and those in the sample matrix such that the concentration of analyte in the extraction phase is equal to the concentration of analyte in the sample. This relationship can be described by Equation (1) which is in keeping with the law of conservation of mass, considering a two phase system – the sample matrix and the fiber coating.[42]

$$C_0 V_s = C_s{}^{\infty} V_s + C_f{}^{\infty} V_f \quad (1)$$

C_0 is the total analyte concentration in the sample, V_s is the sample volume, C_s^{∞} and C_f^{∞} are the analyte concentrations at equilibrium in the sample and on the fiber, respectively and V_f is the fiber coating volume.[42] The distribution of analytes in the coating is determined by its distribution constant K_{fs} which is demonstrated by Equation (2).

$$K_{fs} = \frac{C_f{}^{\infty}}{C_s{}^{\infty}} \quad (2)$$

Equations (1) and (2) can be rearranged and combined to give Equation (3)

$$n = C_f{}^{\infty} V_f = C_0 \frac{K_{fs} V_s V_f}{K_{fs} V_f + V_s} \quad (3)$$

Where *n* is number of moles of analyte extracted by the coating and it is linearly proportional to the analyte concentration in the sample. This equation represents the analytical foundation on which quantitation using SPME is used.[42]

The time required to reach equilibrium can be infinite and thus equilibrium is defined as the time at which 95% of the equilibrium amount of the desired compound is extracted. This relationship is expressed by Equation (4).

$$t_e = t_{95\%} = 3 \frac{\partial K_{fs}(b-a)}{D_s} \quad (4)$$

The time to reach equilibrium t_e, is equal to the amount of time required to extract 95% of the equilibrium amount of the analyte, $t_{95\%}$. ∂ is the thickness of the boundary layer which can be reduced by agitation, ($b - a$) is the fiber coating thickness and D_s is the analyte's diffusion coefficient. It can be noted that this equilibration time is dependent on the analyte distribution constant K_{fs} and the higher the affinity of the analyte for the coating the longer the equilibration time.[42]

1.8.2 *In vivo* SPME

One of the main advantages of SPME is the ability to use this sample preparation tool on-site and moreover for *in vivo* analysis. This is highlighted throughout the thesis in the later chapters (Chapters 4-6) to emphasize the capabilities and potential of SPME for ameliorating current sample preparation workflows for a number of difficult samples as well as for rapid analysis like point-of-care testing. *In vivo* analysis is possible according the fundamentals of the technique. Starting with Equation (3), should the volume of the sample V_s be significantly greater than the product of the volume of the fiber V_f and the distribution constant K_{fs} ($V_s >> K_{fs}V_f$), then the product is essentially negligible and Equation (3) simplifies to Equation (5).

$$n = C_0 K_{fs} V_f \qquad (5)$$

The amount extracted n, according to Equation (5) is now independent of the volume of the sample V_s. This is ideal for *in vivo* investigations since the volume of a system being sampled is generally difficult to ascertain.

1.8.3 Thin-film SPME

There are several SPME configurations available and the choice of which to use is dependent on the nature of the analyte of interest as well as the aim of the research.[42] A few to name include the popular fiber configuration which is commercially available, stir bar sorptive extraction (SBSE), in-tube SPME and thin-film SPME (TF-SPME) otherwise referred to as thin-film microextraction TFME.[29] TF-SPME is an optimal

configuration because it provides better method sensitivity without sacrificing short extraction times.[47] This is due to the increased surface area to volume ratio of the extraction phase allowing for higher mass uptake of the analyte.[47] Theoretically, this increased mass uptake can be demonstrated by referring back to Equation (3) wherein the amount of analyte extracted is linearly proportional not only to analyte concentration in the sample but also to the volume of the extraction phase V_f.[42] Additionally, this thin-film geometry can be modified into a 96 brush format that is compatible with the 96-well plate template, extending SPME capabilities for high throughput analysis.[47]

1.8.4 Biocompatible coatings

Advancements in SPME technology and the development of biocompatible coatings allow for direct immersion of these devices into untreated complex biological matrices.[48] There are a number of research papers regarding the use of various biocompatible coatings in a range of complex matrices. A short summary of recently used biocompatible coatings, respective matrices and methods is shown in

Table 1.1.[29]

Table 1.1 Summary of recently used biocompatible coatings, respective matrices and methods. Excerpted from Souza-Silva et al.[29]

Type of polymer coating	Analyte	Matrix	Extraction Mode	Instrument Method
Polypyrrole (PPY) and polythiophene	amoxicillin	plasma	DI-SPME	LC-UV
PAN-C18	benzodiazepines	plasma	DI-SPME (thin film with Concept-96)	LC-MS/MS
PPY	Diazepam, nordiazepam, oxazepam	rat circulating blood	*In vivo* SPME	LC-MS/MS
C18	More than 100 doping compounds	urine	DI-SPME	LC-MS/MS
C18	Cocaine and diazepam	urine	DI-SPME	CBS-MS/MS

Biocompatible binder-C18	Carbamazepine, carbamazepine-10,11-epoxide	Mice circulating blood	*In vivo*-SPME	LC-MS/MS
PDMS	Ibuprofen and fluoxetine	Fish muscle	DI-SPME	LC-MS/MS
HLB-PAN	25 doping substances	plasma	DI-SPME (thin film using Concept-96)	LC-MS/MS

Due to polyacrylonitrile's (PAN) exceptional properties such as excellent thermal, mechanical and chemical stability, biocompatible coatings are based on a mixture of extraction phase polymer particles with PAN.[48] PAN membranes are extensively used in the biomedical field and are usually the membrane material used for UF and ED.[48] Published works in relation to the use of SPME biocompatible coatings in PK studies include: study of amoxicillin in human plasma by polypyrrole (PPY) and polythiophene coating following analysis by HPLC-MS/MS; *in vivo* SPME studies of carbamazepine in mice; and *in vivo* studies of diazepam in rat circulating blood.[49–51] Other recent research from the Pawliszyn research team on biocompatible SPME coatings and methods used in the related mediums of plasma and urine for *ex vivo* studies include the quantification of prohibited substances in plasma using hyrophillic-lipophillic balance (HLB) coating as well the quantitative analysis of prohibited substances in urine using polyacrilonitrile – octadecyl carbon chain (PAN-C18) coating.[52,53] The use of SPME in clinical field for TDM as well as tissue analysis has been pioneered by Bojko et *al*.(2011; 2013, 2014) with the TDM of tranexamic acid in plasma and the use of *in vivo* SPME for monitoring biomarkers and drugs during surgery in lung tissue.[54–56] Lastly, the use of SPME for clinical metabolomics was pioneered by Vuckovic and Pawliszyn (2011) wherein a systematic evaluation of various coatings for untargeted profiling of biological fluids was performed.[57] These achievements laid the foundation on which the work presented in this thesis is based. The typical SPME workflow employed for the instrumentation used in this thesis is discussed in *section 1.10 "Typical SPME workflow"* following the discussion of the types of instrumentation explored in this thesis.

1.9 Instrumentation

The instrumentation used for separation and quantitation in bioanalysis includes gas chromatography (GC), liquid chromatography (LC), and capillary electrophoresis (CE), while detection is often achieved via mass spectrometry (MS) or spectrophotometry methods such as ultraviolet/visible (UV/Vis) and fluorescence (Flr). The research conducted for this thesis primarily used liquid chromatography coupled to mass spectrometry (LC-MS), as this has become the standard technology used to support and advance PK studies, TDM, and metabolomics.[58–60] Suitable for semi- to low- volatility compounds, LC provides excellent separation resolution and efficiency for a range of compounds due to the availability of numerous stationary phases, while MS enables the identification and quantification of both known and unknown compounds.[59–61] LC coupled with tandem mass spectrometry (MS/MS) or high-resolution mass spectrometry (HRMS) allows for improved specificity, selectivity and greater sensitivity, all while providing reliable and reproducible quantitative and qualitative data.[58–60] TDM assays are usually very specific and/or selective for the compounds of interest. MS-based TDM utilizes sensitive and selective MS/MS, which employs a combination of mass analyzers. Some examples of tandem mass spectrometers include triple quadrupole (QqQ), quadrupole time of flight (Q-ToF), tandem time of flight (ToF-ToF), and ion trap (Q-trap). These mass spectrometers are generally viewed as robust workhorses due the fact that they are typically in constant use for the determination and quantitation of various known analytes, while requiring less maintenance than HRMS.[15,21] Since metabolomics involves the detection of hundreds of unknown compounds from a range of biochemical classes related to the metabolome, mass spectrometers characterized by high resolution, rapid data acquisition, and high mass accuracy are required. Mass analyzers such as the orbitrap, the Fourier-transform ion cyclotron resonance (FT-ICR), and the quadrupole time of flight Q-ToF are all able to meet these requirements, achieving resolving powers ranging from 35, 000 to 1 000 000 and mass accuracies below 15 ppm.[21] As mentioned in *section 1.5 "Rapid analysis"*, unlike TDM and metabolomics, which require LC to be coupled to MS/MS or HRMS, rapid analysis bypasses both the laborious sample preparation step and the chromatographic separation step, thereby increasing sample throughput. Generally,

stand-alone MS with ambient ionization is used specifically for this kind of analysis.[21] Some commonly used ambient ionization techniques include desorption electrospray ionization (DESI), direct analysis in real-time (DART), and matrix-assisted laser desorption ionization (MALDI); notably, DESI and DART have been successfully used with the SPME concept.[62] In this thesis, an ambient ESI-based in-laboratory-developed rapid technology interface—microfluidic open interface (MOI)—was used to couple to biocompatible SPME fibers (Bio-SPME) to MS/MS in order to further explore the potential of SPME for creating a rapid TDM protocol.

1.10 Typical SPME workflow

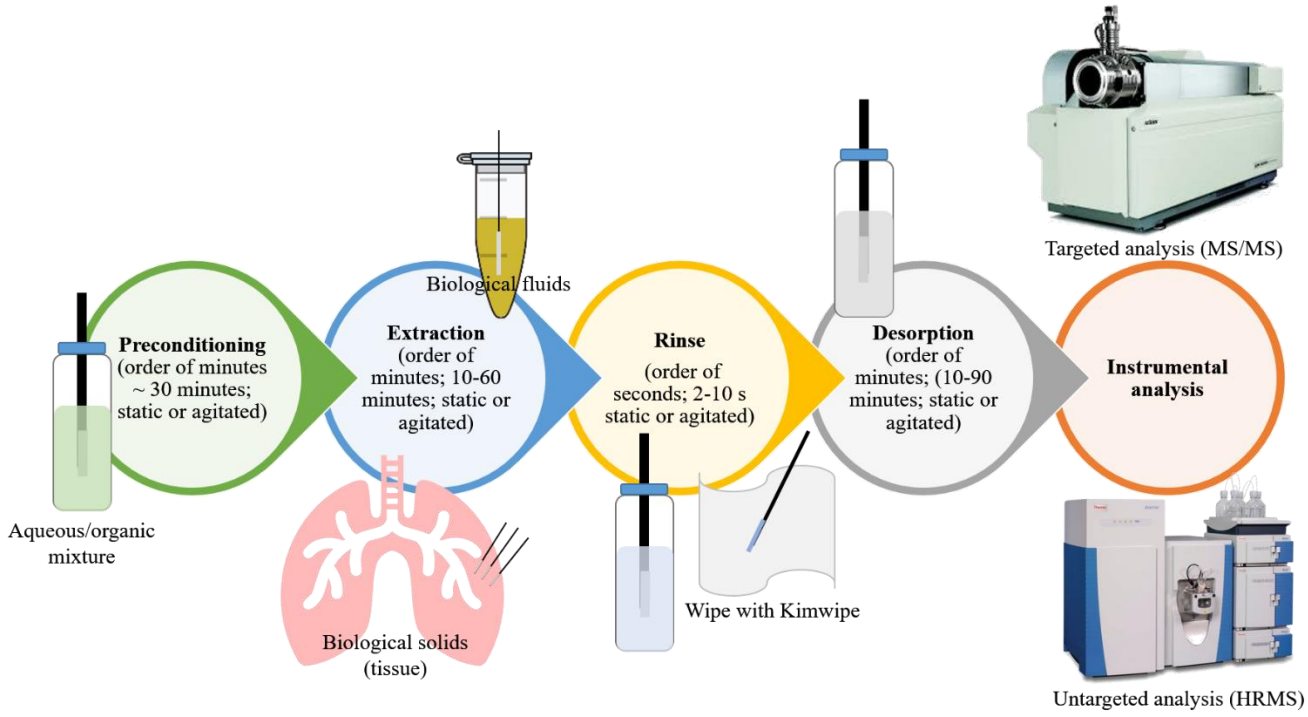

Figure 1.5 Graphical representation of the general SPME workflow.

The typical SPME workflow consists of four steps: preconditioning, extraction, rinse and desorption followed by analysis with various instrumentation (Figure 1.5). Generally, SPME devices used for DI analysis followed by LC require an initial preconditioning step to effectively activate the coating. A mixture of organic/aqueous content is usually sufficient for these purposes but largely depends on the type of coating

employed as some coating have better wettability and require less or little preconditioning time in comparison to other coating types. Post conditioning, the SPME device is exposed to the sample of interest (biofluids or biosolids) *in vivo* or *ex vivo* and remains in the sample for a pre-determined amount of time after which the device is rinsed to remove any loosely attached/adhered matrix components. This rinsing step is critical to reduce interferences coextracted as well as prevents the precipitation of matrix components onto the fiber following the subsequent desorption step, which normally contains some amount of organic solvent. Precipitation can damage the device (via irreversible adsorptive processes) and thus affect device reproducibility and/or reusability. Rinsing is also important for obtaining cleaner extracts that are to be injected for LC analysis, thereby improving separation conditions by helping to extend column lifetime. In the final step, desorption, the presence of some content of organic solvent reduces the distribution constant (K_{fs}) of the analyte for the extraction phase thus facilitating their recovery from the fiber. Suitable desorption solutions depend on the coating used, analytes of interest and initial LC instrumental conditions. Thus, each step of the workflow should be optimized to improve method sensitivity. In the case of rapid analysis however, this final offline desorption step is overlooked, rather desorption is performed online via ambient interfaces that couple the SPME device directly to the mass spectrometer (SPME-MS). SPME-MS is explored more in *Chapter Chapter 7* of this thesis.

1.11 Research objective

The work presented in this thesis aims to exemplify the practicality, feasibility, and suitability of SPME for personalized clinical applications such as TDM, clinical metabolomics, and pharmacometabolomics. In addition, this research aims to further lay the groundwork for the use of SPME in clinical settings by developing SPME-based methods for targeted and untargeted approaches, such as TDM and metabolomics. As a sampling tool that integrates sampling and sample preparation into a single step, one of the main advantages of SPME is its suitability for *in vivo* and on-site analysis. With the exception of microdialysis, this is a characteristic that is uncommon for the bulk of conventional sample preparation practices. As such,

SPME offers an especially promising tool for use in TDM, metabolomics, and point-of-care analysis, one that can ultimately serve to improve personalized approaches to patient care.

Therefore, the objective of this thesis is to demonstrate the use of SPME for: 1) developing robust targeted approaches for therapeutics; 2) determining useful candidate metabolic markers indicative of toxicity or positive response; and 3) showing that these targeted approaches and pre-determined metabolic markers can be rapidly monitored, thereby providing real-time, personalized treatment that can be quickly customized depending on therapeutic concentration or the presence/absence of these indicative metabolic markers. The future direction/goal of this research is to eventually enable the use of SPME as an alternative complementary diagnostic tool that is capable of not only providing reliable, rapid quantitative analyses of a range of therapeutics, but also performing simultaneous rapid chemical biopsies *in vivo* or from a range of clinically relevant biological matrices, such as urine, blood compartments, and lung tissue.

The thesis achieves these research objectives by first illustrating the suitability of SPME for TDM through the development of a method for monitoring tranexamic acid in plasma and urine samples from patients undergoing cardiac surgery (Chapter 2). Next, the applicability of SPME for clinical metabolomics is demonstrated through its use for the determination of disease conversion (psoriasis to psoriatic arthritis) pathophysiology via the untargeted profiling of serum samples from patients with psoriasis and varying degrees of psoriatic arthritis (Chapter 3). The applicability of SPME for clinical metabolomics of more complex samples and dynamic environments is then demonstrated in Chapter 4, where it is used for the *in vivo* monitoring of porcine lung tissue undergoing normothermic *ex vivo* lung perfusion (NEVLP), which is an organ-preservation strategy commonly used to improve lung function and increase the donor pool for transplantation. Chapter 5 and Chapter 6 then demonstrate the use of *in vivo* SPME for simultaneous TDM and proof-of-concept pharmacometabolomics on lung tissue treated with chemotherapy via *in vivo* lung perfusion (IVLP) for pre-clinical and clinical trials. Chapter 5 presents a pre-clinical trial of folinic acid-5-fluorouracil-oxaliplatin (FOLFOX) combination therapy in a porcine model during IVLP, wherein the

developed quantitative SPME method was used for the TDM of FOLFOX in samples collected *in vivo* on-site (in the hospital), followed by pharmacometabolomics. Chapter 6 details a clinical trial in human lungs with the use of doxorubicin (DOX) during IVLP, followed TDM of DOX in lung tissue as well as pharmacometabolomics. The goal in Chapter 6 was to correlate good/successful clinical outcomes with metabolomic data to indicate the effectiveness of the drug combination using the same principles as in the proof-of-concept in Chapter 5. Lastly, Chapter 7 demonstrates the potential of SPME for rapid diagnostics by using SPME-MS for the rapid quantitation of tranexamic acid in the plasma samples acquired from the patients in Chapter 1, thus showing the close correlation between SPME-MS and LC-MS, which is the gold standard for quantitative bioanalysis. As Chapter 7 demonstrates, reliable rapid analysis can theoretically be achieved using any untreated complex biological matrix once the methods have been established. The availability of rapid SPME-based methods for biological fluids means that the same tool that was used for rapid plasma analysis in this research can be easily translated towards more complex matrices, such as tissue, for the rapid quantitation of therapeutics in tissue. In the same way, once metabolomic methods have been better established, useful metabolic markers can also be rapidly monitored quantitatively or qualitatively with the use of SPME-MS.

Chapter 2: Therapeutic drug monitoring of tranexamic acid in plasma and urine of renally impaired patients using solid phase microextraction

2.1 Preamble

The results from this chapter have been used by clinicians to develop a PK profile of TXA for the purposes of correcting the dosing schedule for patients with chronic renal dysfunction who are undergoing cardiac surgery; the results of which are published as an article entitled "Tranexamic acid dosing for cardiac surgical patients with chronic renal dysfuntion" by A. Jerath, Q. J. Yang, S.K. Pang, N. Looby (the author of this thesis), N. Reyes-Garcés, T. Vasiljevic, B. Bojko, J. Pawliszyn, D. Wijeysundera, W. S. Beattie, T. M. Yau, and M. Wasowicz., *Anesthesia & Analgesia*, **2018**, 127(6), 1323-1332. The results in this chapter have not yet been published but have been formatted for submission to *Talanta* and co-authored by T. Vasiljevic, N. Reyes-Garces, A. Roszkowska, B. Bojko, M. Wasowicz, A. Jerath and J. Pawliszyn. Please see *Statement of contributions.* We are grateful to the Natural Sciences and Engineering Research Council (NSERC) of Canada for the financial support provided through the Industrial Research Chair program.

2.2 Introduction

Tranexamic acid (TXA) is extensively employed in hospital and clinical settings to reduce blood loss.[63] TXA inhibits fibrinolysis—which is the breakdown of fibrin, a key constituent of blood clots—by inhibiting plasmin and preventing the activation to plasminogen, the protein responsible for fibrinolysis.[63] Findings have shown that TXA has a much better safety profile than earlier generation antifibrinolytics like aprotinin and ecallantide, and that higher concentrations can be particularly effective for use in high-risk operations, such as cardiac surgery.[64] However, findings have also shown that the continued use of TXA at high concentrations may put some patients at risk of developing post-operative seizures[63,64] due to elevated concentrations of TXA in the cerebrospinal fluid, even after the cessation of intravenous administration.[65] Furthermore, TXA has high inter-patient variability, with drastically different resultant blood plasma

concentrations having been observed in patients that have undergone the same dosing schedule, for both high- and low-dose schedules.[3,64] Given that the body removes tranexamic acid via glomerular filtration, it has been hypothesized that this interpatient variation is due to poor renal clearance among patients suffering from chronic renal dysfunction.[66] Thus, the purpose of the work presented herein was to develop a high-throughput method for the fast and reliable quantitation of TXA in two complementary biological matrices: plasma and urine. Ideally, this new method will prove to be a valuable tool for use in pharmacokinetic (PK) studies aimed at correcting dosing schedules in order to avoid overdosing or high blood plasma concentrations—and thereby reducing the risk of seizures—in patients suffering chronic renal dysfunction.

Classical analytical methods for quantitating TXA in biological fluids often require sample preparation steps such as plasma protein precipitation (PPt) and liquid-liquid extraction (LLE), which are sometimes followed by a sample pH adjustment step depending on the separation method that will be used.[65,67] Other recently reported sample preparation techniques have incorporated microwave-assisted derivatization and phospholipid clean-up prior to PPt.[68,69] Some of the instrumental analytical techniques that have been reported for TXA separation include gas chromatography (GC),[70] high-performance liquid chromatography (HPLC),[71,72] capillary liquid chromatography (CapLC),[69] and capillary or paper electrophoresis (CE, EP).[73] However, the methodologies that have been reported to date are expensive, complex, time-consuming, and require multiple steps, which renders them unsuitable for high-throughput analysis. In contrast, ambient mass spectrometry represents a promising technology for high-throughput clinical applications due to its ability to be coupled to automated sample preparation approaches, high-speed of analysis, and excellent selectivity.[74,75] Despite these advantages, ambient mass spectrometry is also hampered by several drawbacks, such as ion suppression resulting in poor sensitivity, and being prone to instrument contamination, which can lead to additional maintenance costs during routine-based analyses. Fortunately, solid-phase microextraction (SPME) offers an attractive, streamlined sample preparation technique that is capable of both addressing and overcoming the above-noted limitations, and providing the necessities required for superior MS detection, with or without prior liquid chromatographic (LC) separation. As a

non-exhaustive technique, SPME minimizes matrix effects by minimizing the amount of interferences coextracted, providing cleaner extracts, which helps to reduce contamination and ion suppression. Furthermore, SPME also features a simple device design, which enables more efficient workflows and makes it highly suitable for high-throughput analysis—features which are especially useful in clinical settings that require rapid sample turnover.

Since the quantitation of TXA in plasma via SPME has already been validated in numerous publications[54,76] and cross-validated against traditional methods such as PPt and UF,[54] this high-throughput PK study will utilize SPME in conjunction with liquid chromatography tandem mass spectrometry (LC-MS/MS) particularly for urine analysis. Furthermore, given the limited body of literature on the quantification of TXA in urine, special emphasis was placed on developing the SPME method with regards to the analysis of TXA in urine. The clinically relevant results for the quantitation of TXA in the plasma and urine of renally impaired patients using the high-throughput SPME proposed in this work has already been reported.[76] To the best of our knowledge, this is the first documented attempt to use SPME to detect TXA from urine.

2.3 Materials and Methods

2.3.1 Chemicals and materials

96-well polypropylene deep-well plates and LC-MS grade solvents (methanol, water, acetonitrile, isopropanol) were purchased from Thermo Fisher Scientific (New Waltham, USA), and bare stainless-steel blades were obtained from Professional Analytical Systems (PAS) Technologies (Magdala, Germany). Pooled plasma was purchased from Lampire Biological Laboratories (Everett, USA), while urine lots and pooled urine were obtained from 22 volunteers. The following standards and chemicals were obtained from Millipore Sigma (Burlington, USA): sodium chloride, potassium phosphate dibasic, potassium chloride, sodium phosphate, trans-4-(aminomethyl)-cyclohexanecarboxylic acid (TXA), cis-4-

aminocyclohexanecarboxylic acid (TXA-internal standard (IS)), supel-select hydrophilic-lipophilic balance (HLB) particles, N,N-dimethylformamide (DMF), formic acid, and polyacrylonitrile (PAN).

2.3.2 Working solutions and calibration curves

A stock solution of 100 µg/mL was prepared in LC-MS grade water. Calibration curve stock solutions were subsequently prepared via serial dilutions in water from the initial concentrated stock solution at the following concentrations: 50 µg/mL, 100 µg/mL, 200 µg/mL, 500 µg/mL, 1000 µg/mL, 2500 µg/mL, 5000 µg/mL, 7500 µg/mL, 10 000 µg/mL, 12 500 µg/mL, 15 000 µg/mL, 20 000 µg/mL, 22 500 µg/mL, and 50 000 µg/mL. In addition, a quality control (QC) stock solution was prepared at 10 000 µg/mL, and a matrix-matched calibration curve was prepared by spiking 1 ml of the appropriate matrix (plasma or urine) with 10 µL of each of the appropriate stock solutions to produce a calibration curve ranging from 0.5 µg/mL – 1000 µg/mL. The method QC was prepared by spiking 50 µL of QC stock solution into 5 mL of the appropriate matrix (urine or plasma), and the internal standard was prepared in phosphate buffered saline (PBS) or 0.5 M phosphate buffer respectively such that the sample contained a final concentration of 100 µg/mL. All samples were left to equilibrate for 45 minutes under agitation at 500 rpm to establish binding prior to SPME sample preparation.

2.3.3 Instrumental analysis

Gradient elution LC was conducted using two Shimadzu 10ADvp series binary pumps with flow of 300 µl/min, which is consistent with the LC method described by Gorynski *et al*.[77] Chromatographic separation was achieved using a 10 cm x 2.1 mm Discovery HS F5 (PFP) column with a 3 µm particle size; a 2 cm x 2.1mm Discovery HS F5 guard column which also had a 3 µm particle size, was used. Mobile phase A consisted of 99.9% water, while mobile phase B consisted of 99.9% acetonitrile; each mobile phase contained 0.1% formic acid. Samples were stored in a CTC-PAL autosampler at 4 °C, with 10 µL sample volume being injected for analysis. Mass spectrometric detection was performed on an API 4000 LC-

MS/MS system (AB Sciex) equipped with a Turboion spray source. For more information on the chromatographic method and mass spectrometer parameters, see Table 2.1 and Table 2.2 respectively.

Table 2.1 Chromatographic parameters for TXA and its internal standard using a Shimadzu 10ADvp series binary pump.

Time (min) Total flow (300 µL/min)	**% Mobile Phase A: Water + 0.1% formic acid**	**% Mobile phase B: Acetonitrile + 0.1% formic acid**
0.01	90	10
2.00	90	10
5.50	40	60
6.00	40	60
6.10	90	10
8.10	90	10

Table 2.2 MS/MS parameters for the analysis of TXA and its internal standard on an API 4000 (AB Sciex) triple quadruple.

Compound	**Transition**	**Time (msec)**	**DP**	**EP**	**CE**	**CXP**
Tranexamic acid (TXA)	158 > 95	200	60.7	6.8	20.6	6.2
Tranexamic acid internal standard (TXA IS)	144 > 80.9	200	53.4	7	28.2	4.9

DP: declustering potential, EP: entrance potential, CE: collision energy, CXP: cell exit potential

2.3.4 Sampling procedure

The study protocol, urine and plasma sample collection methods, and experimental procedures for patients in both the high- and low-risk cardiac surgery groups were approved by the Toronto General Hospital/ University Health Network's Research Ethics Boards and University of Waterloo's Research Ethics Boards. The dosing schedule for patients in the high-risk group was consistent with the schedule outlined by Blood Conservation Using Antifibrinolytics in a Randomized Trial (BART).[78] Briefly, TXA was initially administered at a bolus dose of 30 mg/kg following the induction of anaesthesia, with an infusion of 16 mg/kg administered over the course of the procedure until the chest closure; an additional bolus of 2 mg/kg was administered via the cardiopulmonary bypass (CPB) pump prime. TXA was administered to patients

in the low-risk group at a bolus dose of 50 mg/kg following the induction of anaesthesia, which is in accordance with the standard institutional practise at Toronto General Hospital. The collection of blood and urine samples remained consistent for all patients across both groups; the collection schedule that was used is detailed in [79]. Briefly, blood samples were collected in standard citrate tubes at baseline prior to TXA administration; 5 min and 10 min following TXA administration; immediately following the sternotomy and prior to chest closure; before the commencement of CPB; and at 30 min intervals after CPB was initiated and 30 minutes after CPB was discontinued. In addition, post-operative blood samples were also collected at 1, 2, 4, 8, 12, 24, and 72 hours. Urine samples were collected in standard plastic urine containers intra-operatively, post-TXA administration pre-CPB, during CPB rewarming, and post-operatively at 1, 2, 4, 8, 12, 24, and 72 hours. All samples were randomly assigned a number to protect patient anonymity.

2.3.5 Preparation of thin-film microextraction devices

Thin-film microextraction (TFME) devices were prepared in accordance with a previously established spraying method.[80] Briefly, a slurry composed of 10% w/v HLB particles, 3% v/v DMF, and PAN solution (7% w/v PAN particles in DMF) was thoroughly stirred inside a flask-type sprayer (Erlenmeyer flask with a sprayer head) in order to obtain a homogenous solution. The solution was sprayed onto a total of 8 combs, each of which had 12 pins. Spray was induced using a high nitrogen flow attached to the flask-type sprayer. Each device (comb) was subsequently cured in an oven at 180 °C after the application of each layer. This spray coating process was continued until a final coating dimension of 2 cm in length and 0.3 mm in thickness had been achieved for each device. Once the coatings had been applied, the 8 combs were assembled to form the TFME brush that would be used for sample preparation. See Figure 2.1

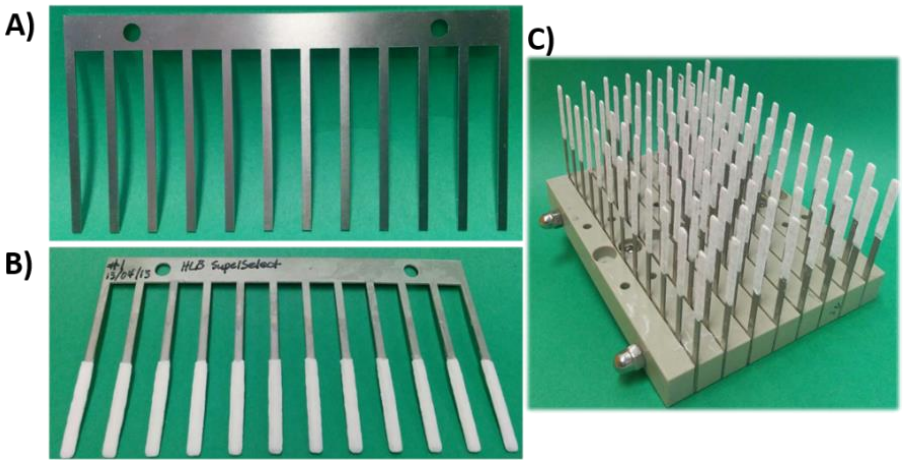

Figure 2.1 Preparation of thin film microextraction (TFME) devices from bare blades to TFME brush. A) Bare blade/comb. B) Coated comb. C) Brush Assembly of 8 coated combs.

2.3.6 Concept-96 for SPME automation

High-throughput sample preparation and the subsequent analysis of both plasma and urine samples were made possible through the use of a Concept-96 autosampler (PAS Technologies, Magdala, Germany). Briefly, this offline software-operated unit automatically performs each step of the SPME sample-preparation protocol—namely, preconditioning, extraction, rinsing, and desorption—via a robotic arm upon which the TFME brush is installed. This brush is compatible with 96-well plates that are immobilized in their respective stations within the unit. Details on the Concept-96 autosampler are provided in elsewhere[79] and shown in Figure 2.2. Agitation conditions were maintained at 1500 rpm at room temperature (23 °C) for each step of the SPME sample-preparation protocol for both plasma and urine samples unless otherwise specified.

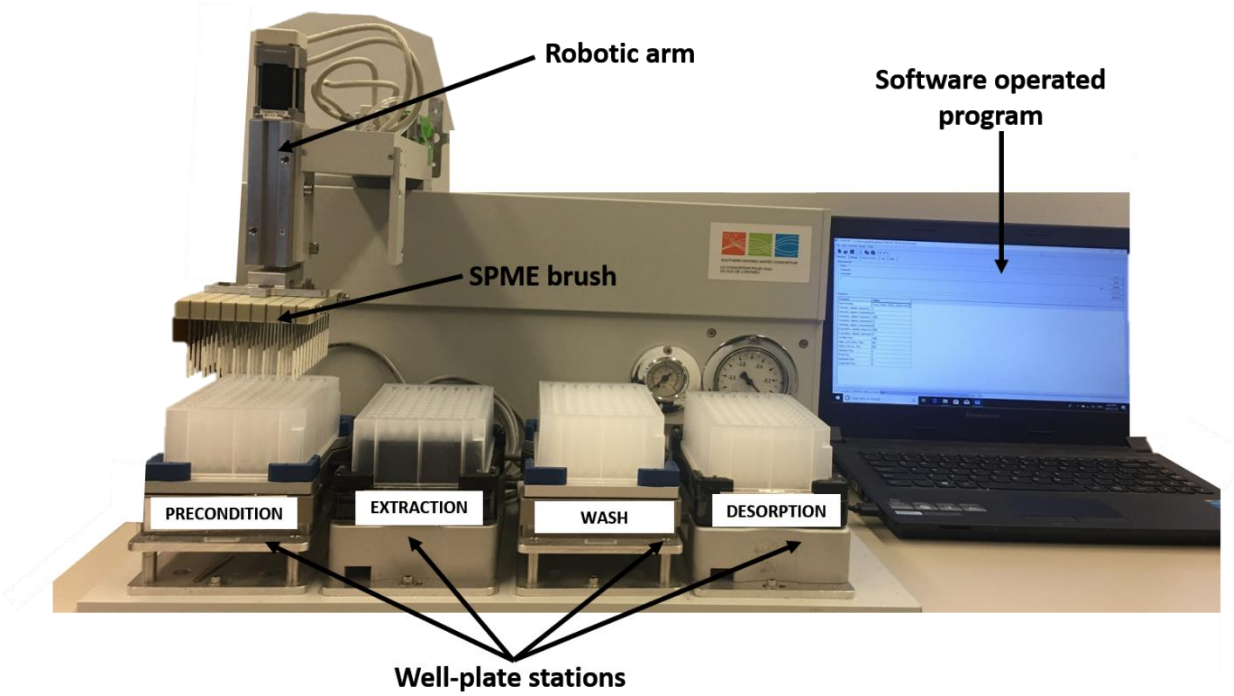

Figure 2.2 Automated software-operated SPME Concept-96 system employed for high throughput analysis of TXA from plasma and urine samples collected from patients undergoing cardiac surgery.

2.3.7 Automated SPME protocol for the analysis of TXA in plasma

The SPME device was first introduced to 1.5 mL of a preconditioning solvent consisting of 50:50 methanol/water (v/v) for 10 minutes. After preconditioning, the device was exposed to 1 mL of plasma sample solution (plasma diluted with PBS) for 5 minutes, and then rinsed in a 1 mL solution consisting of 90:10 water/methanol (v/v) solution for 10 s under static conditions. Following rinsing, the device was desorbed in 1 mL of a solution consisting of 3:3:4 methanol/acetonitrile/water (v/v/v) for 10 minutes.

2.3.8 Automated SPME protocol for analysis of TXA in urine

As in the plasma extractions, the SPME brush was initially preconditioned in 1.5 mL of a 50:50 methanol/water (v/v) solution for 10 minutes before being exposed to a 1 mL urine sample for 5 minutes.

Following extraction from the urine sample, the device was rinsed in 1 mL of water for 10 s under agitated conditions to remove any salts. Finally, the device was desorbed for 10 minutes in 1 mL of a 90:10 water/methanol (v/v) solution.

2.4 Results

2.4.1 Device coating

The method for extracting TXA from urine and plasma developed in this work was based on the use of a hydrophilic-lipophilic balanced (HLB) coating, as previous research has found these coatings to be particularly well-suited for the extraction of polar compounds from aqueous matrices[52,81] such as plasma and urine. This enhanced compatibility is largely due to the fact that HLB coatings contain a higher number of polar groups, which improves the interaction between the analytes and the coating via adsorptive mechanisms, in addition to featuring exceptional wettability.[81] Furthermore, the superior wettability of HLB particles allows for shorter preconditioning and extraction times than are possible with more hydrophobic extraction phases such as polystyrene divinyl benzene (PS-DVB) and silica-core octadecyl (C18). Indeed prior studies that have utilized C18 in the sample preparation process for the analysis of TXA in plasma samples have found that it can lead to preconditioning and extraction times over 10 times higher than an HLB (greater than 45 minutes).[54,82,83] The decreased preconditioning and extraction times enabled by the use of an HLB coating in the SPME protocol results in a decrease in the overall amount of time required for each sample; thus, these reduced time requirements assert SPME as a highly attractive sample preparation technique for high-throughput analyses.

Since there are several published works that focus on the development of an SPME protocol for the extraction of TXA from plasma,[54,77] the present research will place more emphasis on developing an effective protocol for extracting TXA from urine and improving the previously reported plasma-based protocols.

2.4.2 Extraction conditions

One of SPME's main advantages as a sample reparation tool is that it enables the extraction of small target molecules from biological matrices of interest without the need for sample pre-treatment steps such as centrifugation, PPt, or significant pH adjustments. The implementation of PAN-based biocompatible coatings allows the SPME device to exclude high molecular weight matrix components like proteins and enzymes, which are present in biological fluids like plasma. As such, the SPME device can be directly immersed into these samples without concern about damage caused by fouling or the irreversible adsorption of matrix components. This feature further increases sample throughput, as it drastically reduces the time and number of steps required for each sample relative to other sample preparation methods. Furthermore, the HLB coating maintains its stability across the entire pH range (i.e., 0 – 14) and temperatures ranging from ambient to physiologic (20 - 37 °C),[84] which means that it can be used to analyze biological fluids like plasma and urine in their native state. TXA is stable at a physiological pH (7.35 – 7.45) and room temperature for onwards of 72 hours, existing as a zwitterion with a full negative charge in the carboxylic acid moiety and a full positive charge in the amino moiety.[77,85] Unlike plasma, which has a relatively constant pH of between 7.3 and 7.4 regardless of the patient, urine can present wider pH ranges both intra-person and inter-person. As a biological waste product, the pH of one's urine is capable of fluctuating within a range from 4.5-9 due to a number of factors such as their environment, diet, age, or medical conditions.[1] These changes in pH will affect which types of TXA species (pKa of 4.56 and 10.22 for the acidic and basic moieties respectively[86]) are present in the sample, which can in turn affect SPME recovery and the MS ionization of this compound. Furthermore, differences in the ionic strengths of urine samples can significantly alter how the zwitterionic compound interacts with the SPME extraction phase. Given that pH and ionic strength are independent of one another, the pH and ionic strength of the samples were normalized with a buffer solution prior to extraction in order to ensure inter-patient consistency in extraction conditions and the species of TXA present in the sample at the time of extraction.

2.4.3 pH modification

Since plasma has minimal inter-person pH variation due to the requirements of the biological system, the use of PBS adjusted to physiologic pH was sufficient to correct for small inter-person pH differences at a 1:3 patient-plasma-sample:buffer dilution. In contrast, a stronger buffer was required to normalize urine pH and ionic strength. In order to maintain a relatively consistent sample-preparation procedure for the two types of sample matrices, and thus providing a more streamlined workflow, various concentrations of phosphate buffer were evaluated for their effectiveness at correcting urine pH and ionic strength at the same 1:3 dilution used for the plasma samples. Table 2.3 shows the effectiveness of different concentrations of PBS and phosphate buffer in achieving a physiologic pH range for urine samples that had been adjusted to extreme pHs (pH 5 and pH 9), a range which is expected in patient samples. As can be seen, phosphate buffer at a concentration of 0.5 M provided adequate pH correction and proved more suitable than higher concentration buffers, which could result in the precipitation of salts out of the solution with any fluctuation in temperature. Table 2.4 shows the capacity of this 0.5 M phosphate buffer to correct for both pH (pH has been adjusted between 7.35-7.45) and ionic strength (adjusted between 34-37 mS) in real urine samples collected from 13 volunteers.

Table 2.3 Testing the buffering capacity of phosphate-buffered saline (PBS) and varying concentrations of phosphate buffer for pH adjusted urine.

Buffer concentration (M)	Initial urine pH	pH adjusted		Final pH after 1:3 sample dilution with buffer		
		Acidified with 1 M HCl	Basified with 1 M NaOH	Final pH for acidified urine	Final pH for basified urine	Final pH for unadjusted urine
0.1 (PBS)	7.14	5.03	8.89	6.34	8.43	7.36
0.1	7.14	5.06	9.07	7.2	7.63	7.42
0.2	7.14	4.91	9.00	7.25	7.46	7.32
0.5	7.14	5.01	9.18	7.31	7.43	7.30
1.0	7.14	5.02	8.96	7.28	7.37	7.31
2	7.28	4.96	9.01	7.31	7.29	7.48

Table 2.4 Testing the capacity of 0.5M phosphate buffer for correcting the pH and ionic strength of urine samples from 13 volunteers.

Volunteer	Before addition of buffer in 1:3 ratio		After addition of buffer in 1:3 ratio	
	pH	Conductivity (mS)	pH	Conductivity (mS)
Volunteer 1	5.13	26.6	7.33	36.6
Volunteer 2	6.15	18.3	7.43	37.4
Volunteer 3	7.06	6.5	7.47	34.4
Volunteer 4	7.21	10.4	7.46	34.6
Volunteer 5	7.45	26.7	7.46	37.2
Volunteer 6	6.87	22.8	7.45	36.1
Volunteer 7	5.63	9.9	7.43	34.1
Volunteer 8	4.88	20.4	7.41	35.9
Volunteer 9	7.08	5.7	7.50	33.8
Volunteer 10	7.11	9.0	7.47	34.0
Volunteer 11	6.83	13.6	7.45	35.1
Volunteer 12	6.72	27.5	7.40	37.1
Volunteer 13	6.14	18.7	7.42	36.1

2.4.4 Extraction time profile

To determine the extraction time that provided the best compromise of extraction efficiency and throughput, an extraction time profile was developed using a working concentration of 100 µg/mL of TXA in the respective biofluids of interest (urine or plasma) diluted at a ratio of 1:3 (v/v) with the appropriate respective buffers (0.5 M phosphate buffer and PBS). Since SPME is predicated on extraction via free concentration, an extraction time profile was also developed in PBS at the above-noted working concentration in order to assess if matrix effects exist and how matrix components influence the amount of TXA extracted. To this end, the following times were evaluated: 5 min, 10 min, 15 min, 20 min, 30 min, 45 min, 60 min, and 90 min. The extraction time profiles of urine and PBS shown in Figure 2.3A confirm that matrix components do not affect the amount of TXA that is extracted, as the absolute recovery rate of TXA in urine and PBS was approximately 1 % for each. These results are consistent with the 1 % recovery rate for TXA in plasma, which has been documented in previous studies[54] and is shown in Figure 2.3B. The similarity of these findings is largely attributable to the fact that TXA experiences less than 3 % binding, which means that it

is available for extraction from plasma and urine at relatively similar levels. *(This finding is also supported by the evaluation of absolute matrix effects presented section 2.4.9 "Method* validation*").*

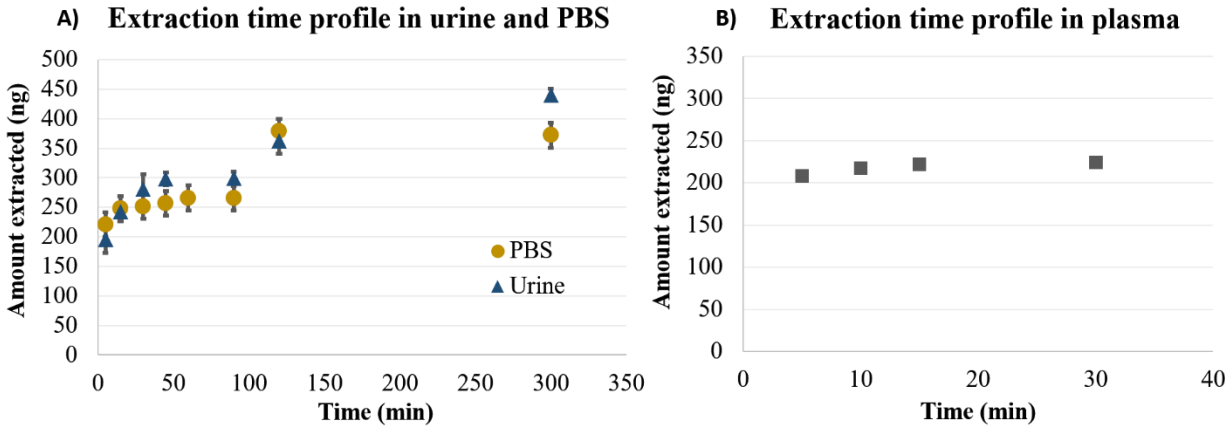

Figure 2.3 A) Extraction time profile of tranexamic acid (TXA) in urine and phosphate buffered saline (PBS). B) Extraction time profile of TXA in plasma.

Although extraction equilibrium was achieved at 15 minutes in urine, adequate method sensitivity could be observed at 5 minutes; thus, an extraction time of 5 minutes was selected, as it dramatically reduced sample preparation time, which in turn enabled considerable high-throughput analysis. Moreover, this reduction in time represents a 12-fold improvement in efficiency over previous methods utilizing a C18 or weak anion exchange (WAX) coating, which both require 60 minutes to achieve equilibrium and comparable recovery.[54,77]

2.4.5 Rinsing conditions

Rinsing is an important and often overlooked step in the development of an SPME protocol, as the conditions under which it is performed can significantly influence the method's sensitivity, reproducibility, and overall cleanliness of the final extract obtained for injection. This step is valuable because it can help to ensure the acquisition of clean extracts through the removal of components that may be loosely adhered to the coating or other potential coeluting/coextracted matrix interferences. A good compromise between length of time, agitation conditions, and solvent choice for the rinsing step is usually recommended. A rinse

solution consisting of a 9:1 water/methanol mixture was selected based on previous research. Figure 2.4A shows the results for the tests comparing various rinsing times and agitation conditions for this particular solvent composition after extraction from plasma. As the results show, a 5s static wash sufficiently removed any loose plasma components without significantly affecting the method's sensitivity or the amount of analyte recovered in the desorption solution, which was comparable to the amounts recovered with no rinsing step.

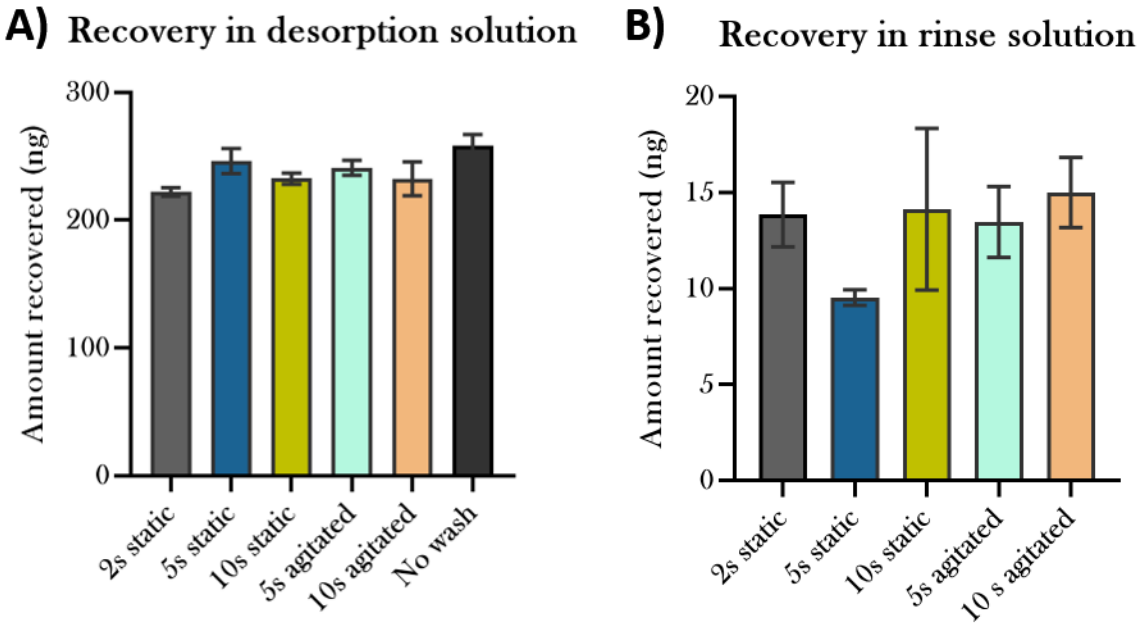

Figure 2.4 Rinsing time and agitation conditions evaluated for solution consisting of a 9:1 water/methanol mixture. A) The amount of TXA recovered from the desorption solution after varying rinse conditions. B) The amount of TXA recovered from the rinse solution after varying rinse conditions.

These results are affirmed by the corresponding data in Figure 2.4B, which show that the lowest amount of TXA was recovered from the rinse solution after this 5s static rinse. While this solvent composition worked well for the coating and minimized the loss of TXA in the final extract, these same conditions could not be applied after the extractions from urine. As such, the devices were rinsed in pure water for 10s under agitated conditions following extractions from urine. Although this approach inadvertently resulted in lower

amounts of TXA in the final extracts, the high salt levels in urine made it necessary to perform a pure water rinse in order to maintain good peak shapes during chromatography.

2.4.6 Desorption conditions and desorption time profile

Suitable desorption conditions ensure maximum desorption efficiency, which is critical for minimizing carryover, maintaining the stability of the final extracts, and ensuring compatibility with the initial liquid chromatographic conditions in order to facilitate effective separation. First, desorption solvents were investigated with a 10 min preconditioning step in a 1:1 methanol/water (v/v) solution. For urine, an extraction time of 5 min from 1:3 sample/diluent (v/v) solution was used, which was followed by rinsing in 100% water under agitation for 10s; for plasma, the same extraction conditions were used, but the rinsing step consisted of 5s of rinsing under static conditions in a 9:1 water/methanol solution. Three solvent formulations were tested during the development of the plasma protocol: 1:1 acetonitrile/water, 1:1:2 acetonitrile/methanol/water, and 3:3:4 acetonitrile/methanol/water (Figure 2.5A). Although the 1:1 acetonitrile/water solution yielded the highest recovery rates—albeit with comparable carryover to the other two desorption solvents (Figure 2.5B)—the 3:3:4 acetonitrile/methanol/water solution was deemed the most appropriate, as the results for this solvent solution showed the greatest agreement with the previously developed LC-silica WCX coating method.[77]

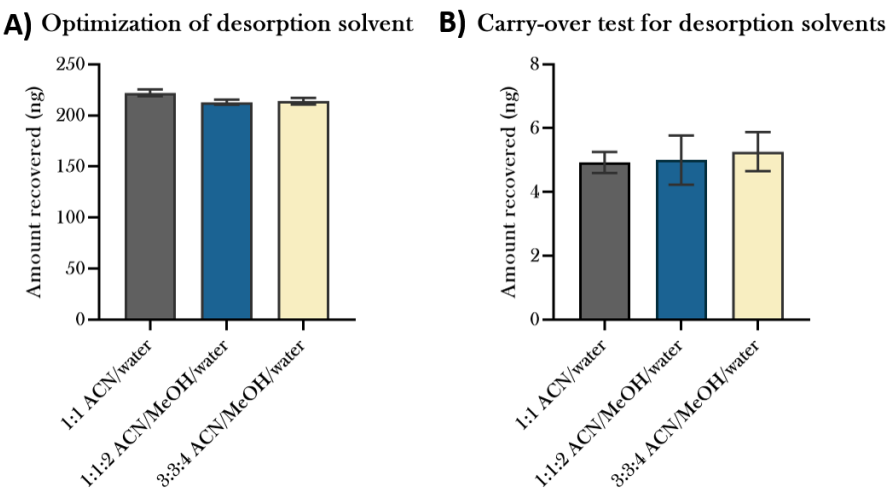

Figure 2.5 A) Optimization of three desorption solvents: 1:1 acetonitrile/water, 1:1:2 acetonitrile/methanol/water, and 3:3:4 acetonitrile/methanol/water. B) Carryover test for each desorption solution.

Regrettably, compounded carry over effects became apparent after a large number of plasma samples were processed (~ 1500 samples) with the selected desorption solvent. A problem not experienced with past SPME-based methods for TXA analysis in plasma due to the significantly smaller number of samples requiring processing in these cases; nor was this problem foreseen with the current research. As such, the desorption conditions and cleaning procedure were re-optimized before processing the urine samples. For more information on the optimization of the cleaning procedure, please see *section 2.4.7 "Device cleaning optimization"*. Increasing ratios of aqueous-to-organic solvent mixtures were studied, accounting for TXA's polarity, in order to increase desorption efficiency (Figure 2.6A). Although the 3:3:4 acetonitrile/methanol/water mixture once again provided the best desorption capabilities, the long-term use of this desorption solvent over hundreds of samples proved to remain challenging. As such, the 9:1 water/methanol mixture was deemed the most optimal desorption solvent, as it provided the best balance between liquid chromatographic compatibility and desorption efficiency, which was confirmed by the carry over test (results not shown). The optimal desorption time was determined by constructing a desorption time profile based on the amount of analyte recovered after 5 min, 10 min, 15 min, 20 min, 30 min, 45 min,

and 60 min of desorption, which took place after a 10 min preconditioning step, a 15 min extraction, and a 10 s rinse in 100% water. As shown in Figure 2.6B, there was no significant increase in the amount of analyte desorbed from the coating beyond 10 minutes; therefore, 10 minutes was chosen as sufficient desorption time.

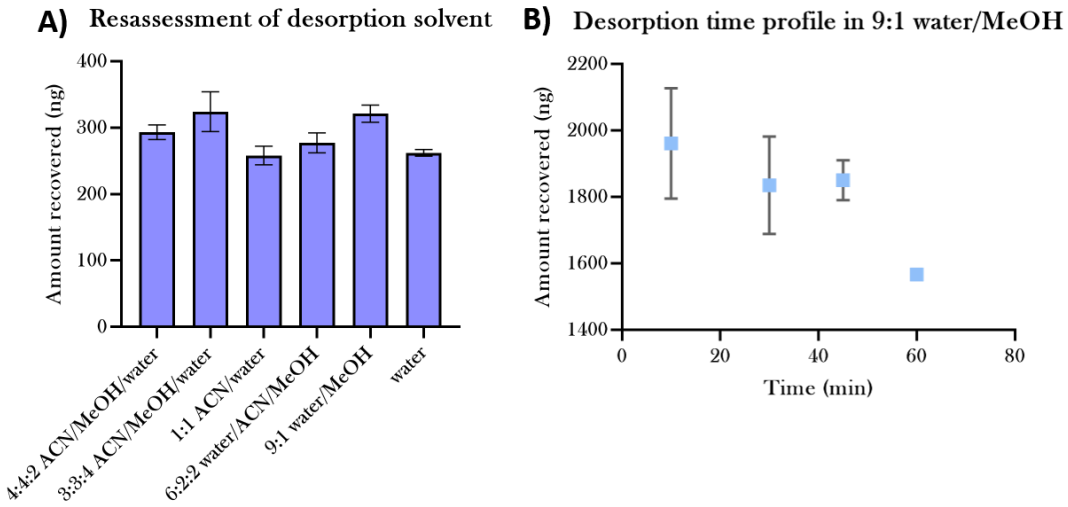

Figure 2.6 A) Reassessment of optimum desorption conditions with increased aqueous content: 2:2:1 acetonitrile/methanol/water, 3:3:4 acetonitrile/methanol/water, 1:1 acetonitrile/water, 6:2:2 water/acetonitrile/methanol, and 9:1 water/methanol and pure water. B) Desorption time optimization in solution consisting of a 9:1 water/methanol mixture.

2.4.7 Device cleaning optimization

Although carryover was evaluated at the highest concentrations expected in patient samples (which was found to be less than 1%), a carryover effect associated with the blades' reusability for high-throughput analysis was still observed for the plasma samples as reported in *section 2.4.6* "*Desorption conditions and desorption time profile*". Once the blades had been exposed to high-concentration samples, the amount of analyte that remained after desorption and cleaning interfered with the quantitation of low-concentration samples and effectively increased the lower limits of quantification, despite being below the acceptable limits for carryover. As such, additional measures were taken prior to preparing the urine samples in order to prevent any carry over effects that could potentially influence the quantitation of lower-concentration

samples. This would be especially detrimental given the dilution effects that can arise during urine processing.

Various solvents and the number of required cleaning steps were explored in order to determine which combination would ensure that the amount of solute remaining on the blade, if any, was less than the amount corresponding to the lower limit of quantification. A strong solvent mixture consisting of 2:1:1 methanol/acetonitrile/isopropanol (v/v/v) that is usually employed for cleaning was studied alongside two other mixtures: 45:45:10 isopropanol/acetonitrile/acetone and 45:45:10 isopropanol/methanol/acetone. Given the polarity of tranexamic acid, each of the three mixtures was diluted with 50% water to evaluate whether this improved cleaning efficiency. Figure 2.7 confirms the hypothesis that the addition of water drastically enhances cleaning efficiency, as all three solutions showed a 50% increase in analyte recovery in solutions that had been mixed with water. Once the 50:25:12.5:12.5 water/methanol/acetonitrile/isopropanol (v/v) mixture had been identified as the optimal cleaning solvent, it was necessary to determine the number of steps required to sufficiently clean the blades. Formic acid is a common mobile-phase additive that is used to improve ionization efficiency for compounds analyzed by mass spectrometry in positive mode; thus, it can also be added to the desorption solution.

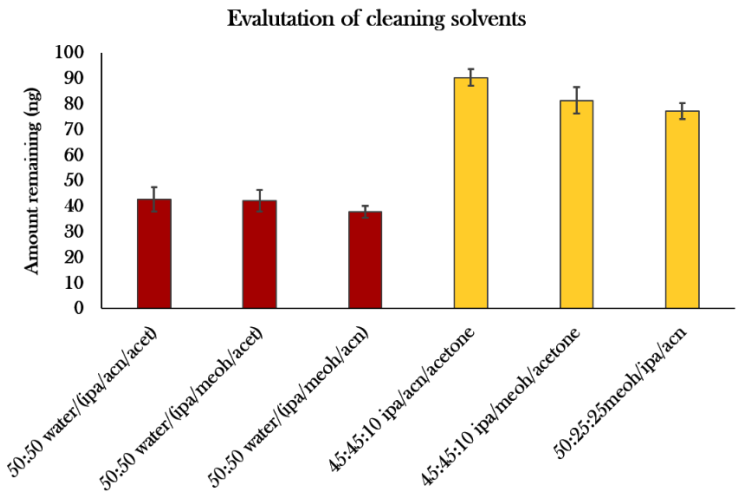

Figure 2.7 Evaluation of three cleaning solutions: 45:45:10 isopropanol/acetonitrile/acetone, 45:45:10 isopropanol/methanol/acetone, and 2:1:1 methanol/isopropanol/acetonitrile (yellow columns). The red columns represent the solutions mixed with 50% water.

However, it is important to assess its effect as an additive in relation to both the coating chemistry of the device used for sample preparation, as well as the composition of the solvent used for desorption. Tests of these relationships showed that the addition of 0.1% formic acid to the 9:1 water/methanol desorption solution decreased desorption efficacy by nearly 50%. In contrast, the addition of formic acid improved the 50:25:12.5:12.5 water/methanol/acetonitrile/isopropanol solution's cleaning efficiency by 50%. Figure 2.8 shows that the blades were sufficiently cleaned after three successive 10-minute immersions in the optimized solution with 0.1% formic acid, as well as in the solution with no additives. While this phenomenon merits further investigation, this falls outside the scope of the present research.

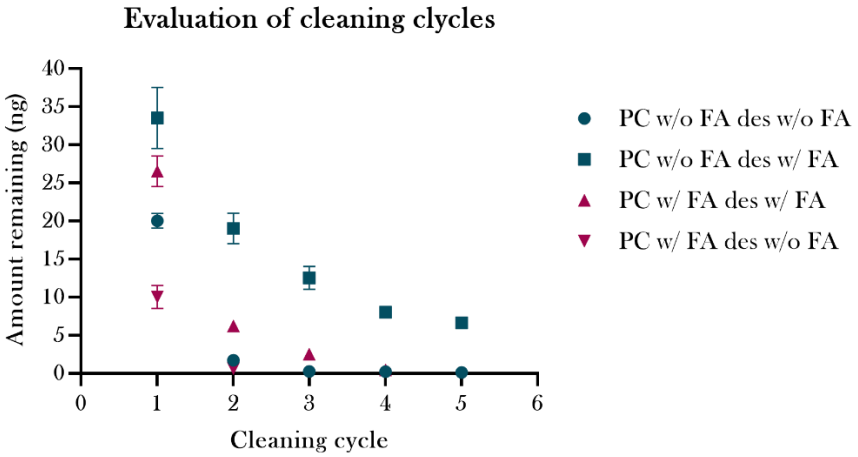

Figure 2.8 Assessment of the number of cleaning cycles required to effectively remove traces of TXA from the device coating. Evaluation of how the addition of formic acid impacts desorption and cleaning efficacy. Devices initially desorbed in optimized desorption solution containing formic acid (des w/ FA) were cleaned in a solution containing formic acid (PC w/ FA) and compared with devices cleaned in a solution containing no formic acid (PC w/o FA). These two cleaning conditions were also evaluated against devices that had been desorbed in optimized desorption solution with no formic acid (des w/o FA).

2.4.8 Evaluation of matrix effects

SPME differs from other sample preparation approaches in that it extracts via free concentration. This suggests that it is unable to extract analytes that are bound to various macromolecules such as proteins, thus decreasing the extraction of possible interferences for an analyte of interest. However, matrices that contain no binding media (i.e., urine) are more challenging due to the increased likelihood of coextracting interfering matrix components that are available in free form such as salts, organic and inorganic content, and metabolites. These instances of coextraction, and subsequent coelution via chromatography, can impact the analytical signal of interest, resulting in signal enhancement or suppression. In order to assess SPME's reliability as a sample preparation tool for the extraction, determination, and quantitation of TXA in a complex and challenging biofluid like urine, absolute and relative matrix effects were evaluated according to the method proposed by Matuszewski *et al*.[87]

To examine absolute matrix effects, urine samples from 14 individuals were assessed at concentrations of 5, 10, 25, 50, and 100 ng/mL, which is consistent with the 1% absolute recovery rate of TXA from samples within the lower part of the expected concentration range. The obtained absolute matrix-effect values largely ranged between 80 and 120%; however, as can be seen in Table 2.5, there were a number of outliers, with enhancements as high as 423% and as low as 76%.

Table 2.5 Evaluation of absolute matrix effects (%) tested at 5 lower-level concentrations in 14 different volunteers. Outliers (values less than 80 % and greater than 120 %) are highlighted in bold font. Each volunteer at each concentration was evaluated with 3 replicates. The values presented for each volunteer at each concentration level had RSD's (n = 3) < 15%.

	Concentration level				
	5 ng/mL	**10 ng/mL**	**25 ng/mL**	**50 ng/mL**	**100 ng/mL**
Volunteer 1	104	102	109	105	92
Volunteer 2	***189***	***133***	115	109	91
Volunteer 3	***213***	75	***149***	96	93
Volunteer 4	96	96	95	105	88
Volunteer 5	87	86	99	90	89
Volunteer 6	***206***	116	99	98	87
Volunteer 7	***251***	103	166	105	***79***
Volunteer 8	106	102	113	98	83
Volunteer 9	103	95	113	101	***79***
Volunteer 10	***180***	100	110	95	82
Volunteer 11	***197***	98	93	82	***76***
Volunteer 12	106	108	***123***	106	***77***
Volunteer 13	95	93	99	104	80
Volunteer 14	***423***	104	102	106	***76***

These outliers suggest that there was some significant ion suppression or enhancement. Therefore, evaluating relative matrix effects are critical to ensure the internal standard used is suitable for correcting these deviations and that the target analyte can be reliably quantitated in urine. As such, a 7-point calibration curve, from 2 μg/mL to 250 μg/mL, was constructed in 8 lots of urine. Figure 2.9 shows that the homologous internal standard employed for the quantification of TXA proved to be suitable for correction, as it produced slopes with an average of 0.024 and a 10% relative standard deviation (RSD) in each lot of urine.

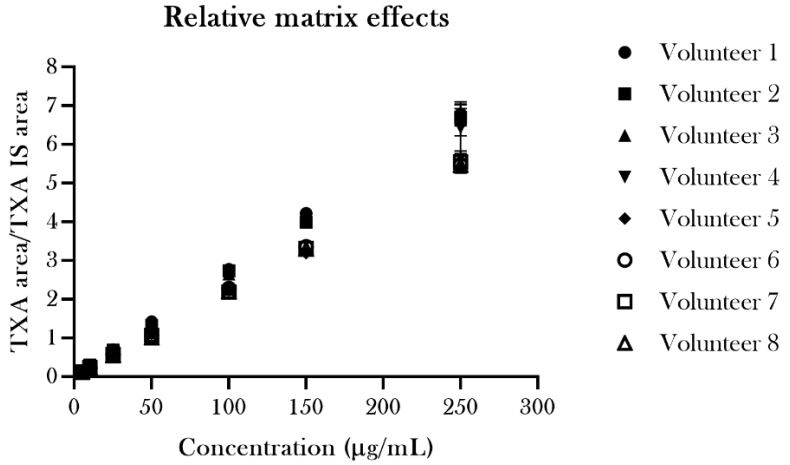

Figure 2.9 Assessment of relative matrix effects. A 7-point calibration curve was constructed in 8 lots of urine, producing an average slope of 0.024 within a 10% relative standard deviation (RSD) and a linearity (R^2) of 0.99 across the 8 volunteers.

2.4.9 Method validation

This method was validated in accordance with the guidelines set forth in the *Food and Drug administration (FDA) Guidance for industry: bioanalytical method validation*. Blank urine from 14 individuals was assessed for interferences, with no cross-talk being observed for the majority of samples under LC-MS chromatographic conditions at the retention times for the analyzed compounds. No significant impact was found in cases where interferences were detected, as they were well below the limit of quantitation (LOQ). The chosen LOQ was the lowest concentration at which the constructed calibration curve determined the nominal concentration with at least 80 % accuracy and a 20% relative standard deviation. This method produced a linear dynamic range over two orders of magnitude—from 25 µg/mL-1000 µg/mL in urine, and from 10 µg/mL-1000 µg/mL in plasma—and achieved LOQs of 25 µg/mL and 10 µg/mL, in urine and plasma respectively. Acceptable linearity (R^2) for TXA in urine and plasma were obtained achieving values of 0.996 and 0.997, respectively.

Accuracy and precision were calculated using 5 replicates of plasma or urine spiked at a working concentration of 100 µg/mL, which is within the expected TXA concentration range for both biofluids.

These replicates were then randomly distributed among a batch of 96 samples prepared in a 96-deep-well plate. Furthermore, 2-3 replicates of blank urine were also randomly distributed among the samples in order to assess and maintain the integrity of the reusable sampling device. Accuracy was considered acceptable if the determined concentration was within 15% of the actual value, and precision was deemed acceptable if the coefficient of variation did not exceed 15%. This figure was increased to 20% for concentrations closer to the limit of quantification. The proposed method achieved intraday accuracy and precision of 105% and 8%, respectively, and inter-day accuracy and precision of 103% and 7%, respectively. The chemical stability of tranexamic acid has already been investigated elsewhere, with findings showing that it is stable under various storage conditions for at least 12 weeks. Furthermore, PK studies have shown that over 95 % of the drug is excreted renally and remains unchanged in urine. Gorynski *et al.*[77] studied TXA's stability during the various stages of the sample preparation protocol, as well as in the final extract obtained, during their development of a method for the concomitant sample preparation of rocuronium bromide and TXA in plasma.

2.5 Discussion

2.5.1 Application of SPME method to clinical samples

The analyzed clinical samples were collected from patients who were undergoing cardiac surgery and had been administered TXA as a means of controlling bleeding during the procedure. Patients were first categorized into low- and high-risk groups depending on the type of cardiac surgery they had undergone and several other health factors. The low-risk group had received a dose of 50 mg/kg as per institutional practise at Toronto General Hospital, while the high-risk group were placed on the relevant dosing schedule outlined in the BART study. Each group contained patients who had healthy kidney function and those with varying degrees of chronic renal dysfunction, from stage 1 to stage 5. As previously noted, suboptimal renal functioning can affect drug clearance, thus leading to heightened blood-drug concentrations of compounds that are largely renally excreted. Since high concentrations of TXA in blood plasma have been associated

with post-operative seizures, it was essential to monitor the TXA concentration over the course of administration in order to gain a better understanding of its PK in individuals suffering from renal impairment. Urine quantitation is much less straightforward than the monitoring and determination of plasma concentrations, which can be done directly, as dilution or pre-concentration can occur while the urine sample is being processed. As such, concentrations were determined via normalization, with creatinine clearance having already been calculated for up to 72 hours. Urine profiles were then constructed and determined as grams of TXA per gram of creatinine (gTXA/gCr). Following this, the developed SPME protocol was used to determine TXA concentrations in plasma and urine from a total of 49 high- and low-risk cardiac patients (25 high-risk and 24 low-risk). Figure 2.10 shows the TXA concentrations in plasma and their corresponding clearance in urine from a total of only 10 patients belonging to both the high- and low-risk groups. As noted above, each group contained patients with varying degrees of chronic renal dysfunction.

For patients on the same dosing schedule, the profiles of those within the same group differed significantly in terms of the maximum TXA concentration in either biofluid. These differences are due to increased mean TXA residence times during CPB due to impaired kidney function, which in turn results in increased concentrations of TXA in the blood. Figure 2.10A demonstrates that the patients suffering from later stages of CRD (Patient 7, Patient 10, and Patient 13 (stages 3-4)) exhibited significantly higher concentrations of TXA during CPB and many hours after the operation. Significantly different corresponding clearance trends in urine are also evident in Figure 2.10B, with higher post-operation concentrations of TXA being observed in patients with stages 3 and 4 chronic renal dysfunction than in patients with earlier stages of the disease. While this particular trend might not be as apparent with the low-risk cardiac patients profiled in Figure 2.10C, it is interesting to note that Patient 10 and Patient 14, who both suffer from stage 1 CRD, have significantly different TXA concentrations in plasma, with Patient 14 exhibiting higher TXA concentrations throughout the entire procedure. These results not only clearly demonstrate the need to adjust dosing schedules to better suit patients suffering from more severe stages of CRD, but also the need to develop

methods capable of rapid analysis and real-time monitoring. These results have already been used to aid clinicians in developing a PK monitoring protocol for TXA [76], while a rapid-analysis method based on SPME coupled directly to MS via a microfluidic open interface (MOI) has also been proposed, developed, and employed for the determination of TXA concentrations in plasma.[79]

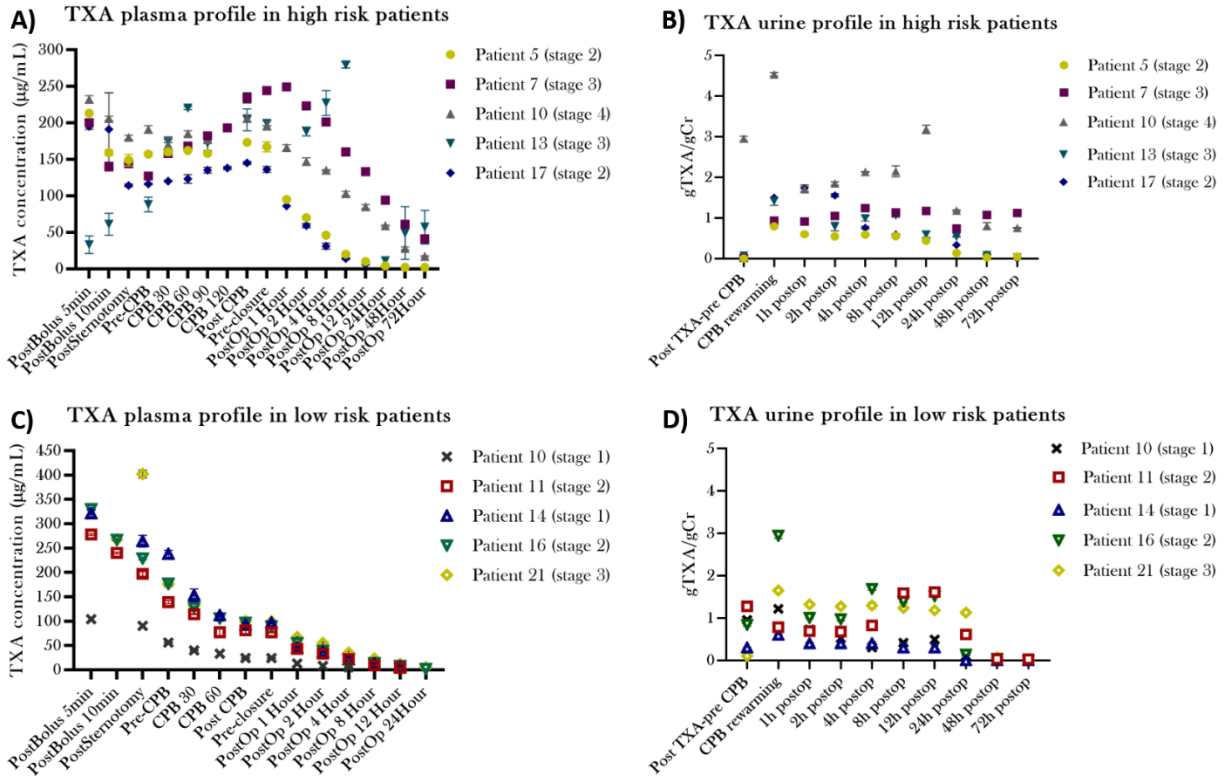

Figure 2.10 TXA profiles in plasma and urine from patients with varying degrees of chronic renal dysfunction who underwent cardiac surgery. A) TXA profiles in plasma from 5 patients undergoing high-risk cardiac surgery. B) Corresponding TXA profiles in urine from 5 patients undergoing high-risk cardiac surgery. C) TXA profiles in plasma from 5 patients undergoing low-risk cardiac surgery. D) Corresponding TXA profiles in urine from 5 patients undergoing low-risk cardiac surgery.

2.6 Conclusion

While numerous publications have focused on the validation and feasibility of using solid phase microextraction for quantitating TXA in plasma, this work marks the first attempt to apply this technique to the development of a protocol for determining TXA in urine. This protocol would allow clinicians to

obtain a more comprehensive patient profile for TXA, which would help to adjust dosing schedules to better suit the needs of individuals with renal impairment. In addition, the open-bed geometry used in the proposed SPME protocol and the use of a biocompatible polyacrylonitrile-based extraction phase help to prevent macromolecules from adversely interacting with the device. These features make this SPME method convenient and easy to use, as it is possible to directly expose the device to a sample without prior sample pre-treatment, such as centrifugation in the case of urine, or PPt in the case of plasma. Furthermore, the proposed method represents an improvement upon previously developed methods of performing extractions from plasma, as the excellent wettability of the HLB phase decreases sample extraction time and increases throughput. The work presented in this paper further emphasizes SPME's suitability and capability for the high throughput monitoring of therapeutic drugs in complementary biological fluids, such as plasma and urine. Since SPME is a non-exhaustive and quantitative microextraction technique, quantitation at high concentrations over three orders of magnitude can be easily achieved without having to dilute the final extracts. Moreover, the use of a Concept-96 autosampler to automate the process enabled over 3500 samples (urine and plasma combined) from 49 patients undergoing low-risk and high-risk cardiac surgery to be processed. This technique's direct amenability to mass sensitive detection methods, such as mass spectrometry, has already facilitated the much needed rapid analysis of TXA in plasma, with the results obtained in this study having been used to cross validate this newly developed technique [79].

Chapter 3: Serum metabolic fingerprinting of psoriasis and psoriatic arthritis patients using solid phase microextraction – liquid chromatography – high-resolution mass spectrometry

3.1 Preamble

Chapter 3 of this thesis has been formatted for submission to the journal *Metabolomics*, with all the writing done by the author of this thesis and co-authored with N. Reyes-Garces, A. Roszkowska, Miao Yu, V. Kulasingam, J. Pawlisyzn and V. Chandran. Collaboration for the work presented in this chapter of the thesis was initiated by J. Pawliszyn, V. Chandran, and V. Kulasingam, with experimental design being conducted by J. Pawliszyn, V. Chandran, V. Kulasingam, N. Reyes-Garcés, and the author of this thesis. All other work presented in this chapter of the thesis were conducted by the author of this thesis with assistance from N. Reyes-Garcés, A. Roszkowska, Miao Yu and I. Batruch. Please see *Statement of contributions*. We are grateful to the Natural Sciences and Engineering Research Council (NSERC) of Canada for the financial support provided through the Industrial Research Chair program, as well as the Canadian Institutes of Health Research (CIHR) through the catalyst grant program.

3.2 Introduction

Approximately 3% of North Americans are affected by psoriasis; a chronic, immune-mediated, inflammatory skin disease.[88,89] While there are many variants of psoriasis—for example, guttate psoriasis, palmoplantar pustulosis, and pustular psoriasis—psoriasis vulgaris, or plaque psoriasis, is the most common, accounting for 85% to 90% of psoriasis-related conditions.[90] Approximately 25% of psoriasis patients also suffer from psoriatic arthritis (PsA), which is a specific form of inflammatory arthritis that may affect peripheral and axial joints and periarticular structures, such as the enthuses.[91] This is a significant problem, as psoriasis and PsA significantly reduce quality of life, and can lead to disability and increased mortality.[92] Thus, it is important to diagnose PsA as early as possible, as doing so can result in better long-term health outcomes.[93] Since PsA often develops after the onset of cutaneous psoriasis, recent research has

tended to focus on converters—psoriatic patients who develop PsA—with the aim of identifying the mechanisms of arthritis development, early diagnosis methods, and measures for impeding the disease's progression, as advances in these areas have the potential to improve patient care tremendously.[94–96] However, progress towards these goals will require the determination of more quantitative biomarkers associated with psoriatic disease pathophysiology.[89]

Researchers have employed several types of untargeted analyses, otherwise known as 'omic-related' approaches, to investigate disease pathology, including transcriptomics, proteomics, and genomics.[97] However, the emergence of metabolomics—which entails the comprehensive investigation of all metabolites in a biological system at a given time—has provided researchers and clinicians with a new approach that enables disease-related changes to be monitored with greater rapidity.[97] Many prior psoriatic-related metabolomics studies have examined mainly the differences between psoriatic and healthy patients. Fewer studies still, investigated PsA at all, with a focus on either how PsA differed in general from patients with psoriasis or how PsA differed from patients suffering from rheumatoid arthritis.[98] Through the analyses of various samples, including skin, blood components (serum and plasma), and urine, the results of these studies yielded biomarkers such as amino acids and various lipids which were associated mainly with psoriasis disease severity or how PsA differed from other forms of arthritis.[98–103] Given the dearth of research related specifically to PsA, the research presented herein attempts to fill that gap by investigating PsA explicitly, in order to determine how it relates to psoriasis disease, and if PsA pathophysiology may provide some insight to disease conversion, thereby indicating a means of prevention or more tailored treatments.

In general, metabolomics studies employ either nuclear magnetic resonance (NMR) or high-resolution mass spectrometry (HRMS), both of which are powerful detectors that scan the broad range of metabolites within a given biological sample. Regardless of which platform is used, sample preparation remains one of the most critical steps in the metabolomics workflow, as sample pre-treatment can inadvertently affect the

outcome of any study. Many HRMS-based metabolomics studies employ standard sample preparation techniques such as protein precipitation (PPt), liquid-liquid extraction (LLE), and solid-phase extraction (SPE). While these methods are effective, they are also labor intensive, as they require multiple steps in order to obtain the final extract for analysis. Furthermore, the considerable amount of sample handling involved in these preparative procedures can easily lead to errors associated with artefact formation. The development of more rapid techniques could both mitigate these issues and increase sample throughput, as the sample would be idle for much less time. Thin-film solid phase microextraction (TF-SPME) coupled to HRMS is one such rapid sample preparation technique that has been reported in numerous metabolomics-related studies.[29,57,62,104] Therefore, this work assesses the viability of TF-SPME coupled to HRMS as a novel and rapid (given the high throughput capabilities) sample preparation tool by using it to perform clinical metabolomics analyses on serum obtained from three sample groups: patients with PsA; patients with psoriasis, but without PsA (PsC); and healthy volunteers.

The objectives of this study were to use TF-SPME-HRMS to find markers or metabolites indicative of:

1. Conversion from psoriasis to PsA;

2. PsA in patients with psoriasis;

3. PsA disease activity.

To the best of our knowledge, this is the first psoriasis-related metabolomics study to investigate the pathology of PsA disease, and further to incorporate the use SPME coupled to HRMS to perform profiling.

3.3 Materials and Methods

3.3.1 Materials

Thin-film stainless steel combs were purchased from PAS technologies (Magdala, Germany), while oasis hydrophilic-lipophilic balanced (HLB) particles (30 – 60 µm) and weak anion exchanger functionalized polystyrene divinylbenzene (PS-DVB-WAX) particles (30 – 60 µm) were purchased from Waters

Corporation (Milford, USA) and Chromatographic Specialties, respectively (Brockville, Canada). A flask-type sprayer and the following internal standards and chemicals were purchased from Millipore Sigma (Burlington, USA): tranexamic acid, phenylalanine-d5, testosterone-d3, codeine-d3, sodium chloride, potassium chloride, sodium phosphate, potassium phosphate, polyacrylonitrile, and N,N-dimethylformamide (DMF). 2 mL deep-well plates were purchased from Thermo Fisher Scientific (Waltham, USA), and the following LC-MS grade solvents were purchased from Fisher Scientific (Ottawa, Canada): formic acid, acetic acid, acetonitrile, methanol, and water. The deionized water that was used to prepare the phosphate buffered saline was obtained using an Milli-Q Reference Water Purification System (EMD Millipore, Fisher Scientific, Ottawa, Canada).

3.3.2 Thin-film microextraction device preparation

The thin-film microextraction (TFME) device was prepared using a well-established spraying method that had been developed in-laboratory.[80] Briefly, a flask-type sprayer was used to coat the stainless-steel support with a slurry mixture consisting of 1:1 HLB and PS-DVB-WAX particles, polyacrylonitrile (to act as a binder), and DMF. After the application of each layer, the coating was placed in an oven to cure at 180 °C for 1 minute. The final coating on the device was 1 cm long with an average thickness of 0.3 mm.

3.3.3 Instrumental analysis: liquid chromatography coupled with high-resolution mass spectrometry

High performance liquid chromatography (HPLC) with HRMS detection was performed using an Accela autosampler and pump coupled to a Q-Exactive mass spectrometer (Thermo Fisher Scientific, Waltham, USA). Chromatographic separation was conducted on a Discovery HS F5-3 column (100 mm x 2.1 mm, 3 µm) with a Discovery HS F5 (20 mm x 2.1mm, 3 µm) pre-column, which were both purchased from Supelco/Sigma Aldrich (Bellefonte, USA). Gradient elution was achieved over 40 minutes in positive mode using mobile phases consisting of 99.9/0.1 water/formic acid (v/v) and 99.9/0.1 acetonitrile/formic acid (v/v). For negative-mode chromatography, 1mM of acetic acid was used instead of formic acid. Sample

extracts were injected at a volume of 10 µL, and the autosampler and column temperature were maintained at 5 °C and 25 °C, respectively. Further details on the gradient elution used for chromatography can be found in Table 3.1.

Table 3.1 Liquid chromatographic gradient used for separation in both positive and negative mode

MS polarity	**Positive mode**	**Negative mode**
Time (min)	**% Mobile phase A (water + 0.1 % formic acid**	**% Mobile phase A (water + 1mM acetic acid**
0.00	100	100
3.00	100	100
25.00	10	10
34.00	10	10
35.00	100	100
40.00	100	100

The Q-Exactive mass spectrometer was equipped with an Ion Max heating source, which contained a heated electrospray ionization (HESI-II) probe. The mass spectrometer was run at high resolution (50, 000), and data was acquired within an m/z range of 100 – 1000 with a balanced automatic gain control and an injection time of 100 milliseconds. The capillary and vaporizer temperatures were each set at 300 °C, while the sheath, auxiliary, and sweep gas were set to 35, 5, and 0, respectively. The electrospray voltages (and lock masses) applied for positive and negative mode were 4 kV (391.2842 m/z) and -2.9 kV (255.2329 m/z), respectively.

MS/MS validation was performed for the desired statistically significant features via parallel reaction monitoring (PRM) on the Q-Exactive. The obtained MS/MS spectrum was then compared to the fragmentation patterns of metabolites from the mzCloud or MS finder databases.

3.3.4 Patients

Serum samples were obtained from the University of Toronto Psoriatic Disease (PsD) Program biobank. Prospective patients with PsA and PsC were enrolled in the program based on careful phenotyping,[105] with samples being collected for both the patients in the program as well as healthy controls without PsD. A scheme outlining the structure of the patient groups is shown in Figure 3.1.

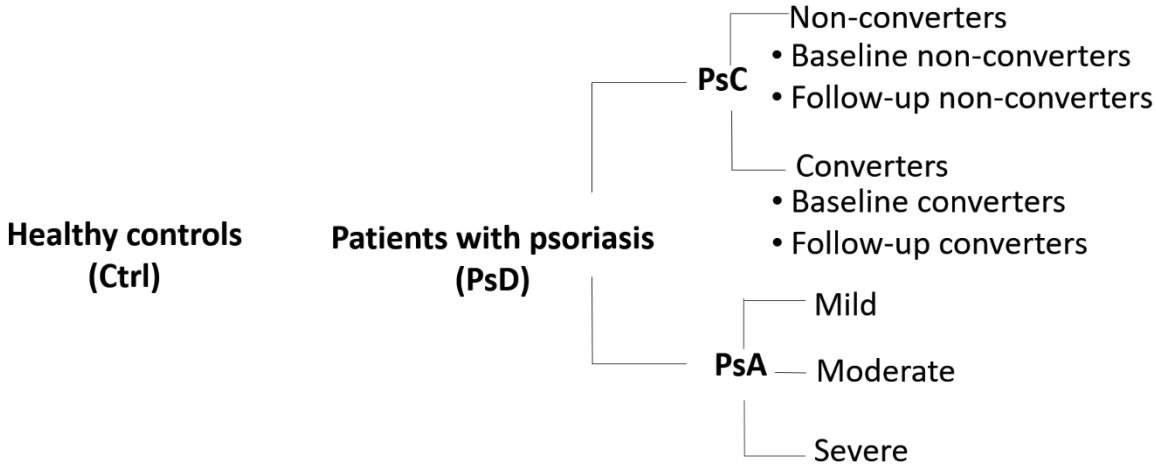

Figure 3.1 Scheme of patient categories and subcategories of samples collected for analysis. Serum samples were obtained from healthy volunteers serving as controls (Ctrl) and patients with psoriasis (PsD). Patients with psoriasis who may or may not have developed psoriatic arthritis are grouped as converters (PsC); psoriatic patients who have developed psoriatic arthritis are classified as converters, while psoriatic patients who have not developed psoriatic arthritis are classified as non-converters. Samples were collected at baseline from both baseline converters and baseline non-converters, and at a subsequent time from both follow-up converters and follow-up non-converters. Patients with psoriatic arthritis (PsA) were categorized based on the severity of their conditions: mild, moderate, or severe. From each group, n = 10 patients were sampled.

Patients with PsD were further categorized into two subgroups at the time of the first sample collection: psoriasis without PsA (PsC), and psoriasis with PsA. The first set of samples was collected at baseline and the second set of samples were collected later from PsC patients who had developed PsA (converters; n=10) and those who had not (non-converters; n=10). Furthermore, patient PsA severity was measured based on the number of actively inflamed (i.e., swollen or tender) joints, with cases being categorized as either mild (<4 actively inflamed and 0 swollen joints; n = 10), moderate (4-5 actively inflamed and <3 swollen joints;

n = 10), or severe (>5 actively inflamed and >3 swollen joints; n = 10). More detailed patient information such as sex, age, duration of psoriasis, duration of PsA, treatment, and associated comorbidities is provided in Table 3.2.

Table 3.2 General information describing the distribution of various biochemical parameters for patients and volunteers involved in the study

Group	Gender (No. of patients)	Age	Dur. PsD (yrs)	Dur. PsA (yrs)	Receiving treat.	Comorbid. (number of patients in group)
PsA (mild)	F (5) M (5)	23 – 74 20 - 53	-0.03 - 53	-0.03 - 16	yes	Lung disease (1) CNS (3) Hyperlipidemia (1) Neuro (1) Autoimmune disease (1) Infection (1) Other med. (8)
PsA (moderate)	F (5) M (5)	35 - 69 47 - 69	19 - 59	0.2 - 26	yes	Hyperlipidemia (1) Diabetes (1) Infection (3) Other med. (7)
PsA (Severe)	F (5) M (5)	24 -71 23 - 48	0.3 - 69	0.3 - 28	yes	Diabetes (2) Cancer (2) Infection (3) Other med. (8)
Converter Baseline	F (3) M (7)	43 – 61 33 - 54	0.4 - 43	N/A -0.04 – 6 (post conversion)	only 2 persons	Lung disease (1) Hyperlipidemia (1) Infection (2) Other med. (5)
Non-Converter Baseline	F (3) M (7)	44 – 60 32 – 53	1 - 28	N/A	only 2 persons	Hyperlipidemia (3) Neuro (2) Osteoporosis (1) Autoimmune (1) Infection (5) Other med. (7)
Control	F (5) M (5)	N/A	N/A	N/A	N/A	N/A

Dur.PsD: duration of psoriasis (in years). Dur. PsA: duration of psoriatic arthritis (in years). Treat.: treatment. Comorbid: patient related comorbidities. Other med: other medications. F: female. M: male. Neuro: Neuropsychiatric disease. N/A: no information available.

3.3.5 Sample preparation

Serum samples were processed using TFME, which consisted of a thin stainless-steel blade that had been coated with an appropriate polymer or sorbent. The coating/extraction phase used in this work was comprised of a mixture of hydrophilic-lipophilic balanced (HLB) functionalized particles and polystyrene divinylbenzene with a weak anion exchanger (PS-DVB-WAX) functionalized particles. Each well of a 96-well plate were filled with 200 µL of serum and 400 µL of phosphate buffered saline (PBS) containing deuterated phenylalanine and testosterone. Thus, each well contained a final sample volume of 600 µL. The device was first conditioned in a mixture of 1:1 methanol:water (v/v) for 30 minutes at 1500 rpm, while the serum samples were incubated at 25 °C during this time. Following conditioning, the device was rinsed in water for 30 seconds at 1500 rpm and then exposed to the serum samples for a period of 1 hour at 1500 rpm. After the extraction process, the device was rinsed in water for 10 seconds at 1500 rpm to remove any loosely attached matrix components from its surface. Finally, the extracted metabolites were desorbed in 550 µL of a mixture consisting of 4:3:3 methanol: acetonitrile:water (v/v/v) for 1 hour at 1500 rpm. The use of a Concept-96 autosampler to automate the TFME protocol enabled a sample preparation time of under 2 minutes per sample. The desorption solution was then diluted with 220 µL of water to produce a final extract composed of 1:1 organic/aqueous content, thus ensuring compatibility with the initial chromatographic conditions of the LC-HRMS metabolomics method that would be used for analysis. A pooled quality control (QC) sample was prepared by combining 10 µL of each sample extract (not including randomly chosen sample replicates) in a separate well. The pooled QC was injected approximately every 10 sample injections.

3.3.6 Data pre-treatment and analysis

The raw LC-MS data files acquired during instrumental analysis were first converted to mzXML files using MSConvert.[106] The converted files were then pre-processed using the XCMS software package and an RStudio script that had been developed in-laboratory; pre-processing involved performing grouping, retention time correction, peak alignment, peak filling, peak picking etc.[107,108] Optimized parameters for

data pre-processing were obtained using the IPO package[109] on selected pooled QC samples run at the beginning, middle, and end of the sequence, while the extracted peaks were annotated using the xMSAnnotator Integrative scoring algorithm[110] in conjunction with the Human metabolome database[111] (HMDB). More detailed statistical analysis was achieved using Metaboanalyst [accessed September 5, 2017][112], and XCMS online[113] and METLIN[114] were also utilized to perform the initial data analysis and feature identification, respectively, on the preliminary results.

The peak-lists generated using the XCMS software package in RStudio were initially filtered using the relative standard deviation (RSD) of the pooled QCs, with any feature in the pooled QC with > 30 % RSD being removed from further analysis. Secondary filtering methods were conducted based on solvent and device blanks, with any feature with a pooled-QC:device/solvent-blank peak-intensity ratio of < 5 also being removed from further statistical evaluation. The resultant peak-lists were uploaded to Metaboanalyst; for this web-based platform, the default settings were used for missing values (wherein a fixed non-zero value is assigned to features with no signal intensity for some samples to eliminate zero values in the data matrix), and no additional feature filtering was applied. A total of 2368 features were detected in positive mode while 935 features were detected in negative mode. In addition, no further data normalization, data transformation, nor scaling (no differences were observed between the PCA's generated for no scaling, autoscaling, or pareto scaling) were performed prior to univariate or multivariate chemometric analyses. Since the distribution of data cannot be assumed, a Kruskal Wallis Test with a false discovery rate (FDR) adjusted p-value of 0.05 was applied for univariate analysis. For multivariate analysis, Principal Component Analysis (PCA), Partial Least Squares–Discriminant Analysis (PLS-DA), and Orthogonal Projection to Latent Structures-Discriminant Analysis (OPLS-DA) were performed as necessary. Given the small number of patients in each group ($n \leq 10$ if there are outliers), model validation for the supervised multivariate analyses (O-PLS-DA and PLS-DA) was conducted using a combination of permutation (at 1000) and leave-one-out cross-validation (LOOCV). Successful model validation for O-PLS-DA was achieved when the original model passed permutation at $p < 0.05$ for model predictability (Q^2) and/or model

fit (R^2). For a PLS-DA model, successful model validation was achieved with a permutation (for separation distance) of $p < 0.05$ and when Q^2 and $R^2 > 0.6$ and/or were within 0.2 units of each other. Only features with a variable of importance (VIP) score of > 1 were investigated further.

3.4 Results

Metaboanalyst was used to generate a visual representation of the overall structure of all the samples as determined by principal component analysis (PCA) (Figure 3.2). This unsupervised multivariate approach is ideal for identifying patterns within the data set from which subsequent supervised models may be constructed. PCA with univariate analysis was largely employed for this study as there were only n = 10 samples per group and very close inter-group association (overlap of clusters) among a number of groups, which may result in overfitting and likely failure during the cross-validation of supervised models. However, data from successfully validated models were used for further analyses.

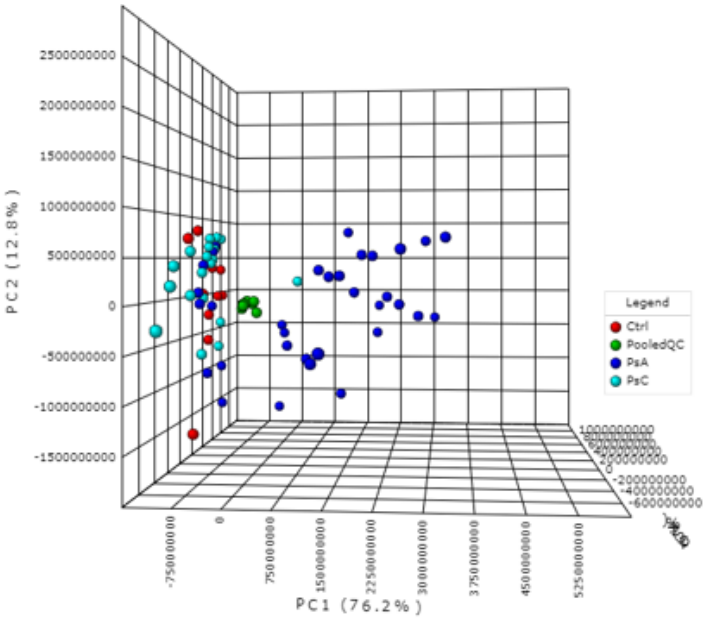

Figure 3.2 Principal component analysis (PCA - PC1:76.2%, PC2: 12.8%, PC3:2.6%) of the pooled QCs and the three patient groups under investigation: healthy volunteers (Ctrl); patients with varying degrees of psoriatic arthritis (PsA); and patients with psoriasis, but without psoriatic arthritis (PsC). The pooled QCs, Ctrls, PsA patients, and PsC patients are represented by green, red, dark blue, and turquoise, respectively. Data shown were obtained via negative mode acquisition and were similar to the results obtained via positive mode acquisition (data not shown).

PCA was used initially to identify any patient-type differentiation amongst patients with PsC (baseline converters and non-converters; n=20), patients with PsA (mild, moderate and severe, n=30), and the healthy controls (Ctrls; n=10). The quality of the resulting data was also assessed via a PCA plot investigating the spread and location of the pooled QC samples on the plot (shown in green). Since the pooled QCs are a pool of each sample, and were injected every 10 samples throughout instrumental acquisition, their very tight clustering in the middle of the plot strongly indicates stability during instrumental acquisition. Finally, in accordance with this project's objectives, further investigations were conducted with respect to the structure of the PsC group, the relationship between PsC and PsA, and PsA severity.

3.4.1 Baseline converters vs. baseline non-converters

No statistically significant differences were found between baseline converters and baseline non-converters, which are represented in green and red, respectively, in Figure 3.3. Detailed information for these patients can be found in Table 3.3.

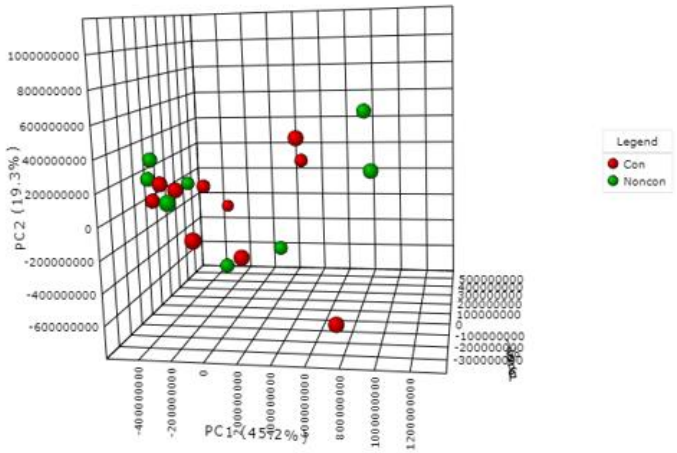

Figure 3.3 PCA (PC1:45.2%, PC2: 19.3%, PC3: 9.6%) plot of patients with psoriasis who developed psoriatic arthritis prior to disease progression (baseline converters) and patients with psoriasis who had not developed psoriatic arthritis (baseline non-converters). Baseline converters and baseline non-converters are represented by red and green, respectively. Data were obtained via negative mode acquisition and were similar to the results obtained in positive mode acquisition (data not shown).

Table 3.3 Information for patients with psoriasis defined as converters or non-converters, prior to conversion (at baseline)

Baseline converters							Baseline non-converters						
ID	**Sex**	**Age**	**Dur. PsD**	**PASI**	**Comorbid.**	**Treat.**	**ID**	**Sex**	**Age**	**Dur. PsD**	**PASI**	**Comorbid.**	**Treat.**
523	F	43	42	3.1	Infection	none	283	F	61	26	1.6	Osteop.	none
597	F	55	3	7.4	Lung dis.	none	524	F	55	1	0.3	Autoimm. Infection	none
647	F	61	16	3.6	N/A	NSAID	541	F	44	20	6.3	Infection	none
495	M	50	10	6	N/A	none	561	M	45	28	7.7	CNS Neuro.	NSAID
529	M	50	44	7.2	Infection	none	609	M	49	24	5.7	GU Hyplipid Infection	none
639	M	54	0.5	16.8	Hyplipid Diabetes	none	611	M	33	4	0.6	N/A	none
687	M	33	6	0.9	N/A	none	629	M	54	20	2.6	Hyplipid	none
717	M	43	29	5.1	N/A	none	797	M	43	27	4.8	N/A	none
755	M	44	14	15.8	N/A	none	808	M	51	7	1.7	Lung dis. Neuro. Infection	none
822	M	49	29	N/A	N/A	Nsaid	824	M	50	4	2.1	N/A	none

Dur.PsD: duration of psoriasis (in years). Dur. PsA: duration of psoriatic arthritis (in years). PASI: psoriasis area and severity index. Comorbid.: patient-related comorbidities. Treat: treatment. Hyplip: hyperlipidemia. Osteop.: osteoperosis. Autoimm.: autoimmune disease. Neuro.: neuropsychiatric disease. CNS: central nervous system. NSAID: nonsteroidal anti-inflammatory drugs. Dmards: disease modifying anti-rheumatic drugs. MTX: methotrexate. Anti-TNF: anti-TNF inhibitor Bio: biologics work up. N/A: no information available

Baseline converters vs. follow-up converters subsequent comparison was made to examine the metabolic changes occurring during the transition from PsC (baseline converter) to PsA (follow-up converter). However, as the PCA plot in Figure 3.4 illustrates, a paired analysis revealed no statistically significant differences between baseline converters (shown in red – group 0) and follow-up converters (shown in green – group 1). Detailed patient information can be found in Table 3.4.

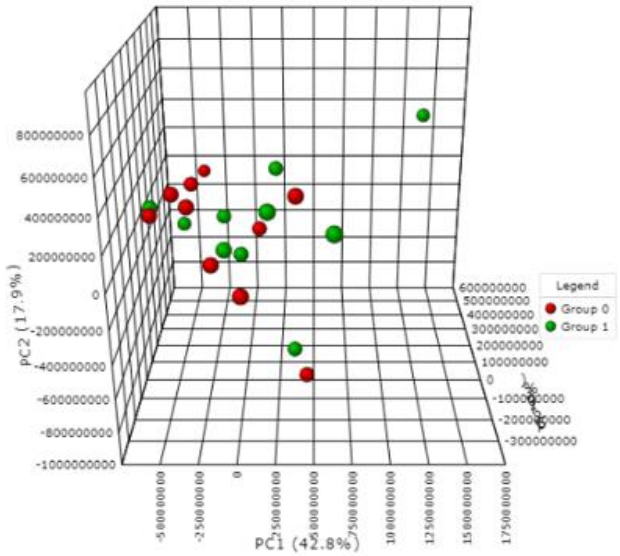

Figure 3.4 PCA (PC1: 42.8, PC2: 17.9%, PC3: 10.3%) plot of a paired analysis of converter (PsC) patients who had psoriasis without psoriatic arthritis at baseline (baseline converters), and developed psoriatic arthritis (follow-up converters). Baseline converters and follow-up converters are represented on the plot by red and green, respectively. Data were obtained via negative mode acquisition and were similar to the results obtained in positive mode acquisition (data not shown).

Table 3.4 Patient information for individuals with psoriasis who develop psoriatic arthritis and patients with mild psoriasis.

Converter									Mild PsA						
Baseline						Post conversion									
ID	**Comorbid.**	**Sex**	**Age**	**PASI score**	**Dur. PsD**	**Dur. PsA**	**Joint info SJ/TJ**	**Treat.**	**ID**	**Sex**	**Age**	**PASI score**	**Dur. PsA**	**Joint info SJ/TJ**	**Treat.**
495	N/A	M	50	2.6	10	0.7	3/7	NSAID	713	M	37	0.9	7	1/1	Dmards NSAID MTX
529	Infection	M	50	13.3	44	-0.04	1/12	Dmards NSAID MTX	**3201**[x]	M	39	0.4	1	0/0	NSAID
639	Hyplip Diabetes	M	54	N/A	0.5	N/A	N/A	Bio	3376	M	20	0.8	0	1/1	none
687	Lung disease	M	33	2.1	6	0	2/2	NSAID	3535	M	49	1.9	0	2/2	NSAID
717	N/A	M	43	5.5	29	0.4	0/0	none	3520	M	53	38.4	8	0/1	Dmards MTX
755	N/A	M	44	38.7	14	1	1/1	Dmards	725	F	23	0.8	5	6/0	Dmards MTX
822*	N/A	M	49	3.1	29	-0.3	0/0	NSAID	3160	F	52	2.6	16	1/1	Bio Dmards NSAID MTX Anti-TNF
523	Infection	F	43	3.8	42	6	3/8	Nsaid	3234	F	30	2.4	1	1/3	Bio NSAID Anti-TNF

597	Lung disease	F	55	0.6	3	1	0/0	Bio Dmards MTX Anti-TNF	3543	F	51	3.6	2	N/A/N/A	Nsaid
647*	N/A	F	61	2.1	16	0.4	3/3	NSAID	3640	F	75	0	3	0/5	Bio NSAID Anti-TNF

(ID*) patients taking treatment at baseline (Nsaid in both cases), prior to conversion. **ID^{x}:** patients excluded from further statistical analysis. SJ: swollen joints. TJ: tender joints. Comorbid.: patient-related comorbidities. Dur.PsD: duration of psoriasis (in years). Dur. PsA: duration of psoriatic arthritis (in years) PASI: psoriasis area and severity index. Treat: treatment. Hyplip: Hyperlipidemia. NSAID: nonsteroidal anti-inflammatory drugs. Dmards: disease modifying anti-rheumatic drugs. MTX: methotrexate. Anti-TNF: anti-TNF inhibitor Bio: Biologics work up. N/A: no information available.

3.4.2 Healthy controls vs. psoriasis without psoriatic arthritis vs mild psoriatic arthritis

Figure 3.5 show that there exists no discrimination between patients with psoriasis and patients with psoriasis newly diagnosed with psoriatic arthritis (follow-up non-converters and follow-up converters represented in Figure 3.5A by green and blue, respectively) with healthy controls (shown as red in Figure 3.5 A and B). Interestingly, no difference was found between these same psoriatic patients newly diagnosed with psoriatic arthritis and mild PsA (shown in blue in Figure 3.5B).

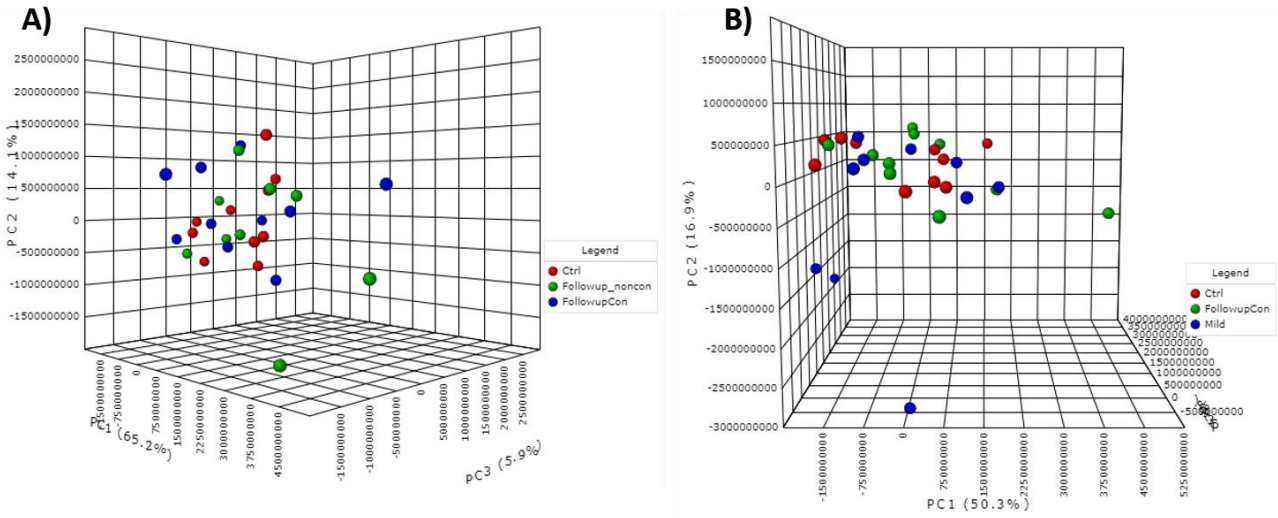

Figure 3.5 A) Principal component analysis (PC1: 65.2%, PC2: 14.1%, PC3: 5.9%) for the comparison of three groups – healthy controls, follow-up non-converters and follow-up converters represented by red, green and blue circles on the plot respectively. B) Principal component analysis (PC1: 50.3%, PC2: 16.9%, PC3: 4.0%) for the comparison of three patient groups – healthy volunteers, follow-up converters and mild psoriatic arthritis represented by red, green and blue on the plot respectively.

3.4.3 PsC vs PsA

It is abundantly clear from Figure 3.2 and Figure 3.6—which explicitly highlights PsA progression or disease severity for PsA patients in comparison to healthy volunteers and PsC patients—that the PsA group dominates the PCA plot. Specifically, compared to the healthy controls (red) and the PsC group (turquoise), the PsA group contains the largest distribution of samples across the plot, accounting for 76.9% of the

variation seen in the first principal component (PC1). Given the considerable variation observed among the PsA group, further investigation was conducted on the PsA group structure.

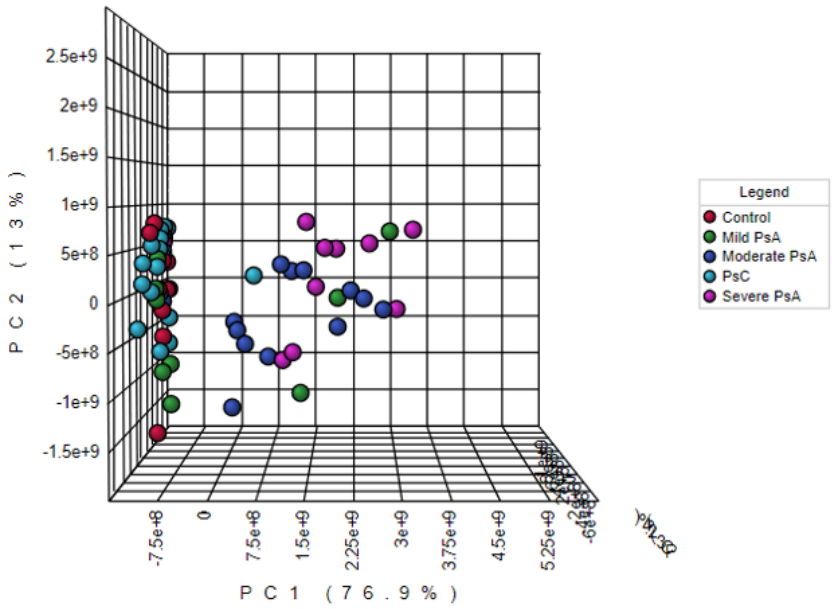

Figure 3.6 PCA (PC1: 76.9, PC2: 13%, PC3: 2.4%) plot of healthy volunteers (control; red) and patients with psoriasis prior to conversion or non-conversion (PsC; turquoise). The plot also distinguishes between PsA patients based on level of disease progression (mild PsA-green; moderate PsA-dark blue; severe PsA-magenta). Data were obtained via negative mode acquisition and were similar to the results obtained in positive mode (data not shown). Pooled QC's were removed.

3.4.4 PsA group

The PCA plot in Figure 3.7 shows a clear separation between PsA groups, such that as those suffering from mild psoriatic arthritis tend towards the left side of the plot, those suffering from severe psoriatic arthritis tend towards the right side of the plot, and those with moderate psoriasis are distributed among and between these two groups. Overall patient information for the PsA group investigated is provided in Table 3.5, while joint related information is provided in Table 3.6.

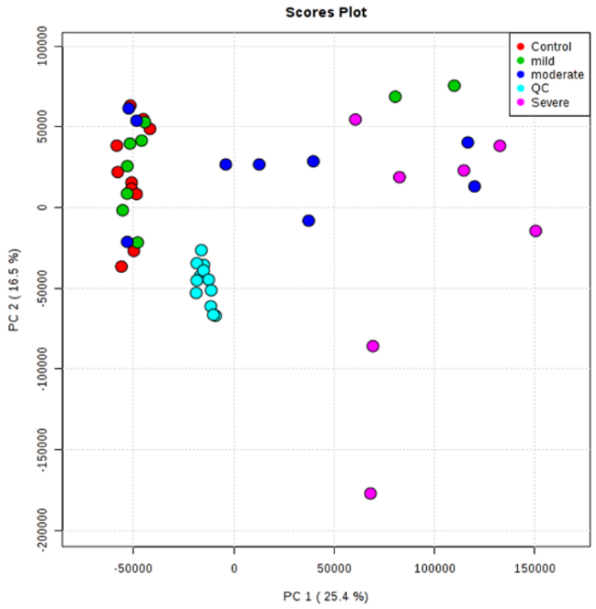

Figure 3.7 PCA (PC1:25.4%, PC2:16.5%) plot of healthy individuals (Ctrls) and patients suffering from varying degrees of psoriatic arthritis (PsA). The control group is represented by red dots, while patients with mild, moderate, and severe PsA are represented by green, dark blue, and magenta dots, respectively. Data were obtained via positive mode acquisition. Data obtained via negative mode acquisition can be found in Online resource 9.

Table 3.5 Patient information for individuals with varying degrees of PsA.

Mild							Moderate							Severe						
ID	**Sex**	**Age**	**Dur. PsD**	**Dur. PsA**	**Comor.**	**Joint info.**	**ID**	**Sex**	**Age**	**Dur. PsD**	**Dur. PsA**	**Comor.**	**Joint info**	**ID**	**Sex**	**Age**	**Dur. PsD**	**Dur. PsA**	**Comor.**	**Joint info**
713	M	37	7	7	N/A	A (1) D(12)	**603**[x]	M	53	25	6	N/A	A (2) D (0)	**192**[x]	M	61	26	33	N/A	A (0) D (26)
3201[x]	M	39	1	1	N/A	N/A	204	M	48	28	25	N/A	A (1) D (14)	242	M	63	10	10	Hyplipid Diabetes	A (0) D (5)
3376	M	20	0	0	Lung dis. Infec.	A (1) D (1)	371	M	52	30	18	Infec.	A (0) D (9)	3103	M	48	0.3	0.3	Infect.	A (21) D (0)
3520	M	53	8	8	N/A	A (1) D (4)	421	M	49	31	24	Infec.	A (1) D (0)	3120	M	24	2	2	N/A	A (8) D (0)
3535	M	49	2	0	N/A	A (2) D (2)	430	M	69	59	19	Hyplipid Diabetes	A (2) D (11)	3316	M	37	31	6	N/A	A (4) D (4)
725	F	23	13	5	CNS	N/A	438	F	62	52	27	N/A	A (2) D (3)	422	F	51	25	21	N/A	A (0) D (32)
3160	F	52	22	16	Hyplipid.	A (1)	23	F	46	35	25	N/A	A (0) D (2)	**706**[x]	F	50	19	19	Diabetes Cancer Infec.	A (18) D (2)
3234	F	30	5	1	CNS Neuro.	A (3)	**3069**[x]	F	50	26	2	N/A	A (0) D (0)	726	F	49	32	28	Lung dis. Liver dis. Autoimm. Infec.	A (15) D (6)
3543	F	51	31	2	N/A	A (N/A) D (0)	3106	F	69	39	0.24	N/A	A (4) D (0)	**3073**[x]	F	72	69	6	Cancer Infec.	A (7) D (2)
3640	F	75	54	3	CNS Autoimm.	A (5) D (3)	3110	F	37	20	7	N/A	A (3) D (1)	3203	F	25	18	18	N/A	A (3) D (0)

ID[x] Patients excluded from further statistical analysis. Dur. PsD: duration of psoriasis (in years). Dur. PsA: duration of psoriatic arthritis (in years). A: number of active joints. D: number of damaged joints. CNS: central nervous system. Neuro.: neuropsychiatric disease. Infec: infection. Hyperlipid.: hyperlipidemia. Autoimm.: autoimmune disease. N/A: no information available.

Table 3.6 Joint information for patients with varying degrees of psoriatic arthritis

Group	ID	SJ	DJ	AJ	notes	Group	ID	SJ	DJ	AJ	notes	Group	ID	SJ	DJ	AJ	notes
Mild	713	1	12	1	severe	Mod.	23	0	2	0		Severe	**192**[x]	0	26	0	
	725	6	0	6	severe		204	1	14	1	severe		242	0	5	0	
	3160	1	0	1			371	0	9	0	severe		**422**[x]	0	32	0	
	3201[x]	0	0	0			421	1	0	1	mild		**706**[x]	2	2	18	
	3234	1	0	3			430	1	11	2	mild		726	10	6	15	
	3376	1	1	1			438	1	3	2			**3073**[x]	3	2	7	
	3520	0	4	1			**603**[x]	2	0	0			3103	16	0	21	
	3535	2	2	2			**3069**[x]	0	0	0			3120	4	0	8	
	3543	N/A	0	N/A			3106	1	0	4			3203	1	0	3	
	3640	0	3	5			3110	1	1	3	mild		3316	3	4	4	mild
avg		1	2	2		avg		1	4	1		avg		4	8	8	

ID[x]: patients excluded from further statistical analysis. SJ: number of swollen joints. DJ: number of damaged joints. AJ: number of active joints Avg: average. N/A: no information available. *Notes: information about which patients were cluster deviations and where they were subsequently found. A blank note suggests patients did not deviate from the cluster.*

3.4.5 Statistically significant features across patient groups

Statistical analysis via univariate analysis yielded 10 statistically significant features across the three PsA groups (mild, moderate and severe), which were putatively identified using xMSAnnotator for negative mode data. For the positive mode data, XCMS online in conjunction with METLIN helped to tentatively identify 7 statistically significant features differentiating healthy individuals from patients with severe PsA. See Table 3.7 and

Table 3.8 and for a complete list of annotated compounds along with their associated annotation confidence levels, statistical parameters and LC-HRMS parameters for both positive and negative modes, respectively.

Table 3.7 Tentatively annotated features showing statistically significant differences via univariate analysis between healthy controls and severe psoriatic arthritis patients for positive mode data.

Feature No.	Tentative ID	m/z	Adduct	Retention time (min)	P value	Q value	Annotation score (max = 3)
57	S-aminomethyldihydrolipoamide	237.1090	$[M+H]^+$	13.25	$8.0x10^{-5}$	$1.8x10^{-2}$	2
130	Hydroxycapric acid	189.1485	$[M+H]^+$	14.84	$2.0x10^{-4}$	$2.0x10^{-2}$	3
304	Glutamyl-tyrosine	310.1159	$[M+H]^+$	14.01	$5.7x10^{-4}$	$4.3x10^{-2}$	2
365	Methyladenosine Isoleucyl glutamate	282.1197 282.1186	$[M+H]^+$ $[M+Na]^+$	12.17	$7.0x10^{-4}$	$2.6x10^{-2}$	2
531/1302	Adenosine or deoxyguanosine Isobutyryl carnitine S-aminomethyldihydrolipoamide	285.1306 254.1363 254.1355	$[M+NH4]^+$ $[M+Na]^+$ $[M+NH4]^+$	11.05	$1.0x10^{-3}$	$3.0x10^{-2}$	0
549	Gamma-glutamyltyrosine	311.1238	$[M+H]^+$	13.45	$1.0x10^{-3}$	$3.0x10^{-2}$	2
715	Arginyl-glycine	254.1224	$[M+Na]^+$	13.33	$2.0x10^{-3}$	$4.0x10^{-2}$	1

Table 3.8 Tentatively annotated features showing statistically significant differences via univariate analysis across patients with varying degrees of psoriatic arthritis for negative mode data.

Feature No.	Tentative ID	m/z	Adduct	Retention time (min)	P value	Q value	Annotation score (max = 3)
4448	2-Hydroxydecanedioic acid, 3-hydroxysebacic acid cis-4-Hydroxycyclohexylacetic acid	217.1077	$[M-H]^-$ $[M+CH3COO]^-$	11.78	$1.5x10^{-3}$	$3.0x10^{-2}$	2
3752	p-Coumaroylagmatine Undecanedioic acid	275.1501	$[M-H]^-$ $[M+CH3COO]^-$	12.15	$8.5x10^{-4}$	$3.0x10^{-2}$	2

1139	3-Hydroxydodecanedioic acid	281.1162	$[M+Cl]^-$	14.00	$1.9x10^{-3}$	$3.0x10^{-2}$	2
3689	Dodecanedioic acid	289.1659	$[M+CH3COO]^-$	12.68	$2.2x10^{-3}$	$3.0x10^{-2}$	2
216	S-aminomethyldihydrolipoamide	295.1163	$[M+CH3COO]^-$	13.36	$9.3x10^{-4}$	$3.0x10^{-2}$	0
2254	1,11-Undecanedicarboxylic acid	303.1818	$[M+CH3COO]^-$	13.40	$6.4x10^{-3}$	$4.0x10^{-2}$	2
2412	Phenylbutyrylglutamine	327.1118	$[M+Cl]^-$	13.03	$1.9x10^{-3}$	$3.0x10^{-2}$	2
2240	Arginyl-Lysine	337.1744	$[M+Cl]^-$	12.30	$1.4x10^{-3}$	$3.0x10^{-2}$	2
2522	6-Keto-PGF1a	429.2488	$[M+CH3COO]^-$	18.90	$1.5x10^{-3}$	$3.0x10^{-2}$	2
2256	N1-(alpha-D-ribosyl)-5,6-dimethyl-benzimidazole	313.0959	$[M+Cl]^-$	12.25	$1.5x10^{-3}$	$3.0x10^{-2}$	2
	L-phenylalanyl-l-hydroxyproline		$[M+Cl]^-$				
	Prolyl-Tyrosine		$[M+Cl]^-$				

Multivariate analysis of baseline converter and severe PsA patients via O-PLS-DA yielded a model with the acceptable criteria of 0.94 (R^2) and 0.78 (Q^2) in positive mode and 0.94 (R^2) and 0.87(Q^2) in negative mode (data for validation is provided in Online Resource 15). The features with a VIP of >1 that had the most significant influence on the model were putatively identified as 3-hydroxytetradecanedioic acid and 3-hydroxydodecanedioic acid for positive and negative mode, respectively. A list of the other features with VIPs of >1, their respective parameters, and their possible biochemical importance for positive and negative mode is provided in Table 3.9 and Table 3.10, respectively.

Table 3.9 Variables of importance isolated from validated O-PLS-DA model that differentiate baseline converters from severe psoriatic arthritis. Data obtained from positive mode acquisition.

Feature No.	Tentative ID	m/z	Adduct	Retention time (min)	VIP score	Biochemical importance
8728	3-Hydroxytetradecanedioic acid	275.1854	$[M+H]^+$	15.72	30	High levels of 3-Hydroxytetradecanedioic acid (and other 3-hydroxydicarboxylic acids) were detected in the urine of a patient with 3-hydroxydicarboxylic aciduria.
8834	3-Hydroxytetradecanedioic acid	297.1673	$[M+Na]^+$	15.70	24	
3800	L-phenylalanine, 3-pyridinebutanoic acid Pyruvophenone, dihydrocoumarin	166.0865	$[M+H]^+$ $[M+NH4]^+$	10.85	15	When present in sufficiently high levels, phenylalanine can act as a neurotoxin and a metabotoxin. A metabotoxin is an endogenously produced metabolite that causes adverse health effects at chronically high levels. Chronically high levels of phenylalanine are associated with at least five inborn errors of metabolism.
9905	9,12-Dioxo-dodecanoic acid	229.1437	$[M+H]^+$	13.8	8	Di-oxo-dicarboxylic acid.
10122	Deoxyadenosine 3-Hydroxydodecanedioic acid	269.1361	$[M+NH4]^+$ $[M+Na]^+$	13.8	8	When present in sufficiently high levels, deoxyadensoine can act as an immunotoxin and a metabotoxin. Chronically high levels of deoxyadenosine are associated with adenosine deaminase (ADA) deficiency, an inborn error of metabolism.
9043	3-Hydroxydodecanedioic acid	247.1542	$[M+H]^+$	13.8	7	A dicarboxylic acid that appears in the urine of children affected with peroxisomal disorders.
8393	2-Phenylglycine	152.0709	$[M+H]^+$	9.1	7	Has a role as a human metabolite and is described in normal human urine.
8434	Ribonic acid, lyxonate, apionic acid, arabinonic acid	184.081	$[M+NH4]^+$	13.8	2	Sugar carboxylic acids.
10328	Biopterin	255.1204	$[M+NH4]^+$	12.9	2	Biopterin concentrations in cerebrospinal fluid from patients with Parkinson's disease are lower than those from age-matched older controls. Lowered levels of urinary biopterin concomitant with elevated serum phenylalanine concentration occur in a variant type of hyperphenylalaninemia.
2321	Creatinine	114.0666	$[M+H]^+$	3.7	1.4	A breakdown product of creatine phosphate in muscle.

2830	L-tyrosine, hydroxy butanoic acid, amino(hydroxyphenyl)propanoate, hydroxyphenylalanine M-coumaric acid, phyenyl pyricin acid	182.0814	$[M+H]^+$ $[M+NH4]^+$	8.78	1.4	Tyrosine is not found in large concentrations throughout the body, likely because it is rapidly metabolized. Most common is the increased amount of tyrosine in the blood of premature infants, which is marked by decreased motor activity, lethargy, and poor feeding. Hydroxybutyric acid (also known as gamma-hydroxybutyrate or GHB) is a precursor and a metabolite of gamma-aminobutyric acid. Hydroxyphenylalanine is an L-phyenylalanine derivative.
8861	3-Hydroxytetradecanedioic acid	292.212	$[M+NH4]^+$	15.71	1.2	See feature No.
1185	Isoleucine	132.1022	$[M+H]^+$	8.93	1.1	Branched amino acids have different metabolic routes: leucine which is solely involved in fats; and isoleucine which is involved in both fats and carbohydrates.
9590	Indoleacetaaldehyde	177.1025	$[M+NH4]^+$	9.4	1	Indoleacetaldehyde participates in a number of enzymatic reactions. In particular, indoleacetaldehyde can be biosynthesized from tryptamine, which is mediated by the enzyme kynurenine 3-monooxygenase. indoleacetaldehyde is involved in tryptophan metabolism.

Table 3.10 Variables of importance isolated from validated O-PLS-DA model that differentiate baseline converters from severe psoriatic arthritis. Data obtained from negative mode acquisition.

Feature No.	Tentative ID	m/z	Adduct	Retention time (min)	VIP score	Biochemical importance
1638	3-hydroxydodecanedioic acid 10-hydroxy-2E-decenoic acid, 2-oxo capric acid	245.1393	$[M-H]^-$ $[M+CH3COO]^-$	14.00	27	3-hydroxydodecanedioic acid is a medium chain hydroxy fatty acid that reportedly appears in children affected with peroxisomal disorders. PMID: 10896310.
77	12-amino-dodecanoic acid	274.2027	$[M+CH3COO]^-$	15.93	6.8	This is an omega-amino medium chain fatty acid and has a role as a bacterial metabolite. (PubChem).
404	n-heptanoyl acetic acid, 3-caproyl propionic acid, 7-methyl-3-oxooctanoic acid, 4-n-valeryl butyric acid	150.0008	$[M+CH3COO]^-$	14.13	6.2	Medium chain oxo-monocarboxylic acids. (PubChem).
1151	2,4-Dideoxy-2-octylpentaric acid 2R-Hydroxy-10-undecenoic acid, 3-capryl propionic acid	259.1552	$[M-H]^-$ $[M+CH3COO]^-$	14.96	3.5	Medium chain hydroxy and “ene”-monocarboxylic acids.
2478	2-Hydroxydecanedioic acid, 3-hydroxy-sebacic acid, 2-hydroxy-decanedioic acid 3-Oxovalproic acid, 4-Hydroxycyclohexylacetic acid, 2-keto-n-caprylic acid	217.1076	$[M-H]^-$ $[M+CH3COO]^-$	12.25	2.6	Medium chain hydroxy dicarboxylic acids. (PubChem) 3-Hydroxysebacic acid is a normal urinary metabolite and can be elevated in patients with peroxisomal disorders. 3-Hydroxysebacic acid and caprylic acid are found to be associated with medium chain acyl-CoA dehydrogenase deficiency, which are inborn errors of metabolism. 4-Hydroxycyclohexylacetic acid is a tyrosine metabolite that has been found in the urine of a patient with a defect of 4-hydroxyphenylpyruvate dioxygenase, an inborn error of metabolism. (HMDB).
2692	p-Cresol sulfate Thiophenecarboxylic acid	187.0062	$[M-H]^-$ $[M+CH3COO]^-$	10.23	2.1	p-Cresol sulfate is a microbial metabolite that is found in urine and likely derives from secondary metabolism of p-cresol. It appears to be elevated in the urine of individuals with progressive multiple sclerosis (HMDB).
2891	Androsterone sulfate	369.1743	$[M-H]^-$	15.93	1.3	Androsterone sulfate is clinically recognized as one of the major androgen metabolites found in urine. (HMDB).
651	1,2-Dihexanoyl-sn-glycerol, 6-hydroxypentadecanedioic acid	287.1865	$[M-H]^-$ $[M+CH3COO]^-$	16.85	1.1	1,2-Dihexanoyl-sn-glycerol is a hexanoic acid derivative. Majority of other tentative compounds are dicarboxylic and carboxylic acid derivatives. (PubChem).

	Keto tridecanoic acid, hydroxy-9-tridecenoic acid, menthenyl lactate, 7-methoxy-dodec-4-enoic acid, 6-hydroxy-4-tridecanolide					
1282	2-Aminoadenosine	341.1223	$[M+CH_3COO]^-$	14.02	1.1	Purine nucleoside. (PubChem).

3.5 Discussion

3.5.1 Baseline converters vs. baseline non-converters

One of the objectives of the study was to investigate the characteristic metabolic differences between converters and non-converters at baseline as a means of possibly determining early markers of disease conversion however, no differences were found to differentiate the two groups contrary to what was expected. Given that both sets of patients have psoriasis and neither group is receiving treatments, this could suggest a very subtle onset of PsA (*this is discussed more in the following section 3.5.2 "Baseline converters vs. follow-up converters"*), further highlighting the challenges of early prognosis.

3.5.2 Baseline converters vs. follow-up converters

Since at baseline, the converter group, according to the results presented herein, are not significantly different from baseline non-converters, strictly monitoring the differences between patients with psoriasis that eventually develop PsA may be more insightful. It is important to note however, that the follow-up samples were collected while patients were receiving treatment. Since these treatments are usually implemented to normalize any metabolic disturbances that may occur due to disease pathophysiology, thereby essentially preventing disease progression, it follows that no separation would be observed between baseline converters and follow-up converters, thus suggesting the effectiveness of the various prescribed treatments.

Another possible reason for the lack of differentiation between the baseline converters and their follow-up samples may be that the follow-up converters had only developed PsA relatively recently (less than 1 year – Table 3.4). As such, it is possible that allowing a longer time period before conducting sampling post conversion may enable the identification of metabolites indicative of disease conversion. However, according to Figure 3.2 and Figure 3.5, the study demonstrates consistency by essentially validating itself, as the follow-up converters (green), who are different from patients with mild PsA (blue), do not exhibit separation. Since the follow-up converters only had mild PsA, the lack of discrimination between them and

the mild PsA patients is therefore logical, suggesting that patients within these two groups may in fact be similar. Table 3.4 shows the similarities between the two groups. Furthermore, there is evidence contradicting the above notion that a longer wait time prior to sample collection post conversion will not yield more valuable information, as disease duration among mild PsA patients ranged from less than a year to 16 years.

The lack of discrimination between the samples collected before and after conversion and between the baseline converters and non-converters may also indicate a small effect size (very subtle changes) for both between-group comparisons. As such, it may be necessary to analyze a very large number of samples from each group before distinctive differences can be observed. Indeed, as a post hoc power analysis revealed (data not shown) that, over 1000 serum samples would be required before any statistically significant differences (power ≥ 0.8) would be observable in the before and after conversion samples, as well as in the baseline samples for the converters and non-converters. It is therefore possible that the metabolic changes related to conversion are perhaps too subtle and/or become diluted due to blood circulation, which would potentially make serum an ineffective biological fluid for detecting and identifying markers specific to conversion.

3.5.3 Healthy controls vs. psoriasis without psoriatic arthritis vs psoriatic arthritis

No discrimination was found among patients with psoriasis, mild PsA, and healthy controls. This result was interesting given the number of metabolomic studies demonstrating visual differences between patients with psoriasis and healthy individuals. Nonetheless, this result is consistent with the patient information provided in Table 3.3 and Table 3.4, which shows that the majority of baseline converters and mild PsA patients had a PASI score of < 10, indicating mild psoriasis. As such, it follows that no discrimination can be discerned amongst these three groups. This is consistent with the results of Li *et al.*'s analysis of serum samples from psoriasis vulgaris patients with varying degrees of psoriasis severity wherein patients with mild psoriasis were similar to the controls and significantly different from patients with severe psoriasis.[99]

3.5.4 PsC vs PsA

Since it is abundantly clear from Figure 3.2 and Figure 3.6 that the PsA group dominates the PCA plot, this result may suggest that the conversion pathophysiology from PsC to PsA is driven by PsA severity.

3.5.5 PsA group—Confounding factors

Considering the patient information described in Table 3.5, and based on the results shown in Figure 3.7, it is clear that neither the duration of psoriasis prior to developing PsA nor the duration of PsA is a predictor of disease conversion or disease severity, respectively. While psoriasis is related to a number of associated comorbidities, such as cardiovascular disease, obesity, insulin resistance, and metabolic syndrome, and the observed patients may be at a risk of other age-related degeneracies ($\geq$ 40 years old), the differentiating pattern on the plot appears to be independent of these factors rather than confounded by them, since all three groups contain patients with and without a range of comorbidities. Additionally, disease severity appears to be independent of sex or age.

3.5.6 PsA group—Severity related to joint information

As demonstrated in Table 3.6, disease severity appears to be correlated with biochemical parameters associated with joints, such as number of swollen joints, number of tender joints, and number of damaged joints. In particular, disease severity appears to be directly related to the number of damaged joints.

3.5.7 PsA group—Cluster deviants

It is worth noting that one or two patients from each group were removed from statistical analysis due to being outliers. Conversely, some patients fell outside the majority of their cluster but were not removed because they did not statistically classify as outliers. For example, two patients with mild PsA (green) and two patients with moderate PsA (dark blue) are located on the extreme right side of the plot with the severe PsA patients (pink), while three moderate PsA patients (dark blue) are located on the left side of the plot with the majority of the mild PsA patients (green) and controls (red). These inconsistent patterns suggest that the current clinical methods being used to evaluate PsA disease severity may not be accurate, thus

highlighting the need to use metabolic markers as a complementary source of information in diagnosis. It is possible that these above-noted outlier patients may be able to provide more information or a better indication as to the pathophysiology of PsA. Interestingly, while some of these deviations seem to correlate more closely with patient joint information (provided in Table 3.6), some do not. This discrepancy further emphasizes the challenges of disease categorization, even with very stringent phenotyping protocols.

3.5.8 Statistically significant features across patient groups

Prior metabolomics studies have found that some of these putatively identified compounds, such as 1,11-undecanedicarboxylic acid, tend to be common in individuals suffering from peroxisomal disorders.[103] Other tentatively identified compounds annotated from both the positive and negative mode data, such as S-aminomethyldihydrolipoamide, have been associated with the serine and threonine metabolism pathways. In particular, Kamleh et al. [100] discovered that these pathways are affected in psoriatic patients, which results in higher serine and threonine levels when compared to healthy individuals. All putatively identified compounds were found to increase in relation to disease severity, with mild PsA patients exhibiting the lowest levels, moderate PsA patients exhibiting much higher levels, and severe PsA patients exhibiting the highest levels of the three groups. An example of this relationship is demonstrated Figure 3.8.

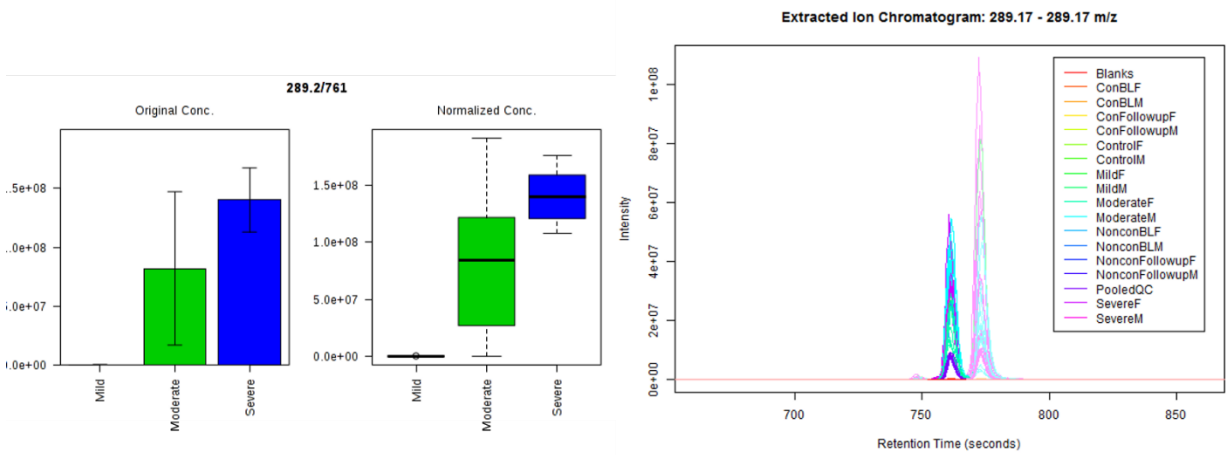

Figure 3.8 The box plots on the left are representative of a statistically significant feature across the PsA group – m/z 289.2 (exact m/z: 289.1659) at a retention time 761 seconds (12.68 min). On the right is the extracted ion chromatogram of that feature. This was tentatively identified as dodecanedioic acid, and putatively identified as such with an annotation score of 2 using xMSAnnotator.

Elevated levels of 3-hydroxytetradecanedioic acid have been implicated in the inhibition of CoA, which is an enzyme involved in fatty acid biosynthesis. Moreover, 3-hydroxydodecanedioic acid has also been linked to inhibited fatty acid oxidation [115–117]. Interestingly, the majority of the other VIPs, especially those from negative mode analysis, were tentatively identified as various dicarboxylic and carboxylic acid derivatives (i.e. 3-hydroxysebacic acid implicated as a result of fatty acid beta-oxidation defects [118]), thus indicating a potentially strong correlation between the dysregulation of the fatty acid or lipidome profile and disease conversion. However, further investigation is required to confirm these findings due to the challenges associated with correlating circulating organic acids with specific metabolic processes. For examples, elevated levels on their own may represent a non-specific response, while ratios of various kinds of organic acids may indeed be more informative [117].

3.6 Conclusion and future direction for research

This paper demonstrates that the use of rapid-sampling TF-SPME for untargeted metabolomics of serum is a feasible method for assessing disease pathophysiology via PsA severity. The heterogeneity of the patient data presented herein (i.e., the large ranges in age, duration of psoriasis, duration of PsA, sex imbalances

in some cases, range of treatments, and comorbidities) and the relatively small sample sizes (n = 10 for each group) made it difficult to exclude samples for the purpose of producing more uniform data sets, which are customary for statistical comparisons of patient groups in clinical applications. Nevertheless, the findings were interesting, as they showed no apparent trends or influence of potential confounding factors (comorbidities) of the patients' biochemical parameters on the patterns observed via multivariate analysis. The aim of this study was to determine biomarkers of the conversion from psoriasis to PsA, biomarkers differentiating PsA from PsC, and biomarkers of PsA severity. Based on the data presented herein, it is apparent that dysregulated fatty acid enzymes related to synthesis or degradation of various fatty acids, is strongly associated with PsA severity as many of these features differentiated baseline converters (PsC) from severe PsA with elevated levels in the latter. This pattern is also more evident for PsA pathology given the increasing levels of important fatty-acid-related features across the PsA group with the lowest levels in mild PsA and the highest levels in severe PsA. Futhermore, there are at least 20 statistically significant features associated with PsA severity, while there are no statistically significant features that differentiate between patients with psoriasis prior to and post conversion. This finding suggests that, while serum may be useful for finding markers of PsA severity, the differences in terms of PsA conversion from psoriasis may be too subtle to generate a significant effect. Therefore, we propose the use of synovial fluid for future metabolic analyses. As the joint fluid found closest to the origin of PsA disease manifestation, synovial fluid can likely provide a better indication of discriminating metabolic biomarkers, specifically for conversion. Since collection of synovial fluid may be quite difficult, it would be beneficial to develop a protocol for *in vivo* SPME sampling, as this would provide a minimally invasive approach for obtaining potentially more useful biological material directly from the source, while avoiding removal/collection from the patient. Furthermore, an *in vivo* SPME technique would enable sampling and sample preparation to be combined into one step, which would drastically minimize the number of analytical steps required to obtain the final extract, thereby preserving the initial integrity of the true metabolome. Finally, while this preliminary data provides a good direction for future directions of the research, due to the relatively small

sample sizes used, we suggest that a more expansive follow-up study be conducted to confirm the findings. This expanded study should increase the number of patients examined, utilize parallel *in vivo* skin-lesion analysis, synovial fluid analysis and include fatty acid profiling and/or lipidome fingerprinting, and more in-depth and rigorous MS/MS validation, as these steps would provide a more supplemented and comprehensive approach to metabolomics for PsA research.

Chapter 4: Metabolomic fingerprinting of porcine lung tissue during pre-clinical prolonged normothermic *ex vivo* lung perfusion (NEVLP) using *in vivo* solid phase microextraction

4.1 Preamble

Chapter 4 of this thesis has not yet been published. The work presented in this chapter of the thesis stemmed from a collaboration with Toronto General Hospital initated by B. Bojko, J. Pawlisyzn, A. Roszkowska, and M. Cypel who were also responsible for the initial experimental design. Further modifications to the experimental design and all other work presented in this chapter of the thesis were equally shared between the author of this thesis and A. Roszkowska. Please see *Statement of contributions*. This work was funded by the Canadian Institute of Health Research (CIHR) - Natural Sciences and Engineering Research Council (NSERC) of Canada Collaborative Health Research Projects program [grant 355935 entitled "Supervised *in vivo* lung perfusion strategy for treatment of cancer metastases to the lungs. Real-time monitoring of chemotherapy by on-site analytical platform"] and the Natural Sciences and Engineering Research Council of Canada Industrial Research Chair (IRC) program.

4.2 Introduction

Lung transplantation remains the single most effective form of treatment for patients suffering from end-stage pulmonary diseases, such as terminal metastatic lung cancer, chronic obstructive pulmonary diseases (COPD), emphysema and cystic fibrosis.[119–121] Unfortunately, the number of patients awaiting transplantation far exceeds the pool of available donor organs. This shortage of donor organs is exacerbated by the fact that only 20% meet the strict criteria for transplantation, largely due to the various intensive care unit (ICU) related complications that can occur in both donation after brain death (DBD) and donation after cardiac death (DCD) donors, including gastric aspiration, bacterial infection, and longer warm ischemic times, among others. Furthermore, 20% of transplanted lungs experience acute lung injury and/or primary graft dysfunction, which are both signs of early rejection and eventual patient mortality.[119,121]

Normothermic *ex vivo* lung perfusion (NEVLP or EVLP) is a modernized organ preservation technique wherein perfusion fluid is circulated throughout the isolated lung at physiological temperature via a specialized circuit set up. This method improves the function of marginalized lungs (lungs that had multiple different injuries and were thus declined for transplantation) by enabling the innate protective metabolic processes that occur under normothermic conditions.[121–123] Additionally, NEVLP allows specific appropriate targeted therapies to be administered within the circuit via the perfusion fluid in order to treat the above-noted ICU-related complications or other donor-borne illnesses prior to transplantation.[121,124] Moreover, NEVLP also allows for more detailed assessments of organ function prior to transplantation.[122,123,125] These advantages have been instrumental in increasing the donor pool, thereby decreasing patient waiting list morbidity and mortality. While a number of "omics" studies—including genomics, transcriptomics, epigenomics, and proteomics[126,127]—have explored the pathophysiology of these end-stage lung diseases, specifically the differences between COPD's, while other "omics" studies, particularly metabolomics, have been employed to assess the effectiveness of the NEVLP approach itself.[120] Metabolomics is an emerging field in systems biology that is able to assess and elucidate the biochemical status of an organism through the analysis of small endogenous molecules (metabolites) at a certain period of time.[128] Since changes in small metabolites are a more rapid indicator of an immediate system response, the use of metabolomics may potentially be more advantageous than genomics or proteomics in determining markers of improved lung function or markers of potential graft dysfunction that may emerge over the course of NEVLP.

Previous research has shown that the evaluation of perfusate (Steen^{TM} solution) collected periodically during the NEVLP procedure can provide biomarkers of improved lung function.[120] Although perfusate analysis has been shown to be useful, it is possible to obtain even more information via direct tissue analysis. However, tissue analysis can be impractical due to the complexities associated with organ heterogeneity, the need for various laborious tissue homogenization techniques and the regular collection of biopsies, usually via invasive procedures. Accordingly, this approach is often avoided. In order to overcome the

limitations of typical tissue analysis workflows, *in vivo* solid phase microextraction (SPME) is evaluated herein as a non-exhaustive, minimally invasive alternative sample preparation technique for use in metabolomics analyses of lung tissue during NEVLP. The device's simplicity and size—a coated needle measuring 240 µm in diameter—allows for repeated insertions into the tissue during the time course of the procedure, thereby eliminating the need for multiple tissue biopsies. The use of SPME has previously been reported in various bioanalytical and clinical applications, including tissue sampling and tissue metabolomics applications[56,129–131] ranging from the *in vivo* sampling and quantitation of pharmaceuticals in live fish muscle[129] to the *in vivo* metabolomic fingerprinting of brain tissue in living and moving rats subject to deep brain stimulation.[132] In addition, prior research has also investigated the effectiveness of various coatings for the non-specific global extraction of metabolites, with findings showing that hydrophilic-lipophilic balanced (HLB) coatings are able to provide excellent recovery for a wide range of analytes (more polar as well as non-polar molecules).[57] Thus, SPME is suitable for metabolomics, as the device's biocompatible coating and extraction phase type, allows for the exclusive extraction of small molecules—both hydrophobic and hydrophilic compounds, including lipids, fatty acids, amino acids and other endogenous or exogenous molecules—directly from live complex biological matrices, such as lung tissue, without significantly interfering with the biochemical transformations of the system under study, or adversely affecting the system itself or the sampling device.[133]

In the present study, HLB-coated SPME fibers were used to sample porcine lung tissue *in vivo* during pre-clinical prolonged NEVLP in order to identify potential metabolic markers of lung function, markers of primary graft dysfunction, and/or markers of general organ stress, as well as to monitor other ways in which the lung may have changed during the procedure. The perfusate was also sampled extensively using two types of SPME devices: SPME HLB fibers and HLB thin-film microextraction (TFME). Perfusate was collected periodically during NEVLP and split into three portions: portion one was sampled on-site during NEVLP using SPME HLB fibers that were similar to those used to sample the lung tissue; portion two was snap frozen in dry ice, transported and stored at –80 °C until later sampling in the lab with SPME HLB

fibers; and portion three was snap frozen and stored under the same conditions as portion two until later sampling in the lab with the HLB TFME device. The perfusate samples were processed in this way in order to: 1) evaluate the differences in the information obtained from the tissue and parallel perfusion fluid samples; 2) investigate the changes in the perfusate samples and compare them to the metabolic results reported in prior biomarker studies; 3) assess whether metabolic changes had occurred due to the sample storage procedure, which was consistent with that used in a typical metabolomics workflow (i.e., collecting and storing samples for analysis at a later date); and 4) evaluate the analytical differences between the two types of SPME devices. This multilevel approach will provide insight into whether lung tissue or perfusate samples are sufficient on their own for providing pertinent metabolic information, or whether it is more advantageous to employ a complementary approach that uses both types of samples simultaneously. Furthermore, few studies have reported on metabolome stability under the typical storage conditions used in metabolomics. This study may help in developing and implementing improved strategies for preserving and storing samples for metabolomics processing at a later time. Finally, this study explores whether using both types of SPME devices in conjunction with one another during on-site sample collection may be optimal for obtaining maximum information—for example, using SPME fibers for *in vivo* metabolomics and TFME for *ex vivo* on-site perfusate analysis.

4.3 Materials and Methods

4.3.1 Animals and research ethical approval

The Animal Care Committee at the Toronto General Hospital Research Institute approved the experimental protocol used for male Yorkshire domestic pigs. Full ethics approval was received through the University Health Network (UHN) Research Ethics Board and the University of Waterloo Office of Research Ethics.

4.3.2 Normothermic ex vivo lung perfusion (NEVLP) strategy

A more detailed outline of the NEVLP procedure is provided elsewhere [123]. In this study, the heart of a male Yorkshire domestic pig was initially excised from the heart-lung block at the left atrium post explantation.

After the left atrial (LA) appendage and the pulmonary artery (PA) had been cannulated, the lungs were transferred to the XVIVO™ chamber (Vitrolife, Denver, CO) and connected to the EVLP circuit, which consisted of a centrifugal pump that was responsible for circulating perfusate (Steen™ solution, Vitrolife) through the circuit. The perfusate first passed through a membrane gas exchanger that was connected to a heater-exchanger, wherein it was de-oxygenated and warmed to normothermic conditions over scheduled time intervals. Once the perfusion fluid had reached normothermic conditions, it was passed through a leukocyte filter and then into the lungs—which were ventilated using an ICU type ventilator—via the PA. After passing through the lungs, the perfusion fluid exited via the LA into a hard-shell reservoir adjusted at a specific height to maintain the appropriate pressures. While 4 hours is the usual length of time for NEVLP, a prolonged schedule requiring a total of 19 hours of perfusion was employed during these experiments to assess lung sustainability for gene therapy.

4.3.3 Chemicals and materials

The nitinol wires used as SPME fiber supports were purchased from Confluent (Palo Alto, USA), while the stainless-steel combs used for thin-film microextraction (TFME) were purchased from PAS Technologies (Magdala, Germany). Oasis hydrophilic-lipophilic balance (HLB) 5 µm particles were kindly provided by Waters Corporation, and 45-60 µm HLB particles were obtained from SPE cartridges purchased from Millipore Sigma (Burlington, USA). LC-MS-grade acetonitrile, methanol, and water were purchased from Millipore Sigma, as were the additives, formic acid and acetic acid, and other chemicals, including polyacrylonitrile (PAN), N,N-dimethylformamide (DMF), and hydrochloric acid. A flask-type sprayer was also purchased from Millipore Sigma.

4.3.4 SPME fiber coating methodology

Nitinol wires were measured and cut to 4 cm in length. The dip-coating procedure was carried out using a specialized software-operated dip-coating machine that had been developed in-laboratory, and was consistent with the protocol reported by Gomez-Rios *et al.* [134]. Briefly, the protocol used in this study

consisted of the following steps: first, a slurry of 10% w/v of 5 µm HLB particles suspended in 7% PAN was prepared; next, the fibers were dipped in the slurry to the desired length and then cured for 1 minute at 125 °C; finally, the dipping/curing process was repeated until the final fiber coating dimensions measured 15 mm in length and 40 µm in thickness.

4.3.5 TFME blade coating methodology

Thin-film microextraction devices were prepared according to a well-established spray coating method developed in-laboratory and reported by Mirnaghi *et al.*.[80] First, the stainless-steel blades were etched for 1 hour in concentrated hydrochloric acid and then thoroughly rinsed in deionized water. After rinsing, the blades were dried in an oven for 45 minutes. Next, a slurry consisting of 10% w/v 45-60 µm HLB particles with 25% v/v DMF in PAN solution (7%) was prepared and mixed thoroughly in a flask-type sprayer. The slurry was then sprayed onto each stainless-steel comb individually using a maximum flow of nitrogen gas. After both sides of the comb had been coated, it was cured for 1 minute at 150 °C. The final TFME coating measured 1 cm in length and 0.5 mm in thickness.

4.3.6 Lung and perfusate sampling with SPME fiber

The overall experimental design is graphically represented in Figure 4.1. The 15 mm HLB-coated fibers were initially sterilized/preconditioned in 50:50 methanol/water for at least 30 minutes under static conditions before being exposed to the lung tissue. Once this preconditioning step had been completed, the fibers were inserted into the left lung in triplicate for an extraction time of 30 minutes. The fibers were then removed from the lung, rinsed manually in water for 5 s, and wiped with a kim-wipe to remove any loosely adhered biological fragments. Next, the fibers were placed in empty 300 µl vials and immediately snap frozen in dry ice for transportation to the laboratory where they were desorbed in 137.5 µL of 40:30:30 v/v/v methanol/acetonitrile/water. Water was then added to the extracts to obtain a 50:50 aqueous/organic ratio, as this ratio would be more amenable to the initial chromatographic conditions. A total of 2 pigs underwent lung sampling during NEVLP.

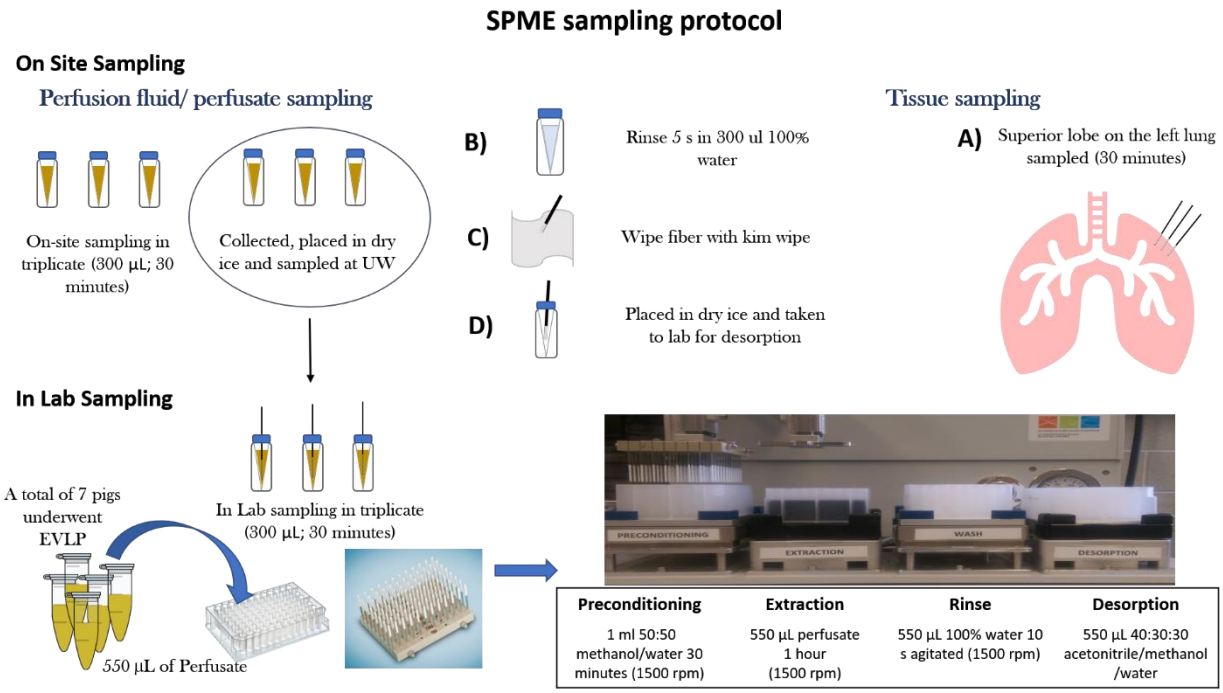

Figure 4.1 Graphical representation of overall experimental design. The SPME sampling protocol is demonstrated in the center under "SPME sampling protocol" whereby steps B), C) and D) represent the rinsing, wipe with Kimwipe and dry ice storage after *in vivo* SPME lung sampling events or on-site extraction of perfusate. Perfusate samples were split into three portions: the first portion was sampled on-site using SPME fibers (in parallel with lung sampling events); the second portion (collected during lung sampling events) was stored in dry ice and transported to the lab for in-laboratory sampling with SPME fibers; the third portion (collected hourly) was stored in dry ice and transported to the lab for in-laboratory sampling with TFME.

Lung sampling was performed during cold ischemia (CIT) before the start of NEVLP, and at 1 hr, 3 hr, 5 hr, 8 hr, 11 hr, 12hr and 13 hr after the start of NEVLP (denoted by blue stars in Figure 4.2B). In addition, perfusate samples were collected hourly by clinicians and separated into three portions for analysis. The first portion (1500 µL) was sampled on-site (in-hospital) in triplicate (3-300 µL portions) for 30 minutes under static conditions using the SPME fibers and the above-described protocol for rinsing, storage, and desorption. On-site SPME fiber sampling was only performed using perfusate samples that were acquired at the same time the lung sampling was taking place. The second portion (1500 µL) was snap frozen in dry ice for transportation to the laboratory. These samples were later prepared using SPME fibers, at the same volume (300 µL) as used in-hospital in triplicate and using the same sampling protocol as described earlier in this section. Only perfusate samples obtained during lung sampling were used for the in-laboratory

extractions with the SPME fibers. TFME was used to perform extractions on the third portion of perfusate samples. This process is described in more detail in *section 4.3.7 "Perfusate sampling with TFME"*.

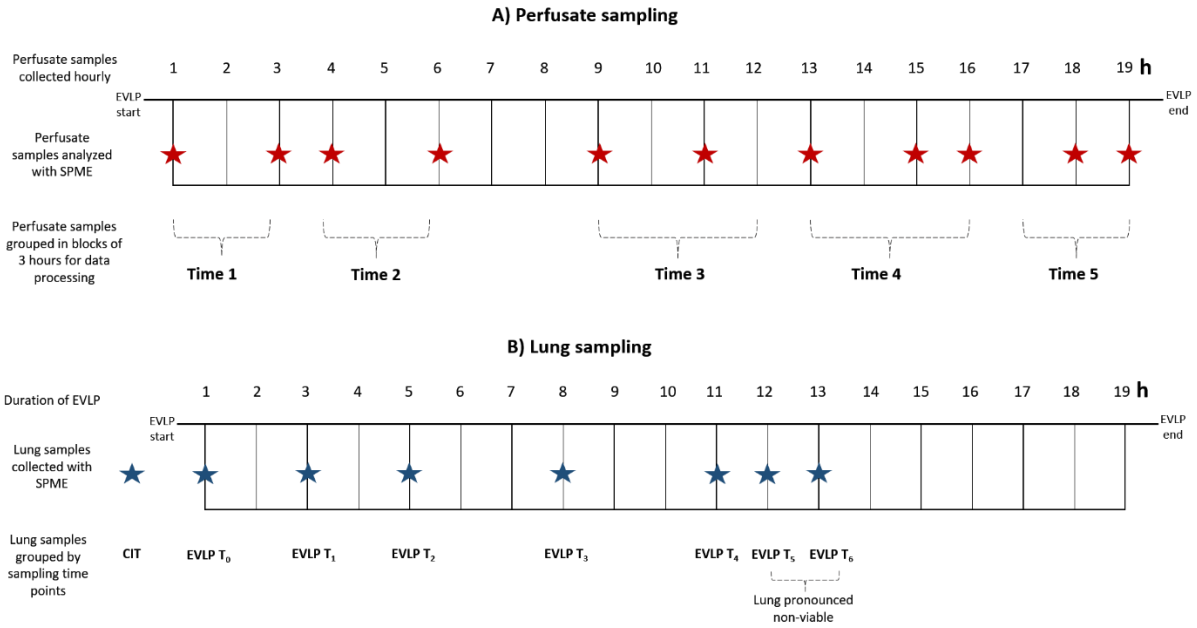

Figure 4.2 Prolonged normothermic ex vivo lung perfusion (NEVLP/ EVLP) conducted over 19 hours. A) Perfusate sampling schedule during NEVLP for samples prepared using thin-film microextraction (TFME). Perfusate samples were collected hourly for 7 pig lungs, with red stars denoting samples that were used for further analysis. The samples prepared via TFME were collected at 1h, 3h, 4h, 6h, 9h, 11 h, 13h 15h, 16h, 18 h, and 19h after the start of NEVLP; the organ had been pronounced non-viable by the last two sampling points. Time 1 to Time 5 illustrate the 3-to-4 hour blocking strategy used to group the collected samples for data processing. B) Lung sampling schedule during NEVLP. SPME fiber lung sampling were conducted for 2 pig lungs. The blue stars denote the time points at which SPME fiber lung sampling events took place. Lung were sampled before the start of EVLP and at 1h, 3h, 5h, 8h, 11 h, 12h and 13h after the start of NEVLP.

4.3.7 Perfusate sampling with TFME

Perfusate samples were collected by clinicians hourly during the 19-hour EVLP procedure and immediately snap frozen in liquid nitrogen as per institutional practice at Toronto General Hospital. These samples, which were later transported to the laboratory in dry ice, constituted the third portion of perfusate samples. From the 19 perfusate samples collected per animal (7 animals in total), a few samples at specific time points (denoted by red stars in Figure 4.2A) were selected from each case for further analysis, with 550 µL of each selected sample being placed into a 96-well plate. Prior to performing the extractions, the TFME

brush device, which is compatible with 96-well plates, was preconditioned for 30 minutes in 50:50 v/v methanol/water at 1500 rpm followed by a quick 10 s rinse in water at 1500 rpm. After preconditioning, the TFME brush device was inserted into the samples for 30 minutes at 1500 rpm and a temperature of 25 °C. The blades were then rinsed in water for 10 s at 1500 rpm and desorbed in 550 µL of 40:30:30 v/v/v methanol/acetonitrile/water for 1 hour at 1500 rpm. A Concept-96 autosampler (PAS technologies) was used to automate the above-described SPME sample preparation process. This method was used to perform extractions from perfusate samples obtained from a total of 7 pigs subjected to NEVLP.

4.3.8 Instrumental analysis

Analysis of the extracts obtained from the lung and perfusate samples was conducted via liquid chromatography (LC) coupled to high-resolution mass spectrometry (HRMS). Chromatographic separation was achieved on a 10 cm x 2.1 mm (5 µm particle size) Discovery HS F5-3 (PFP) column, which was protected by a 2 cm x 2.1 mm (3 µm particle size) guard column (Millipore Sigma). A 40-minute gradient elution was employed using a Thermo Fisher Scientific Accela binary pump and autosampler. Mobile phase A consisted of water, while mobile phase B consisted of acetonitrile. For positive and negative mode polarity, 0.1% formic acid or 1mM acetic acid were added, respectively. A Thermo Fisher Scientific Exactive mass spectrometer equipped with an Ion Max heated electrospray ionization (HESI II) source was used to perform acquisition in high resolution (50, 000) mode, with a balanced automatic gain control (AGC), an injection time of 100 ms, and a scan range of 100 – 1000 m/z.

A pooled quality control (pooled QC) was prepared for each set of samples (fibers vs TFME) by pooling 10 µL of each sample in a single vial. These pooled QCs were injected every 10 samples to ensure instrumental stability for the duration of the acquisition process. Samples were run completely randomly for both sets of data to avoid confounding the resulting data with any instrumental variation.

4.3.9 Data pre-processing

The raw LC-MS data files were first converted into mzXML files via MSConvert[106] before being pre-processed using the XCMS software package[107] in RStudio with an in-laboratory developed script.[108] The IPO package[109] used the pooled QC samples to optimize the data pre-processing parameters used to perform peak alignment, retention time correction, normalization, peak filling, and peak picking. The paired mass difference (PMD) function was also employed to reduce the number of redundant features that might be investigated.[135] This function was used in combination with other filtering methods to remove features with: a) low spray stability or high variation in the pooled QCs (features in the pooled QCs with RSDs > 30% were eliminated); b) signal intensities that were similar to those of the blank fibers and blank blades (features with a pooled QC:blank fiber/blank blade ratio of < 5 were eliminated); c) a similar signal intensity to the blank solvent (features with a pooled QC:blank solvent ratio of < 5 were eliminated); and d) a similar signal intensity to the pure steen solution (features with a pooled QC:steen solution ratio at a baseline of < 5 were eliminated). These filtering methods substantially reduced the total number of features included in subsequent chemometric analyses, thereby improving data manageability and mitigating potential artefacts. The extracted peaks were annotated using the xMSannotator Integrative Scoring Algorithm in conjunction with the human metabolome database (HMDB).[110] For metabolite profiling, unique and multiple features with medium-to-high confidence annotations were selected. xMSannotator annotated these features based on their intensity profiles, retention times, mass defect, and the isotope/adduct patterns of their peaks. For high-confidence matches, the following requirements are satisfied: a non-zero score for database matching, user specified required adducts are present (i.e. M+H or M-H for positive and negative modes respectively), N, O, P, S/C ratio checks, hydrogen/carbon ratio check, abundance ratio checks for isotopes, multimers, and multiply charged adducts. For medium-confidence matches, pathway level correlation is satisfied.

4.3.10 Data pre-treatment, data processing and model validation

Metaboanalyst was the sole platform used to perform a range of multivariate and univariate statistical analysis after pareto scaling. The original unbiased structure of the data was analyzed using principal

component analysis (PCA) in order to evaluate the stability of the instrumental acquisition via the pooled QCs, and to assess true patterns in the data structure that could be further investigated via other supervised multivariate methods. Orthogonal Projections onto Latent Structures Discriminant Analysis (OPLS-DA) was used to further compare two groups in order to identify features of differentiation, while Partial Least Squares Discriminant Analysis was used to identify features of discrimination among three or more groups. Given that the obtained data had a high degree of dimensionality—that is, the number of features was substantially larger than the number of samples—cross validation techniques were used to confirm model reliability, as well as the stability of the features the model deemed to be important. To this end, quality parameters such as goodness of fit (R^2) and predictability (Q^2) were assessed. Cross validation is particularly important for supervised methods, as it ensures that separation between groups is based on significant differences as opposed to noise, which is a common pitfall of these techniques. Methods such as Leave One Out Cross Validation (LOOCV), *k*-fold cross validation, and permutation testing were performed within their respective limitations with respect to the sample size. A t-test was used to perform univariate analysis of changes in individual features between two time groups, while a non-parametric analysis of variance (ANOVA), a Kruskal Wallis test, was used to examine these changes among three or more time groups. In addition, parametric and non-parametric univariate analyses were employed based on the limitations of the sample or the feature size using a false-discovery-rate adjusted p-value of 0.05. Since the selection of the appropriate method was based on the distribution of the data being investigated, non-parametric analysis was used most often, as no assumptions were made with respect to the data being normally distributed. Finally, heat maps were also used to visualize the data in order to find dysregulated features across the groups. This approach was generally employed in the event of a failed cross-validated model or when statistically insignificant features were deemed to be of interest.

4.4 Results

4.4.1 Rationale and data analysis

A total of 2 pigs underwent lung sampling whereby for the first pig, the lung was sampled in triplicate at all time points, while for the second pig, lung was only sampled during the first two sampling points (CIT and NEVLP at 1 hr) and at the end of NEVLP (NEVLP at 12 hr). While a total of 19 hours was the predetermined NEVLP schedule, at 12 hr, the lung was pronounced non-viable. The relative lack of lung sampling for the second pig, as well as the lack of total animals for this aspect of the study (lung sampling with SPME fibers), was due to unexplained and extensive lung damage sustained during NEVLP and other unforeseen surgical and research circumstances. However, a total of 7 NEVLP cases were used for perfusate sampling with TFME.

The lung samples from both pig cases were grouped based on the time point at which they were collected during NEVLP. For example, samples collected during cold ischemic time for both pig 1 and pig 2 (CIT) were assigned to one time group, while samples collected in the first hour of NEVLP—NEVLP at 1hr (EVLP t_0 as outlined in Figure 4.2B)—were assigned to a separate time group, and so forth. See Figure 4.2B for further details on the grouping of lung samples collected via SPME fibers. Many of the SPME fiber time groups only contained a small number of samples (3-6 samples, 3 technical replicates, 2 biological replicates) since the number of lungs sampled with these devices was small (2 cases), and the number of lungs sampled to the completion of the NEVLP procedure was even smaller (1 case). This is an unfavorable statistical circumstance and limitation of the study.

Although perfusate samples were collected on an hourly basis throughout the 19-hour NEVLP process for 7 pigs, they were ultimately processed in blocks/groups of 3 hours due to the preliminary nature of the study, and for sake of practicality with regards to instrumental analysis. Grouping perfusate samples in 3-hour time blocks was advantageous because it would be easier to validate potentially important features, as these features would be persistently present in the lung during NEVLP. As such, each group contained

samples that were obtained within a 3-hour time block. For example, group 1, otherwise referred to as Time 1 in Figure 4.2A, contained perfusate samples from 7 cases that were collected within 1-3 hours after the start of NEVLP. See Figure 4.2 for further details on groupings for perfusate samples. While this data processing design limits the capturing of possibly important short-lived species, this compromise was implemented for improved data manageability.

The study design also allowed for the analysis of overall metabolite stability and sample storage by enabling a comparison of samples collected and sampled on-site and those that were transported back to the laboratory for further analysis. The perfusate samples collected during lung sampling were essential for this analysis, as a portion of these samples were collected and sampled on-site, while another portion was transported back to the laboratory for sampling.

4.4.2 Unsupervised multivariate analysis

The Principal Component Analysis (PCA) in Figure 4.3 shows that the pooled QCs for both sets of analyses are clustered tightly on the respective plots. While the pooled QCs for the perfusate samples (Figure 4.3A, shown in red) are located in the middle of the time groups—which is the most common trend observed for these types of analyses—the pooled QCs for the lung samples (Figure 4.3B, black dots) are closer to a particular time group. This clustering behavior may be the result of some features (metabolites) from this time group exerting a greater influence on the overall variation of the data, possibly due to a higher or lower relative abundance of certain features in comparison to other groups. Nevertheless, tight clustering of the pooled QCs implies instrumental stability throughout data acquisition, which means that the plot captures true and reliable patterns in the data structure. PCA also revealed similar patterns of distinct transitions from the initial time groups through to the final time group at the end of NEVLP for both perfusate (Figure 4.3A) and lung samples (Figure 4.3B). As can be seen in Figure 4.3A Figure 4.3B, the biggest differences occur between the initial and final time groups, while time groups directly preceding or following one another exhibit some graphical overlap.

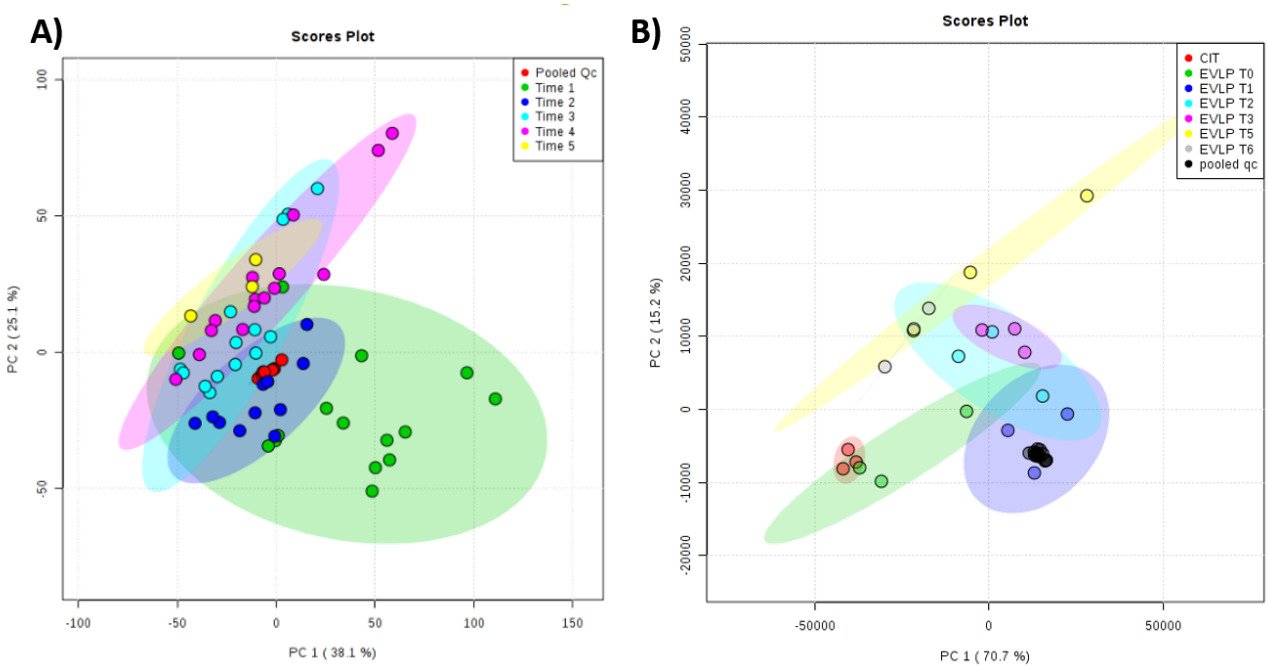

Figure 4.3 Principal Component Analysis (PCA). A) PCA (PC1: 38.1%; PC2: 25.1%) of the perfusate samples collected during NEVLP and prepared via TFME. Samples grouped by Time 1, Time 2, Time 3, Time 4, and Time 5 are represented by green, blue, turquoise, pink, and yellow, respectively. Each time point is comprised of a progressive 3-hour time block throughout the NEVLP process. B) PCA (PC1: 70.7%, PC2:15.2%) of the lung sampling events with the SPME fibers. The seven time groups—cold ischemic time (CIT), EVLP t_0, EVLP t_1, EVLP t_2, EVLP t_3, EVLP t_5 and EVLP t_6—are represented by red, green, blue, turquoise, pink, yellow, and gray, respectively. Each time point represents lung samples collected prior to the start of NEVLP, and 1h, 3h, 5h, 8h, 11h, 12h, and 13 h after the start of NEVLP. The pooled QCs are represented by red and black on the plot for the perfusate and lung samples, respectively.

Interestingly, for both sample types, the differences between groups becomes less discrete after Time Group 3. Time Group 3 is denoted by EVLP T_2 for lung samples (Figure 4.3B) and Time 3 for perfusate samples (Figure 4.3A), which correspond to 5 and 12 hours after the start of perfusion, respectively (Figure 4.2). Furthermore, the 7-hour difference in the onset of this apparent equilibrium between lung and perfusate samples may indicate that tissue sampling provides more accurate insight into when certain changes start to manifest in the organ. This 7-hour time lag can be explained by differences in the processes by which metabolites are diffused from the lung to the bulk of the perfusion fluid and from the lung directly to the SPME fiber exposed in the tissue.

The overlap between the Time 4 and Time 5 clusters for perfusate samples suggests that additional hours of perfusion may neither improve nor deteriorate the state of the organ after a certain point; that is, after a certain point, it appears as though the rate of change reaches a maximum and an equilibrium is established. In general, the decrease in intergroup variation from the initial time group to the last also suggests that all pig lungs, regardless of their initial states—as evidenced by the larger intergroup variation in Time 1 for perfusate samples—undergo the same distinct changes.

4.4.3 Supervised multivariate analysis

Partial least squares discriminant analysis (PLS-DA) was used for both sets of data in order to identify statistically relevant discriminatory features from the initial NEVLP conditions through to the final conditions. Permutation cross validation (CV) was used to validate the PLS-DA models. Permutation CV aims to validate the model by systematically randomly assigning the known class labels to different random samples and comparing the separation generated with the randomly assigned classification with the original data classification. Both PLS-DA models (perfusate sampled with TFME and lungs sampled with SPME fibers) passed permutation CV (2000/1000 permutations for perfusate and lung respectively), yielding significant ($p < 0.05$) quality parameters for the original models (Figure 4.4A and Figure 4.4B for perfusate and lung samples, respectively). This means that the observed statistics for the original data classifiers (groups) produced significant separation compared to the distribution of the permuted data sets. The PLS-DA model for the perfusate samples yielded quality parameters of $R^2 = 0.82$ and $Q^2 = 0.69$ after a 10-fold cross validation with an optimal of 4 latent components, while the lung samples yielded quality parameters of $R^2 = 0.96$ and $Q^2 = 0.64$ after LOOCV with an optimal of 8 latent components. Although the quality parameters for the lung samples fall outside the desired range threshold (0.2 units apart), it is important to note that the number of samples per group for this data set was quite small in comparison to the perfusate samples. Nonetheless, Q^2 for this data set was still above the acceptable limit of 0.5.

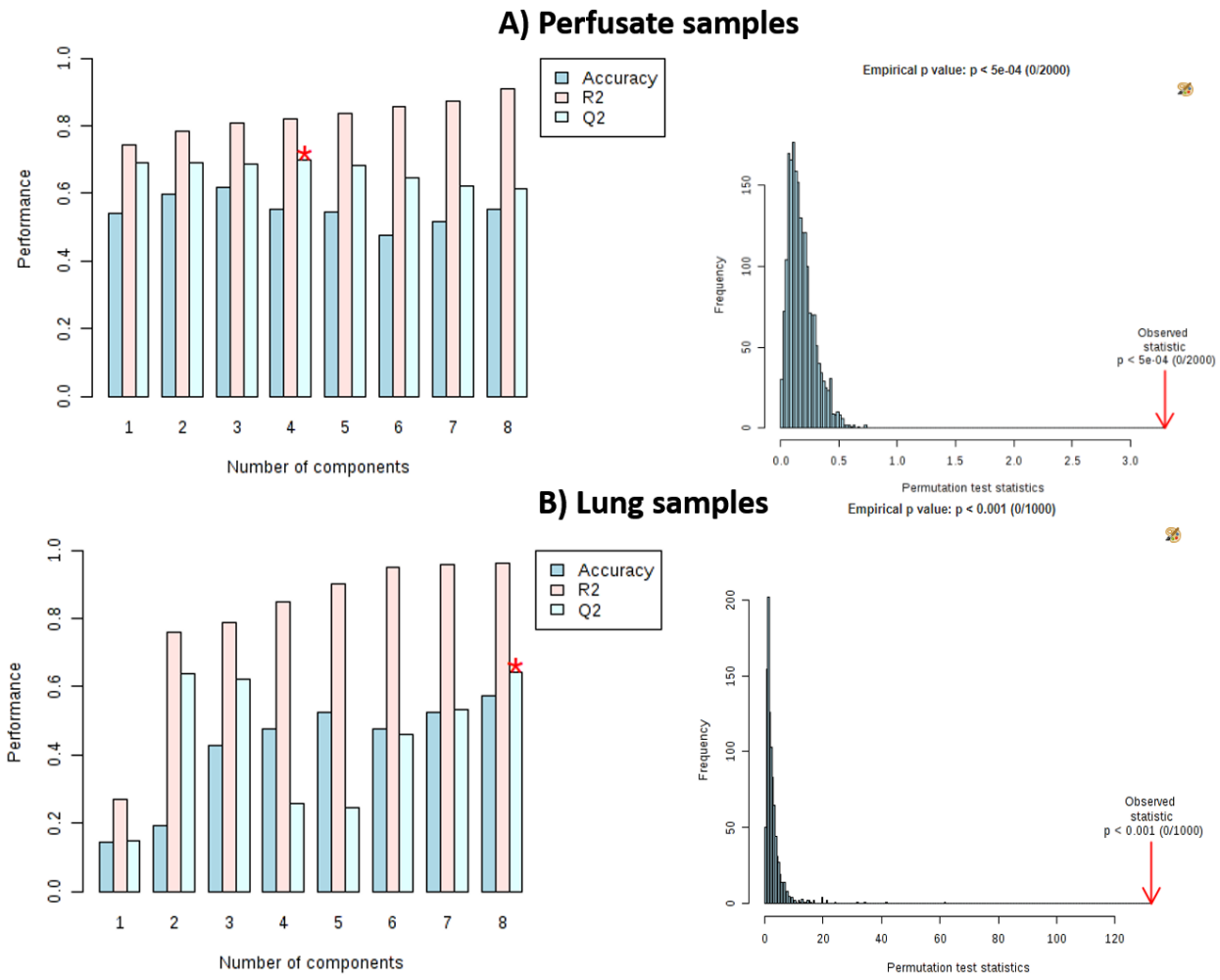

Figure 4.4 Cross validation (CV) of PLS-DA models via k-fold CV, *leave one out cross validation (*LOOCV*)*, and permutation. A) CV for perfusate samples. On the left side, the optimized number of latent variables for a 10-fold CV was found to be 4 (denoted by a red star) with quality parameters $R^2 = 0.82$ and $Q^2 = 0.69$. B) CV for lung samples. On the left side, 8 latent variables (denoted by red star) were found to be the optimum for a LOOCV with $R^2 = 0.96$ and $Q^2 = 0.64$. On the right side for both sets of data, the observed statistics for the original data set was $p < 0.0005$ and $p < 0.001$ for perfusate and lung samples, respectively (highlighted by the red arrows).

Only features with VIP scores > 1.5 for each component up until the optimized number of latent components were investigated since these are features found to influence the discriminatory patterns observed in the data. Therefore, 100 and 200 features were assessed for the perfusate collected on site and lung samples, respectively. See Table 4.1 and Table 4.2 for the list of VIPs obtained from multivariate analysis and their respective statistical and LC-HRMS parameters for perfusate and lung samples. Tentatively identified metabolites or features significant changing (increase or decrease with respect to any time point over the

duration of NEVLP) over the time course of NEVLP (Time 1 to Time 5) for lungs sampled with SPME fibers and perfusate sampled with TFME are found in Table 4.3 and Table 4.4 respectively and are discussed in more detail in *section 4.5.1 "Statistically significant metabolites and their biochemical relevance".*

Table 4.1 VIPS > 1 obtained from validated PLS-DA model for perfusate samples collected during NEVLP. Shown are statistically significant features changing from Time 1 to Time 5, all time points inclusive. Data from positive mode analysis with a mass tolerance of less than or equal to 5 ppm.

Compound classification	Feature parameters				Tentative ID
	m/z	Retention time (min)	Adduct	Average VIP score	
Important features also found via METLIN and annotation	375.2164	13.2	$[M+H]^+$	12.5	Resolvin D1, HDOPA
	226.0807	14.3	$[M+Na]^+$	3	Alanyl-asparagine
	324.059	10.1	$[M+H]^+$	2.4	5'-CMP, 2',3'-Cyclic UMP
	255.087	3.75	$[M+H]^+$	1.9	3-Hydroxy-DL-kynurenine
	146.0039	9.3	$[M+Na]^+$	1.7	Taurine
Other endogenous compounds found via METLIN	375.2164	13.2	$[M+H]^+$	12.5	Prostaglandin E1
	323.1701	9.8	$[M+NH_4]^+$	8.0	Threoninyl-tryptophan
	378.3213	15.7	$[M+Na]^+$	5.3	Arachidonoyl-EA(d8)
	359.2215	14.3	$[M+H]^+$	5.3	4S-Hydroxy-8-oxo-(5E,9Z,13Z,16Z,19Z)-neuroprostapentaenoic acid-cyclo[7S,11S], 17Beta-hydroxyandrost-4-ene-3,11-dione propionate
	321.1849	14.5	$[M+H]^+$	3.9	4,7,10,13,16-Docosapentaynoic acid
	175.1191	1.3	$[M+H]^+$	2.9	D-Arginine
	750.429	13.2	$[M+Na]^+$	2.5	PS(12:0/20:4(5Z,8Z,11Z,14Z))

Table 4.2 VIPS > 1 obtained from validated PLS-DA model for SPME fiber lung sampling events during NEVLP. Shown are statistically significant features changing from EVLP t_0 to EVLP t_5, all time points inclusive. Data from positive mode analysis.

Compound classification	Feature parameters				Tentative feature ID
	m/z	Retention time (min)	Adduct	Average VIP score	
Important features found via METLIN and annotation	247.1077	12.29	$[M+H]^+$	21.8	N-acetyltryptophan
	166.0863	9.7	$[M+H]^+$	6.0	Phenylalanine
	226.0808	19.6	$[M+Na]^+$	6.2	Alanyl-asparagine
	269.0897	12.29	$[M+Na]^+$	5.7	N-acetyltrptophan
	205.0974	12.29	$[M+H]^+$	4.4	Tryptophan
	132.102	7.6	$[M+H]^+$	3.6	L-isoleucine
	182.0813	7.6	$[M+H]^+$	2.4	L-tyrosine
	147.0764	1.4	$[M+H]^+$	2.0	L-glutamine
	156.0768	2.1	$[M+H]^+$	1.2	Histidine
Other Endogenous compounds found via METLIN	240.0965	23	$[M+Na]^+$	13	N-a-acetylcitrulline, Alanyl-glutamine, 5-Hydroxysebacate
	184.0577	12.3	$[M+Na]^+$	3.8	DL-2-aminoadipic acid, N-methylglutamic acid
	137.0458	1.6	$[M+H]^+$	2.9	Hypoxanthine
	270.093	12.2	$[M+NH_4]^+$	2.1	Cysteinl-methionine
	209.0543	19.5	$[M+Na]^+$	1.9	AMPA
	269.0881	1.6	$[M+H]^+$	1.9	Inosine,
	156.0768	2.1	$[M+NH_4]^+$		Urocanic acid
	268.1041	7.6	$[M+H]^+$	1.5	Adenosine, Deoxyguanosine
			$[M+Na]^+$		Glutamyl-valine

4.4.4 Univariate analysis

Univariate analysis was conducted via a Kruskal Wallis Test in order to evaluate changes among individual features throughout the NEVLP procedure. The results of this analysis yielded (Figure 4.5) upwards of 2000 statistically significant features for perfusate samples, and more than 1700 statistically significant features for lung samples.

Figure 4.5 Univariate analysis via *a non-parametric* analysis of variance (ANOVA)–*Kruskal Wallis test*. A false discovery rate (FDR) adjusted p-value of 0.05 was used as the cut-off for the selection of statistically significant features. Statistically significant features are highlighted in red, while non-significant features are highlighted in blue. *On the* right, shows the patterns over time for a single statistically significant feature.

4.5 Discussion

In the current study, two SPME formats were employed for the metabolomic fingerprinting of lung and perfusate samples sampled over the course of NEVLP. Minimally invasive *in vivo* SPME fibers were directly introduced into the lung for the purpose of selectively extracting small endogenous molecules in order to gain insight into ongoing biochemical processes originating specifically in the tissue over the course of NEVLP (*in vivo* SPME). Additionally, SPME fibers were also used to extract metabolites from fresh perfusate samples collected at the same time as the lung sampling events (on-site *ex vivo* SPME), as well as for a portion of perfusate samples that were snap frozen and transported back to the laboratory for further analysis (in-lab *ex vivo* SPME). Furthermore, TFME was also used to perform extractions on a portion of the samples that had been snap-frozen and transported to the laboratory (in-lab *ex vivo* TFME). This multi-tiered approach to collecting perfusate samples and the use of various devices to perform extractions yielded important information about metabolite alterations during NEVLP and the biochemical stability of the metabolome under typical storage and sample handling procedures (Table 4.4).

4.5.1 Statistically significant metabolites and their biochemical relevance

The features that were putatively identified via annotation and the variables of importance (VIP > 1.5) selected from/indicated by multivariate analysis (PLS-DA) show that it is possible to identify the presence of several endogenous metabolites related to the modulation of immune responses in a living system through *in vivo* SPME and on-site *ex vivo* SPME sampling at particular time-points during lung perfusion. Notably, multiple bioactive lipids (oxylipins) derived from polyunsaturated fatty acids (PUFAs) with either pro-inflammatory or anti-inflammatory properties were extracted with the use of SPME fibers over the course of NEVLP (Table 4.3). For instance, neuroprostanes, which are prostaglandin-like compounds formed *in vivo* via the peroxidation of fatty acids (primarily docosahexaenoic acid), were detected in lung tissue and fresh perfusate extracts during the first hours of lung perfusion. These oxygenated essential fatty acids possess potent anti-inflammatory properties and are considered to be biomarkers of oxidative stress, as well as inhibitors of macrophage activity.[136,137] The presence of neuroprostanes was observed up to the

5th hour of NEVLP in lung tissue and up to the 8th hour in perfusate samples, after which the presence of other signaling molecules related to the metabolism of prostaglandins began to emerge. Specifically, the number of prostaglandin-derived compounds began to increase significantly during the 3rd hour of NEVLP, with a tremendous number of these compounds being reached in the 11th-12th hour (Table 4.3). During this time period, several pro-inflammatory tissue components, putatively identified as prostaglandin F3α and prostaglandin E2, were extracted from the lung tissue and perfusate samples. Conversely, prostaglandin D2 and its derivatives, which have been previously shown to play an anti-inflammatory role in acute lung inflammation, were also detected in the analyzed matrices during this time period.[138] These results strongly indicate pro-inflammatory and anti-inflammatory responses in lungs, especially in the later hours of lung perfusion. However, since particular prostaglandins may produce various, and sometimes opposite, effects in different tissues, the exact role of the detected prostaglandins requires further investigation via the targeted analysis of detected metabolites and also their respective receptors in lung tissue.

In addition to prostaglandins, other eicosanoids, mainly leukotrienes and, to a lesser extent, lipoxins and thromboxanes, were also observed during NEVLP. Leukotrienes are potent local mediators of immune hypersensitivity and inflammation, and, similar to prostaglandins, the highest number of these compounds and their derivatives was detected in both lung tissue and fresh perfusate samples in the 11-12th hour of lung perfusion (Table 4.3), thus highlighting the intense immune system activity during this particular time-point of lung perfusion. Moreover, various oxygenated lipid metabolites, including hydroxyeicosatrienoic acids (e.g., 11,12-DiHETrE and 5,6-DHET) and epoxy fatty acids (e.g., 9(10)-EpODE), were formed during lung perfusion, with significantly higher numbers of these metabolites being observed in lung tissue during the 11-12th hour of NEVLP. However, the lab extractions performed on the stored perfusate samples with SPME probes and TFME revealed a decrease in the number of these signaling lipid molecules (Table 4.4). These results are consistent with the findings of recent research on the effectiveness of performing extractions from rat brain *in vivo* and post-mortem.[139] Specifically, the findings of the present research show that *in vivo* SPME is more effective for sampling living systems, such as lungs undergoing NEVLP, as it is

able to provide insight into the true oxylipin profile of the lung that cannot be achieved via the *ex vivo* analysis of stored samples. Overall, intense lipid peroxidation may occur under many conditions associated with pro- and anti-inflammatory responses within an organism; therefore, the elucidation of the mechanisms that drive these processes could enable the development of novel or improved targeted treatments for inflammatory diseases or processes.

Other compounds with significant anti-inflammatory and anti-apoptotic activities were also extracted using SPME fibers. In particular, resolvins and neuroprotectins, which belong to a group of autacoids possessing strong *in vivo* immunoregulatory activity, were detected in lung tissue and perfusate samples during the first hours of lung perfusion. As previously reported, these new mediator families act locally and may strongly affect the action of the immune system.[140] Resolvins are formed from omega-3 essential fatty acids and occur in trace amounts in tissues; nonetheless, the application of SPME probes facilitated their successful extraction. In addition, while neuroprotectins were detected in live tissue and from perfusate extracts during sampling conducted on-site in-hospital, these compounds were barely detectable in the stored perfusate samples (Table 4.4), which may be due to their lability and/or short lifetime. As such, these results suggest that neuroprotectin levels should be monitored using preferably *in vivo* tools. Overall, the presence of pro-inflammatory endogenous compounds may indicate ongoing inflammatory processes in the lung during NEVLP; however, these compounds are efficiently regulated or balanced by the production of specialized mediators that stimulate anti-inflammatory responses. Along with resolvins and neuroprotectins, lipoxins are among the most potent antagonists of endogenous inflammation, and, as novel chemical mediators, they have been considered potential targets in the development of new approaches to treating inflammation-related diseases.

The use of SPME fibers to directly sample lung tissue and perfusate samples during lung perfusion enabled the monitoring of changes in the number and composition of other endogenous molecules, such as amino acids, acyl carnitines, steroid hormones, purines, and pyrimidines (Table 4.3). Moreover, on-site *in vivo*

sampling of lung tissue and perfusate samples revealed the presence of oleamide, which is a fatty acyl amide that has previously been reported as a potential biomarker for predicting primary graft dysfunction (PGD 3) during lung transplantation[120] (Table 4.3). In contrast, this compound was scantily detected in the stored perfusate extracts sampled via TFME, which suggests that its stability is negatively affected during storage (Table 4.4). Acyl carnitines, which are endogenous compounds related to fatty acid metabolism, were also extracted from lung tissue, the perfusate samples collected on-site during NEVLP, and the stored perfusate samples. These compounds play a crucial role in the β-oxidation of fatty acids, which is an alternative pathway for energy production in the tissues when the supply of glucose is insufficient to maintain a normal level of energy. Elevated levels of these compounds may be related to inefficient mitochondrial importation of fatty acids by carnitine-acylcarnitine shuttle and could indicate metabolic disorders. However, decanoylcarnitine—a metabolite in carnitine metabolism that is involved in lipid catabolism and energy production and has previously been proposed as a marker of PGD3 that could improve donor lung selection and the outcomes of lung transplantation—was present solely in the stored perfusate samples. On the contrary, other acyl carnitines, including oxo (keto) and hydroxy fatty acids, were detected during lung perfusion, with significant increases in the number of those compounds during the 3rd hour of NEVLP. In addition, the occurrence of malonylcarnitine in lung tissue from the 3rd hour of NEVLP onwards may suggest disruptions in fatty acid oxidation caused by the impaired entry of long-chain acylcarnitine esters into the mitochondria.

Table 4.3 A comparison of unique features annotated by HMDB with medium-to-high confidence matches obtained by lung sampling and on-site perfusate sampling during NEVLP

	CIT	1st hour		3rd hour		5th hour		8th hour		11th-12th hours		13th-14th hours	
	LUNG_*in vivo*	LUNG_*in vivo*	PERFUSATE_on site	LUNG_*in vivo*	PERFUSATE_on site	LUNG_*in vivo*	PERFUSATE_on site	LUNG_*in vivo*	PERFUSATE_on site	LUNG_*in vivo*	PERFUSATE_on site	LUNG_*in vivo*	PERFUSATE_on site
amino acids	N-Acetylhistamine	N-Acetylhistamine	L-Phenylalanine	L-Histidine	N-Acetylhistamine	L-Histidine	N-Acetylhistamine	L-Histidine	L-Histidine	N-Acetylhistamine	L-Tryptophan	N-Acetylhistamine	L-Histidine
	DL-Glutamate	L-Cystine	L-Tryptophan	N-Acetylhistamine	N-acetyltryptophan	L-Tryptophan	L-Tryptophan	L-Tryptophan	N-Acetylhistamine	L-Tryptophan	L-Kynurenine	Kynurenic acid	N-Acetylhistamine
	L-Glutamic acid	L-Asparagine	Kynurenic acid	L-Tryptophan	Indoleacetyl glutamine	L-Kynurenine	Indoleacetyl glutamine	Indoleacetyl glutamine	L-Glutamine	Indoleacetyl glutamine	L-Glutamine	L-Glutamine	L-Kynurenine
	L-4-Hydroxyglutamate semialdehyde	L-Threonine	L-Leucine	L-Kynurenine	L-Glutamic acid	L-Glutamic acid	L-Glutamine	Quinaldic acid	L-Glutamic acid	Quinaldic acid	L-Glutamic acid	L-Glutamic acid	Indoleacetyl glutamine
	N-Methyl-D-aspartic acid	L-Proline	L-Isoleucine	Indoleacetyl glutamine	L-Glutamine	L-Glutamic acid	L-Glutamic acid	L-Glutamine	L-Tryptophan	L-Kynurenine	Pyroglutamic acid	L-Phenylalanine	2-Aminomuconic acid
	O-Acetylserine	L-Glutamine	L-Methionine	L-Glutamic acid	Pyroglutamic acid	Pyroglutamic acid	Pyroglutamic acid	L-Lysine	N-acetyltryptophan	L-Glutamic acid	L-Threonine	L-Methionine	L-Glutamine
	N-Undecanoylglycine	L-Arginine	L-Arginine	Pyroglutamic acid	L-Valine	D-Arginine	L-Proline	L-Phenylalanine	L-Kynurenine	D-Glutamic acid	L-Proline	L-Cystine	Pyroglutamic acid
	Tetracosanoylglycine	L-Glutamic acid	L-Cystine	Gamma-Glutamyltyrosine	L-Cystine	L-Valine	L-Phenylalanine	Ne,Ne dimethyllysine	Indoleacetyl glutamine	L-4-Hydroxyglutamate semialdehyde	L-Cystine	L-Lysine	L-Lysine
	N-Nonanoylglycine	5-Aminopentanamide	L-Proline	L-Leucine	L-Lysine	L-Leucine	Capryloylglycine	L-Leucine	L-Leucine	O-Acetylserine	N(6)-(Octanoyl)lysine	L-Proline	L-Phenylalanine
		Creatine	L-Tyrosine	L-Isoleucine	Creatinine	L-Arginine	Tridecanoylglycine	L-Isoleucine	L-Phenylalanine	N-Acetylserine	L-Methionine	L-Tyrosine	L-Leucine
		Creatinine	L-Glutamic acid	L-Phenylalanine	N-Acryloylglycine	L-Isoleucine	N-Undecanoylglycine	L-Methionine	Pyroglutamic acid	Creatinine	L-Arginine	Creatine	L-Isoleucine
		N-Decanoylglycine	L-alpha-glutamyl-L-hydroxyproline	D-Serine	Tridecanoylglycine	L-Phenylalanine	N-Nonanoylglycine	L-Cystine	L-Isoleucine	N-Undecanoylglycine	Creatine	N-Undecanoylglycine	N-(5-Methyl-3-oxohexyl)alanine
		N-Nonanoylglycine	Creatine	L-Methionine	N-Decanoylglycine	NNAL-N-glucuronide	Palmitoylglycine	L-Asparagine	L-Methionine	Tridecanoylglycine	Creatinine	N-Acryloylglycine	L-Arginine
		Palmitoylglycine	N-Undecanoylglycine	L-Cystine	Palmitoylglycine	N-Acetyl-S-(N-methylcarbamoyl)cysteine	N-Acryloylglycine	L-Threonine	L-Arginine	Tricosanoylglycine	N-Undecanoylglycine	Tridecanoylglycine	L-Tyrosine
			Tridecanoylglycine	L-Threonine	N-Undecanoylglycine	N-Undecanoylglycine	Tridecanoylglycine	Creatine	L-Cystine	Tetracosanoylglycine	Valproylglycine	Pristanoylglycine	Tetracosanoylglycine
			Tetracosanoylglycine	L-Tyrosine	Tridecanoylglycine	Valproylglycine	N-Decanoylglycine	Creatinine	L-Lysine	N-Nonanoylglycine	5-L-Glutamylglycine	N-Nonanoylglycine	N-Acryloylglycine
			Pristanoylglycine	L-Valine		Tridecanoylglycine	Valproylglycine	Tetracosanoylglycine	L-Threonine	Palmitoylglycine	Capryloylglycine	N-Lauroylglycine	Capryloylglycine
			N-Nonanoylglycine	5-Oxoprolinate		Tetracosanoylglycine		N-Undecanoylglycine	L-Proline		Tridecanoylglycine	N-Decanoylglycine	N-Undecanoylglycine
			N-Lauroylglycine	Creatinine		Stearoylglycine		N-Decanoylglycine	Creatine		Tetracosanoylglycine	Tridecanoylglycine	N-Nonanoylglycine
			Dimethylglycine	Creatine		N-Nonanoylglycine		Tridecanoylglycine	N-Undecanoylglycine		Pristanoylglycine		N-Nonanoylglycine
				N-Acryloylglycine		N-Lauroylglycine		Pristanoylglycine	N-Acryloylglycine		N-Nonanoylglycine		Palmitoylglycine
				Tetracosanoylglycine		N-Decanoylglycine		N-Nonanoylglycine	Tridecanoylglycine		N-Lauroylglycine		

				Pristanoylglycine N-Undecanoylglycine N-Nonanoylglycine Palmitoylglycine Tridecanoylglycine N-Decanoylglycine		Palmitoylglycine N-Acryloylglycine		N-Lauroylglycine Palmitoylglycine Capryloylglycine Tridecanoylglycine N-Decanoylglycine 5-L-Glutamylglycine	Tetracosanoylglycine Stearoylglycine N-Nonanoylglycine N-Lauroylglycine N-Decanoylglycine Dimethylglycine Tridecanoylglycine 5-L-Glutamylglycine		N-Decanoylglycine Palmitoylglycine N-Acryloylglycine		
peptides			Phenylalanyl-Arginine Arginyl-Phenylalanine		Arginyl-Phenylalanine		Phenylalanyl-Arginine Arginyl-Phenylalanine L-Cysteinylglycine disulfide	Phenylalanyl-Arginine Aspartyl-Alanine Arginyl-Phenylalanine Alanyl-Aspartate Valproylglycine Gamma-Glutamyltyrosine L-Cysteinylglycine disulfide	Phenylalanyl-Arginine Aspartyl-Alanine Arginyl-Phenylalanine Alanyl-Aspartate	Arginyl-Arginine	Aspartyl-Alanine Alanyl-Aspartate L-Cysteinylglycine disulfide	Phenylalanyl-Arginine Arginyl-Phenylalanine	
acylcarnitines	6-Keto-decanoylcarnitine 12-Hydroxy-12-octadecanoylcarnitine	6-Keto-decanoylcarnitine L-Acetylcarnitine	Propionylcarnitine Arachidonyl carnitine	6-Keto-decanoylcarnitine L-Acetylcarnitine Malonylcarnitine L-Palmitoylcarnitine L-Carnitine	Propionylcarnitine Arachidonyl carnitine Malonylcarnitine L-Acetylcarnitine	6-Keto-decanoylcarnitine	L-Acetylcarnitine Propionylcarnitine	6-Keto-decanoylcarnitine Malonylcarnitine	6-Keto-decanoylcarnitine Propionylcarnitine L-Acetylcarnitine	12-Hydroxy-12-octadecanoylcarnitine L-Acetylcarnitine L-Carnitine	12-Hydroxy-12-octadecanoylcarnitine L-Acetylcarnitine Malonylcarnitine Arachidonyl carnitine	6-Keto-decanoylcarnitine L-Acetylcarnitine	6-Keto-decanoylcarnitine L-Acetylcarnitine Malonylcarnitine
autacoids	Resolvin D1 Resolvin D2		Resolvin D5 Neuroprotectin D1	Resolvin D1 Resolvin D2	Resolvin D1 Resolvin D2 Resolvin D5 Neuroprotectin D1	Resolvin D1 Resolvin D2 Resolvin D5 Neuroprotectin D1	Resolvin D1 Resolvin D2		Resolvin D1 Resolvin D2 Resolvin D5 Neuroprotectin D1	Resolvin D5 Neuroprotectin D1	Resolvin D5 Neuroprotectin D1	Resolvin D5 Neuroprotectin D1	
OXYLIPINS:													
I. EICOSANOIDS													

1. prostaglandins	7-hydroxy-D4-neuroprostane 4-hydroxy-D4-neuroprostane 20-hydroxy-E4-neuroprostane 17-hydroxy-E4-neuroprostane 14-hydroxy-E4-neuroprostane			7-hydroxy-D4-neuroprostane 4-hydroxy-D4-neuroprostane 20-hydroxy-E4-neuroprostane 17-hydroxy-E4-neuroprostane 14-hydroxy-E4-neuroprostane 5,6-Dihydroxyprostaglandin F1a	7-hydroxy-D4-neuroprostane 4-hydroxy-D4-neuroprostane 20-hydroxy-E4-neuroprostane 17-hydroxy-E4-neuroprostane 14-hydroxy-E4-neuroprostane	7-hydroxy-D4-neuroprostane 4-hydroxy-D4-neuroprostane 20-hydroxy-E4-neuroprostane 17-hydroxy-E4-neuroprostane 14-hydroxy-E4-neuroprostane PGF2a ethanolamide	7-hydroxy-D4-neuroprostane 4-hydroxy-D4-neuroprostane 20-hydroxy-E4-neuroprostane 17-hydroxy-E4-neuroprostane 14-hydroxy-E4-neuroprostane 13,14-Dihydro PGF-1a 13,14-Dihydro-15-keto-PGD2 11b-PGE2 8-isoprostaglandin E2 8-iso-15-keto-PGF2a 15-Keto-prostaglandin F2a 13,14-Dihydro-15-keto-PGE2 8-iso-PGF3a Prostaglandin F3a Prostaglandin D2 Prostaglandin H2 PGF2a ethanolamide Prostaglandin E2		4-hydroxy-D4-neuroprostane 20-hydroxy-E4-neuroprostane 17-hydroxy-E4-neuroprostane 14-hydroxy-E4-neuroprostane 7-hydroxy-D4-neuroprostane	Prostaglandin B1 Prostaglandin A1 23-Dinor-6-keto-prostaglandin F1 a 8-iso-PGA1 Prostaglandin C1 9-Deoxy-delta12-PGD2	Levuglandin E2 13,14-Dihydro-15-keto-PGD2 11b-PGE2 8-iso-PGF3a Prostaglandin F3a Prostaglandin D2 Prostaglandin H2 Prostaglandin I2 Prostaglandin E2 8-isoprostaglandin E2 8-iso-15-keto-PGF2a 15-Keto-prostaglandin F2a 13,14-Dihydro PGF-1a (5Z)-(15S)-11alpha-Hydroxy-9,15-dioxoprostanoate (13E)-11a-Hydroxy-9,15-dioxoprost-13-enoic acid		
2. thromboxanes							Thromboxane A2			2,3-Dinor-TXB2	Thromboxane A2		
3. leukotrienes	Leukotriene C5 Leukotriene E4	Leukotriene E4	Omega-Carboxy-trinor-leukotriene B4 10,11-dihydro-20-trihydroxy-leukotriene B4	Leukotriene E4 67-dihydro-12-epi-LTB4 12-Oxo-20-trihydroxy-leukotriene B4 1011-dihydro-leukotriene B4 12-Keto-tetrahydro-leukotriene B4	Omega-Carboxy-trinor-leukotriene B4 Leukotriene C5	Omega-Carboxy-trinor-leukotriene B4 10,11-dihydro-20-trihydroxy-leukotriene B4 20-Hydroxy-leukotriene B4	12-Oxo-20-trihydroxy-leukotriene B4 1011-dihydro-20-trihydroxy-leukotriene B4 Leukotriene E4 Leukotriene C5	Leukotriene E4	67-dihydro-12-epi-LTB4 12-Keto-tetrahydro-leukotriene B4 Omega-Carboxy-trinor-leukotriene B4 Leukotriene C5 Leukotriene E4	67-dihydro-12-epi-LTB4 10,11-dihydro-leukotriene B4 20-Hydroxy-leukotriene B4 Omega-Carboxy-trinor-leukotriene B4 Leukotriene C5	6,7-dihydro-12-epi-LTB4 10,11-dihydro-leukotriene B4 12-Keto-tetrahydro-leukotriene B4 Leukotriene E4	Leukotriene E4

										67-dihydro-5-oxo-12-epi-LTB4 1011-dihydro-12-oxo-LTB4 12(S)-Leukotriene B4 6-trans-12-epi-Leukotriene B4 6-trans-Leukotriene B4 Leukotriene B4	10,11-dihydro-20-trihydroxy-leukotriene B4 12-Keto-tetrahydro-leukotriene B4 Leukotriene E4	
4. lipoxins							15-Epi-lipoxin A4 13,14-Dihydro-15-oxo-lipoxin A4 Lipoxin B4 Lipoxin A4				15-Epi-lipoxin A4 13,14-Dihydro-15-oxo-lipoxin A4 Lipoxin A4 Lipoxin B4	
II. OTHER OXYLIPINS			9,10-DiHODE 15,16-DiHODE 12,13-DiHODE 12(13)Ep-9-KODE 9(S)-HPODE	9,10,13-TriHOME 9,12,13-TriHOME 12(13)Ep-9-KODE	9,10-DiHODE 15,16-DiHODE 12,13-DiHODE 9,10,13-TriHOME 9,12,13-TriHOME 9(S)-HPODE 5,6-DHET 11,12-DiHETrE 8,9-DiHETrE 14,15-DiHETrE	9,10,13-TriHOME 9,12,13-TriHOME	9,10-DiHODE 15,16-DiHODE 12,13-DiHODE 9,10,13-TriHOME 9,12,13-TriHOME 9(S)-HPODE 12(13)Ep-9-KODE	9,10-DiHODE 15,16-DiHODE 12,13-DiHODE 9(S)-HPODE 12(13)Ep-9-KODE	15,16-DiHODE 12,13-DiHODE 9,10,13-TriHOME 9,12,13-TriHOME 9-HOTE 13-HOTE 9(S)-HPODE 9(10)-EpODE A-12(13)-EpODE 9-OxoODE	9,10,13-TriHOME 9,12,13-TriHOME 5,6-DHET 8,15-DiHETE 5,15-DiHETE 17,18-DiHETE 14,15-DiHETE 15H-11,12-EETA 11H-14,15-EETA 11,12-DiHETrE 8,9-DiHETrE 14,15-DiHETrE 12,20-DiHETE 5-HPETE 8(S)-HPETE 11(R)-HPETE 12(R)-HPETE 15(S)-HPETE 12(S)-HPETE	9,10-DiHODE 15,16-DiHODE 12,13-DiHODE 9,10,13-TriHOME 9,12,13-TriHOME 9(S)-HPODE 5,6-DHET 11,12-DiHETrE 8,9-DiHETrE 14,15-DiHETrE	9,10-DiHODE 15,16-DiHODE 12,13-DiHODE 9,12,13-TriHOME 9(S)-HPODE 12(13)Ep-9-KODE 5,6-DHET 11,12-DiHETrE 8,9-DiHETrE 14,15-DiHETrE	
hormones	11beta-Hydroxy-3,20-dioxopregn-4-en-21-oic acid Estradiol-17beta 3-sulfate	17a-Estradiol Estradiol Methyltestosterone	Methyltestosterone 6-Dehydrotestosterone glucuronide	6-Dehydrotestosterone glucuronide 11beta-Hydroxy-3,20-dioxopregn-4-en-21-oic acid 21-Hydroxy-5b-pregnane-3,11,20-trione 19-Hydroxydeoxycorticosterone 21-Deoxycortisol Corticosterone Cortexolone	6-Dehydrotestosterone glucuronide 11beta20-Dihydroxy-3-oxopregn-4-en-21-oic acid	6-Dehydrotestosterone glucuronide 11beta20-Dihydroxy-3-oxopregn-4-en-21-oic acid	Methyltestosterone 6-Dehydrotestosterone glucuronide 11beta-Hydroxy-3,20-dioxopregn-4-en-21-oic acid	6-Dehydrotestosterone glucuronide 5a-Dihydrotestosterone sulfate Androsterone sulfate	6-Dehydrotestosterone glucuronide Methyltestosterone 11beta-Hydroxy-3,20-dioxopregn-4-en-21-oic acid		Methyltestosterone 6-Dehydrotestosterone glucuronide	6-Dehydrotestosterone glucuronide Estradiol-17beta 3-sulfate	6-Dehydrotestosterone glucuronide

purines, pyrimidines		5-Aminoimidazole ribonucleotide	5-Methylthioadenosine Cytidine 2,3-cyclic phosphate Cytidine monophosphate	5-Methylthioadenosine Cytosine Deoxycytidine	5-Methylthioadenosine Cytidine 2,3-cyclic phosphate		5-Methylthioadenosine Biotinyl-5-AMP 2-Deoxyinosine triphosphate	5-Methylthioadenosine Cytidine 2,3-cyclic phosphate Cytidine monophosphate 2-Deoxyinosine triphosphate	5-Methylthioadenosine Cytidine 2,3-cyclic phosphate Deoxycytidine Cytosine	5-Methylthioadenosine Cytidine 2,3-cyclic phosphate	5-Methylthioadenosine Cytidine 2,3-cyclic phosphate 2-Deoxyinosine triphosphate Cytidine monophosphate Cytosine	5-Methylthioadenosine Cytidine 2,3-cyclic phosphate Deoxycytidine Cytosine	5-Methylthioadenosine Cytidine 2,3-cyclic phosphate Deoxycytidine Cytosine
lipids	3-O-Sulfogalactosylceramide (d18:124:0) 3-O-Sulfogalactosylceramide (d18:124:1(15Z)) Oleamide Arachidonic acid	3-O-Sulfogalactosylceramide (d18:122:0) 3-O-Sulfogalactosylceramide (d18:124:0) Oleamide	3-O-Sulfogalactosylceramide (d18:122:0) 3-O-Sulfogalactosylceramide (d18:124:0) Oleamide	3-O-Sulfogalactosylceramide (d18:126:1(17Z)) 3-O-Sulfogalactosylceramide (d18:122:0) 3-O-Sulfogalactosylceramide (d18:120:0) 3-O-Sulfogalactosylceramide (d18:124:0) Oleamide	3-O-Sulfogalactosylceramide (d18:124:0) 3-O-Sulfogalactosylceramide (d18:120:0) 3-O-Sulfogalactosylceramide (d18:122:0) Oleamide Arachidonic acid	3-O-Sulfogalactosylceramide (d18:122:0) 3-O-Sulfogalactosylceramide (d18:122:0) Oleamide	3-O-Sulfogalactosylceramide (d18:124:0) 3-O-Sulfogalactosylceramide (d18:120:0) Oleamide Arachidonic acid	3-O-Sulfogalactosylceramide (d18:122:0) 3-O-Sulfogalactosylceramide (d18:124:0) Oleamide Arachidonic acid	3-O-Sulfogalactosylceramide (d18:122:0) 3-O-Sulfogalactosylceramide (d18:124:0) Oleamide Arachidonic acid	3-O-Sulfogalactosylceramide (d18:122:0) 3-O-Sulfogalactosylceramide (d18:124:0) Oleamide	3-O-Sulfogalactosylceramide (d18:124:0) 3-O-Sulfogalactosylceramide (d18:124:1(15Z)) 3-O-Sulfogalactosylceramide (d18:122:0) 3-O-Sulfogalactosylceramide (d18:120:0) Oleamide	3-O-Sulfogalactosylceramide (d18:122:0) 3-O-Sulfogalactosylceramide (d18:124:0)	3-O-Sulfogalactosylceramide (d18:122:0) 3-O-Sulfogalactosylceramide (d18:124:0) Oleamide
other	Taurine		L-Urobilin Melanin Farnesyl pyrophosphate Betaine	L-Urobilin N-Acetylserotonin sulfate Melatonin glucuronide Porphobilinogen 5-Hydroxyindoleacetic acid	cyclic 6-Hydroxymelatonin Betaine L-Urobilin Taurine	Betaine Melatonin glucuronide Arachidonoyl Serinol	Farnesyl pyrophosphate Urothion Porphobilinogen	Pentaporphyrin I L-Urobilin Melanin Melatonin glucuronide Norepinephrine sulfate Taurine Betaine	cyclic 6-Hydroxymelatonin Norepinephrine sulfate Farnesyl pyrophosphate Taurine	Norepinephrine sulfate Taurine 5-Hydroxyindoleacetic acid	Taurine cyclic 6-Hydroxymelatonin Norepinephrine sulfate Melatonin glucuronide L-Urobilin	Norepinephrine sulfate Taurine	cyclic 6-Hydroxymelatonin Melatonin glucuronide Porphobilinogen L-Urobilin L-Urobilinogen

Table 4.4 A comparison of unique features annotated by HMDB with medium-to-high confidence matches obtained from perfusate samples prepared in laboratory with SPME fibers and TFME (blades)

	1st hour		**3rd hour**	**5th hour**		**8th hour**	**11th-12th hours**		**13th-14th hours**		**17th-19th hours**
	FIBERS	BLADES	FIBERS	FIBERS	BLADES	FIBERS	FIBERS	BLADES	FIBERS	BLADES	BLADES
amino acids	L-Histidinol N-Acetylhistamine	Histidinal L-Histidine	N-Acetylhistamine L-Phenylalanine	N-Acetylhistamine Indoleacetyl glutamine	NaNa-Dimethylhistamine N-Acetylhistamine	N-Acetylhistamine Beta-Leucine	N-Acetylhistamine L-Histidinol	Na,Na-Dimethylhistamine N-Acetylhistamine	N-Acetylhistamine L-Phenylalanine	Na,Na-Dimethylhistamine N-Acetylhistamine	Na,Na-Dimethylhistamine Histidinal

D-Leucine	L-Glutamine	L-Tyrosine	Quinaldic acid	3-Methylhistamine	L-Cystine	L-Glutamine	L-Histidine	L-Tryptophan	Histidinal	L-Histidinol
N-acetyltryptophan	L-Asparagine	L-Tryptophan	Indoleacetyl glutamine	1-Methylhistamine	L-Norleucine	L-Proline	Histidinal	Pyroglutamic acid	L-Histidinol	L-Histidine
Beta-Leucine	L-Threonine	L-Valine	L-Cystine	Histidinal	L-Tryptophan	N-acetyltryptophan	L-Histidinol	L-Phenylalanine	N-acetyltryptophan	N(6)-(Octanoyl)lysine
L-Norleucine	L-Proline	Kynurenic acid	D-Leucine	L-Histidinol	L-Homoserine	L-Glutamine	N-acetyltryptophan	Indoleacetyl glutamine	N-Acetylserotonin	L-Tryptophan
L-Tryptophan	L-Phenylalanine	Pyroglutamic acid	D-Tryptophan	N-Acetylvaline	L-Leucine	L-Tryptophan	L-Tryptophan	L-Valine	N-Decanoylglycine	Indoleacetyl glutamine
L-Leucine	Creatine	Indoleacetyl glutamine	L-Allothreonine	Creatinine	L-Glutamine	Kynurenic acid	Indoleacetyl glutamine	L-Methionine	Indoleacetyl glutamine	L-Tryptophan
L-Alloisoleucine	5-Hydroxykynurenine	N-acetyltryptophan	Alanylglycine	L-Proline	L-Alloisoleucine	L-Leucine	N(6)-(Octanoyl)lysine	L-Glutamine	N(6)-(Octanoyl)lysine	Creatinine
L-Isoleucine	L-3-Hydroxykynurenine	Creatine	Beta-Leucine	Methylglutaric acid	L-Allothreonine	Pyroglutamic acid	L-Cystine	L-Arginine	Ornithine	Ornithine
L-Phenylalanine	Cycloserine	L-Methionine	D-Glutamine	Ketoleucine	Pyroglutamic acid	L-Isoleucine	L-Glutamine	L-Cystine	L-Proline	L-Proline
Indoleacetyl glutamine	L-Tryptophan	L-Glutamine	L-Norleucine	Pyroglutamic acid	L-Isoleucine	L-Carnitine	Creatinine	L-Histidine	N-Acetylvaline	Creatine
Tridecanoylglycine	Methylglutaric acid	Indoleacetyl glutamine	L-Tryptophan	Ornithine	L-Threonine	Valproylglycine	L-Arginine	L-Threonine	L-Asparagine	NeNe dimethyllysine
Tetracosanoylglycine	Hydroxykynurenine	Capryloylglycine	L-Homoserine	L-Fucose	L-Phenylalanine	N-Acryloylglycine	Ornithine	L-Tyrosine	L-Carnitine	N(6)-(Octanoyl)lysine
N-Undecanoylglycine	2-Methylglutaric acid	Tridecanoylglycine	L-Leucine	3-Methoxytyramine	Creatine	Capryloylglycine	L-Lysine	L-Glutamic acid	Creatinine	Farnesylcysteine
N-Nonanoylglycine	Pyroglutamic acid	Stearoylglycine	L-Glutamine	N-Acetyl-L-glutamate 5-semialdehyde	Indoleacetyl glutamine	Tridecanoylglycine	L-Asparagine	Indoleacetyl glutamine	Indoleacetaldehyde	N-Acetyl-L-glutamate 5-semialdehyde
	Ketoleucine	Pristanoylglycine	L-Alloisoleucine	D-Serine	N-Undecanoylglycine	Stearoylglycine	L-Proline	N-Acryloylglycine	23-Dimethyl-3-hydroxyglutaric acid	N6N6N6-Trimethyl-L-lysine
	Dimethylglycine	N-Undecanoylglycine	Pyroglutamic acid	L-Tryptophan	Palmitoylglycine	N-Undecanoylglycine	Allysine	Tridecanoylglycine	Ketoleucine	L-Glutamic acid 5-phosphate
	NaNa-Dimethylhistamine	N-Nonanoylglycine	L-Isoleucine	L-Tyrosine	Tridecanoylglycine	N-Nonanoylglycine	Methylglutaric acid	Tetracosanoylglycine	Ribitol	Quinaldic acid
	Indoleacetyl glutamine	N-Acryloylglycine	L-Threonine	Indoleacetyl glutamine	Tetracosanoylglycine	N-Lauroylglycine	Urocanic acid	N-Undecanoylglycine	Urocanic acid	L-Glutamine
	N-acetyltryptophan		L-Phenylalanine	N(6)-(Octanoyl)lysine	N-Nonanoylglycine	N-Lauroylglycine	Pyroglutamic acid	N-Nonanoylglycine	N-Acetyl-L-glutamate 5-semialdehyde	L-Cysteine
	8-Methoxykynurenate		Creatine	L-Cystine	N-Nonanoylglycine	N-Decanoylglycine	L-Phenylalanine	N-Lauroylglycine	D-Serine	L-Arginine

L-Cystine

Quinaldic acid
N-Undecanoylglycine
N-Nonanoylglycine
N-Acryloylglycine
N-Decanoylglycine

Tridecanoylglycine
Tetracosanoylglycine
N-Nonanoylglycine
N-Lauroylglycine
N-Decanoylglycine
Palmitoylglycine

N-Acryloylglycine
Tridecanoylglycine
N-Undecanoylglycine
N-Nonanoylglycine
Valproylglycine
5-L-Glutamylglycine

o-Tyrosine
Beta-Tyrosine
L-Threo-3-Phenylserine
N-Undecanoylglycine
N-Decanoylglycine
Tridecanoylglycine
N-Nonanoylglycine
Myristoylglycine
N-Acryloylglycine
Valerylglycine
Isovalerylglycine
N-Nonanoylglycine
N-Undecanoylglycine
N-Lauroylglycine
N-Decanoylglycine

N-Lauroylglycine
N-Lauroylglycine
N-Decanoylglycine
Valproylglycine
5-L-Glutamylglycine
Alanylglycine

N-Acryloylglycine
Capryloylglycine
Tridecanoylglycine
N-Decanoylglycine

Palmitoylglycine

NeNe dimethyllysine
N(6)-(Octanoyl)lysine
D-Serine
N6N6N6-Trimethyl-L-lysine
Citrulline
L-Valine
Quinaldic acid
Ureidosuccinic acid
L-Methionine
L-Cystine
L-Threonine
L-Tyrosine
L-Glutamic acid
Creatine
5-L-Glutamylglycine
N-Acryloylglycine
Tiglylglycine
N-Butyrylglycine
Isobutyrylglycine
N-Lauroylglycine
N-Decanoylglycine
N-Undecanoylglycine

N-Decanoylglycine
Palmitoylglycine
N-Undecanoylglycine

N-Undecanoylglycine
Valproylglycine
N-Heptanoylglycine
Valerylglycine
Capryloylglycine
Isovalerylglycine
2-Methylbutyrylglycine
Tridecanoylglycine
N-Lauroylglycine
Myristoylglycine

L-Cystine
L-Lysine
L-Asparagine
L-Threonine
L-Tyrosine
L-Glutamic acid
L-Carnitine
Kynurenic acid
2-Methylglutaric acid
N-Undecanoylglycine
N-Lauroylglycine
N-Decanoylglycine
N-Undecanoylglycine
N-Nonanoylglycine
N-Decanoylglycine
Tridecanoylglycine
Stearoylglycine
Myristoylglycine
Palmitoylglycine
Valproylglycine

								N-Lauroylglycine Palmitoylglycine Tridecanoylglycine Stearoylglycine			
peptides		Valyl-Hydroxyproline Prolyl-Asparagine Phenylalanyl-Arginine Hydroxyprolyl-Valine Aspartyl-Phenylalanine Asparaginyl-Proline Arginyl-Phenylalanine Arginyl-Arginine	Arginyl-Phenylalanine	Phenylalanyl-Arginine Aspartyl-Alanine Arginyl-Phenylalanine Alanyl-Glycine Alanyl-Aspartate Arginyl-Arginine	Valyl-Aspartate Threoninyl-Hydroxyproline Hydroxyprolyl-Threonine Aspartyl-Valine Histidinyl-Cysteine Cysteinyl-Histidine Arginyl-Arginine	Phenylalanyl-Arginine Aspartyl-Alanine Arginyl-Phenylalanine Alanyl-Glycine Alanyl-Aspartate	Phenylalanyl-Arginine Arginyl-Phenylalanine	Tryptophyl-Arginine Phenylalanyl-Arginine Histidinyl-Alanine Aspartyl-Alanine Arginyl-Tryptophan Arginyl-Phenylalanine Alanyl-Histidine Alanyl-Aspartate	Phenylalanyl-Arginine Arginyl-Phenylalanine	Arginyl-Arginine	Arginyl-Arginine gamma-Glutamyl-S-methylcysteinyl-beta-alanine
acylcarnitines	Hydroxypropionylcarnitine Decanoylcarnitine	Propionylcarnitine L-Acetylcarnitine Malonylcarnitine	L-Acetylcarnitine L-Carnitine Malonylcarnitine 6-Keto-decanoylcarnitine	6-Keto-decanoylcarnitine L-Acetylcarnitine	L-Carnitine L-Acetylcarnitine 3-Dehydrocarnitine 3-Dehydroxycarnitine Tiglylcarnitine Propionylcarnitine Hydroxypropionylcarnitine	6-Keto-decanoylcarnitine L-Acetylcarnitine	Arachidonylcarnitine Malonylcarnitine 3-Hydroxy-9-hexadecenoylcarnitine	L-Acetylcarnitine Propionylcarnitine Tiglylcarnitine 3-Dehydroxycarnitine Hydroxypropionylcarnitine L-Carnitine	6-Keto-decanoylcarnitine L-Acetylcarnitine	Propionylcarnitine L-Acetylcarnitine 3-Dehydroxycarnitine Tiglylcarnitine Hydroxypropionylcarnitine 3-Dehydrocarnitine	3-Dehydrocarnitine Propionylcarnitine L-Acetylcarnitine Malonylcarnitine 2-Octenoylcarnitine Heptanoylcarnitine Hydroxypropionylcarnitine Tiglylcarnitine Dodecanoylcarnitine 3-Dehydroxycarnitine
autacoids			Resolvin D1 Resolvin D2	Resolvin D1 Resolvin D2		Resolvin D1 Resolvin D2	Resolvin D5 Neuroprotectin D1	Resolvin D1 Resolvin D2		Resolvin D1 Resolvin D2	Resolvin D1 Resolvin D2

OXYLIPINS											
I. EICOSANOIDS											
1. prostaglandins	PGF2a ethanolamide	6-Keto-prostaglandin F1a 15-Deoxy-d-12,14-PGJ2 Prostaglandin G1 20-Hydroxy-PGF2a	7-hydroxy-D4-neuroprostane 4-hydroxy-D4-neuroprostane 20-hydroxy-E4-neuroprostane 17-hydroxy-E4-neuroprostane 14-hydroxy-E4-neuroprostane	7-hydroxy-D4-neuroprostane 4-hydroxy-D4-neuroprostane 20-hydroxy-E4-neuroprostane 17-hydroxy-E4-neuroprostane 14-hydroxy-E4-neuroprostane 15-Deoxy-d-12,14-PGJ2	15-Deoxy-d-12,14-PGJ2	7-hydroxy-D4-neuroprostane 4-hydroxy-D4-neuroprostane 20-hydroxy-E4-neuroprostane 17-hydroxy-E4-neuroprostane 14-hydroxy-E4-neuroprostane 15-Deoxy-d-12,14-PGJ2	Prostaglandin G1 20-Hydroxy-PGF2a	7-hydroxy-D4-neuroprostane 4-hydroxy-D4-neuroprostane 20-hydroxy-E4-neuroprostane 17-hydroxy-E4-neuroprostane 14-hydroxy-E4-neuroprostane 6-Keto-prostaglandin F1a PGF2a ethanolamide 20-Hydroxy-PGF2a	13,14-Dihydro PGF-1a	7-hydroxy-D4-neuroprostane 4-hydroxy-D4-neuroprostane 20-hydroxy-E4-neuroprostane 17-hydroxy-E4-neuroprostane 14-hydroxy-E4-neuroprostane 20-hydroxy-E4-neuroprostane 15-Deoxy-d-12,14-PGJ2	7-hydroxy-D4-neuroprostane 4-hydroxy-D4-neuroprostane 20-hydroxy-E4-neuroprostane 17-hydroxy-E4-neuroprostane 14-hydroxy-E4-neuroprostane Prostaglandin D2 Prostaglandin H2 Prostaglandin I2 Prostaglandin E2 PGF2a ethanolamide 13,14-Dihydro-15-keto-PGD2 11b-PGE2 8-iso-15-keto-PGF2a 15-Keto-prostaglandin F2a 8-iso-PGF3a Prostaglandin F3a 56-Dihydroxyprostaglandin F1a (5Z)-(15S)-11alpha-Hydroxy-9,15-dioxoprostanoate
2. thromboxanes		Thromboxane B2					Thromboxane B2	Thromboxane B2			Thromboxane A2
3. leukotrienes	Leukotriene C5 Leukotriene E4	10,11-dihydro-20-dihydroxy-LTB4	Leukotriene E4 Omega-Carboxy-trinor-leukotriene B4	Omega-Carboxy-trinor-leukotriene B4 Leukotriene C5	6,7-dihydro-12-epi-LTB4 10,11-dihydro-leukotriene B4	Omega-Carboxy-trinor-leukotriene B4 Leukotriene C5	12-Oxo-20-trihydroxy-leukotriene B4 10,11-dihydro-20-dihydroxy-LTB4	10,11-dihydro-20-dihydroxy-LTB4 10,11-dihydro-20-trihydroxy-leukotriene B4	Leukotriene E4		10,11-dihydro-20-trihydroxy-leukotriene B4 Leukotriene B4 ethanolamide

	Omega-Carboxy-trinor-leukotriene B4		Leukotriene C5	Leukotriene E4	12-Keto-tetrahydro-leukotriene B4	Leukotriene E4	Leukotriene E4				20-Hydroxy-leukotriene B4
	12-Oxo-20-trihydroxy-leukotriene B4						10,11-dihydro-20-trihydroxy-leukotriene B4				
								9-HODE			
								15-Deoxy-d-12,14-PGJ2			
								Prostaglandin G1			
4. lipoxins											15-Epi-lipoxin A4
											13,14-Dihydro-15-oxo-lipoxin A4
II. OTHER OXYLIPINS		9,10,13-TriHOME		9,10-DiHODE	5,6-DHET	9,10-DiHODE		9,10,13-TriHOME	12(13)Ep-9-KODE	Tetranor 12-HETE	9-HODE
		9,12,13-TriHOME		15,16-DiHODE	11,12-DiHETrE	15,16-DiHODE		9,12,13-TriHOME	9,10,13-TriHOME	9,10,13-TriHOME	9,10-DiHODE
				12,13-DiHODE	8,9-DiHETrE	12,13-DiHODE		12,13-EpOME	9,12,13-TriHOME	9,12,13-TriHOME	15,16-DiHODE
				9(S)-HPODE	14,15-DiHETrE	9(S)-HPODE		Tetranor 12-HETE			12,13-DiHODE
				9,10,13-TriHOME	9,10,13-TriHOME	9,10,13-TriHOME		9(S)-HPODE			9(S)-HPODE
				9,12,13-TriHOME	9,12,13-TriHOME	9,12,13-TriHOME					9,10,13-TriHOME
											9,12,13-TriHOME
											12,13-EpOME
hormones	17a-Estradiol	19-Oxo-deoxycorticosterone	17a-Estradiol	11beta-Hydroxy-3,20-dioxopregn-4-en-21-oic acid	Methyltestosterone	17a-Estradiol	17a-Estradiol	11beta-Hydroxy-3,20-dioxopregn-4-en-21-oic acid	5b-Dihydrotestosterone	Cortisone	21-Deoxycortisol
	Estradiol	19-Hydroxydeoxycorticosterone	Estradiol	Estradiol	19-Oxo-deoxycorticosterone	Estradiol	Estradiol	19-Oxo-deoxycorticosterone	4-Androstenediol	18-Oxocortisol	6-Dehydrotestosterone glucuronide
		2-Hydroxy-3-methoxyestrone	11beta-Hydroxy-3,20-dioxopregn-4-en-21-oic acid	6-Dehydrotestosterone glucuronide	19-Hydroxydeoxycorticosterone	6-Dehydrotestosterone glucuronide	6-Dehydrotestosterone glucuronide	19-Hydroxydeoxycorticosterone	5-Androstenediol	Aldosterone	19-Oxo-deoxycorticosterone
		Adrenosterone	6-Dehydrotestosterone glucuronide	17a-Estradiol	11beta20-Dihydroxy-3-oxopregn-4-en-21-oic acid	Methyltestosterone		11beta20-Dihydroxy-3-oxopregn-4-en-21-oic acid	Dihydrotestosterone	11beta-Hydroxy-3,20-dioxopregn-4-en-21-oic acid	19-Hydroxydeoxycorticosterone
		19-Oxoandrost-4-ene-3,17-dione			21-Hydroxy-5b-pregnane-3,11,20-trione	11beta-Hydroxy-3,20-dioxopregn-4-en-21-oic acid		Adrenosterone	Epiandrosterone	11beta20-Dihydroxy-3-oxopregn-4-en-21-oic acid	11beta-Hydroxy-320-dioxopregn-4-en-21-oic acid
		21-Hydroxy-5b-pregnane-			21-Deoxycortisol			19-Oxoandrost-4-ene-3,17-dione	Androsterone		11beta20-Dihydroxy-3-

		3,11,20-trione									oxopregn-4-en-21-oic acid
		6b-Hydroxymethandienone			11-Dehydrocorticosterone			21-Hydroxy-5b-pregnane-3,11,20-trione	6-Dehydrotestosterone glucuronide		21-Hydroxy-5b-pregnane-31120-trione
		21-Deoxycortisol			18-Oxocortisol			21-Deoxycortisol	11beta20-Dihydroxy-3-oxopregn-4-en-21-oic acid		21-Deoxycortisol
		11-Dehydrocorticosterone			Cortexolone			11-Dehydrocorticosterone			11-Dehydrocorticosterone
		Corticosterone			3b16a-Dihydroxyandrostenone sulfate			Corticosterone			Corticosterone
		Cortexolone			Corticosterone			3b16a-Dihydroxyandrostenone sulfate			Androstanedione
		2-Methoxyestrone						Cortexolone			Epitestosterone
		3b16a-Dihydroxyandrostenone sulfate						2-Methoxyestrone			18-Oxocortisol
								6-Dehydrotestosterone glucuronide			Testosterone
											Dehydroepiandrosterone
											Cortexolone
											3b16a-Dihydroxyandrostenone sulfate
											21-Hydroxy-5b-pregnane-31120-trione
											19-Hydroxydeoxycorticosterone
purines, pyrimidines	6-Thioinosinic acid	Cytosine	5-Aminoimidazole ribonucleotide	Cytidine 2,3-cyclic phosphate	Deoxyadenosine monophosphate	Cytidine 2,3-cyclic phosphate	5-Methylthioadenosine	5-Methylthioadenosine	Cytidine monophosphate	dUMP	dUMP
	Cytidine 2,3-cyclic phosphate	Cytidine monophosphate	Allopurinol riboside	5-Methylthioadenosine	Biotinyl-5-AMP	5-Methylthioadenosine		Deoxyadenosine monophosphate	5-Methylthioadenosine	3-Methylcytosine	3-Methylcytosine
	2-Deoxyinosine triphosphate	3-Methylcytosine			dUMP			Cytidine 2,3-cyclic phosphate		2-O-Methylcytosine	2-O-Methylcytosine
	5-Methylthioadenosine	5-Methylcytosine			3-Methylcytosine			Cytidine monophosphate		5-Methylcytosine	8-Hydroxypurine
		Dihydrouracil			Cytosine			Cysteine-S-sulfate		Thymine	Thiocysteine

		2-O-Methylcytosine						Cytosine Dihydrouracil Deoxycytidine 8-Hydroxypurine		Dihydrouracil 8-Hydroxypurine	5-Methylthioadenosine Cytosine Deoxycytidine 13-Dimethyluracil N-Acetyl-S-(N-methylcarbamoyl)cysteine 24-Diamino-6-hydroxypyrimidine Dihydrothymine 6-Dimethylaminopurine 5-Thymidylic acid
lipids	3-O-Sulfogalactosylceramide (d18:122:0) 3-O-Sulfogalactosylceramide (d18:124:0) Oleamide	Oleamide	3-O-Sulfogalactosylceramide (d18:124:0) 3-O-Sulfogalactosylceramide (d18:126:1(17Z)) 3-O-Sulfogalactosylceramide (d18:122:0) Arachidonic acid	3-O-Sulfogalactosylceramide (d18:120:0) 3-O-Sulfogalactosylceramide (d18:124:0)		3-O-Sulfogalactosylceramide (d18:122:0) 3-O-Sulfogalactosylceramide (d18:120:0) 3-O-Sulfogalactosylceramide (d18:124:0)	3-O-Sulfogalactosylceramide (d18:122:0) 3-O-Sulfogalactosylceramide (d18:124:0)	3-O-Sulfogalactosylceramide (d18:124:0) 3-O-Sulfogalactosylceramide (d18:124:1(15Z)) 3-O-Sulfogalactosylceramide (d18:120:0) 3-O-Sulfogalactosylceramide (d18:118:0) 3-O-Sulfogalactosylceramide (d18:112:0) Oleamide	3-O-Sulfogalactosylceramide (d18:122:0) 3-O-Sulfogalactosylceramide (d18:120:0) Arachidonic acid		3-O-Sulfogalactosylceramide (d18:124:1(15Z)) 3-O-Sulfogalactosylceramide (d18:122:0) 3-O-Sulfogalactosylceramide (d18:120:0) 3-O-Sulfogalactosylceramide (d18:118:0) 3-O-Sulfogalactosylceramide (d18:124:0) 3-O-Sulfogalactosylceramide (d18:112:0) Arachidonic acid Oleamide
other	Melatonin glucuronide cyclic 6-Hydroxymelatonin Farnesyl pyrophosphate	Urothion Fucose 1-phosphate Allantoin	Mevalonic acid-5P 2-Aminomuconic acid Melatonin glucuronide	D-Fucose Fucose 1-phosphate Allantoin	Taurine	Norepinephrine sulfate Farnesyl pyrophosphate Melatonin glucuronide	Allantoin Porphobilinogen dUMP	NNAL-N-glucuronide Taurine	Histamine Phosphate Acetylcholine Fucose 1-phosphate	Lipoyl-AMP Biotinyl-5-AMP Porphobilinogen

Taurine	Serotonin	cyclic 6-Hydroxymelatonin	Porphobilinogen	L-Urobilin	Neuromedin N (1-4)	Allantoin	Bilirubin
	cyclic 6-Hydroxymelatonin	Betaine			Fucose 1-phosphate	Taurine	Melatonin glucuronide
	Melatonin glucuronide	Taurine			Taurine	Porphobilinogen	Allantoic acid
	Melanin	L-Urobilin			Melanin	3-O-Methyl-a-methyldopamine	FAPy-adenine
	Ribitol	Melanin			Norepinephrine sulfate		L-Urobilin
	L-Fucose				L-Urobilin		Melanin
	Histamine Phosphate				Bilirubin		DOPA sulfate
					Carnosine		Taurine
					4E15Z-Bilirubin IXa		Protoporphyrinogen IX
					cyclic 6-Hydroxymelatonin		Phosphohydroxypyruvic acid
					3-O-Methyl-a-methyldopamine		4E,15Z-Bilirubin IXa
							Urocanic acid

4.5.2 Metabolite stability

The typical metabolomics workflow requires an initial sampling step wherein samples of interest are collected, and then followed by one of the most crucial steps in the protocol: sample preparation. SPME was used for lung fingerprinting analysis during NEVLP because it integrates sampling and sample preparation into a single step, thereby offering superior and easy sample clean up. Importantly, in comparison to other sample preparation methods, SPME also features a simultaneous quenching step via the exclusive extraction of a wide range of small molecules representative of the metabolome. This is advantageous because interferences or changes to the sample that would occur due to the presence of coextracted enzymes, inherent with conventional sample preparation approaches, would be avoided. Furthermore, these enzymes would otherwise need to be inactivated separately prior to analyte isolation thus increasing sample handling.

One of the aims of this multi-tiered study was to compare the information recovered from samples collected via the typical metabolomics workflow with the information obtained via on-site extraction of these samples, while using SPME as the main sample preparation tool. Given the dynamics of a biological system, snap freezing is often employed after sample collection to mitigate changes to the sample after it has been extracted from the system, thereby maintaining its integrity and ensuring an accurate representation of the metabolome. As such, the same methods were employed in order to determine whether there were any significant differences between the samples that were collected and prepared with SPME fibers on-site, and those that were immediately snap-frozen after collection and sampled in the laboratory. Figure 4.6 shows the differences between the three main sample groups, namely: lung tissue sampled *in vivo* on-site; perfusate sampled on-site at the same time as the lung tissue sampling; and perfusate that was snap-frozen and transported back to the laboratory for sampling. As can be seen in Figure 4.6, there is a distinct difference between the *in vivo* lung samples and all of the perfusate samples (a more obvious separation can be seen in the 3D PCA plot in Figure 4.6), which is likely due to their respective compositional differences (i.e, semi-solid vs fluid); however, there is also a distinct difference between the perfusate

samples that were collected and prepared on-site and those that were snap-frozen and sampled in the laboratory. This difference is interesting considering that these samples were collected at the same time point, with the same types of vials being used for collection, storage, and sampling. Although overlapping between the two perfusate groups can be observed for certain time points, the differences between them are clearly observable overall.

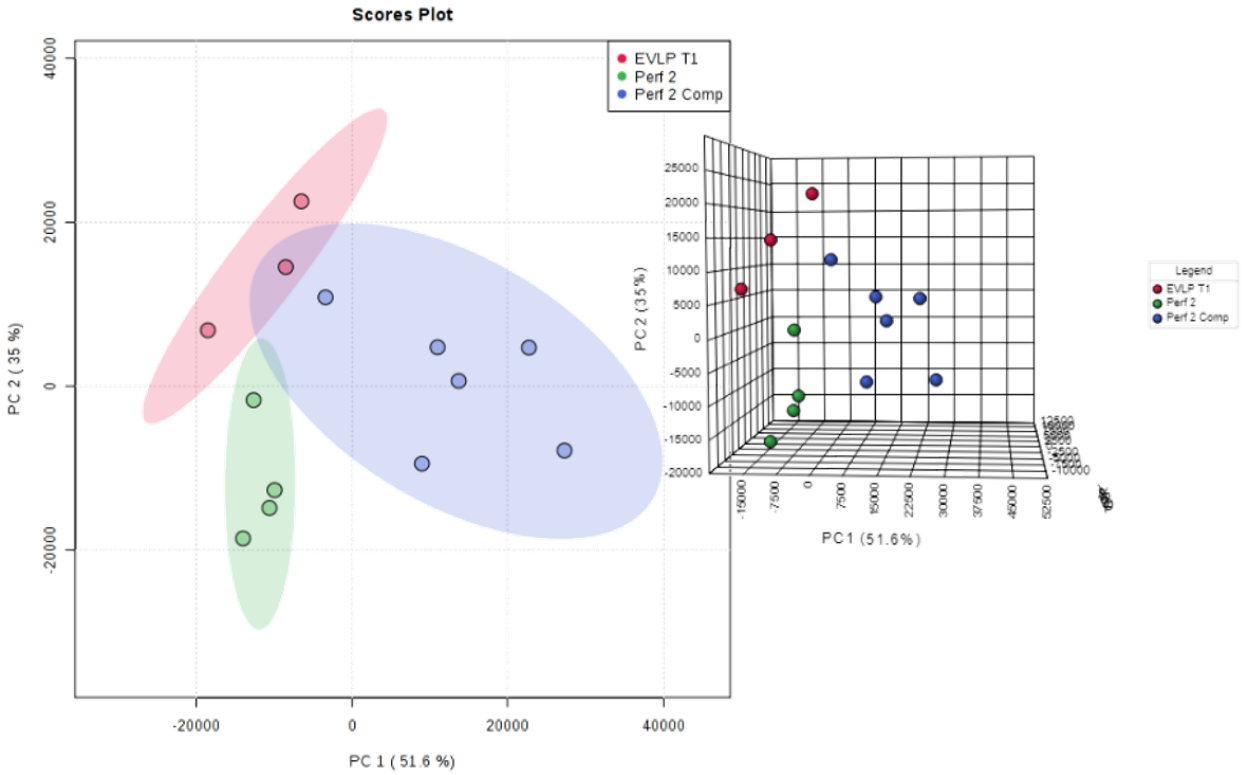

Figure 4.6 PCA (PC1:51.6%; PC2: 35%; PC3: 6.5%) plot of samples collected *in vivo* from lung (red), perfusate samples collected on-site in the operating room (green), and perfusate samples collected, snap-frozen and sampled *ex vivo* in the laboratory (blue).

Figure 4.7 shows a heat map for three sampling time points (1 hour, 3 hours, and 6 hours) for the three main sample groups (lung samples, on-site perfusate, and in-lab perfusate denoted by red, green, and blue class markers, respectively). Given that the perfusate samples were collected under the same conditions, one would expect to observe similar profiles in terms of the relative abundance of their respective features. This is true for some features, which is evidenced in the lower section of the heat map in Figure 4.7B and the

upper section of the heat map in Figure 4.7C; however, the dark red and dark blue squares in Figure 4.7A to Figure 4.7C indicate that there are a number of upregulated or down regulated features distinguishing the on-site and in-laboratory perfusate samples. This trend can be seen throughout the NEVLP process and for a wide range of compounds/features as demonstrated for hour 1, 3 and 6 of NEVLP in Figure 4.7. This result is quite surprising as it reveals that the typical metabolomics workflow can give rise to misleading results wherein prospective biomarkers may be a result of artefact formation. Nonetheless, it is important to note that, while there are differences between the on-site and in-laboratory prepared samples, the untargeted nature of the study makes it difficult to predict whether these particular statistically significant features are of any biochemical relevance. It is therefore important to emphasize that prospective biomarkers discovered during metabolomics studies may or may not be workflow dependent. As such, it is necessary to rigorously and intensively investigate such biomarkers before widespread use.

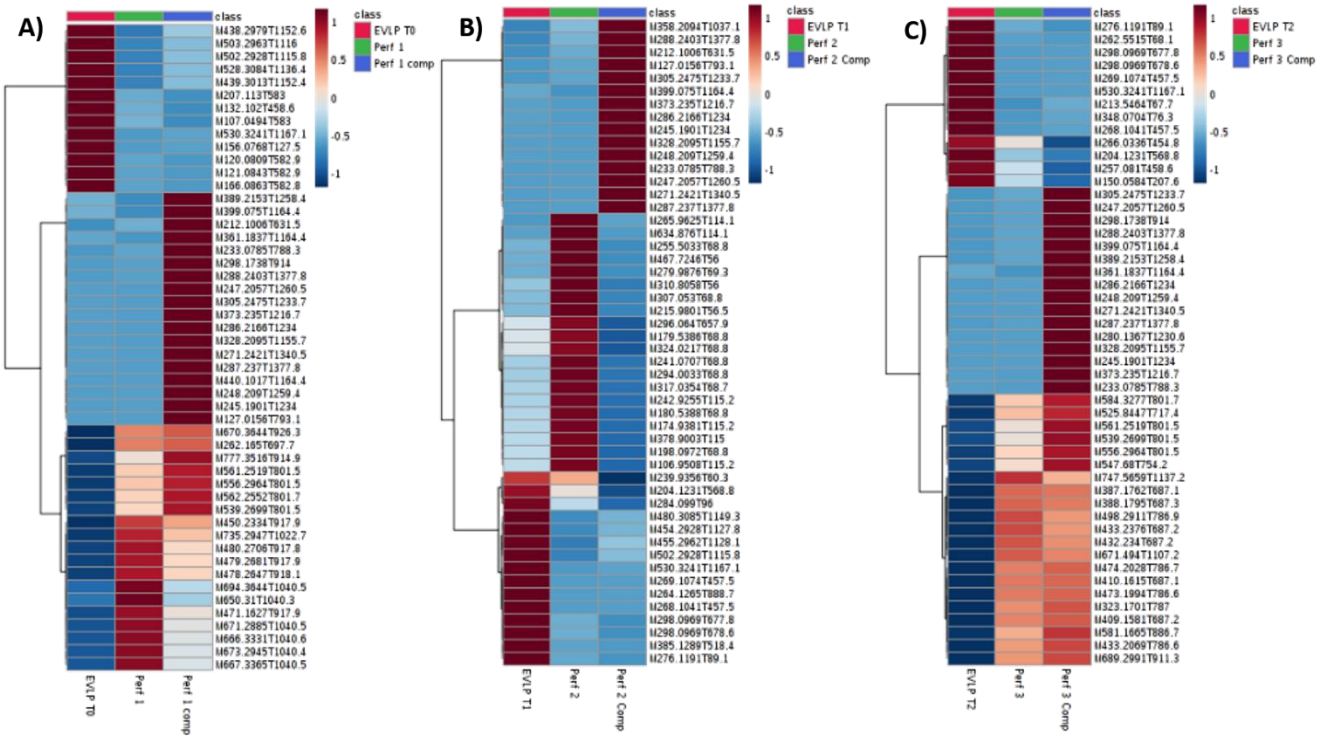

Figure 4.7 Group averaged heat maps of samples collected *in vivo* from lung (red), perfusate samples collected on-site in the operating room (green), and perfusate samples collected, snap-frozen, and prepared in the laboratory (blue). Dark red squares on the heat map indicate a very high abundance of that particular feature in a specific group of samples, while dark blue indicates a very low abundance. A) Heat map for samples collected after the first hour of perfusion (EVLP T_0). B) Heat map for samples collected after 3 hours of perfusion (EVLP T_1). C) Heat map for samples collected after 6 hours of perfusion (EVLP T_2).

Since SPME has also been reported to enable the extraction of short-lived and unstable metabolites [104,129,141], another aim of the study was to examine the advantages of using specifically tissue sampling to complement perfusate sampling as indeed, there are an indefinite number of biochemical processes occurring within the lung during NEVLP that may not be detectable in perfusate samples. This could be due to short-lived metabolites produced in lung by sometimes very rapid biochemical reactions. This advantage of tissue sampling is thus illustrated by the heat map in Figure 4.7 and requires an understanding of the dynamics and fundamentals of the SPME protocol. For example, some features/compounds (i.e. m/z 438.3, 503.3, 502.3, 439.3, 207.1, 132.1, 107.0, 530.3, 156.1…) are highly abundant in lung tissue (represented by red class label in Figure 4.7A) but are not present in either set of perfusate samples. This disparity highlights the advantage of SPME as an *in vivo* technique, as these features may represent short-lived species only

present in lung tissue. Moreover, it is possible that these features diffuse from the lung to the perfusate more slowly during perfusion and are therefore not seen in the perfusion fluid collected at the time of SPME tissue sampling. This supposition supports the observation that lung samples exhibit a more rapid transition in comparison to metabolomic profiles observed in perfusate samples (*as discussed in section 4.4.2 "Unsupervised multivariate analysis"*). Another aspect of interest that highlights the complementary information obtained via *in vivo* lung sampling and on-site sampling concerns the fundamentals of SPME, namely, that it performs extraction via free concentration. This is demonstrated in the heat map in Figure 4.7, which shows a high abundance of features in the perfusate samples collected on-site and a low abundance of these same features in the corresponding *in vivo* lung samples. Since SPME, as a non-exhaustive technique, extracts only a portion of the free concentration being sampled, it is possible that the features with apparent low-to-zero abundance may have very high binding to the lung tissue, thus resulting in a lower free concentration available for extraction. However, given the continuous perfusion of the organ and various diffusive processes, these features may have a higher free concentration in perfusion fluid due to lower binding processes in comparison to a denser semi-solid biomatrix, such as lung. These dynamics and interconnected processes not only emphasize the importance of performing simultaneous and complementary sampling, but they also emphasize the importance of having sample preparation tools with rapid on-site capabilities, as such tools can help to minimize sample handling and the number of required sample processing steps while providing reliable real-time pertinent biochemical information.

4.6 Conclusion

In summary, the use of prolonged NEVLP to extend the lifetime of the lungs may induce the cellular reprogramming of the organ to accommodate for or adjust to the biosynthetic demands of the applied procedure. The application of *in vivo* SPME fibers directly into the lungs allowed changes occurring in the organ at the metabolite level to be monitored during NEVLP. Several upregulated biochemical pathways mainly involved in pro- and anti-inflammatory responses, as well as in lipid metabolism, were observed during extended lung perfusion, especially between the 11^{th} and 12^{th} hours of the procedure. These changes

were also observed in the perfusate composition, wherein the majority of compounds were diffused from the lung during perfusion. However, a number of unstable and/or short-lived metabolites were solely extracted from lung tissue *in vivo* via SPME fibers. Moreover, the perfusate samples that had been stored and prepared in the laboratory according to the typical metabolomics workflow provided less complementary information about the metabolome/metabolomic profile of extracted compounds than *in vivo* tissue samples or perfusate samples collected in real-time on-site during NEVLP. In addition, the samples that were prepared in the laboratory also exhibited a tendency to be misleading by potentially producing artefacts associated with tentative features that have been previously reported as potential biomarkers for lung injury. In the future, secondary and tertiary cohort metabolomic studies, more targeted metabolomic approaches and substantial MS/MS validation, should be explored to confirm the possibility of artefact formation and the other tentative results of this untargeted metabolomic study. Furthermore, future research should also monitor the metabolomic status of lungs after transplantation to the recipient patient in order to find and confirm potential candidate biomarkers of lung function or injury during prolonged NEVLP; and a better association of the metabolic data and clinical data should be implemented.

Chapter 5: Therapeutic drug monitoring of FOLFOX and screening of drug metabolites followed by pharmacometabolomic fingerprinting of porcine lung tissue during pre-clinical *in vivo* lung perfusion (IVLP) using *in vivo* solid phase microextraction

5.1 Preamble

Chapter 5 of this thesis has not yet been published. The research presented in this chapter stemmed from a collaboration with Toronto General Hospital initiated by B. Bojko, J. Pawliszyn, and M. Cypel. Further modifications to the experimental design were overseen by G.A. Gomez-Rios. The work presented in this chapter of the thesis related to untargeted analysis, LC method development, experimental design for quantitative SPME method development, *in vivo* sample analysis, sample and data processing and stability study were conducted by the author of this thesis with assistance from G.A Gomez-Rios, A. Roszkowska, and Miao Yu. Please see *Statement of contributions.* Funding: We are grateful to the Canadian Cancer Society for their support in the development of IVLP via innovation grants. We are also grateful to the Canadian Institute of Health Research (CIHR) - Natural Sciences and Engineering Research Council (NSERC) of Canada Collaborative Health Research Projects program for their financial support [grant 355935 entitled "Supervised *in vivo* lung perfusion strategy for treatment of cancer metastases to the lungs. Real-time monitoring of chemotherapy by on-site analytical platform"] and the Natural Sciences and Engineering Research Council of Canada Industrial Research Chair (IRC) program.

5.2 Introduction

The *in vivo* lung perfusion (IVLP) method employed at the Toronto General Hospital is a modified form of isolated lung perfusion (ILP) that was adapted from the Toronto *ex vivo* lung perfusion (EVLP) method in order to treat terminal pulmonary diseases like end-stage metastatic cancer *in situ*.[142,143] This targeted drug delivery system enables high doses of chemotherapy to be administered exclusively to the lung, thus

minimizing common adverse drug-toxicity related effects of systemic exposure to chemotherapy, such as hair loss, nausea, vomiting, and weakened immune system. When used in conjunction with metastasectomy—which is currently the most effective treatment for lung cancer metastases—it is believed that IVLP can help to prevent disease recurrence by treating any undetected micrometastases remaining in the peripheral tissue following tumor resection.[143] This combined approach may be able to improve the daunting 20% - 40% 5-year survival rate of patients with lung cancer metastases, as they tend to be particularly vulnerable to the appearance of new unresectable tumours.[142,143] In this Chapter, the use of *in vivo* SPME is explored for the simultaneous monitoring of combination drugs concentrations in the lung as well as the lung metabolome during pre-clinical IV and IVLP administration in porcine models.

Combination chemotherapy approaches—for example, the use of Folinic acid (FOL), 5-fluorouracil (F), and oxaliplatin (OX) (FOLFOX)—have been shown to be effective for treating a wide range of solid tumors found in areas of the body including, but not limited to, the breasts, the head and neck, the ovaries, and, most notably, the colon.[144–147] Despite these advantages, the intravenous (IV) administration of these therapies can lead to serious pulmonary side effects in a small subsection of patients (less than 1.5%);[147] however, since the risk of these side effects is so small, it is worth exploring the use of FOLFOX in conjunction with IVLP. Each drug in this FOLFOX combination exhibits a complex mechanism of action. One of the biologically active pathways (< 20%), specifically for folinic acid-5-flurouracil (FOLF) combination, works by exploiting the thymidylate synthase (TS) pathway, which is an enzyme that is overly expressed in cancerous cells due to proliferation.[145] Briefly, deoxyuridine monophosphate (dUMP) is enzymatically converted to deoxythymidine monophosphate (dTMP) via methylation on the C-5 position of uracil in the presence of 5,10-methylenetetrahydrofolate (5,10-methyleneTHF)—one of the metabolite of FOL. dTMP is subsequently phosphorylated and integrated into the DNA as deoxythymidine triphosphate (dTTP), which is vital for DNA repair and replication.[1,145] However, the introduction of F, which can mimic both uracil, and thymine, leads to the formation of an irreversible ternary complex between F, the TS enzyme, and 5,10-methyleneTHF during attempts to methylate the C-5 position on uracil,

which now has a fluorine substituent instead. This inhibits the TS enzyme, consequently depleting the cellular availability of thymidine.[1,145,146] The use of FOL in the therapy is to essentially inundate the folic acid pool with 5,10-methyleneTHF since increased concentrations of this folate lead to the stabilization of the ternary complex.[146] Moreover, F can be further integrated into the DNA inadvertently via anabolism (building up of smaller molecules to complex molecules) to 5-fluorodeoxyuridine (5FdUrd) and then subsequent phosphorylation of 5-fluorodeoxyuridine monophosphate (5FdUMP), which produces 5-fluorodeoxyuridine triphosphate (5FdUTP). The integration of F into the RNA occurs via the formation of 5-fluorouridine (5FUrd) and the subsequent phosphorylation to 5-fluorouridine triphosphate (5FUTP).[145,147,148] Replacing the thymidine and uridine substituent in DNA and RNA respectively, induces mutations in the DNA specifically as a result of the misincorporation of the incorrect base pair, which in turn leads to DNA and/or RNA damage and, ultimately, apoptosis.[1] Meanwhile, the biological inactivation (> 80%) of F is mediated by the catabolic (breakdown of larger molecules to smaller molecules) metabolism of F via the dihydropyrimidine dehydrogenase (DPD) enzyme, which varies not only in concentration, but also in activity from patient to patient.[147] DPD leads to the formation of inactive F catabolites, including dihydrofluorouracil (FUH_2), fluoroureidopropionic acid (FUPA), and fluoro-beta-alanine (FBAL), none of which exhibit any therapeutic benefits.[144,147,148] OX, which is a third-generation platinum-based chemotherapeutic drug,[149] has various mechanisms of action but is known to largely exert its cytotoxic effect via the formation of DNA-protein crosslinks and especially the formation of DNA intra- and inter-strand crosslinks by binding usually to the N7 atom of guanine, forming links with two adjacent guanines and to a lesser extent to guanine-adenine base pair.[149,150] OX undergoes rapid non-enzymatic transformation wherein the oxalate group is displaced, and the following transient reactive species are formed, namely, dichloro-, monochloro-, and diaquo- diaminocyclohexane (DACH). These reactive species readily complex with amino acids and proteins or other plasma and tissue macromolecules.[149,151] The dichloro(DACH) complex enters the cells and the formation of these DNA lesions lead to DNA synthesis arrest and subsequently apoptosis. OX-DNA adduct conformation is postulated to more effectively inhibit the binding

of the mismatch repair (MMR) protein complex compared to first- and second- generation platinum-based agents cisplatin and carboplatin. Additionally, the bulky DACH group on OX better prevents DNA synthesis in comparison to cisplatin and carboplatin.[150] OX has also been implicated in reducing F catabolism by inhibiting DPD activity, emphasizing the synergistic effects of namely the FOX combination in chemotherapy.[144]

While a number of studies have established that FOLFOX provides satisfactory antitumor activity, standard dosing methods are hampered by high inter-patient variability with regards to FOLFOX concentrations in the blood plasma, which results in drug under- or over-exposure.[10,147,152] Given the serious circumstances under which these drugs are administered, their accompanying cytotoxicity, and large inter-patient variability due to factors such as sex, weight, medical history, DPD activity and concentration, it is imperative to know the impact of these drugs throughout the treatment process. Personalizing treatment by monitoring the concentrations of these drugs can help to prevent under- or over-dosing, effectively maximizing therapeutic outcomes and minimizing adverse events. Therapeutic drug monitoring (TDM) is employed to measure the concentration of a drug in biological matrices such as blood, plasma, or tissue following administration, and it is required for drug combinations like FOLFOX, which have narrow or unknown therapeutic ranges and large inter-patient variability.[10] Some challenges in TDM, specifically in the field of chemotherapy, include: a lack of available assays for the many possible therapies that can be administered; no agreed upon universal therapeutic range for drugs used in these treatments; and, in combination therapies, changes in the synergistic effects of one or more components due to the presence of other chemotherapies or patient medications at other various doses.[10] Moreover, while plasma concentrations may be easier to monitor, this is not always suitable since it may not reflect the concentrations of a drug in specific tissues or organs requiring treatment, which can further exacerbate TDM-related challenges with respect tissue analysis.[25] In clinical settings, performing TDM on tissue matrices requires the invasive collection of multiple biopsies over the course of treatment, as well as time-consuming sample preparation procedures that are laborious and require multiple steps, such as cryogenic

pulverization or various other homogenization methods in tandem with solid-liquid extraction (SLE).[25] Nevertheless, it is critical to define the relationship of the administered chemotherapeutic dose and the effective concentration in the respective biofluid and tissue.

Metabolomics is an emergent "omic" strategy in systems biology that has been proposed as an alternative means of assessing (combination) chemotherapy efficacy.[153] Briefly, metabolomics entails the study of all metabolites in a system at a given time.[128,154] The use metabolomics or pharmacometabolomics—the study of the metabolome in response to pharmaceuticals—to monitor one or a multitude of metabolic biomarkers for a particular combination or dose of chemotherapy could yield vital information about drug resistance, development of resistance, and overall positive, negative, or indifferent responses to treatment.[153] Though metabolomics in general studies remain tremendously difficult to implement due to challenges associated with validating biomarkers, validating the methods used to obtain these biomarkers, and correctly interpreting candidate biomarkers, metabolomics could nevertheless help to guide treatment and provide information about treatment response.[153]

Despite the availability of targeted approaches like TDM and the potential for untargeted approaches such as metabolomics, it remains difficult to obtain precise information regarding drug concentrations and the efficacy of combination therapy especially during IVLP, particularly in lung tissue. Another challenge of employing metabolomics is the requirement that the system under study not be disturbed by external stimuli, including the sample preparation method. However, biopsies entail removing a piece of the organ from the bulk, which can lead to changes in the metabolic profile of the collected lung sample, as well as in the metabolic profile of the lung itself due to injury sustained during the biopsy. In the case of TDM, current methods for tissue-based determinations of drugs utilize lung biopsies collected prior to the start of IVLP, and biopsies taken from peripheral locations in the lung following the completion of IVLP prior to chest closure at the end of reperfusion. Thus, the current tissue-sampling protocol is not sufficient for determining drug concentrations in the lung during the actual IVLP procedure. Furthermore, the biopsies

obtained after IVLP are usually from areas that are farther away from the bulk of the organ, often producing misleading or erroneous information due to the non-homogenous distribution of the drug within this heterogeneous organ.

Solid phase microextraction (SPME) is a novel alternative sample preparation approach that involves the introduction of a small needle (200 µm in diameter) coated with a biocompatible polymeric extraction phase (40 µm thickness)[55,62,129,155] into the lung, thus eliminating the need for biopsy collection. The simple design of the device and negligible depletion not only facilitate *in vivo* sampling, thereby overcoming an inherent limitation of other tissue sampling preparation techniques, but also integrates sampling and sample preparation into a single step. The polyacrylonitrile-based (PAN) extraction phase allows for the diffusive partitioning of a broad range of small molecule compounds (< 1000 Da) from complex biological matrices through adsorption,[57,104] thus enabling the extraction and monitoring of targeted and untargeted small molecules. In addition, SPME eliminates the need for the solvent or solvent/perfusate-based extraction methods used in other *in vivo* methods, like microdialysis (MD), or other *ex vivo* methods, such as SLE.[55,131,155] When coupled with liquid chromatography (LC) and highly specific and sensitive detectors like tandem mass spectrometry (MS/MS) or high-resolution mass spectrometry (HRMS), this method permits the targeted and untargeted analysis of all compounds removed from the biological tissue.[62] Furthermore, the amenability of SPME for direct coupling to mass spectrometry[156] via a microfluidic open interface (MOI)[79] easily enables rapid therapeutic analysis of drugs or metabolites in typically challenging matrices like tissues, especially under *in vivo* conditions.

The present study had a number of objectives, which were informed by the following factors: the cytotoxicity of the FOLFOX combination therapy; the large inter-patient variations in FOLFOX drug concentrations within the plasma; unknown drug concentrations in the lung tissue; the unknown rate at which metabolites form in the lung, particularly during IVLP (wherein metabolism via the liver is bypassed) as well as IV; and the lack of information regarding organ status during IVLP and IV FOLFOX treatments.

To address these issues, SPME is proposed as an *in vivo* sampling technique for the simultaneous therapeutic monitoring of FOLFOX and metabolites in pig lungs during administration via pre-clinical IVLP and IV, with the chemotherapeutic efficacy of these administration routes being subsequently assessed via pharmacometabolic fingerprinting. To this end, a retrospective SPME protocol was developed for the quantitation of FOLFOX in lung tissue undergoing IVLP; this method was also used to determine FOLFOX concentrations in sample extracts obtained during the pre-clinical IVLP and IV trials. In addition, a retrospective dual mode quantitative LC-MS/MS method was developed for the comprehensive targeted monitoring of FOLFOX and the screening of drug metabolites, including the metabolites of FOL, such as 5-methyltetrahydrofolate (5-methylTHF), 5,10-methyleneTHF, and tetrahydrofolate (THF), and the metabolites of F, including anabolites such as 5FUrd, 5FdUrd, FdUMP, FUTP, and FdUTP, and catabolites such as FBAL and FUPA. Pharmacometabolic fingerprinting was performed using LC-HRMS as a proof of concept to illustrate the ability of SPME to characterize changes in lung tissue over the course of the IVLP procedure. The ability to characterize changes in the lung throughout the IVLP procedure could enable interpretation about the state of the tissue during therapy or provide possible useful biochemical information to indicate potentially promising markers/features of drug effectiveness or toxicity. Furthermore, a supplementary study was conducted to assess metabolic profile stability under the standard storage conditions currently employed in metabolomics; the objective of this supplementary study was to determine whether these standard storage conditions (-80 ^{o}C) reliably preserve precious samples. To the best of our knowledge, this is the first time a dual LC-MS/MS method encompassing FOLFOX and all of its metabolites has been proposed in conjunction with the novel pharmacometabolic fingerprinting methodology to assess chemotherapeutic efficacy during pre-clinical IVLP and IV administration in a porcine model. This is also the first time an SPME-based method has been developed for quantitation of FOLFOX in lung tissue.

5.3 Materials and Methods

5.3.1 Materials

(6R,S)-5,6,7,8-tetrahydrofolic acid hydrochloride (THF) and the internal standard (IS), 5-fluoro-2'-deoxyuridine (5FdUrd), were purchased from Cayman Chemical Company (Ann Arbor, USA), while Uridine-$^{15}N_2$5'-monophosphate (UMP-IS), uridine$^{15}N_2$5'-triphosphate (UTP-IS), folinic acid (FOL)/leucovorin calcium, and 5-fluorouracil (F) were purchased from Sigma-Aldrich (St. Louis, USA). The following compounds were purchased from Sierra Bioresearch (Tucson, USA): 5-fluoro-2'-deoxyuridine-5'-triphosphate (5FdUTP), 5-fluoro-2'-deoxyuridine-5'-monophosphate (5FdUMP), and 5-fluorouridine-5'-triphosphate (5FUTP). Finally, 5,10-methylenetetrahydrofolic acid (5,10-methylTHF), 5-methyltetrahydrofolic acid (5-methylTHF), folic acid-d2 (FA-d2), (2R)-3amino-2-fluoropropanoic acid (FUPA), ureidopropionic acid (FUPA-IS), alpha-fluoro-b eta-alanine (FBAL), alpha-fluoro-beta-alanine-$^{13}C_3$ (FBAL-IS), 5-fluorouridine-$^{13}C,^{15}N_2$ (5FUrd-IS), 5-fluoro-2'-deoxyuridine-$^{13}C,^{15}N_2$ (5FdUrd-IS), oxaliplatin (OX), carboplatin, and chlorouracil (CU) were purchased from Toronto Research Chemicals (Toronto, Canada).

5.3.2 Animals

Four Yorkshire pigs with an average weight of 35 kg were used for the IVLP (3) and IV (1) experiments. This study was approved by the Animal Care Committee of the Toronto General Research Institute and all animals received humane care in compliance with the *Principles of Laboratory Animal Care* outlined by the National Society for Medical Research and the *Guide for the Care of Laboratory Animals* instituted by the National Institutes of Health.

5.3.3 IVLP procedure

This procedure is described in more detail elsewhere.[142,143] Briefly, post induction of general anesthesia, the left pulmonary artery (PA) and the left pulmonary veins (PV) were dissected and isolated via a left thoracotomy, with ventilation to the left lung being maintained by an intensive care unit (ICU) ventilator.

After heparin administration, the left PA and PVs were cannulated and clamped before initiating IVLP in order to isolate the left lung from systemic circulation. 1.2 L of Steen™ solution/perfusion fluid (XVIVO Perfusion, Göteburg, Sweden) was then circulated through the isolated organ by a centrifugal pump, which first passed the perfusion fluid through a membrane gas exchanger that was connected to a heater/cooler which modulated perfusate temperature to normothermic conditions. The warmed solution then passed through a leucocyte filter, entered the lung via the left PA, and exited through the left PV into a hard-shell reservoir maintained at a certain height to ensure suitable PA and PVs pressures. After entering the reservoir, the fluid was then recirculated through the circuit. Drug doses were calculated based on the body weight and body surface area (BSA) of the pigs using Brody's formula.[157] 400 mg/m^2 of FOL was administered intravenously. Once maximum circuit flow was reached, FOX was administered directly into the perfusion circuit through the reservoir as a bolus at a concentration of 400 mg/m^2 for F, and concentrations of either 255 mg/m^2 or 170 mg/m^2 for OX. After 4 hours of IVLP, a 10 to 15-minute washout with 500 mL of pure perfusate (Perfadex; XVIVO Perfusion) was conducted, followed by the removal of the cannulas from the PA and PVs. The lung was then reconnected to systemic circulation and reperfusion (normal systemic circulation) was initiated for a two-hour period.

5.3.4 IV procedure

A left thoracotomy was performed in order to allow the sampling fibers access to the lung; however, no further surgical processes took place. FOLFOX was administered intravenously at 400 mg/m^2 for FOLF and 85 mg/m^2 for OX for a period of approximately 2 hours.

5.3.5 Lung sampling protocol

The SPME fibers used to perform *in vivo* lung sampling during IVLP and IV consisted of an octadecyl-strong-cation-exchange (C18-SCX) coating and were kindly provided by Supelco. The fibers were initially sterilized for a minimum of 30 minutes in a solvent mixture consisting 50:50 methanol/water. Following sterilization, the fibers were removed from the conditioning solvent and inserted by surgeons into the lung

in triplicate approximately 1-2 cm apart from each other at predetermined time points as outlined in Figure 5.1 and described in more detail below. After the extractions had been completed, the fibers were removed from the lung tissue, rinsed manually in water for 5 s to remove any loosely adhered biological matter, wiped with a Kimwipe, and placed in empty 300 µL polypropylene vials. The vials were then snap frozen in dry ice for transportation to the lab. The fibers remained stored in the empty vials at –80 ^{0}C until the time of instrumental analysis.

The left lung was sampled according to the schedule outlined in Figure 5.1 (*In vivo Lung Perfusion (IVLP) SPME fiber Sampling Schedule*). Briefly, the lung was initially sampled at baseline (IVLP Lung Blank) post sternotomy and prior to the addition of FOLFOX; it was then sampled 10 minutes after the intravenous administration of FOL (Time L0), and again 60 minutes after the initial FOL administration (Time L1). Due to surgical time restrictions, an extraction time of 10 minutes was used for each of these three sampling points prior to IVLP. The next round of sampling was conducted following the administration of FOX into the perfusion circuit, 10 minutes (IVLP T0) after the commencement of IVLP (full flow established), with subsequent samplings taking place at 1-hour intervals during the 4 hours of perfusion (IVLP T1-IVLP T3), and at 1-hour intervals during the 2 hours of reperfusion (IVLP T4-IVLP T5). An extraction time of 30 minutes was used for sampling during IVLP and reperfusion.

During the intravenous administration (IV) of FOLFOX, the lung was sampled according to the schedule outlined in Figure 5.1 (*Intravenous SPME Fiber Sampling Schedule*). Briefly, the lung was sampled at baseline (IV lung blank) prior to the administration of FOLFOX, and again at 40 minutes (IV TL) after the start of bolus administration of FOLFOX. The lung was subsequently sampled hourly at 100 minutes, 160 minutes, 220 minutes, and 280 minutes (IV T0 – IV T3). Infusion lasted approximately 2 hours.

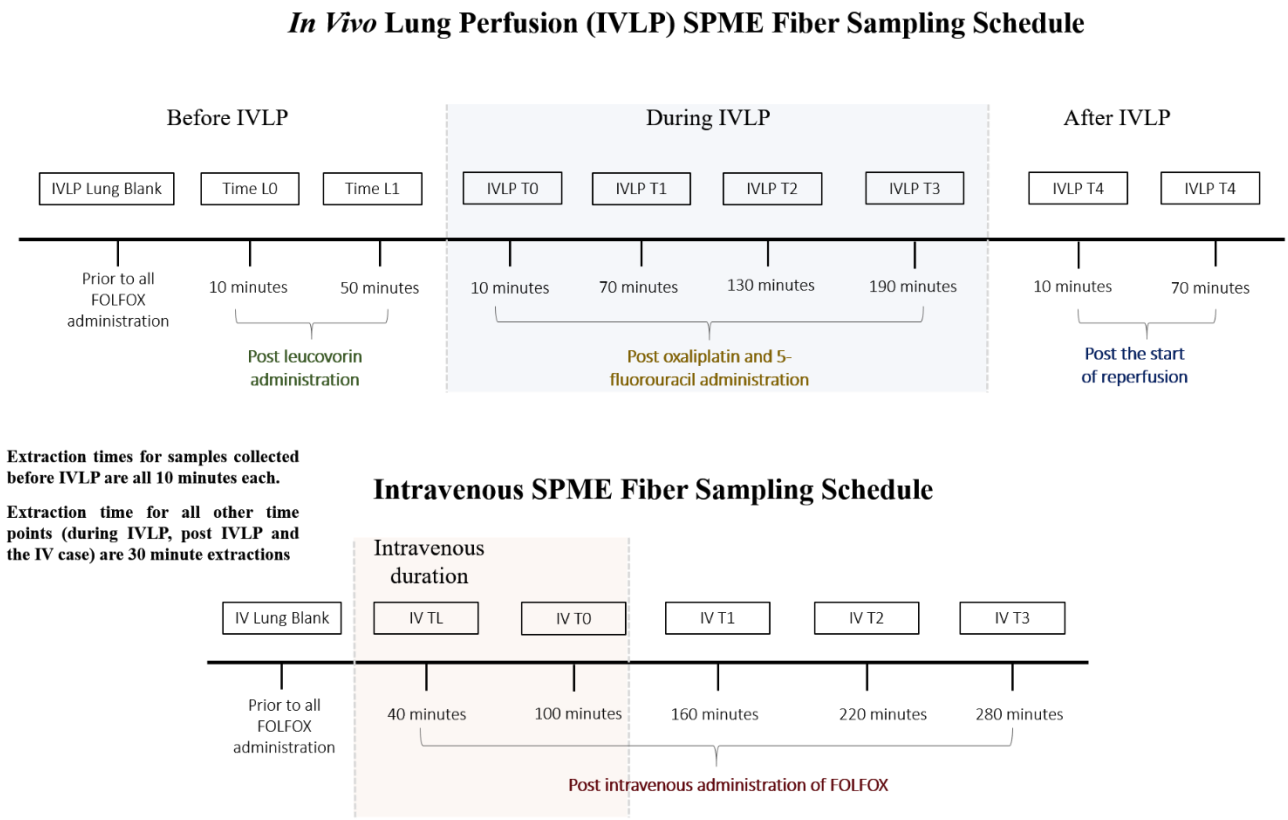

Figure 5.1 Lung sampling schedule using SPME fibers during *in vivo* lung perfusion (IVLP) (top schedule) and intravenous (IV) FOLFOX administration (bottom schedule).

5.3.6 Perfusate sampling protocol

Single perfusate samples were collected in parallel with the IVLP sampling schedule outlined in Figure 5.1 following the same protocol that was used for lung sampling. C18-SCX fibers were sterilized/conditioned in 50:50 methanol/water and then exposed to 300 µL of perfusion fluid for a total of 30 minutes under static conditions. The fibers were then removed, rinsed manually for 5 s in pure water, and stored in empty 300 µL vials, which were snap frozen in dry ice and stored at –80 ^{0}C until further analysis.

5.3.7 Fiber coating procedure

Hydrophilic-lipophilic balance (HLB) was investigated separately, alongside octyl-strong-cation-exchange (C8-SCX) as alternative extraction phase that can compete with C18-SCX, as it has been reported to be particularly useful for isolating compounds characterized by low logP values. To this end, an in-house

developed coating procedure was used to coat nitinol wires with 5 µm HLB particles—which were kindly provided by Waters Corporation—until the coating dimensions measured 1.5 cm in length and 40 µm in thickness.[134,158,159] Briefly, this dip-coating method utilized an automated software-operated computer system to dip the 4 cm nitinol wires into a homogenously mixed slurry composed of 10 % (w/v) particles, 1 % glycerol (v/v), and 89 % (v/v) of 7 % (w/v) PAN. This dipping process was repeated until the desired coating dimensions had been achieved.

5.3.8 Sample preparation and sample extracts

Sampling and sample preparation, which are integrated into a single step in SPME, was conducted at the hospital during pre-clinical IVLP and IV trials as described above. Just prior to instrumental analysis, the fibers were removed from storage at –80 ^{0}C and desorbed at room temperature in 50:50 acetonitrile/water for 60 minutes at 1500 rpm. At the end of the 60-minute desorption period, the fibers were removed from desorption solution and discarded, and LC-HRMS was used to perform instrumental analysis on the final solvent extracts. Once the quantitative method for FOLFOX had been developed, a portion of these extracts were transferred from their original vials (20 µL) to separate vials and mixed with 6 µL of internal standard mixture to produce a final concentration of 200 ng/mL (IS). The quantitative analysis of FOLFOX and the screening of FOLFOX metabolites was then conducted by subjecting these newly prepared solutions to LC-MS/MS.

5.3.9 Mass spectrometric parameters and conditions

Folinic acid, 5,10-methyleneTHF, 5-methylTHF, and THF were tuned and analyzed in positive mode, while oxaliplatin, F, 5FdUMP, 5FdUTP, 5FUTP, 5FUrd, 5FdUrd, FUPA, and FBAL were tuned and analyzed in negative mode. All compounds were initially tuned at a concentration of 1 µg/mL in a 50:50 acetonitrile/water solution containing 0.1% acetic acid, with flow rates of 5 µL/min and 7-10 µL/min for positive and negative mode ionization, respectively. For poor ionizers, infusion was instead performed at either 5 µg/mL or 10 µg/mL. The tuning parameters and conditions are outlined in Table 5.1.

Table 5.1 Mass spectrometric parameters and conditions used for tuning compounds and metabolites in positive and negative mode.

MS Parameters	Positive mode	Negative mode
Source position	B	D
Voltage (kV)	3-3.5	2 - 2.5
Sheath gas (AU)	2-5	15-30
Auxiliary gas (AU)	0 - 2	0 - 2
Capillary temperature (°C)	275	275
Sweep gas (AU)	0	0

5.3.10 LC-MS/MS method for FOLFOX and metabolites screening

The chromatographic separation of F, 5-FUrd, 5-FdUrd, 5-FUTP, 5-FdUTP, 5-FdUMP, FBAL, FUPA, OX and their respective internal standards was performed using a Sequant® Zic®-pHILIC column (100 x 2.1 mm, 5 µm particle size; MilliporeSigma: Darmstadt, Germany) protected by a corresponding Sequant® Zic®-pHILIC column guard column (20 x 2.1 mm, 5 µm particle size). LC-MS/MS was conducted using a Thermo Vanquish quaternary pump and an autosampler coupled to a Thermo TSQ Vantage triple quadrupole mass spectrometer equipped with an Ion Max™ atmospheric pressure ionization (API) heated electrospray source (HESI). Water (mobile phase A) and acetonitrile (mobile phase B), each with 0.1% acetic acid and 5mM ammonium acetate, were employed at a total flow rate of 300 µL/min. An injection volume of 5 µL was utilized, with the samples and column being maintained at 5 °C and 25 °C, respectively. The above-noted compounds were ionized in negative mode at 2 kV in position D. More information on the LC gradient, the HESI source parameters, and the MS parameters is provided in Table 5.2 and Table 5.3.

Table 5.2 LC gradient conditions used with the Sequant® Zic®-pHILIC column (100 x 2.1 mm, 5µm particle size) for OX, F, and F metabolites.

Time (min) Total flow = 300 µL/min	% Mobile phase A: water + 0.1 % acetic acid + 5mM ammonium acetate	% Mobile phase B: acetonitrile + 0.1 % acetic acid + 5mM ammonium acetate
0.00	10	90
1.00	10	90
4.00	70	30
4.70	70	30
4.90	10	90
8.00	10	90

Table 5.3 MS conditions and observed chromatographic retention times for OX, F, and F metabolites. Negative mode ionization was employed.

Compound	Parent mass	Product mass	S-LENS	Collision energy	Retention time (min)
FBAL	106	86	46	11	5.66
FBAL-IS	109	89	47	11	5.66
5-fluorouracil	129	42	49	19	1.26
5-chlorouracil	145	42	52	20	1.21
FUPA	149	86	41	18	5.51
		106 *		12	
FUPA-IS	131	88	38	12	5.30
5-FdUrd	245	155	69	17	1.09
5-FdUrd-IS	248	132	69	16	1.11
		158 *		17	
5-FUrd	261	129	72	10	1.55
		171*		16	
5-FUrd-IS	264	132*	72	17	1.57
		171		16	
5-FdUMP	325	79	82	53	5.54
		129 *		23	
UMP-IS	325	97	105	24	5.74
		113 *		28	
5-FUTP	501	159 *	112	39	6.63
		403		20	
5-FdUTP	485	159	104	35	6.56
		257		27	
		387 *		20	
Oxaliplatin	396	89	95	19	4.60
		196 *		37	
		284		21	
Carboplatin	370	352	133	12	5.22

Some compounds had more than one transition. Transitions which are denoted by (*) were used as the quantifier ion. The other transition(s) were used as qualifier ions. IS means internal standard. The Ion Max heated electrospray ionization source was run at 2 kV at position D with a vaporizer and capillary temperature of 275 °C, and a sheath gas, ion sweep gas, and auxiliary gas of 35, 0, and 5, respectively.

A Discovery® HS F5-3 (PFP) column (100 x 2.1 mm, 3 µm particle size; MilliporeSigma: Bellefonte, PA) protected by a corresponding Discovery® HS F5-3 guard column (20 x 2.1 mm, 3 µm particle size), was employed for the separation of FOL, 5,10-methylTHF, 5-methylTHF, THF and folic acid-d2 on the above-mentioned LC-MS/MS system. Mobile phases A and B consisted of water and acetonitrile, respectively, with 0.25% acetic acid and 0.05% formic acid added to each. The same flow rate and autosampler conditions noted above were applied, but the column was maintained at 30 ^{0}C and an injection volume of

10 µL was used. The compounds were ionized in positive mode at 1.3 kV in position B. More information on the LC gradient, HESI source parameters, and the MS parameters is provided in Table 5.4 and Table 5.5.

Table 5.4 LC gradient conditions for the Discovery HS F5-3 (PFP) column (100 x 2.1 mm, 5µm particle size) used for FOL and its metabolites, 5-methylTHF, 5-methylTHF, and THF.

Time (min) Total flow = 300 µL/min	Mobile phase A: water + 0.25% acetic acid + 0.05% formic acid	Mobile phase B: acetonitrile + 0.25% acetic acid + 0.05% formic acid
0	95	5
0.33	95	5
0.83	85	15
2.17	76	24
2.50	50	50
2.67	10	90
4.20	10	90
7.00	95	5
8.50	95	5

Table 5.5 MS conditions and observed chromatographic retention times for FOL and its metabolites, 5-methylTHF, 5-methylTHF, and THF. Positive ionization was employed.

Compound	Parent mass	Product mass	S-LENS	Collision energy	Retention time
Folinic acid	474	327	109	18	1.33
5,10-methylTHF	458	311	79	20	5.00
5-methylTHF	460	180	56	39	5.46
		313 *		19	
THF	446	299	113	19	5.14
Folic acid-d2	444	297	95	17	1.35

The Ion Max heated electrospray ionization source was run at 1.3 kV at position B with a vaporizer and capillary temperature of 275 °C, and a sheath gas, ion sweep gas, and auxiliary gas of 30, 2, and 30, respectively

5.3.11 Calibration curve and quality control

Study limitations (the release of external compounds (internal standard) was not permitted) inherent to this *in vivo* study conditions precluded the use of pre-loaded internal standards on the SPME fiber and as such, kinetic calibration methods could not be used for quantitation. Consequently, a matrix-matched external calibration curve was instead constructed in 15 g of lamb lung homogenate with a range of 2 µg/g-2000 µg/g. Previous research showed that there was no statistical difference between the amount of drug (doxorubicin) extracted from intact tissue (biopsy collected during pre-clinical IVLP trials with

doxorubicin) vs. tissue homogenate (same biopsy homogenized) using SPME fibers.[160] Internal standards were then only added to the desorption solution, thus correcting for LC-MS injection, but not for extraction. This matrix-matched external calibration curve was made to correspond to an instrumental curve that ranged from 0.001 µg/mL to 1 µg/mL for F and 0.01µg/mL to 3.5 µg/mL for FOL in order to reduce the use of large amounts of lung homogenate and to simplify the quantitation process. Ultimately, a limit of detection (LOD) of 25 µg/g and a limit of quantitation (LOQ) of 50 µg/g was achieved for both F and FOL. This is discussed in *section 5.4.8 "Standard solutions, calibration curves, method validation and quality control"*. A quality control at concentrations of 100 µg/g and 500 µg/g were internally assessed via the back calculation of the validated matrix-matched lung homogenate calibration curve with these points excluded.

5.3.12 LC-HRMS for untargeted analysis

Pharmacometabolic fingerprinting was performed on the porcine lung and perfusate extracts collected during the pre-clinical IVLP and IV trials using a Thermo Exactive orbitrap mass analyzer mass spectrometer coupled to an Accela binary pump and autosampler. Chromatography was done on a Discovery® HS F5-3 column (100 x 2.1, 3 µm particle size: MilliporeSigma: Bellefonte, PA) protected by a Discovery® HS F5-3 guard column (20 x 2.1 mm, 3 µm particle size), using a 40-minute method that had previously been developed in laboratory.[57] Mobile phases A and B consisted of water and acetonitrile, respectively, with 0.1% formic acid added to each for positive mode analysis, and 0.1% acetic acid added to both for negative mode analysis. The column was maintained at 30 ^{0}C, and the samples were kept in the autosampler at 4 ^{0}C. A pooled quality control (QC) consisting of 10 µL of each sample extract was collected in a separate vial and injected every 10 samples during instrumental acquisition. An injection volume of 10 µL was used for LC-HRMS analysis.

5.3.13 Data pre-processing for untargeted analysis

After instrumental analysis via LC-HRMS, the raw files were converted to mzXML files via MSConvert. Initially, the IPO package from the XCMS software package was used with an in-laboratory-developed

script in RStudio in order to optimize the peak-picking parameters based on the pooled QCs.[106–108] These optimized parameters were then used to perform data pre-processing functions, such as noise filtering and baseline correction, peak detection and deconvolution, retention time and mass-to-charge ratio (m/z) alignment and correction, and normalization. The final data matrix, which contained all sample names, all features, their respective retention times, and feature intensity across the samples, was filtered by eliminating features in the pooled QCs with relative standard deviations (RSD) > 30% and a pooled QC-to-blank ratio of < 5. The xMSAnnotator Integrative Scoring Algorithm[110] was used to annotate features from each group in the data via retention time clusters, adduct formation, isotope patterns and abundance and pathway analysis. Only high- and medium-confidence matches with unique or multiple feature identities were considered for further data interpretation.

5.4 Results

5.4.1 Chemometric analysis and model validation

Statistical analysis, including multivariate and univariate analysis, was performed using Metaboanalyst. Principal Component Analysis (PCA) was initially used to assess the quality of the instrumental run via analysis of the pooled QCs' structures, with Partial Least Squares Discriminant Analysis (PLS-DA) and Orthogonal Projection to Latent Structures Discriminant Analysis (O-PLS-DA) being subsequently employed to fingerprint/classify the clustered groups. Univariate analysis by way of the Kruskal-Wallis test was employed to identify any features that changed significantly (false discovery rate (FDR) adjusted p value < 0.05) across two or more time points during IVLP or IV. Only models that passed crossed validation were further considered. The PLS-DA model generated for time points taken during IVLP (IVLP T0 to IVLP T3) was validated using a permutations test (at 1000) and a 10-fold cross validation (CV). Both CV's passed with the original data classification generating a significant difference ($p < 0.01$) in comparison to the remaining permuted distribution of the data while the 10-fold CV produced a model fit of $R^2 = 0.90$ and a predictability of $Q^2 = 0.79$. A such the Variables of Importance (VIP) with scores greater than 1.5 (VIP >

1.5) were further investigated and tentatively identified using METLIN and cross referenced via annotation. Features of interest are shown in the Table 5.6 and tentatively and putatively identified with a mass accuracy of less than 5 ppm.

Table 5.6 VIPs > 1 obtained from a validated PLS-DA model for lung sampling events performed during IVLP with FOLFOX. Shown are statistically significant features changing from IVLP T0 to IVLP T3. Data obtained from positive mode analysis

Compound classification	Feature parameters				Tentative ID
	m/z	Retention time (min)	Adduct	Average VIP score	
Important features found via METLIN and annotation	375.2164	13.9	$[M+H]^+$	28	16-phenyl tetranor prostaglandin E1, 8-oxo-resolvin D1
	378.3	16.6	$[M+Na]^+$	7.1	Arachidonoyl-EA(d8) (not found in annotation)
	282.2792	21.4	$[M+H]^+$	5	oleamide
	377.2324	12.9	$[M+H]^+$	2.1	Resolvin D1 - D4, HDOPA
Other endogenous compounds found via METLIN	247.1075	11.7	$[M+H]^+$	32	N-acetyl-DL-tryptophan
	166.0863	9.0	$[M+H]^+$	6.1	L-phenylalanine
	132.102	7.1	$[M+H]^+$	4.4	L-isoleucine, L-alanine
	205.0973	12.0	$[M+H]^+$	3.9	L-tryptophan
	195.1189	5.1	$[M+H]^+$	2.5	L-arginine
	323.1702	10.0	$[M+NH_4]^+$	2.0	Threoninyl-tryptophan
	182.0813	7.1	$[M+H]^+$	1.5	L-Tyrosine, L-threo-3-Phenylserine, N-Hydroxy-L-phenylalanine
			$[M+NH_4]^+$		Phenylpyruvic acid
	104.1072	6.4	$[M+H]^+$	1.1	Choline

5.4.2 LC method development

Although the FOLFOX compounds are used in combination with one another for chemotherapy, these compounds and their metabolites possess a wide range of polarities (log(p) values provided are a mix of experimental and predicted values obtained from drugbank[161]) and mass ranges (Figure 5.2). Generally, these compounds have been ionized exclusively in either positive (OX, FOL, and FOL metabolites) or negative mode (F and F metabolites), which effectively renders the use of a single LC-MS/MS method impractical unless instruments capable of polarity switching are utilized. Furthermore, various column types have been successfully used for separation of only subsets of these compounds,[162] thus requiring the use of three or more LC-MS/MS methods for the screening and/or quantitation of all FOLFOX drugs and

drug metabolites. To address this challenge, several columns were evaluated during the development of an LC method that could encompass all the target compounds (FOLFOX drug and drug metabolites): a Hypercarb column (100 x 2.1 mm, 5µm particle size; Thermo Scientific), a Kinetex pentafluorophenyl (PFP) column (100 x 2.1 mm, 2.6 µm particle size; Phenomenex), a Discovery® HS F5-3 (PFP) column (100 x 2.1 mm, 3 µm particle size; MilliporeSigma), an Atlantis C18 column (70 x 2.1 mm, 5 µm particle size; Waters Corp), and a Sequant® Zic®-pHILIC column (100 x 2.1 mm, 5 µm particle size; MilliporeSigma). Acetonitrile, water, and methanol were tested as mobile phases, while formic acid, acetic acid, ammonium acetate, or a mixture thereof were tested as mobile phase additives.

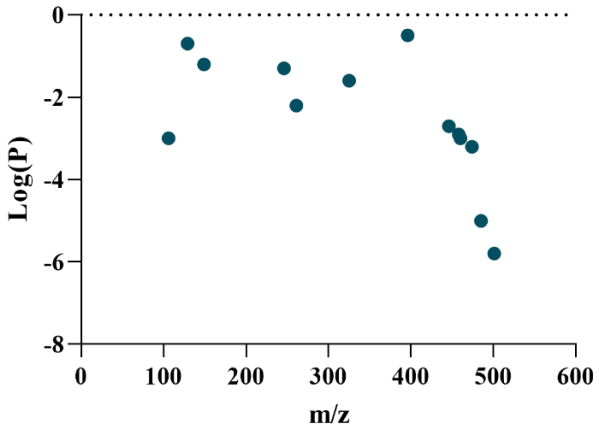

Figure 5.2 Distribution of FOLFOX compounds and their metabolites according to their mass-to-charge ratio (m/z) and physiochemical properties (LogP).

Given the limitations associated with the physiochemical properties of the compounds and their preferred MS polarity analysis modes, the aim was the development of an LC-MS/MS method that ideally used a single column and a dual mode additive, such as acetic acid, that is suitable for both positive and negative modes. This would result in a more streamlined LC-MS/MS analytical process as positive- and negative-mode analysis could be efficiently executed without the need for solvent change over or column conditioning. Therefore, FOL, FOL metabolites, and OX were initially grouped together for analysis in positive mode, while F and F metabolites were grouped together for analysis in negative mode. However,

separation on any particular column was only successful for either positive- or negative-mode groups individually, but not for both at the same time. While the Hypercarb column provided good separation for OX, F, and F metabolites, it was unable to elute folates, even with the increased elution strength of the various MS-compatible mobile phases listed above. This phenomenon was also observed for the Zic-pHILIC column, which provided improved separation and retention of OX, F, and F metabolites, with all folates being eluted close to the void volume. The opposite effect was seen with the Atlantis C18, Discovery, and Kinetex F5 columns; that is, these columns provided good separation for FOL and FOL metabolites, with OX, F, and F metabolites all being eluted in the void volume. It became clear that two LC methods utilizing two separate columns would be necessary for the comprehensive separation and quantification of FOLFOX and the screening its of metabolites. However, the literature contains no reports of oxaliplatin being ionized in negative mode.[163] Considering that it was not feasible to attain OX retention on reversed-phase columns in the same manner as other positively ionized compounds, such as FOL and FOL metabolites, a third LC-MS/MS method would have been necessary to analyze oxaliplatin on a separate column. To avoid the laborious and time-consuming prospect of having to use three separate LC methods, the goal of the method-development process was altered to focus on minimizing the number of LC methods required for the comprehensive analysis and separation of FOLFOX and metabolites. Therefore, for the first time, OX was tuned and analyzed in negative mode, and grouped together with similar polarity compounds like F and F metabolites in an effort to maintain a maximum of two LC-MS/MS methods.

Methanol was found to be a sub-optimal eluent for FOL and FOL metabolites, as it produced extremely poor peak shapes that were either very late-eluting or required a longer LC method; in contrast, acetonitrile produced much better results for the same gradient, with narrower, sharper, gaussian peak shapes and acceptable elution times. A concentration of less than 5 mM of ammonium acetate buffer produced much broader peaks for some metabolites; conversely, while it was more challenging to dissolve 10 mM of ammonium acetate buffer in acetonitrile containing 0.1% acetic acid, this formulation produced a

tremendous increase in the spray current of the ESI needle. However, this volume did not provide significant improvement in peak shape in comparison to the 5 mM ammonium acetate concentration. A similar trend was observed for acetic acid as an additive, as less than 0.25% produced broader peaks during the analysis of FOL and FOL metabolites. A literature review revealed that existing methods for separating and quantitating F and F metabolites generally use mobile phases that require pH adjustment, high salt concentrations (> 10 mM), or the use of a regularly scheduled separate LC run for cleaning.[162,164–168] These types of modifications can be time consuming, potentially error-prone, and lead to MS fouling, which can affect instrument sensitivity. Furthermore, no singular method encompassing all F metabolites has been developed; rather, the developed methods are only able to quantitate/screen for a class of metabolites, like the anabolites specifically, or the catabolites separately. The method developed herein is capable of quantitating and separating all F metabolites, without the need for pH adjustment or the use of high salt concentrations.

5.4.3 Selectivity and specificity of LC-MS/MS method

To ensure that the developed LC-MS/MS method was free of interferences from co-extracted or co-eluted endogenous compounds, C18-SCX-, HLB- and C8-SCX-coated fibers were used to perform extractions from the blank (non-spiked) homogenized lamb lung tissue that had been used to prepare the matrix-matched external calibration curve. In addition, neat solvent blanks were also tested. Neither the solvent blanks nor the blank lung extractions showed any interferences for the specific transitions of any of the desired target compounds or metabolites. The chromatograms illustrating the LC-MS/MS method's specificity and selectivity can be seen in Figure 5.3 (data shown for HLB- and C8-SCX-coated fibers).

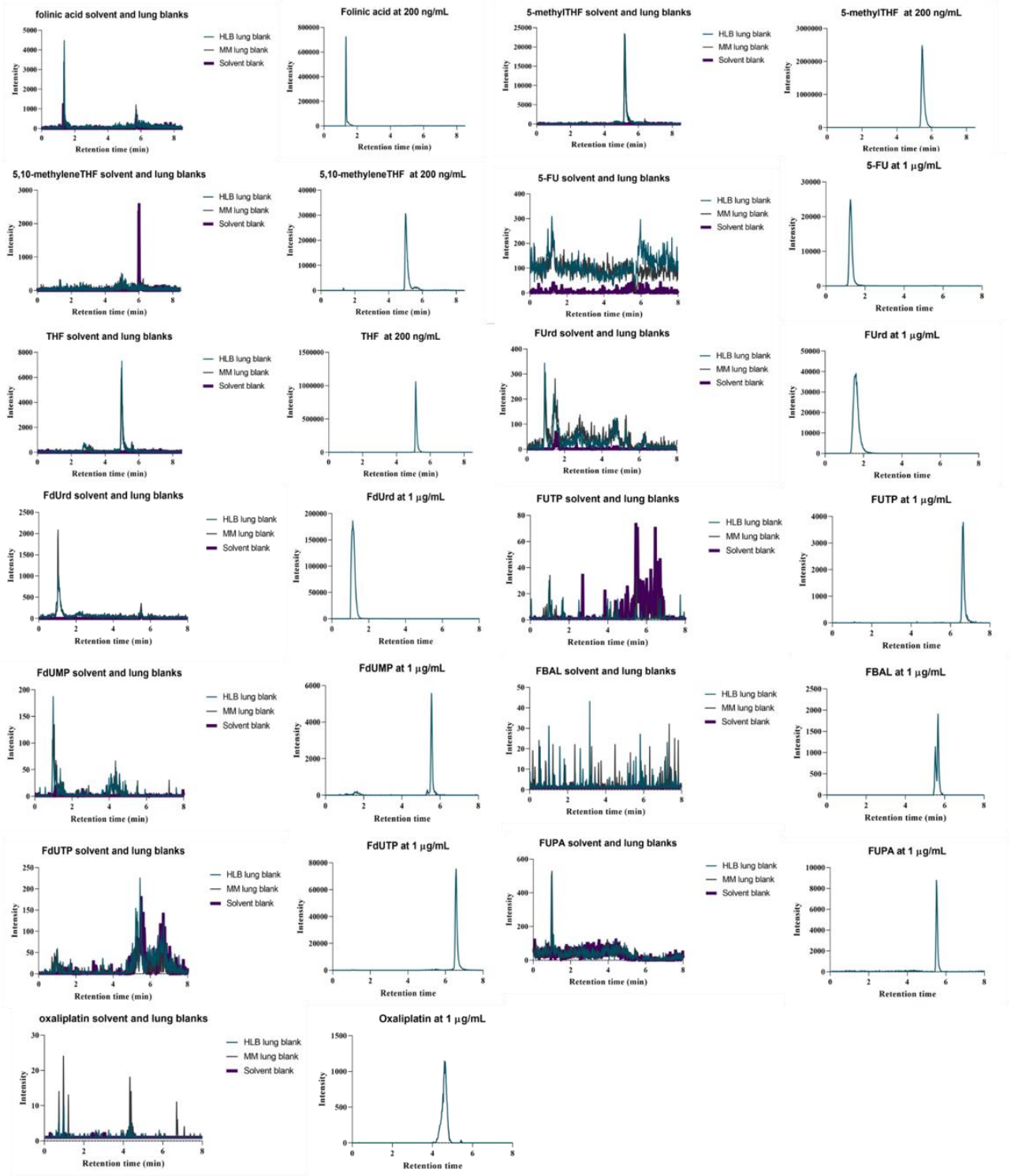

Figure 5.3 Evaluation of LC-MS/MS selectivity and specificity. Neat solvent blank and extracts obtained from blank (non-spiked) lung homogenate with the hydrophilic-lipophilic balance (HLB) and C8-SCX (MM) coatings were injected and monitored at the mass spectrometric transitions of the target analytes. The blank signal from the HLB coating is shown in turquoise, the signal from MM is shown in dark gray, and the signal from the neat solvent is shown in dark purple bolded.

5.4.4 FOLFOX compounds and drug metabolites stability

The OX, F, and F metabolites investigated in this study have previously been reported as being stable in solvent and in extracts from a range of biological matrices, including plasma, cell lines, and tissue.[163–169] As such, the stability of these metabolites was not evaluated further in this study. Since SPME provides quenching by exclusively extracting small molecules from very complex matrices via free concentration while selectively excluding red blood cells, macromolecules such as proteins, and large molecules (>1000 Da). The direct desorption of the fibers into the desorption solvent is comparable to the storage of each compound or metabolite under solvent conditions. For example, DPD, the major enzyme that catabolizes F, is found in red blood cells and in tissues. However, SPME does not extract red blood cells or tissue fragments; rather, its PAN-based coating essentially acts as a high-molecular-weight sieve that allows it to extract only small molecules available in free concentrations. Thus, the extracted drugs and metabolites desorbed into the desorption solution will behave similarly to how they would in pure solvent, as they will not undergo enzymatic degradation. However, folates such of FOL and FOL metabolites are prone to rapid degradation in light, air, and under various pH conditions and temperatures; therefore these compounds require the presence of an antioxidant in the solution.[170] Thus, 1% ascorbic acid was added to the 50:50 acetonitrile/water desorption solution used throughout the development of the proposed method.

5.4.5 Coating performance and absolute recoveries

At the inception of this study, the clinical application of SPME was rather novel. Moreover, access to various coating types and in-house coating protocols were limited at the time, which led to the exclusive use of LC- and bio-compatible C18-SCX-coated fibers that were also newly commercially available. Given that this study involved both targeted and untargeted analyses, these devices were deemed ideal, as they featured good inter-fiber reproducibility, which is essential for reliable data collection, especially for metabolomics. Unfortunately, production of these C18-SCX coatings was halted near the end of the study and were replaced by octyl-strong-cation-exchange (C8-SCX) coatings. This posed a problem, as there were very few remaining C18-SCX fibers available for extensive method development. As such, a

retrospective evaluation was completed to compare these newly available C8-SCX coatings against both the previously employed C18-SCX coating and a newly developed (at the time) in-laboratory coating method that produced HLB-coated devices.

The performances of all three coatings were evaluated via recovery tests in phosphate buffered saline (PBS), with the results shown in Figure 5.4. The absolute recoveries from PBS and homogenized tissue, as shown in Figure 5.5, were only tested for HLB and C8-SCX due to the limited number of C18-SCX fibers remaining (results in Figure 5.5 shown only for C8-SCX as these were the commercially available replacements for C18-SCX). PBS and tissue were spiked at clinically expected concentrations for FOLFOX and all associated metabolites. PBS was spiked at 300 µg/mL and 100 µg/mL for FOLFOX and the metabolites, respectively, while lamb lung homogenate was spiked at 300 µg/g for FOLFOX and 100 µg/g for the metabolites. The sampling protocol for both PBS and lung tissue homogenate were as outlined for lung and perfusate in *section 5.3 "Materials and Methods" namely sections 5.3.5 "Lung sampling protocol" and 5.3.6 "Perfusate sampling protocol"*, with 5 replicates being performed for each coating at each time point.

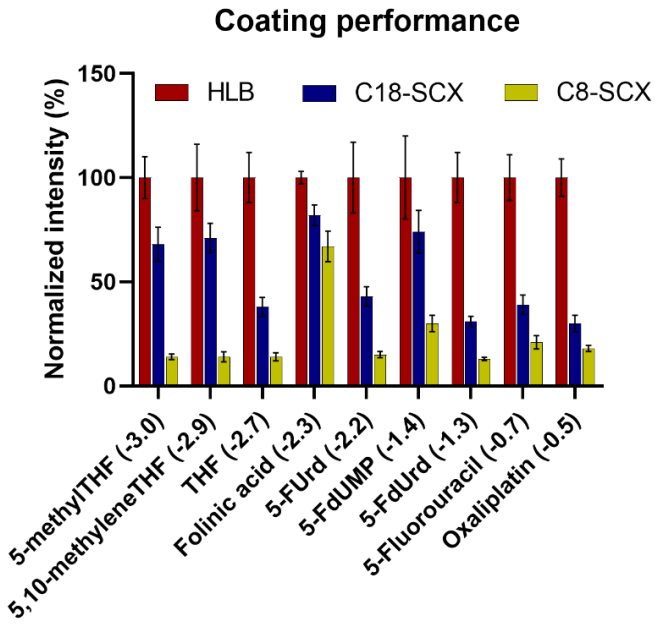

Figure 5.4 Evaluation of coating performance based on extractions from PBS spiked at clinically expected concentrations. Values were normalized based on the intensity observed with HLB. The HLB coating is shown in red, the C18-SCX is shown in blue, and the C8-SCX coating is shown in yellow. The relative recoveries are shown for each compound along with their log P values in parentheses.

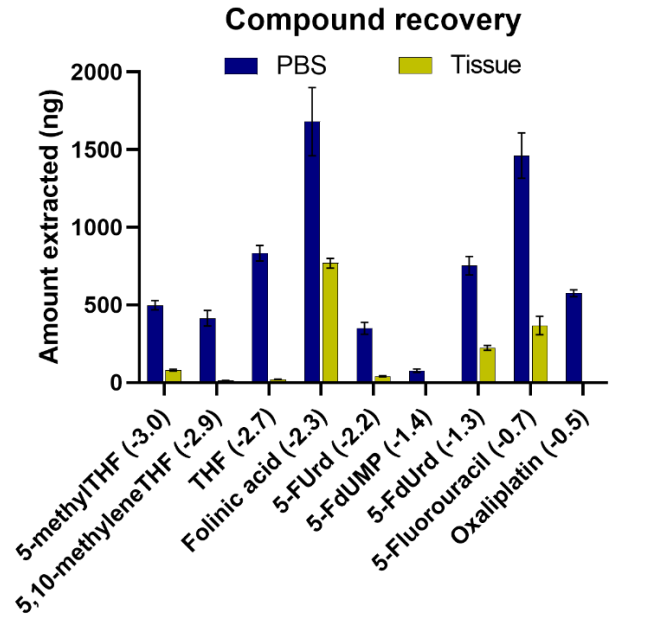

Figure 5.5 Absolute recoveries of FOLFOX and its metabolites from PBS and homogenized lamb lung tissue spiked at clinically expected concentrations. The log(p) value for each compound is provided in parentheses. Results shown only for the C8-SCX coating.

The HLB coating exhibited superior recovery for the majority of the compounds (Figure 5.4), a result that is consistent with previous findings showing its ability to provide excellent extraction, especially for very polar compounds like FOLFOX from aqueous matrices.[52,53] HLB showed as little as 1.5 times improvement in extraction efficiency compared to C18-SCX, and as much as 10 times improvement for some compounds compared to C8-SCX. Interestingly, C18-SCX demonstrated the next best recovery for these compounds, followed by its replacement C8-SCX. This trend is likely due to the strong interactions between the polar moieties of the target compounds and metabolites and the polar N-vinylpyrrolidone group on the HLB coating. Furthermore, it also appears that many of these compounds and metabolites contain aromatic or ring groups that better interact with the divinylbenzene group on the HLB coating via dispersion forces. This speculation is supported by the lower recoveries for slightly smaller but comparatively linear metabolites, such as FUPA and FBAL (results not shown), which would have less overall interaction due to their decreased molecular surface area. Thus, weak interaction between short hydrocarbon chains and aromatic extraction phases could explain the decreased recovery of these compounds via HLB. Moreover, the greater recovery for the majority of compounds and metabolites with the C18-SCX coating, as opposed to its short-chain counterpart, C8-SCX, supports the deduction that extraction efficiency is influenced by the degree of surface area interaction between the compounds and the coatings. While this would suggest improved recoveries for ring-containing metabolites with larger molecular weights, such as 5-FdUTP and 5-FUTP, the observed negligible recoveries (results not shown) could also be due to slower diffusion kinetics since the PBS extractions were performed under static conditions, or simply that these compounds are extremely polar with log(p) values of less than -5.0 and thus have a very low affinity (partition coefficient) for the coating. The coating performance trends observed in tissue homogenate mirrored those observed in PBS, with HLB providing better extraction efficiency and coverage of compounds than C8-SCX. However, the much lower recovery rates from homogenized tissue compared to PBS (Figure 5.5-yellow bars, shown only for C8-SCX) suggest significant matrix binding for many analytes, which therefore affects the free concentration available for SPME extraction. Additionally, some metabolites that were

already difficult to extract from PBS, such as 5FdUTP, 5FUTP, FUPA, and FBAL due to their polarity or structure, failed to be extracted altogether even when spiked at the same concentration in tissue as the parent compound F, which is much higher than the expected metabolite concentration.

5.4.6 Extraction time profile

30 minutes was arbitrarily selected as the generic extraction time for sampling during the pre-clinical IVLP and IV trials. It is important, however, to determine whether this 30-minute extraction time falls under the pre-equilibrium, kinetic or equilibrium conditions of the time profile in order to appropriately account for any reproducibility issues that may result from slight variations during the active sampling protocol as a result of unforeseen surgical circumstances. As such, an extraction time profile was constructed using lamb lung homogenate in order to investigate the time at which the equilibrium was achieved for the HLB and C8-SCX coatings (Figure 5.6). Extraction times of 1 min, 5 min, 10 min, 20 min, 30 min, 45 min and 60 min were selected given the time limitations imposed by the surgical procedure. After being exposed to the lung homogenate for the predetermined extraction time, the fibers were removed, manually rinsed in 300 µL of water for 5 s, wiped with a Kimwipe, and then desorbed in 100 µL of 50:50 acetonitrile/water containing 200 ng/mL of internal standards.

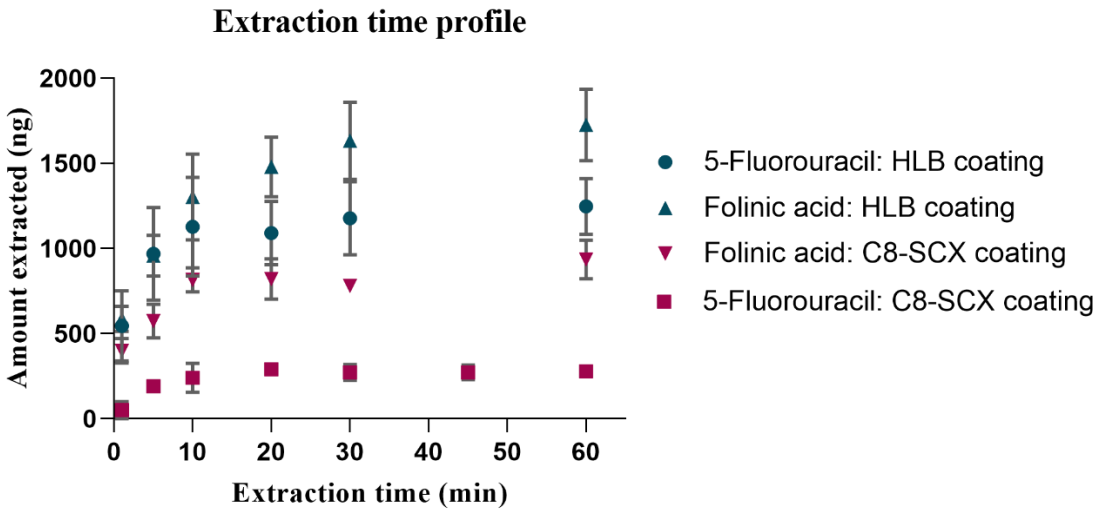

Figure 5.6 Extraction time profile of FOLFOX from lamb lung homogenate. The following extraction times were tested: 1 min, 5 min, 10 min, 20 min, 30 min, 45 min, and 60 min. The HLB and C8-SCX coatings were evaluated using 5 replicates for each coating at each time point.

The extraction conditions used in this retrospective analysis were set to closely mimic clinical conditions in terms of the drug concentration administered into the perfusate. Therefore, lamb lung homogenate was spiked at concentrations of approximately 300 µg/g and 170 µg/g for FOLF and OX, respectively. The spiked homogenate was then left to equilibrate at 500 rpm for 3 hours before performing extractions at various times. While it is common practice to allow a minimum of 8 hours for drug equilibration in tissue to permit various binding equilibria to be established, *in vivo* lung sampling occurred as early as 10 minutes after drug administration during IVLP. As such, 3 hours was deemed a suitable compromise between common bioanalytical practice and the clinical conditions of the experiment. 15 g of lung homogenate was weighed for each time point of the extraction time profile, with 5 replicates being investigated for each the two extraction phases. Extraction was timed and performed under static conditions for all time points simultaneously to avoid any differences due to fluctuating binding equilibria as a function of time.

As shown in Figure 5.6, extraction equilibrium was reached at 20 minutes for FOL and 30 minutes for F using HLB-coated fibers, and at 10 minutes for both compounds using C8-SCX. These results are in accordance with SPME fundamentals, which hold that longer equilibration times and higher amounts of

extracted analyte are directly proportional to an increased affinity between the targeted compound and the coating. This explains why HLB coatings provide better method sensitivity, but also require equilibration times that are 2-3 times longer than those required for the C8-SCX coatings. Unfortunately, OX could not be recovered from tissue due to high binding and rapid non-enzymatic transformation, which results in a half-life of only 14 minutes in biological systems.[150] Considering the 3-hour equilibration time after spiking the lung tissue with FOLFOX, the results for OX correlate with the experimental conditions. Based on the results shown in Figure 5.4, it would be safe to assume that the C18-SCX coating used for sample collection during experiments would have achieved equilibrium between 10 and 30 minutes as a function of analyte affinity and coating performance. Therefore, it can be concluded that a 30-minute extraction time was suitable for SPME sampling during pre-clinical IVLP and IV trials as it remains within the desired SPME equilibrium conditions.

5.4.7 Calibration under *in vivo* conditions

SPME fibers were used to perform *in vivo* sampling in the left lung during IVLP. The advantage of SPME as a sample preparation method is related to its fundamentals, shown in Eq (6), which permit *in vivo* sampling when the sample volume (V_s) is sufficiently larger than the product of the sampling device coating volume (V_f) and the analyte's affinity for the coating (K_{fs}) Eq (7), such that the amount of analyte extracted (n) becomes independent of the sample volume (V_s) Eq (8).

$$n = \frac{K_{fs}V_f C_0 V_s}{K_{fs}V_f + V_s} \tag{6}$$

$$V_s \gg K_{fs}V_f \tag{7}$$

$$n = K_{fs}V_f C_0 \tag{8}$$

Thus, it is important to perform calibration under the same *in vivo* conditions in the surrogate lamb lung matrix by determining the sample volume/weight above which *in vivo* conditions would dominate. Under the appropriate *in vivo* conditions, the amount of analyte extracted becomes independent of the sample

weight or volume. The experiment was conducted in accordance with the procedure outlined by Roszkowska et al.[160] Briefly, a bulk amount of lamb lung homogenate was spiked at the expected clinical FOLFOX concentration of 300 µg/g and then homogenized and agitated at 500 rpm for 1-2 hours. The bulk lung homogenate was then portioned at weights of 1 g, 5 g, 10 g, and 15 g, with extractions being performed simultaneously from each weight in replicates of 5 to avoid any errors associated with time delay or binding equilibria. An extraction time of 30 minutes was employed. Figure 5.7 (results for F shown, similar results obtained for FOL) shows that the extracted amount of F becomes independent at 10 g of lamb lung homogenate, which is consistent with SPME-related research for the quantification of doxorubicin from lung tissue.[160] Nonetheless, 15 g of lamb lung homogenate was used to construct the calibration curve in order to ensure that conditions were within the acceptable *in vivo* range for quantification. Furthermore, the external matrix-matched calibration curve was made to correspond to an instrumental curve in order to avoid the use of lamb lung homogenate each time. This procedure is detailed in the following *section 5.4.8 "Standard solutions, calibration curves, method validation and quality control"*.

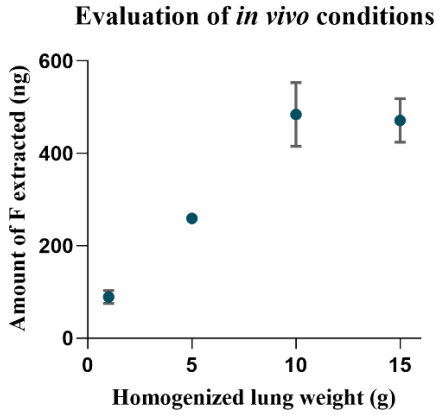

Figure 5.7 The assessment of *in vivo* conditions for appropriate calibration. The following weights of homogenized lamb lung were tested: 1g, 5g, 10g, and 15g. This test sought to find the conditions under which the amount of extracted F becomes independent of the sample weight.

5.4.8 Standard solutions, calibration curves, method validation and quality control

Folates are especially susceptible to degradation by oxidation and thus need to be protected with antioxidants. Dimethylsulfoxide (DMSO) has been documented as an antioxidant that is tissue compatible, miscible with LC-MS-compatible solvents,[171] and is generally and effective cosolvent. Thus, in order to mimic the high FOLFOX concentrations that are administered in perfusate and expected to be observed in tissue during IVLP, DMSO was employed as a solvent to produce the highest resultant concentrations for FOL (100 mg/mL), OX (100 mg/mL), F (100 mg/mL), 5,10-methyleneTHF (10 mg/mL), 5-methylTHF (20 mg/mL), and THF (20 mg/mL). Conversely, water was used to produce the highest concentrations for 5FUrd (20 mg/mL), 5FdUrd (25 mg/mL), FBAL (10 mg/mL), FUPA (5 mg/mL), 5FdUMP (5 mg/mL), 5FdUTP (29 mg/mL), and FUTP (16 mg/mL). All standards were stored at –80 ^{0}C until further use. To reduce the number of freeze-thaw cycles these high-concentration standards would be subjected to, each standard was diluted to 100 µg/mL working solutions, which were further diluted for method development and MS tuning. The limited availability (small amounts) and high costs of all metabolite standards, as well as their very low recoveries in matrix-deficient and especially matrix-abundant environments via SPME extraction, precluded their quantitation in tissue in compliance with the *in vivo* SPME calibration method. However, it did allow for metabolite screening.

A matrix-matched external calibration curve with no internal standard correction was constructed for FOLFOX compounds such that 1 mL of standard mix at a specific concentration could be added to 15 g of lamb lung homogenate. This approach was appropriate, as internal standards were neither present nor could be used during *in vivo* sampling due to clinical limitations imposed by the hospital as a safety precaution for the animals. Thus, 1.5 mL of FOLFOX stock standards diluted with water were made at the following concentrations: 30 µg/mL, 75 µg/mL, 150 µg/mL, 375 µg/mL, 750 µg/mL, 1 125 µg/mL, 1 500 µg/mL, 3 750 µg/mL, 7 500 µg/mL, 15 000 µg/mL, and 30 000 µg/mL; in order to produce an external lung homogenate calibration curve corresponding to concentrations of 2 µg/g, 5 µg/g, 10 µg/g, 25 µg/g, 50 µg/g, 75 µg/g, 100 µg/g, 250 µg/g, 500 µg/g, 1000 µg/g, and 2000 µg/g. In accordance with the *FDA's guidelines*

for bioanalytical method validation, the limits of detection (LOD) and limits of quantitation (LOQ) were found to be 25 µg/g and 50 µg/g, respectively, for FOL and F, with an achieved linearity (R^2) of 0.99 for both compounds (Figure 5.8A and Figure 5.8C).

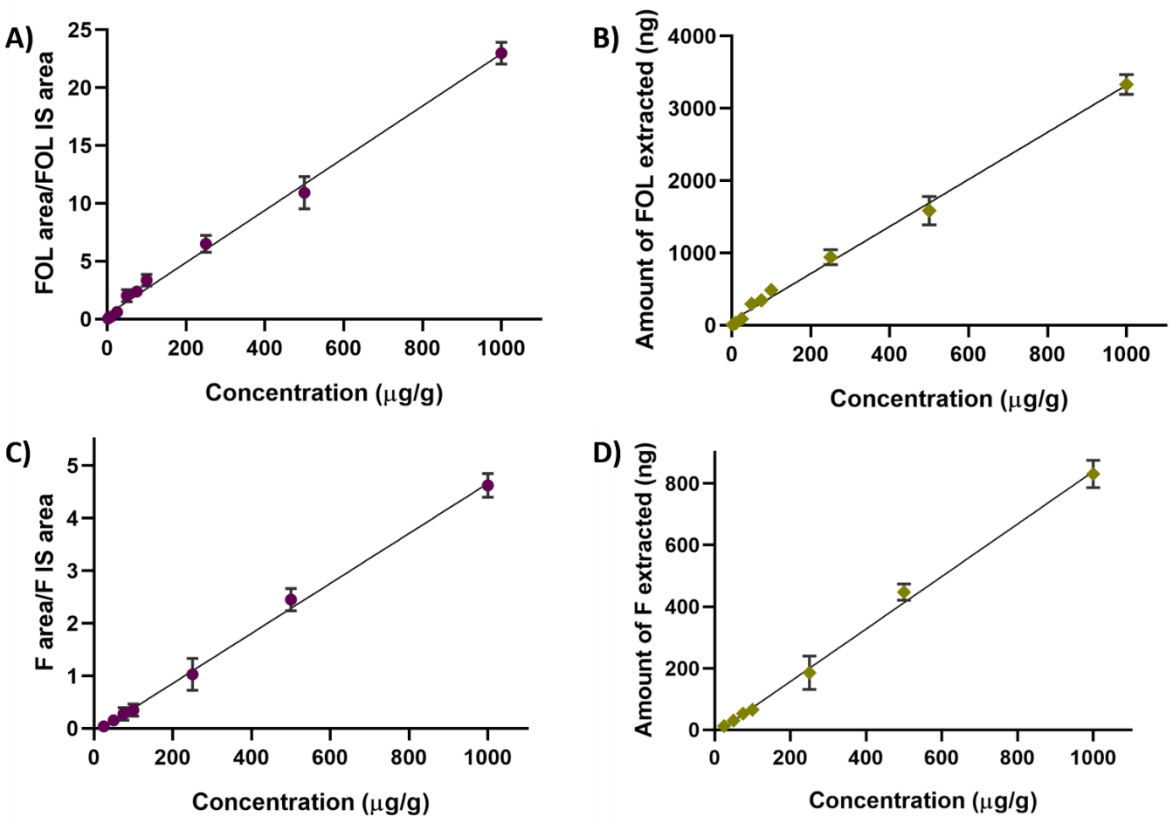

Figure 5.8 Matrix-matched external calibration curve in lamb lung homogenate for FOL (A) and F (C). A linear dynamic range from 50 µg/g to 1000 µg/g with a linearity (R^2) of 0.99 was achieved for both compounds. Each calibration curve was correlated with the amount of extracted FOL (B) and F (D) in order to streamline the analytical process. Linear dynamic ranges corresponding to 295 ng to 3000 ng and 30 ng to 800 ng were achieved for FOL and F, respectively.

In an attempt to provide more practical measurements, the matrix-matched calibration curve was related to an instrumental curve based on the amount extracted. This approach eliminates the need to continuously use lamb lung homogenate, which can be arduous to prepare, and it also reduces the use of the very high-concentration standards required for the appropriate weight of lung used, which proved difficult to achieve for some standards due to solubility limitations. Figure 5.8B and Figure 5.8D show the absolute amounts

(ng) of FOL and F that were extracted at each point of the matrix-matched external lung calibration curve. While this method of quantification allows for a more efficient and sustainable workflow, it is worth mentioning that it is only useful for 1.5 cm length C8-SCX coated fibers with a thickness of 40 µm. Furthermore, the instrumental calibration curve should be constructed in the same way each time, to avoid issues with accuracy and precision. As such, the instrumental curve used herein was constructed via serial dilutions of a 40 µg/mL stock solution such that 10 µL of each instrumental stock from 10 ng/mL to 40 µg/mL could be diluted to 100 µL, thereby producing an instrumental curve that ranged from 1 ng/mL to 4 µg/mL. The obtained LODs and LOQs corresponded to an extracted amount of 90 ng and 295 ng for FOL, and 12.5 ng and 30 ng for F. The instrumental curve was used to determine the absolute amounts of FOL and F obtained in clinical IVLP and IV samples that were below the LOQs of the lung calibration curve. In addition, only the absolute amounts (ng extracted) of FOL and F were determined for perfusate samples instead of the appropriate concentration (µg/mL). This drawback was due to the restricted availability of Steen solution to persons strictly within clinical settings. These restrictions were a result of the very high cost of this commodity (approx. 2000-3000 CAD per 500 mL) and its exclusive use for organ preservation. The instrumental curves for FOL and F, which were correlated to the matrix-matched external lamb lung homogenate calibration curve, was used to provide the absolute amounts (ng extracted) of drugs from lung samples and perfusate samples that fell below the LOQ (50 µg/g) of the matrix-matched calibration curve. The instrumental curve produced a linearity (R^2) of 0.999, with an LOD and LOQ of 1 ng/mL and 5 ng/mL for FOL, and an LOD and LOQ of 5 ng/mL each for F. A quality control (QC) at concentrations of 100 µg/g and 500 µg/g was internally assessed via the back calculations of the validated matrix-matched lung homogenate calibration curve with the respective point excluded prior to calculation. An accuracy and precision of 99.8% and 8% was achieved for the QC internally assessed at 100 µg/g while an accuracy and precision of 101% and 20% was achieved for the QC internally assessed at 500 µg/g.

5.4.9 Sterilization and preconditioning

Clinical protocol requires the sterilization of all devices that will be used on patients. While solvent sterilization was sufficient for these animal experiments, there are cases that may require more rigorous sterilization approaches. This type of preconditioning may affect the extraction efficiency of the fibers, which may in turn affect the various conditions that were evaluated. In this work, the following preconditioning solutions were tested and assessed: 50:50 methanol/water, which is the typical solution employed for SPME conditioning; saline solution, which is often used in clinical settings; pure sterilized water; and no solution at all. These various solutions were tested for both autoclaved and non-autoclaved C8-SCX fibers since these fibers were the commercially available replacement for the C18-SCX fibers used to perform active sampling during the pre-clinical trials. During these tests, all fibers were preconditioned under their respective conditions for a minimum of 30 minutes, which was followed by a 30-minute static extraction in PBS solution spiked with 300 ug/mL of FOLFOX and metabolites, a 5 s manual rinse in water, and desorption in 50:50 acetonitrile/water for 60 minutes at 1500 rpm. Figure 5.9A and Figure 5.9B reveal that the autoclaved and non-autoclaved fibers that were conditioned in 50:50 methanol/water performed significantly better than those that had been conditioned in saline, pure water, and no solution at all. Although saline appeared to outperform pure water and no solution conditioning on average, there were no significant differences ($p < 0.05$) in the amounts of FOLFOX or metabolites extracted using the autoclaved and non-autoclaved devices, both within and between groups, that had been preconditioned using these solutions. However, there were significant differences ($p < 0.05$) in the amount of F and FOL extracted by the autoclaved and non-autoclaved fibers that had been conditioned with 50:50 methanol/water; specifically, non-autoclaved fibers extracted more of both compounds. This contrasts with previous results for the quantitation of doxorubicin in lung tissue,[160] wherein autoclaved fibers out-performed non-autoclaved fibers. These results suggest that device pre-treatment and preconditioning have various effects that are compound-specific. Interestingly, the metabolite, 5,10-methyleneTHF, showed significantly ($p < 0.05$) improved recoveries under autoclaved conditions and preconditioning with 50:50 methanol/water

compared to non-autoclaved conditions with the same preconditioning solvent. Conversely, no significant differences were observed for OX under the same conditions (Figure 5.9C). It is also important to mention that the autoclaved and non-autoclaved fibers were visibly different after being removed from the 50:50 methanol/water preconditioning solution. In contrast to the other solutions/conditions (saline, pure water, no preconditioning solution), which left the fibers with a white appearance, the 50:50 methanol/water solution left both the autoclaved and non-autoclaved fibers with a hydrated dark grey appearance.

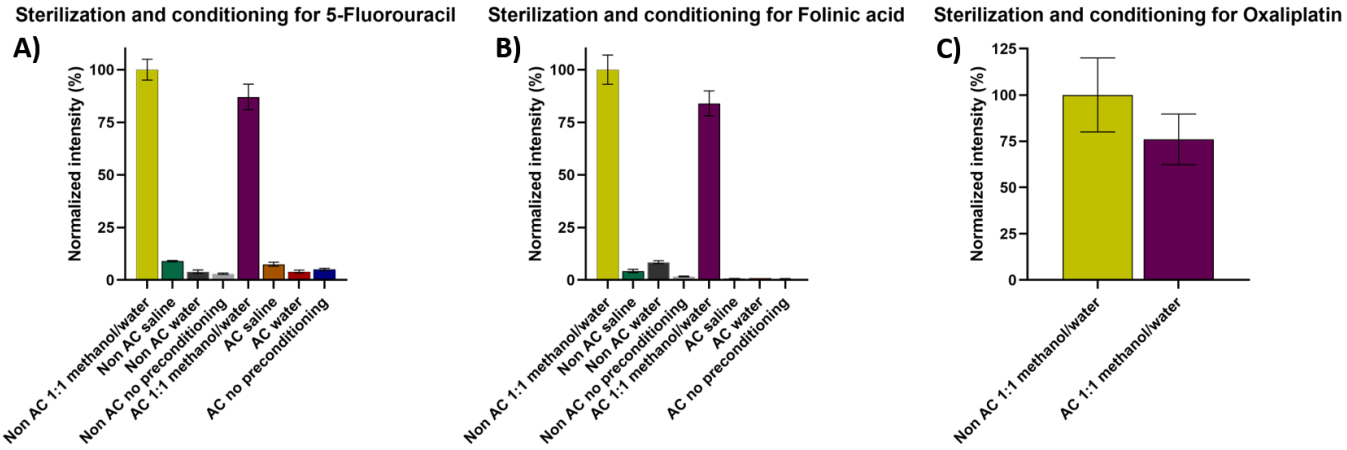

Figure 5.9 Evaluation of sterilization and preconditioning of C8-SCX-coated fibers for F (A), FOL (B), and OX (C). Sterilization by autoclave was tested against non-autoclaved fibers. For each category of steam sterilization, preconditioning solutions of 50:50 methanol/water, saline solution, pure water, and no solution were tested

5.5 Discussion

5.5.1 Application of the developed SPME-LC-MS/MS protocol on samples obtained from pre-clinical trials of FOLFOX chemotherapy using IVLP

The retrospective SPME-LC-MS/MS method development revealed that the HLB coating provided the best sensitivity for the compounds and metabolites of interest. However, the tests conducted during method development also showed that the C18-SCX-coated fibers, which were used during these pre-clinical IVLP and IV trials, were rather suitable as well. In addition, preconditioning in 50:50 methanol/water was shown to be an acceptable sterilization method for non-autoclaved SPME devices, as it enabled good coating

extraction efficiency to be maintained. Furthermore, an extraction time of 30 minutes, which was used during sampling prior to method development, was also revealed to be within equilibrium conditions for the investigated HLB and C8-SCX coatings, with the supposition that the C18-SCX coating would achieve equilibrium within comparable times. Nonetheless, since the C8-SCX-coated fibers were used to build the calibration curve and the C18-SCX-coated fibers were used to perform sampling, it is only possible to form a close estimate of FOLFOX concentrations in the collected pre-clinical samples, while allowing for a 20% to 50% difference in these obtained values for FOL and F, respectively. These limits are based on the differences observed in the recovery of these compounds during the coating performance tests (Figure 5.4). Briefly, FOL was administered intravenously prior to the start of IVLP. Once the IVLP circuit was assembled and full flow was established, FOX was administered directly into the perfusion fluid, with perfusion of the left lung continuing for 4 hours. A final lung flush was performed after IVLP and prior to the start of reperfusion. In all three pre-clinical IVLP cases, no FOLFOX was detected in any of the pig lung blanks; however, F was quantifiably recovered only in samples collected after the administration of FOX and during the 4 hours of IVLP from IVLP T0 to IVLP T3 (Figure 5.10A). As Figure 5.10A shows, F appears to maintain a steady concentration between 250 µg/g and 350 µg/g throughout IVLP. This trend could be indicative of F's low protein binding of 8-12% (information provided by DrugBank[161]), which leaves the majority of the drug available in free form during IVLP. The larger error bars for some of the sampling points are likely related to the non-homogenous distribution of the drug in the lung and the 1 to 2 cm spacing of the fibers during sampling.

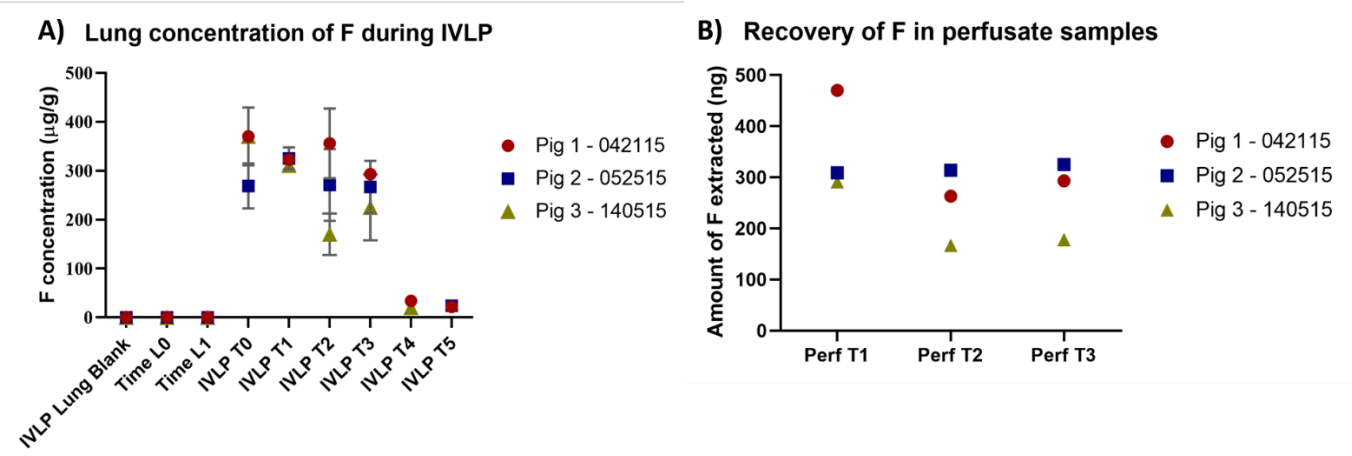

Figure 5.10 Application of *in vivo* SPME protocol and developed LC-MS/MS method for the quantification of F in pre-clinical IVLP samples. (A) Lung concentration of F throughout the IVLP procedure. (B) Absolute recovery of F obtained from perfusate samples collected during IVLP. Refer to Figure 5.1 on page141 for the *"Figure 5.1 Lung sampling schedule using SPME fibers during in vivo lung perfusion (IVLP) (top schedule) and intravenous (IV) FOLFOX administration (bottom* schedule*)."*

This steady state trend is mirrored in the results for the perfusate samples shown in Figure 5.10B. Notably, the amount of available F appears to drop at Perf T2 and Perf T3 for Pigs 1 and 3 (compared to Perf T1), while no such drop is observable for Pig 2. This might be a result of different rates of enzymatic activation or degradation among the pigs, however, it is difficult to reliably conclude what this trend signifies, as only one perfusate sample was taken at each time point. It is important to remember that, given the differences in the devices used for calibration and sample collection, the actual concentration can be estimated to be about twice that reported above, resulting in a concentration between 500 µg/g and 700 µg/g. Trace amounts of F were detected in the samples collected during the two hours of reperfusion, which suggests that the flushing step with fresh perfusion fluid before reperfusion prevents systemic exposure to high drug concentrations. 5FdUrd and 5FUrd were also detected in lung samples, but these compounds were mostly found in perfusate samples on an inconsistent basis. For example, 5FdUrd was detected in one pig's lung as early as one hour after the start of IVLP (IVLP T0) and approximately 30 minutes after FOX administration, but not in the other two pigs at the same time point. Furthermore, it could be detected at IVLP T1 for all pigs but was undetectable by IVLP T3. 5FUrd was mostly detected at IVLP T2, IVLP T3,

and, in some cases, IVLP T4 and IVLP T5 for pigs 1 and 2. These fluctuations might be the product of the dynamics of drug administration and distribution rather than the processes of metabolism due to the minimal presence of various concentrations of the F-dependent enzymes responsible for anabolism. Traces of 5FdUTP and 5FUTP were also observable in a few perfusate and lung samples from as early as IVLP T1 to as late as IVLP T5. Neither F nor its metabolites were found in the lungs during the IV case using the developed LC-MS/MS method. FBAL and FUPA were not detected in any of the samples in the IVLP and IV cases, which may simply be the result of the poor analyte affinity for the coating rather than an indication of their nonexistence, as was earlier demonstrated in the coating performance tests (Figure 5.4).

No F was detected prior to the start of IVLP when only FOL had been administered; at these earlier time points, namely, 10 minutes (Time L0) and 50 minutes (Time L1) after the initial IV administration of FOL, only FOL was detectable (Figure 5.11A). However, the amount of FOL recovered from the lung was inconsequential, falling below the 25 µg/g LOQ for determining its concentration in the tissue (interpolated to be between 5-25 µg/g). Thus, the tissue concentration of FOL could not be reliably quantified with this method, and the amount recovered (ng) was used instead. There is a decreasing trend in the amount of FOL recovered for the IVLP cases over the course of 60 minutes from Time L0 to Time L1 (Figure 5.11A). This decreasing trend is observed again during the IV application (Figure 5.11B), with the FOL concentration appearing to peak 100 minutes after the commencement of FOLFOX infusion (IV T0) and then slowly decreasing. This trend suggests that the drug is either partitioning into cells, experiencing elimination, or is being metabolized. It should be noted that 5-methylTHF has been reported as the final product of FOL metabolism[172,173] and has been shown to be most stable of all FOL-related metabolites[174], especially under a wide pH range (pH 2-10). While 5,10-methyleneTHF could not be detected, 5-methylTHF was detected at Time L0 and Time L1 (10 minutes and 60 minutes after the infusion of FOL) in the IVLP cases and throughout the IV cases starting as early as IV T0, 100 minutes after FOL administration at the peak of FOL concentration. It is important to consider a few limitations in the analysis of these samples for folate derivatives including: the tendency of 5,10-methyleneTHF to rapidly convert to THF under various

temperature and pH conditions (low pH, pH below 8); the instability of THF also at low pH (pH below 5); the fact that these samples were unfortunately not stored with an antioxidant after being initially desorbed; and that the chromatographic conditions used produced a pH between 3-5. Therefore, it is difficult to screen for or accurately quantify the absolute amounts of each of these folate species in this particular application, with the exception of 5-methylTHF that is stable between a pH range of 2-10 and thus could indeed be detected/screened for. The use of an antioxidant is therefore strongly recommended for future research.

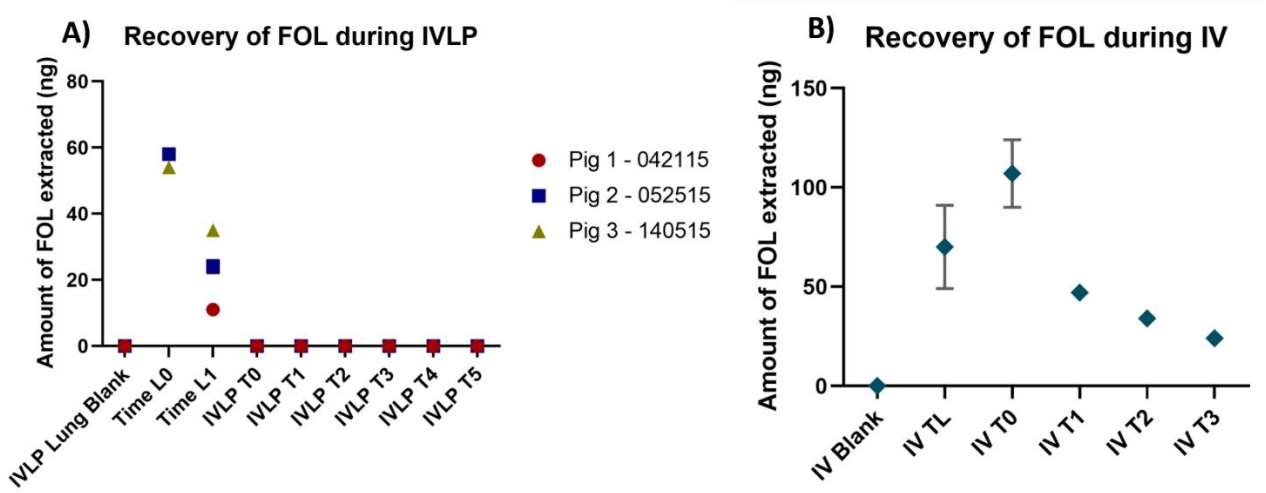

Figure 5.11 Application of *in vivo* SPME protocol and developed LC-MS/MS method for the quantification of FOL in preclinical IVLP samples. (A) Absolute recoveries of FOL from lung tissue during IVLP. (B) Absolute recoveries of FOL from lung tissue during IV administration of FOLFOX.

5.5.2 Untargeted pharmacometabolomic analysis

In order to monitor the biochemical profile of the living system during IVLP and IV with anticancer polytherapy (FOLFOX), a novel microextraction technology, SPME, was applied to isolate endogenous and exogenous small molecules from lung tissue and perfusate samples. SPME fibers, which are the size of acupuncture needles, were inserted directly into the left lung of the pig during IVLP, as well as during the IV administration of drugs. Additionally, SPME fibers were used to extract metabolites from perfusate samples that were collected in parallel with the lung sampling events during IVLP. The annotation and

identification of the molecular features (metabolites) detected in the SPME extracts via the developed LC-MS/MS method revealed changes in the metabolomes of these analyzed matrices (Table 5.7 to Table 5.9).

In examining the overall data structure of the samples, which were initially analyzed in 2015, it is evident that the instrumental analysis was reliable, as the pooled QCs clustered well in the center of all the samples on the PCA plot (Figure 5.12A and Figure 5.12B). It is important to note that, given the three biological replicates (3 pigs sampled) included in the analysis and the three technical replicates (3 fibers) collected during each sampling time for each pig, specifically for the lung sampling events, there is a clear and significant difference between the samples. This can be seen in the categorical clustering of each group, namely, samples collected prior to the start of IVLP (lung blanks and samples collected after FOL administration); those collected during IVLP (IVLP T0 to IVLP T3); and those collected during reperfusion after IVLP (IVLP T4 and IVLP T5). Interestingly, contrary to expectations, there is no clustering corresponding to the progression of the IVLP procedure from the first hour to the fourth hour. However, the IV case from the same time period (2015) (Figure 5.12B and Figure 5.12C with pooled QCs removed) shows distinct clustering of the lung samples collected prior to FOLFOX administration (IV Blank – represented in red) and clear separation between these samples and the last two sampling time points (IV T2 and IV T3), with overlap occurring between the three interim sampling time points (IV TL0, IV T0, and IV T1).

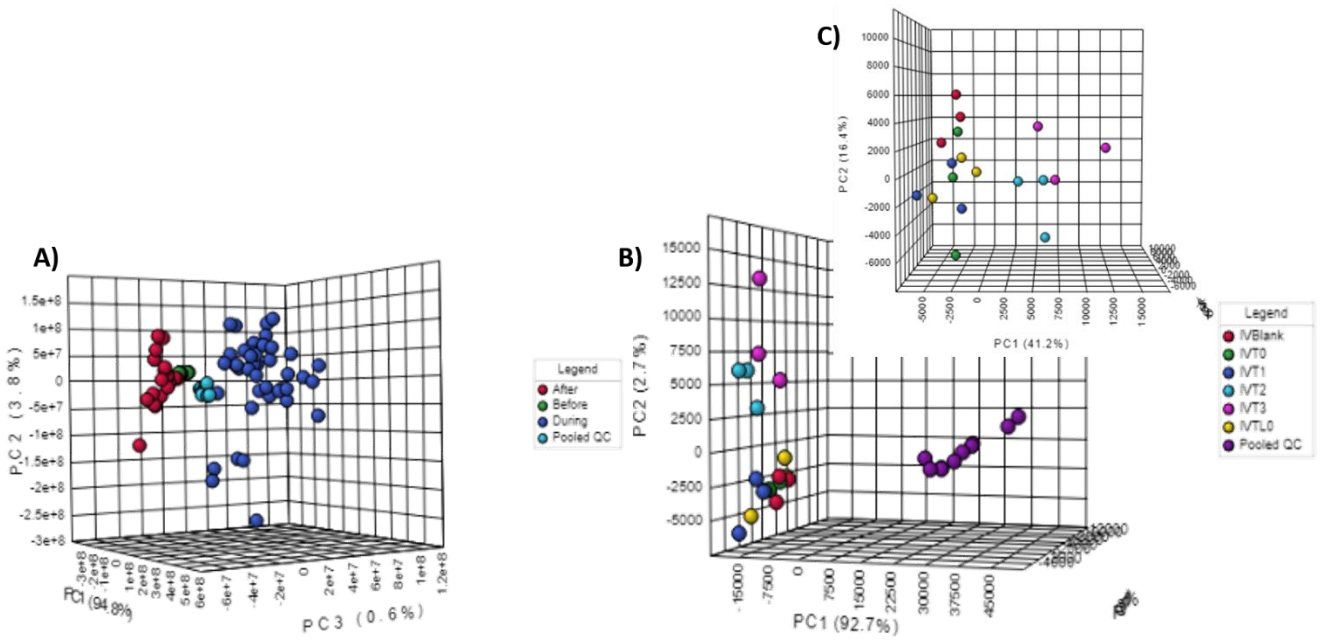

Figure 5.12 Principal component analysis (PCA) plots of the overall structure of the data for lung samples taken during IVLP and IV administration of FOLFOX. A) PCA (PC1:94.8%, PC2: 3.8%, PC3: 0.6%) plot for lung sampling events over the course of IVLP. Samples taken before, during, and after IVLP (during reperfusion) are represented in green, blue, and red, respectively. Pooled QC's are represented in turquoise. B) PCA (PC1: 92.7%, PC2:2.7%; PC 3: 1.1%) plot of lung sampling events during IV administration. Samples collected at baseline and hourly for 5 hours after the start of infusion are shown in red, yellow, green, blue, turquoise, and pink, respectively. Pooled QC's are represented in purple. C) PCA (PC1: 41.2%, PC2: 16.4%, PC3: 12.6%) plot for samples shown in B) with pooled QCs removed to enable closer observation.

Over the course of IVLP, the observed compositional changes of endogenous metabolites in the lung tissue were related to the metabolism of amino acids, acylcarnitines, purines and pyrimidines, lipids, and pro- and anti-inflammatory compounds, among others (Table 5.7). Moreover, these metabolomic alterations were also reflected in the composition of the perfusate samples (Table 5.8). For instance, the number of amino acids initially detected in the lung tissue significantly decreased approximately 60 minutes after the administration of FOL (Time L1 in Figure 5.1) and remained low until the end of the reperfusion period. Concurrently, the number of dipeptides significantly increased starting at 70 minutes post FOX administration (IVLP T1 in Figure 5.1), which may be related to the intense metabolism of these compounds after the local administration of anticancer drugs into the perfusion circuit. However, analysis of the perfusate samples collected during IVLP not only revealed a higher number of dipeptides, but also a higher

number of free amino acids (Table 5.8). Since SPME extracts only a portion of the unbound analytes, it is possible that the certain metabolites may be present in the lung in lower abundance due to their higher binding affinity to the lung tissue components, thus reducing their level of free concentration for SPME extraction. Conversely, there may be higher free concentrations of these metabolites in perfusion fluid due to their lower binding affinity for perfusate components; this explains why a higher number of free amino acids were observed in the perfusate samples than were observed in lung tissue. Interestingly, the systemic administration of FOLFOX did not significantly affect the number of amino acids and dipeptides, as the composition of these compounds stayed relatively constant in lung tissue for more than 4 hours after IV drug administration (Table 5.9). In addition, after systemic drug administration, the number of detected free amino acids was much higher in comparison to the number of these compounds extracted from the lungs during IVLP, which may be a result of different drug administration routes.

Although low numbers of several lipid species were detected early in the IVLP procedure, including bioactive lipids (oxylipids) with either pro- or anti-inflammatory activity, the number of these compounds significantly increased by the second hour post FOX administration (IVLP T2) (Table 5.7). These observed alterations were even more profound in perfusate samples (Table 5.8). Interestingly, a similar trend was observed in lung tissue after the IV administration of anticancer polytherapy, as a tremendous release of pro- and anti-inflammatory compounds was observed approximately three hours (IV T1) post drug administration. This strongly indicates that, for oxylipins specifically, the changes with respect to these compounds in lung tissue over time are more related to the polytherapy activity than the route of drug administration (IVLP vs. IV).

Apart from the above-mentioned group of compounds, the overall metabolomic profile of lung tissue after systemic drug administration differed significantly from the lung tissue profile observed during IVLP (Table 5.7). For instance, a group of endogenous compounds known as autacoids—specifically, resolvins and neuroprostanes—were detected in lung tissue and perfusate samples solely during the IVLP procedure

(i.e., 60 minutes post FOX administration). These locally acting compounds possess potent immunoregulatory properties and may strongly affect the activity of the immune system.[140] Interestingly, these autacoids were not detected in lung tissue after IV administration of FOLFOX, which indicates that FOX's distinct impact on the metabolomic profile of lung tissue—and, consequently, the pharmacokinetics and pharmacodynamics of the polytherapy in the targeted organ—is strongly dependent on the administration route. It should also be noted that the concentration of metabolites, or intermediates of purine and pyrimidine metabolism remained relatively constant in lung tissue after the systemic administration of FOLFOX (Table 5.9) but decreased significantly during the local administration of FOLFOX via IVLP (Table 5.7). However, the most prominent finding relates to the identification of the main active metabolite of F, FdUMP[175], solely in lung tissue after IV drug administration. FdUMP was detected in lung tissue about 100 minutes after the systemic administration of F and remained present until the end of SPME sampling (up to 280 minutes). The lack of FdUMP in lung tissue during IVLP may indicate the crucial role of liver metabolism in both the catabolic and anabolic pathways of F biochemical transformations. While the presence of this metabolite might seem to contradict the results (or lack thereof) obtained via the developed targeted LC-MS/MS method (wherein no F metabolites were detected during IV administration), this discrepancy can be explained by the improved sensitivity in terms of resolution experienced with HRMS instruments and other nuances related to data processing, which is outside the scope of this research. This highlights the benefits of implementing both types of instrumentation (MS/MS and HRMS) for the comprehensive analysis of newly explored systems.

5.5.3 Storage conditions and metabolite stability

Sampling were performed at Toronto General Hospital in 2015. Upon the completion of sampling, the fibers were snap frozen in dry ice and stored in empty 300 µL vials for transportation to the laboratory where they were stored at –80 ^{0}C until instrumental analysis. After analysis, the sample extracts were re-stored at –80 ^{0}C until they were analyzed again two years later in 2017. These sample extracts were consistently stored

under the above conditions and were not subjected to multiple freeze-thaw cycles (less than two cycles). Figure 5.13 shows a loss of approximately 40% of the information corresponding to nearly 1400 features.

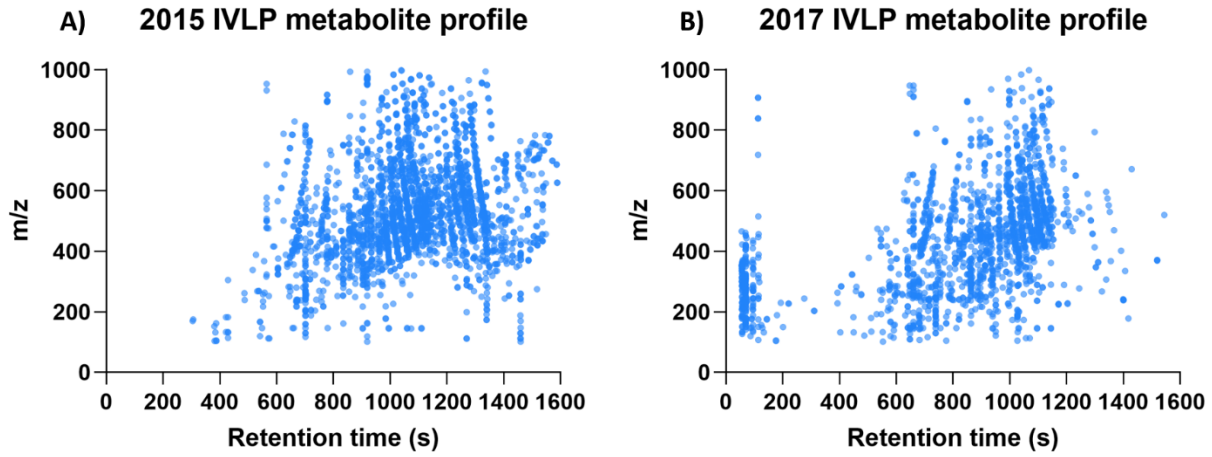

Figure 5.13 (A) Metabolite profile of pre-clinical IVLP samples obtained and analyzed via LC-HRMS in 2015. (B) Metabolite profile of the same pre-clinical IVLP samples upon re-analysis in 2017. Both sets of data were filtered in the same way.

While the PCAs obtained from both sets of data maintain a similar structure (Figure 5.14A and Figure 5.14B), the metabolite profiles for the lung samples before, during, and after IVLP are noticeably different (Figure 13). For example, a significant loss of features within a large m/z range between retention times of 1200 s to 1600 s can be observed from 2015 to 2017. Additionally, a loss in the number of features greater than 600 m/z between retention times of 600 s to 800 s, and the appearance of features below 500 m/z with retention times of less than 200 s can also be observed, which could be products of degradation.

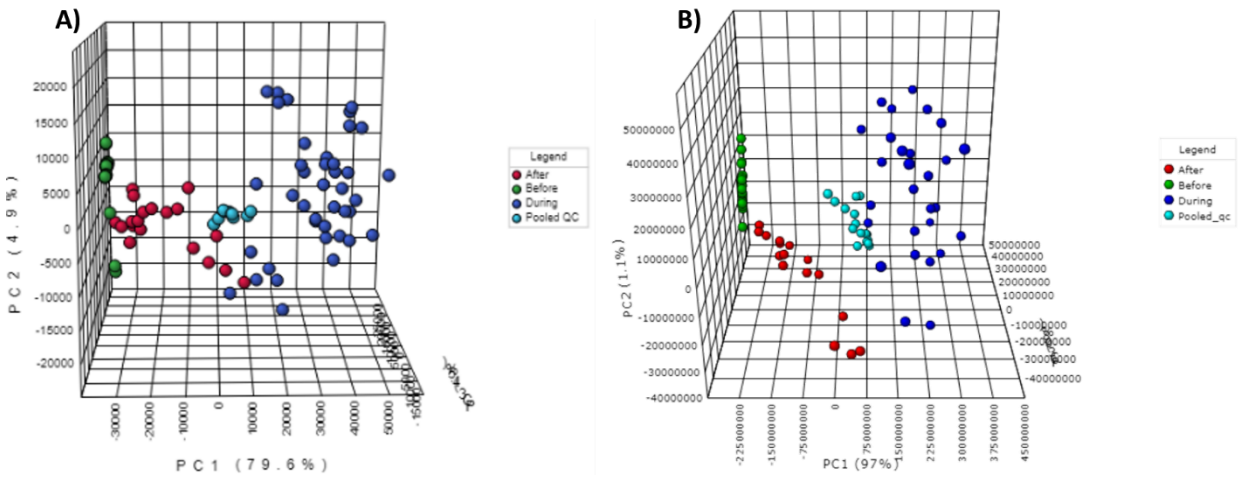

Figure 5.14 Principal component analysis (PCA) of lung samples taken before the start of IVLP (IVLP Lung Blank, Time L0, Time L1), during IVLP (IVLP T1 to IVLP T3), and post IVLP during reperfusion (IVLP T4 and IVLP T5). Each group of samples is represented by green, red, and blue, respectively. A) PCA (PC1: 79.6%, PC2:4.9%, PC3:1.1%) of samples acquired in 2015. B) PCA (PC1: 97%, PC2: 1.1%, PC3: 1%) of the same samples in 2017. Each data set shows the clustering of the pooled QCs at the center of the data (represented by turquoise).

While it is difficult to pinpoint what causes these changes during storage under these conditions, the profiles clearly highlight the degradation of data integrity over prolonged storage times. Given the time-consuming nature of metabolomics data processing, it may be quite challenging to employ tandem mass spectrometry for metabolite validation if discriminating features or features of importance have degraded. Indeed, as was observed in this study, the analysis done before and after storage showed a drastic difference in the same data sets for samples taken before, during, and after IVLP. Moreover, annotation of the 2017 data revealed almost no information of importance due to the loss of almost half the data initially annotated in 2015. Briefly, the annotated peaklist from 2017 data showed most amino acids were retained in the data from 2015 but only a few peptides were present, indicating peptide degradation during sample storage. In addition, a few lipids were scantily detected in the 2017 data in comparison to the 2015 data, indicating the substantial degradation of these classes of compounds during storage.

5.6 Conclusion

In vivo lung perfusion (IVLP) is a novel isolated lung technique and adapted EVLP strategy developed for the local administration of high-dose chemotherapy *in situ* in order to treat metastatic lung cancer. Combination therapy involving folinic acid-5-fluorouracil-oxaliplatin (FOLFOX) is routinely employed to treat a number of solid tumors in various types of tissues. However, the most active drug, F, requires close monitoring during administration, as it has been found to exhibit large interpatient variability with regards to plasma concentration. Since plasma concentrations are not always reflect the drug concentration in tissue, it is also essential to employ sample preparation methods that are specific to monitoring drug concentrations in tissue. Thus, *in vivo* SPME was proposed as an effective tool for sampling lung tissue during pre-clinical IVLP and IV trials using FOLFOX. To overcome the limitations of current sample preparation and separation techniques, a retrospective SPME-LC-MS/MS method capable of providing improved tissue analysis was developed. In the proposed method, SPME is utilized for repeated and easy *in vivo* sampling of complex biological matrices, such as lung, which is followed by comprehensive quantitative and qualitative separation methods aimed at determining FOLFOX concentration in lung tissue, screening of FOLFOX metabolites, and general pharmacometabolic profiling. This marks the first documented attempt to develop a complementary, all-encompassing LC-MS/MS method for the quantitation and screening of FOLFOX and its metabolites. Furthermore, the extraction of other endogenous and exogenous small molecules and their detection via LC-HRMS made it possible to assess the impact of polytherapy on the metabolomic profile of the lung, which revealed metabolic pathways specifically associated with the route of administration (IVLP vs. IV) as well as those related to the therapy itself. Additionally, while both methods of administration seemed to produce relevant metabolites indicative of effective therapy, these metabolites were produced to a lesser extent via IVLP, as the formation of important anabolites occurs via enzymatic transformation in the liver. In addition, the lack of change in the lung metabolic profile over the course of IVLP may indicate that 1) the lungs are still performing well during treatment and perhaps higher doses of chemotherapy can be tolerated; 2) and the use of a different fluorinated pro-drug might be more

efficient. It would also be worth investigating potential long-term complications by assessing the lungs up to days after treatment with IVLP. Furthermore, the results of the supplementary study, which evaluated the metabolome stability of extracts stored at –80 °C over a long period of time (2 years), illustrates the challenges associated with metabolomic studies, as the observed loss of data emphasizes the importance of performing analysis and MS/MS validation as soon as possible after sample collection. Considering not only the time-consuming aspect of this type of analyses with the plethora of data processing techniques available but also the untargeted nature of these studies, it is difficult to process and interpret data quickly enough as well as predict which features or compounds are likely to be problematic in terms of degradation, since reliable metabolite identification in itself remains the bottleneck of translating metabolomics into clinical practice. In summary, this study successfully demonstrated that SPME is an effective *in vivo* sampling tool for the concomitant quantitative monitoring of polychemotherapy and qualitative lung assessment via pharmacometabolomic fingerprinting during the IVLP and IV administration of FOLFOX.

Table 5.7 High- and medium confidence annotated features changing over the course of IVLP (Lung blank until the end of reperfusion IVLP T5) with FOLFOX administration

	Lung Blank	IVLP L0	IVLP L1	IVLP T0	IVLP T1	IVLP T2	IVLP T3	IVLP T4	IVLP T5
	L-Glutamine	L-Tryptophan	Lipoyllysine	Beta-Citryl-L-glutamic acid	L-Asparagine	Beta-Citryl-L-glutamic acid	Lipoyllysine	Beta-Citryl-L-glutamic acid	Beta-Citryl-L-glutamic acid
	L-Phenylalanine	L-Phenylalanine	D-Tryptophan	Lipoyllysine	L-Threonine	Lipoyllysine	N(6)-(Octanoyl)lysine	Lipoyllysine	Lipoyllysine
	L-Tyrosine	Lipoyllysine	L-Tryptophan	N-acetyltryptophan	Beta-Citryl-L-glutamic acid	L-Tryptophan	N-Acetylglutamine	L-Tryptophan	L-Tryptophan
	D-Serine	N-Acetyl-L-methionine	Kynurenic acid	D-Tryptophan	Lipoyllysine	Kynurenic acid	D-Lysine	L-Asparagine	Kynurenic acid
	N6,N6,N6-Trimethyl-L-lysine	L-Aspartic acid	L-Phenylalanine	(E)-2-Methylglutaconic acid	L-Aspartic acid	L-Phenylalanine	Kynurenic acid	L-Threonine	Tridecanoylglycine
	Lipoyllysine	L-Serine	N-Acetylhistamine	L-Tryptophan	N-acetyltryptophan	N-Acetylhistamine	L-Lysine	2-Hydroxyglutarate	N-Undecanoylglycine
	L-Methionine	L-Lysine	Tridecanoylglycine	L-Phenylalanine	N-Acetylglutamine	N-Undecanoylglycine	L-Histidine	N-acetyltryptophan	Myristoylglycine
	Homocitrulline	L-Histidine	N-Undecanoylglycine	N-Acetylhistamine	N-Acetylglutamic acid	Myristoylglycine	L-Phenylalanine	D-Glutamine	Palmitoylglycine
	L-Cystine	L-Asparagine	N-Nonanoylglycine	N-Undecanoylglycine	Kynurenic acid	Palmitoylglycine	N-Acetylhistamine	L-Phenylalanine	
amino acids	L-Lysine	L-Threonine	N-Lauroylglycine	Tridecanoylglycine	3-Hydroxymethylglutaric acid	Tridecanoylglycine	Tridecanoylglycine	N-Acetylhistamine	
	L-Asparagine	o-Tyrosine	N-Decanoylglycine	N-Nonanoylglycine	L-Phenylalanine	N-Nonanoylglycine	N-Undecanoylglycine	Tridecanoylglycine	
	L-Threonine	D-Glutamine		N-Decanoylglycine	N-Acetylhistamine	N-Decanoylglycine	N-Nonanoylglycine	N-Undecanoylglycine	
	L-Proline	N-Acetylglutamic acid		Myristoylglycine	Pristanoylglycine		N-Lauroylglycine	Palmitoylglycine	
	L-Glutamic acid	Kynurenic acid			Myristoylglycine		N-Decanoylglycine	N-Nonanoylglycine	
	N-Acetylglutamic acid	L-2-Hydroxyglutaric acid			Palmitoylglycine			N-Lauroylglycine	
	Kynurenic acid	L-Glutamine			Tridecanoylglycine			N-Decanoylglycine	
	L-Leucine	D-2-Hydroxyglutaric acid			N-Undecanoylglycine			Dimethylglycine	
	L-Isoleucine	3-Hydroxyglutaric acid			N-Nonanoylglycine				
	N-Acetyl-L-methionine	L-Tyrosine			N-Decanoylglycine				
	L-Arginine	N-Acetylhistamine							

	L-Histidine	o-Tyrosine								
	L-Tryptophan	Beta-Tyrosine								
	Ne,Ne dimethyllysine	L-Tyrosine								
	Tridecanoylglycine	N-Undecanoylglycine								
	Pristanoylglycine	Tridecanoylglycine								
	N-Undecanoylglycine	N-Nonanoylglycine								
	Guanidoacetic acid	N-Lauroylglycine								
	3-Hydroxymethylglutaric acid	N-Decanoylglycine								
	Pyroglutamic acid	Beta-Tyrosine Dimethylglycine								
peptides	Glu-Val	Phenylalanyl-Lysine	L-gamma-glutamyl-L-valine	Glu-Val	Tyrosyl-Glutamate	L-gamma-glutamyl-L-valine	Glu-Val	Glu-Val	Leucyl-Aspartate	
	L-gamma-glutamyl-L-valine	Lysyl-Phenylalanine	L-beta-aspartyl-L-leucine	L-gamma-glutamyl-L-valine	Leucyl-Aspartate	L-beta-aspartyl-L-phenylalanine	Prolyl-Asparagine	Tyrosyl-Glutamate	Isoleucyl-Aspartate	
	L-beta-aspartyl-L-leucine	Alanyl-Glycine	Arginyl-Arginine	L-beta-aspartyl-L-leucine	Isoleucyl-Aspartate	L-beta-aspartyl-L-leucine	Phenylalanyl-Aspartate	Leucyl-Aspartate	Histidinyl-Histidine	
	Cysteineglutathione disulfide	L-alpha-glutamyl-L-hydroxyproline		L-alpha-glutamyl-L-hydroxyproline	Glycyl-Hydroxyproline	L-Aspartyl-L-phenylalanine	Leucyl-Aspartate	Isoleucyl-Aspartate	Hydroxyprolyl-Cysteine	
	L-Cysteinylglycine disulfide	Alanylglycine			Glutamyl-Tyrosine	Arginyl-Arginine	Isoleucyl-Aspartate	Glutamyl-Tyrosine	Cysteinyl-Hydroxyproline	
	Glutarylglycine	L-Threo-3-Phenylserine			Aspartyl-Leucine		Histidinyl-Histidine	Aspartyl-Leucine	Aspartyl-Leucine	
		Glutarylglycine			Aspartyl-Isoleucine		Glycyl-Hydroxyproline	Aspartyl-Isoleucine	Aspartyl-Isoleucine	
		Arginyl-Arginine			L-glycyl-L-hydroxyproline		Aspartyl-Phenylalanine	Alanyl-Glycine	L-gamma-glutamyl-L-valine	
					L-gamma-glutamyl-L-valine		Aspartyl-Leucine	L-gamma-glutamyl-L-valine	L-beta-aspartyl-L-leucine	
					L-beta-aspartyl-L-leucine		Aspartyl-Isoleucine	L-beta-aspartyl-L-leucine		
					Glutarylglycine		Asparaginyl-Proline	Alanylglycine		
					Arginyl-Arginine		L-glycyl-L-hydroxyproline	Oxidized glutathione		
							L-gamma-glutamyl-L-valine			

							L-beta-aspartyl-L-phenylalanine L-beta-aspartyl-L-leucine L-alpha-glutamyl-L-hydroxyproline L-Aspartyl-L-phenylalanine Oxidized glutathione		
acylcarnitines	3-Dehydroxycarnitine L-Acetylcarnitine 2-trans4-cis-Decadienoylcarnitine 6-Keto-decanoylcarnitine 12-Hydroxy-12-octadecanoylcarnitine Hydroxyvalerylcarnitine Propionylcarnitine L-Carnitine	3-Dehydroxycarnitine Heptadecanoylcarnitine Propionylcarnitine L-Acetylcarnitine	3-Dehydroxycarnitine 12-Hydroxy-12-octadecanoylcarnitine Hydroxybutyrylcarnitine Propionylcarnitine	3-Hydroxyhexadecadienoylcarnitine 3-Hydroxy-9-hexadecenoylcarnitine 12-Hydroxy-12-octadecanoylcarnitine Hydroxybutyrylcarnitine Propionylcarnitine Arachidonyl carnitine	3-Hydroxyhexadecadienoylcarnitine 3-Hydroxy-9-hexadecenoylcarnitine Pimelylcarnitine 2-trans4-cis-Decadienoylcarnitine 12-Hydroxy-12-octadecanoylcarnitine Hydroxybutyrylcarnitine Propionylcarnitine Heptadecanoyl carnitine Propionylcarnitine Malonylcarnitine	Hydroxybutyrylcarnitine 3-Hydroxyhexadecadienoylcarnitine 3-Hydroxy-9-hexadecenoylcarnitine Pimelylcarnitine 12-Hydroxy-12-octadecanoylcarnitine Hydroxybutyrylcarnitine Propionylcarnitine Malonylcarnitine	Arachidonyl carnitine 3-Hydroxyhexadecadienoylcarnitine 3-Hydroxy-9-hexadecenoylcarnitine Pimelylcarnitine 12-Hydroxy-12-octadecanoylcarnitine Hydroxybutyrylcarnitine Propionylcarnitine Malonylcarnitine	Hydroxybutyrylcarnitine Pimelylcarnitine 2-trans4-cis-Decadienoylcarnitine 12-Hydroxy-12-octadecanoylcarnitine Propionylcarnitine 3-Hydroxy-5 8-tetradecadiencarnitine	3-Dehydroxycarnitine 3-Hydroxy-9-hexadecenoylcarnitine 2-trans4-cis-Decadienoylcarnitine Hydroxybutyrylcarnitine Propionylcarnitine Malonylcarnitine
autacoids					7-hydroxy-D4-neuroprostane 4-hydroxy-D4-neuroprostane 20-hydroxy-E4-neuroprostane 17-hydroxy-E4-neuroprostane 14-hydroxy-E4-neuroprostane Resolvin D1 Resolvin D2		7-hydroxy-D4-neuroprostane 4-hydroxy-D4-neuroprostane 20-hydroxy-E4-neuroprostane 19-Oxo-deoxycorticosterone 17-hydroxy-E4-neuroprostane 14-hydroxy-E4-neuroprostane Resolvin D1 Resolvin D2	7-hydroxy-D4-neuroprostane 4-hydroxy-D4-neuroprostane 20-hydroxy-E4-neuroprostane 17-hydroxy-E4-neuroprostane 14-hydroxy-E4-neuroprostane Resolvin D1 Resolvin D2	
eicosanoids	Omega-Carboxy-trinor-leukotriene B4 18-Carboxy-dinor-LTE4	18-Carboxy-dinor-LTE4 13,14-Dihydro PGF-1a	Omega-Carboxy-trinor-leukotriene B4 13,14-Dihydro PGF-1a	Leukotriene B4 ethanolamide 5-Oxo-6-trans-leukotriene B4	Omega-Carboxy-trinor-leukotriene B4 18-Carboxy-dinor-LTE4	Leukotriene B4 ethanolamide 67-dihydro-5-oxo-12-epi-LTB4	Omega-Carboxy-trinor-leukotriene B4 18-Carboxy-dinor-LTE4	18-Carboxy-dinor-LTE4 6,7-dihydro-5-oxo-12-epi-LTB4	Omega-Carboxy-trinor-leukotriene B4 18-Carboxy-dinor-LTE4

Leukotriene B4 ethanolamide	12,13-DHOME	12,13-DHOME	Leukotriene B5	Leukotriene B4 ethanolamide	1011-dihydro-12-oxo-LTB4	Leukotriene B4 ethanolamide	10,11-dihydro-12-oxo-LTB4	6,7-dihydro-5-oxo-12-epi-LTB4
Leukotriene B5	9,10-DHOME	9,10-DHOME	12-Keto-leukotriene B4	PGF2a ethanolamide	12(S)-Leukotriene B4	Leukotriene B5	12(S)-Leukotriene B4	10,11-dihydro-12-oxo-LTB4
12-Keto-leukotriene B4			PGF2a ethanolamide	15-Deoxy-d-1214-PGJ2	6-trans-12-epi-Leukotriene B4	12-Keto-leukotriene B4	6-trans-12-epi-Leukotriene B4	12(S)-Leukotriene B4
10,11-dihydro-20-dihydroxy-LTB4			Prostaglandin-c2	1314-Dihydro PGF-1a	6-trans-Leukotriene B4	PGF2a ethanolamide	6-trans-Leukotriene B4	6-trans-12-epi-Leukotriene B4
Prostaglandin E2 ethanolamide			bicyclo-PGE2		Leukotriene B4	13,14-Dihydro PGF-1a	Leukotriene B4	6-trans-Leukotriene B4
13,14-Dihydro PGF-1a			15d PGD2		PGF2a ethanolamide	Prostaglandin-c2	Omega-Carboxy-trinor-leukotriene B4	Leukotriene B4
Prostaglandin-c2			15-Deoxy-d-12,14-PGJ2		1314-Dihydro PGF-1a	bicyclo-PGE2	1314-Dihydro PGF-1a	5-Oxo-6-trans-leukotriene B4
bicyclo-PGE2			Delta-12-Prostaglandin J2		Prostaglandin C1	15d PGD2	Prostaglandin C1	Leukotriene B5
15d PGD2			Prostaglandin B2		9-Deoxy-delta12-PGD2	Delta-12-Prostaglandin J2	9-Deoxy-delta12-PGD2	12-Keto-leukotriene B4
Delta-12-Prostaglandin J2			Prostaglandin A2		15-Deoxy-d-12,14-PGJ2	Prostaglandin B2	Prostaglandin B1	Prostaglandin C1
Prostaglandin B2			Prostaglandin J2		Prostaglandin B1	Prostaglandin A2	Prostaglandin A1	9-Deoxy-delta12-PGD2
Prostaglandin A2			15-Keto-13,14-dihydroprostaglandin A2		Prostaglandin A1	Prostaglandin J2	8-iso-PGA1	15-Deoxy-d-12,14-PGJ2
Prostaglandin J2			12,13-DHOME		8-iso-PGA1	15-Keto-1314-dihydroprostaglandin A2	PGF2a ethanolamide	Prostaglandin B1
15-Keto-13,14-dihydroprostaglandin A2			9,10-DHOME		13,14-Dihydro PGF-1a	13,14-Dihydro PGF-1a	12,20-DiHETE	Prostaglandin A1
Prostaglandin G1					12,20-DiHETE	12,13-DHOME	5-HPETE	8-iso-PGA1
20-Hydroxy-PGF2a					17-HETE	9,10-DHOME	8,15-DiHETE	PGF2a ethanolamide
6-Keto-prostaglandin F1a					13-HETE		5,15-DiHETE	13,14-Dihydro PGF-1a
13,14-Dihydro PGF-1a					10-HETE		17,18-DiHETE	Prostaglandin-c2
17-HETE					19(S)-HETE		14,15-DiHETE	bicyclo-PGE2
13-HETE					5-HETE		15H-11,12-EETA	15d PGD2
10-HETE					11,12-EpETrE		12,13-DHOME	Delta-12-Prostaglandin J2
19(S)-HETE					9-HETE		9,10-DHOME	Prostaglandin B2
5-HETE					8,15-DiHETE		8(S)-HPETE	Prostaglandin A2
11,12-EpETrE					5,15-DiHETE		11(R)-HPETE	Prostaglandin J2
9-HETE					17,18-DiHETE		11H-14,15-EETA	15-Keto-13,14-dihydroprostaglandin A2

						14,15-DiHETE		12(R)-HPETE	12,20-DiHETE
						12-HETE		15(S)-HPETE	5-HPETE
						15H-11,12-EETA		12(S)-HPETE	8,15-DiHETE
						8(S)-HPETE			5,15-DiHETE
						11(R)-HPETE			17,18-DiHETE
						11H-14,15-EETA			14,15-DiHETE
						12(R)-HPETE			15H-11,12-EETA
						11(R)-HETE			12,13-DHOME
						16(R)-HETE			9,10-DHOME
						15(S)-HPETE			8(S)-HPETE
						12(S)-HPETE			11(R)-HPETE
						15(S)-HETE			11H-14,15-EETA
						14R,15S-EpETrE			12(R)-HPETE
						9-HODE			15(S)-HPETE
						9,10,13-TriHOME			12(S)-HPETE
						12,13-EpOME			9-HODE
									12,13-EpOME
steriod hormones				Cortisone Aldosterone 11beta20-Dihydroxy-3-oxopregn-4-en-21-oic acid	5a-Dihydrotestosterone sulfate 11beta-Hydroxy-3,20-dioxopregn-4-en-21-oic acid	11beta20-Dihydroxy-3-oxopregn-4-en-21-oic acid	19-Hydroxydeoxycorticosterone 11beta-Hydroxy-3,20-dioxopregn-4-en-21-oic acid 11beta20-Dihydroxy-3-oxopregn-4-en-21-oic acid 21-Hydroxy-5b-pregnane-3,11,20-trione 21-Deoxycortisol 11-Dehydrocorticosterone Corticosterone Cortexolone Aldosterone	5a-Dihydrotestosterone sulfate Androsterone sulfate 11beta-Hydroxy-3,20-dioxopregn-4-en-21-oic acid 11beta20-Dihydroxy-3-oxopregn-4-en-21-oic acid	11beta20-Dihydroxy-3-oxopregn-4-en-21-oic acid
purines, pyrimidines	Thymidine 35-cyclic monophosphate 5-Methylthioadenosine	7-Methylguanosine Cytosine	Cytosine Deoxycytidine	Allopurinol riboside 2-Deoxyinosine triphosphate	Cytidine triphosphate 5-Amino-6-ribitylamino uracil	5-Amino-6-ribitylamino uracil Inosine triphosphate	Cytosine Deoxycytidine	5-Methylthioadenosine Cytosine	5-Methylthioadenosine Cytosine

	Cytosine	Deoxycytidine	Deoxyguanosine	Inosine	Thymidine 5-triphosphate		2-Deoxyinosine triphosphate			Deoxycytidine
	Deoxycytidine	Pseudouridine	Adenosine		Pseudouridine		5-Aminoimidazole ribonucleotide			Inosine triphosphate
	Pseudouridine	Uridine			Uridine					
	Uridine	Inosine triphosphate			2-Deoxyinosine triphosphate					
	Adenosine phosphosulfate	Inosine			Inosine triphosphate					
	Adenosine monophosphate									
	Inosine triphosphate									
	Inosine									
	Oleamide	Oleamide	Oleamide	Arachidonoyl Serinol	Arachidonoyl Serinol	Arachidonoyl Serinol	Arachidonoyl Serinol	Arachidonoyl Serinol	S-Adenosylhomocysteine	
	NADH	Porphobilinogen	Porphobilinogen	Oleamide	Oleamide	Oleamide	Oleamide	Oleamide	Porphobilinogen	
	Fucose 1-phosphate	Ureidoisobutyric acid	Riboflavin	Porphobilinogen	Porphobilinogen	Porphobilinogen	Fucose 1-phosphate	Fucose 1-phosphate		
	S-Adenosylhomocysteine	DOPA sulfate	Taurine	Taurine			Porphobilinogen	Taurine		
other	Homocysteine	Taurine					Taurine			
	Porphobilinogen	Creatinine								
	Norepinephrine sulfate									
	DOPA sulfate									
	FAD									
	Creatinine									
	Taurine									
	Creatine									

Table 5.8 High- and medium confidence annotated features from perfusate samples sampled on-site with SPME fibers in the hospital during IVLP with FOLFOX administration

	T0	T1	T2	T3
amino acids	Beta-Citryl-L-glutamic acid	Beta-Citryl-L-glutamic acid	Beta-Citryl-L-glutamic acid	Beta-Citryl-L-glutamic acid
	L-Tryptophan	N-acetyltryptophan	D-Tryptophan	N(6)-(Octanoyl)lysine
	Kynurenic acid	N-Acetylhistamine	L-gamma-glutamyl-L-valine	N-acetyltryptophan
	Lipoyllysine	L-Tryptophan	L-Tryptophan	D-Tryptophan
	N-Acetylhistamine	L-Valine	L-Valine	N-Acetylglutamine
	Tridecanoylglycine	Kynurenic acid	Kynurenic acid	L-Tryptophan
	N-Decanoylglycine	Lipoyllysine	N-Acetylhistamine	Kynurenic acid
	N-Undecanoylglycine	N-Undecanoylglycine	Lipoyllysine	L-Phenylalanine
	N-Nonanoylglycine	Tridecanoylglycine	N-Undecanoylglycine	N-Acetylhistamine
	Myristoylglycine	N-Decanoylglycine	N-Nonanoylglycine	Lipoyllysine
	Palmitoylglycine	Palmitoylglycine	N-Decanoylglycine	N-Undecanoylglycine
	Dimethylglycine	Pristanoylglycine	Myristoylglycine	Tridecanoylglycine
		Myristoylglycine	Palmitoylglycine	N-Nonanoylglycine
		Dimethylglycine	Methylglutaric acid	N-Decanoylglycine
		Histidinal	L-2-Hydroxyglutaric acid	Pristanoylglycine
			Histidinal	Palmitoylglycine
				Methylglutaric acid
				Histidinal
peptides	Histidinyl-Histidine	Gamma-glutamyl-Cysteine	Glu-Val	Glu-Val
	Glu-Val	Prolyl-Asparagine	Gamma-glutamyl-Phenylalanine	Tyrosyl-Glutamate
	Prolyl-Asparagine	Hydroxyprolyl-Cysteine	Tyrosyl-Glutamate	Tryptophyl-Arginine
	Phenylalanyl-Lysine	Glycyl-Hydroxyproline	Tryptophyl-Arginine	Prolyl-Asparagine
	Lysyl-Phenylalanine	Glutaminyl-Cysteine	Threoninyl-Arginine	Leucyl-Hydroxyproline
	Leucyl-Aspartate	Cysteinyl-Gamma-glutamate	Prolyl-Asparagine	Leucyl-Aspartate
	Isoleucyl-Aspartate	Cysteinyl-Hydroxyproline	Phenylalanyl-Gamma-glutamate	Isoleucyl-Hydroxyproline
	Aspartyl-Leucine	Cysteinyl-Glutamine	Phenylalanyl-Glutamine	Isoleucyl-Aspartate
	Aspartyl-Isoleucine	Asparaginyl-Proline	Phenylalanyl-Aspartate	Hydroxyprolyl-Leucine
	Asparaginyl-Proline	Oxidized glutathione	Leucyl-Leucine	Hydroxyprolyl-Isoleucine
	L-gamma-glutamyl-L-valine		Leucyl-Isoleucine	Hydroxyprolyl-Cysteine
	L-beta-aspartyl-L-leucine		Leucyl-Hydroxyproline	Glycyl-Hydroxyproline
	Arginyl-Arginine		Leucyl-Aspartate	Glutamyl-Tyrosine
	Gamma-Glutamyltyrosine		Isoleucyl-Leucine	Cysteinyl-Hydroxyproline
	Oxidized glutathione		Isoleucyl-Isoleucine	Aspartyl-Leucine
			Isoleucyl-Hydroxyproline	Aspartyl-Isoleucine

			Isoleucyl-Aspartate	Asparaginyl-Proline
			Hydroxyprolyl-Isoleucine	Arginyl-Tryptophan
			Hydroxyprolyl-Cysteine	L-glycyl-L-hydroxyproline
			Glutamyl-Tyrosine	L-gamma-glutamyl-L-valine
			Glutaminyl-Phenylalanine	L-beta-aspartyl-L-leucine
			Cysteinyl-Hydroxyproline	Gamma-Glutamyltyrosine
			Aspartyl-Phenylalanine	Arginyl-Arginine
			Aspartyl-Leucine	Oxidized glutathione
			Aspartyl-Isoleucine	
			Asparaginyl-Proline	
			Arginyl-Tryptophan	
			Arginyl-Threonine	
			L-beta-aspartyl-L-phenylalanine	
			L-beta-aspartyl-L-leucine	
			L-alpha-glutamyl-L-hydroxyproline	
			L-Aspartyl-L-phenylalanine	
acylcarnitines	Pimelylcarnitine	Pimelylcarnitine	3-Hydroxyhexadecadienoylcarnitine	Pimelylcarnitine
	2-trans4-cis-Decadienoylcarnitine	3-Hydroxyhexadecadienoylcarnitine	Pimelylcarnitine	Hydroxybutyrylcarnitine
	12-Hydroxy-12-octadecanoylcarnitine	3-Hydroxy-9-hexadecenoylcarnitine	trans-2-Dodecenoylcarnitine	Arachidonyl carnitine
	Hydroxybutyrylcarnitine	3-Hydroxy-5 8-tetradecadiencarnitine	12-Hydroxy-12-octadecanoylcarnitine	6-Keto-decanoylcarnitine
	Propionylcarnitine	2-trans4-cis-Decadienoylcarnitine	Hydroxybutyrylcarnitine	12-Hydroxy-12-octadecanoylcarnitine
	Malonylcarnitine	12-Hydroxy-12-octadecanoylcarnitine	Hydroxypropionylcarnitine	Propionylcarnitine
	Hydroxypropionylcarnitine	Hydroxybutyrylcarnitine	Propionylcarnitine	Arachidonyl carnitine
		Propionylcarnitine	Malonylcarnitine	2,6 Dimethylheptanoyl carnitine
		Malonylcarnitine	3-Hydroxy-9-hexadecenoylcarnitine	Malonylcarnitine
autacoids	7-hydroxy-D4-neuroprostane	7-hydroxy-D4-neuroprostane	7-hydroxy-D4-neuroprostane	7-hydroxy-D4-neuroprostane
	4-hydroxy-D4-neuroprostane	4-hydroxy-D4-neuroprostane	4-hydroxy-D4-neuroprostane	4-hydroxy-D4-neuroprostane
	20-hydroxy-E4-neuroprostane	20-hydroxy-E4-neuroprostane	20-hydroxy-E4-neuroprostane	20-hydroxy-E4-neuroprostane
	17-hydroxy-E4-neuroprostane	17-hydroxy-E4-neuroprostane	17-hydroxy-E4-neuroprostane	17-hydroxy-E4-neuroprostane
	14-hydroxy-E4-neuroprostane	14-hydroxy-E4-neuroprostane	14-hydroxy-E4-neuroprostane	14-hydroxy-E4-neuroprostane
	Resolvin D1	Resolvin D1	Resolvin D1	Resolvin D1
	Resolvin D2	Resolvin D2	Resolvin D2	Resolvin D2
				Resolvin D5
				Neuroprotectin D1
eicosanoids	Omega-Carboxy-trinor-leukotriene B4	Omega-Carboxy-trinor-leukotriene B4	Omega-Carboxy-trinor-leukotriene B4	Omega-Carboxy-trinor-leukotriene B4
	18-Carboxy-dinor-LTE4	18-Carboxy-dinor-LTE4	18-Carboxy-dinor-LTE4	18-Carboxy-dinor-LTE4
	6,7-dihydro-5-oxo-12-epi-LTB4	13E-Tetranor-16-carboxy-LTE4	Leukotriene B4 ethanolamide	Leukotriene B4 ethanolamide

6,7-dihydro-12-epi-LTB4
12-oxo-20-dihydroxy-leukotriene B4
12-oxo-10,11-dihydro-20-COOH-LTB4
10,11-dihydro-leukotriene B4
10,11-dihydro-12-oxo-LTB4
20-Carboxy-leukotriene B4
12(S)-Leukotriene B4
6-trans-12-epi-Leukotriene B4
6-trans-Leukotriene B4
12-Keto-tetrahydro-leukotriene B4
Leukotriene B4
PGF2a ethanolamide
13,14-Dihydro PGF-1a
Prostaglandin C1
9-Deoxy-delta12-PGD2
Prostaglandin B1
Prostaglandin A1
8-iso-PGA1
13,14-Dihydro PGF-1a
12,20-DiHETE
5-HPETE
8,15-DiHETE
5,15-DiHETE
17,18-DiHETE
14,15-DiHETE
15H-11,12-EETA
12,13-DHOME
9,10-DHOME
8(S)-HPETE
11(R)-HPETE
11H-14,15-EETA
12(R)-HPETE
15(S)-HPETE
12(S)-HPETE
5,6-DHET
11,12-DiHETrE
8,9-DiHETrE
Leukotriene B4 ethanolamide
PGF2a ethanolamide
1314-Dihydro PGF-1a
12(13)Ep-9-KODE
9,10,13-TriHOME
9,12,13-TriHOME
12,13-DHOME
9,10-DHOME

6,7-dihydro-12-epi-LTB4
5-Oxo-6-trans-leukotriene B4
10,11-dihydro-leukotriene B4
Leukotriene B5
12-Keto-leukotriene B4
12-Keto-tetrahydro-leukotriene B4
PGF2a ethanolamide
13,14-Dihydro PGF-1a
Prostaglandin-c2
bicyclo-PGE2
15d PGD2
Delta-12-Prostaglandin J2
Prostaglandin B2
Prostaglandin A2
Prostaglandin J2
15-Keto-13,14-dihydroprostaglandin A2
13,14-Dihydro PGF-1a
17-HETE
13-HETE
10-HETE
19(S)-HETE
5-HETE
11,12-EpETrE
9-HETE
12-HETE
12,13-DHOME
9,10-DHOME
11(R)-HETE
16(R)-HETE
8-HETE
15(S)-HETE
5,6-DHET
11,12-DiHETrE
89-DiHETrE
14R,15S-EpETrE
14,15-DiHETrE
9,10,13-TriHOME
5-Oxo-6-trans-leukotriene B4
Leukotriene B5
12-Keto-leukotriene B4
13,14-Dihydro PGF-1a
PGF2a ethanolamide
5,6-Dihydroxyprostaglandin F1a
Prostaglandin-c2
bicyclo-PGE2
15d PGD2
Delta-12-Prostaglandin J2
Prostaglandin B2
Prostaglandin A2
Prostaglandin J2
15-Keto-1314-dihydroprostaglandin A2
13,14-Dihydro PGF-1a
12(13)Ep-9-KODE
17-HETE
13-HETE
10-HETE
19(S)-HETE
5-HETE
11,12-EpETrE
9-HETE
12-HETE
12,13-DHOME
9,10-DHOME
11(R)-HETE
16(R)-HETE
8-HETE
15(S)-HETE
14R,15S-EpETrE
9,10,13-TriHOME
9,12,13-TriHOME

	14,15-DiHETrE		9,12,13-TriHOME	
	9-HODE			
	12,13-EpOME			
steriod hormones	Aldosterone	11beta-Hydroxy-3,20-dioxopregn-4-en-21-oic acid	19-Oxo-deoxycorticosterone	Aldosterone
	11beta-Hydroxy-3,20-dioxopregn-4-en-21-oic acid	11beta20-Dihydroxy-3-oxopregn-4-en-21-oic acid	11beta-Hydroxy-3,20-dioxopregn-4-en-21-oic acid	19-Oic-deoxycorticosterone
	11-Dehydrocorticosterone			11beta-Hydroxy-3,20-dioxopregn-4-en-21-oic acid
	Cortisone			11beta20-Dihydroxy-3-oxopregn-4-en-21-oic acid
purines, pyrimidines	Inosine triphosphate	5-Amino-6-ribitylamino uracil	Inosine triphosphate	7-Methylguanosine
		2-Deoxyinosine triphosphate	Cytosine	5-Amino-6-ribitylamino uracil
		7-Methylguanosine	2-Deoxyinosine triphosphate	2-Deoxyinosine triphosphate
		Inosine triphosphate	Pseudouridine	Cytosine
		Pseudouridine	Uridine	Inosine triphosphate
		Uridine		5-Fluorouridine (LEV2,MULTI)
other	Arachidonoyl Serinol	Arachidonoyl Serinol	Arachidonoyl Serinol	L-Urobilinogen
	Oleamide	Oleamide	Oleamide	Arachidonoyl Serinol
	Porphobilinogen	Fucose 1-phosphate	Norepinephrine sulfate	Ubiquinol-10
	Riboflavin	5-Aminoimidazole ribonucleotide		Oleamide
		Porphobilinogen		5-Aminoimidazole ribonucleotide

Table 5.9 High- and medium confidence annotated features from lungs sampled *in vivo* with SPME fibers in the hospital during IV administration with FOLFOX.

	IV_Blank	IV_TL	IV_T0	IV_T1	IV_T2	IV_T3
amino acids	L-Tryptophan	L-Tryptophan	N-Acetyl-L-methionine	L-Tryptophan	Beta-Citryl-L-glutamic acid	D-Serine
	L-Glutamine	L-Phenylalanine	N6,N6,N6-Trimethyl-L-lysine	L-Glutamine	N6,N6,N6-Trimethyl-L-lysine	L-Glutamine
	L-Arginine	Beta-Citryl-L-glutamic acid	L-Methionine	L-Tyrosine	L-Methionine	L-Proline
	L-Lysine	N-Acetyl-L-methionine	L-Arginine	N-Acetyl-L-methionine	L-Arginine	L-Phenylalanine
	L-Proline	N6,N6,N6-Trimethyl-L-lysine	L-Histidine	L-Methionine	L-Lysine	Beta-Citryl-L-glutamic acid
	L-Phenylalanine	L-Valine	L-Phenylalanine	L-Arginine	L-Histidine	N-Acetyl-L-methionine
	Beta-Citryl-L-glutamic acid	L-Methionine	L-Tyrosine	L-Aspartic acid	L-Tyrosine	L-Methionine
	N6,N6,N6-Trimethyl-L-lysine	L-Glutamine	D-Leucine	L-Histidine	L-Glutamic acid	L-Lysine
	L-Methionine	L-Arginine	Beta-Leucine	L-Proline	N-Acetylglutamic acid	L-Asparagine
	L-Cystine	L-Proline	N-Acetylglutamic acid	L-Phenylalanine	Kynurenic acid	L-Threonine
	L-Aspartic acid	L-Tyrosine	Kynurenic acid	N-Acetylglutamic acid	L-Tryptophan	L-alpha-glutamyl-L-hydroxyproline
	L-Histidine	L-gamma-glutamyl-L-valine	L-Leucine	L-Leucine	L-Methionine	o-Tyrosine
	L-Asparagine	D-Lysine	L-Alloisoleucine	D-2-Hydroxyglutaric acid	L-Arginine	Beta-Tyrosine
	L-Tyrosine	Kynurenic acid	L-Isoleucine	L-Isoleucine	L-Histidine	Kynurenic acid
	L-Glutamic acid	L-Leucine	N-Acetylhistamine	L-Glutamine	L-Phenylalanine	L-Leucine
	N-Acetylglutamic acid	L-Lysine	L-Glutamine	L-Arginine	L-Tyrosine	Pyroglutamic acid
	Kynurenic acid	L-Isoleucine	L-Arginine	L-Histidine	N-Lauroylglycine	L-Isoleucine
	L-Leucine	N-Acetylhistamine	L-Tyrosine	L-Histidine	Glutarylglycine	L-Tyrosine
	L-Isoleucine	o-Tyrosine	Tridecanoylglycine	L-Phenylalanine	Palmitoylglycine	L-Glutamic acid
	L-Arginine	Beta-Tyrosine	N-Undecanoylglycine	L-Tyrosine	N-Undecanoylglycine	Urocanic acid
	L-Glutamic acid	L-Tyrosine	N-Nonanoylglycine	L-Glutamic acid	N-Decanoylglycine	L-Cysteinylglycine disulfide
	L-Lysine	Pristanoylglycine	N-Decanoylglycine	L-Tryptophan	Tridecanoylglycine	Cysteineglutathione disulfide
	L-Tyrosine	N-Decanoylglycine	Pristanoylglycine	L-2-Hydroxyglutaric acid	Pristanoylglycine	Ornithine
	D-Tryptophan	Myristoylglycine	Margaroylglycine	3-Hydroxyglutaric acid	Pentacosanoylglycine	Dimethylglycine
	L-Tryptophan	Palmitoylglycine	Methylglutaric acid	N-Undecanoylglycine	N-Nonanoylglycine	Tridecanoylglycine
	Pristanoylglycine	N-Undecanoylglycine		N-Decanoylglycine	Myristoylglycine	Pristanoylglycine
	N-Decanoylglycine	Tridecanoylglycine		Tridecanoylglycine	Lipoyllysine	N-Undecanoylglycine
	Myristoylglycine	N-Nonanoylglycine		Pristanoylglycine	Ornithine	N-Nonanoylglycine
	Palmitoylglycine	N-Lauroylglycine		Palmitoylglycine		N-Decanoylglycine
	Glutarylglycine	Lipoyllysine		Glutarylglycine		Myristoylglycine
	N-Undecanoylglycine	Ornithine		N-Nonanoylglycine		N-Lauroylglycine
	Tridecanoylglycine	Dimethylglycine		N-Lauroylglycine		Palmitoylglycine
	N-Nonanoylglycine			Lipoyllysine		Lipoyllysine

	Lipoyllysine			Ornithine		
	Ornithine			Dimethylglycine		
	Dimethylglycine			3-Methylglutaconic acid		
	Hippuric acid			Urocanic acid		
	3-Methylglutaconic acid					
peptides	Histidinyl-Histidine	Histidinyl-Histidine	L-Cysteinylglycine disulfide	Cysteinyl-Cysteine	Glutamyl-Glutamate	Histidinyl-Histidine
	L-Cysteinylglycine disulfide	Glutamyl-Glutamate	Glutarylglycine	Glutamyl-Glutamate	Cysteinyl-Cysteine	L-Cysteinylglycine disulfide
	Cysteinyl-Cysteine	L-Cysteinylglycine disulfide	Arginyl-Arginine	L-Cysteinylglycine disulfide	Gamma-Glutamyltyrosine	L-Threo-3-Phenylserine
	Oxidized glutathione	Leucyl-Aspartate	Carnosine	Asparaginyl-Arginine	L-Cysteinylglycine disulfide	Glutarylglycine
	Glutathione	Isoleucyl-Aspartate	Oxidized glutathione	Arginyl-Asparagine	Oxidized glutathione	Cysteinyl-Cysteine
	Cysteineglutathione disulfide	Hydroxyprolyl-Cysteine		Carnosine		Arginyl-Arginine
		Cysteinyl-Hydroxyproline		Oxidized glutathione		Oxidized glutathione
		Aspartyl-Leucine		Glutathione		
		Aspartyl-Isoleucine		L-Cystathionine		
		L-beta-aspartyl-L-leucine				
		Arginyl-Arginine				
		Oxidized glutathione				
		L-Cystathionine				
acylcarnitines	Hydroxybutyrylcarnitine	L-Acetylcarnitine	Pimelylcarnitine	Hydroxybutyrylcarnitine	Pimelylcarnitine	L-Acetylcarnitine
	9,12-Hexadecadienoylcarnitine	Pimelylcarnitine	2-trans4-cis-Decadienoylcarnitine	L-Acetylcarnitine	2-trans4-cis-Decadienoylcarnitine	3-Hydroxy-9-hexadecenoylcarnitine
	3-Hydroxy-9-hexadecenoylcarnitine	2-trans4-cis-Decadienoylcarnitine	6-Keto-decanoylcarnitine	9,12-Hexadecadienoylcarnitine	6-Keto-decanoylcarnitine	2-trans4-cis-Decadienoylcarnitine
	Pimelylcarnitine	6-Keto-decanoylcarnitine	12-Hydroxy-12-octadecanoylcarnitine	Pimelylcarnitine	12-Hydroxy-12-octadecanoylcarnitine	6-Keto-decanoylcarnitine
	2-trans4-cis-Decadienoylcarnitine	12-Hydroxy-12-octadecanoylcarnitine	Hydroxybutyrylcarnitine	2-trans4-cis-Decadienoylcarnitine	Butenylcarnitine	12-Hydroxy-12-octadecanoylcarnitine
	6-Keto-decanoylcarnitine	Hydroxybutyrylcarnitine	3-Dehydroxycarnitine	6-Keto-decanoylcarnitine	Propenoylcarnitine	Propenoylcarnitine
	12-Hydroxy-12-octadecanoylcarnitine	Butenylcarnitine	Tiglylcarnitine	12-Hydroxy-12-octadecanoylcarnitine	3-Dehydroxycarnitine	3-Dehydroxycarnitine
	Butenylcarnitine	Propenoylcarnitine	Propionylcarnitine	Hydroxyvalerylcarnitine	Propionylcarnitine	Propionylcarnitine
	Propenoylcarnitine	3-Dehydroxycarnitine	L-Acetylcarnitine	Butenylcarnitine	L-Acetylcarnitine	
	Tiglylcarnitine	Propionylcarnitine	L-Carnitine	Propenoylcarnitine		
	Propionylcarnitine	L-Carnitine		3-Dehydroxycarnitine		
	L-Acetylcarnitine			Propionylcarnitine		
	L-Carnitine			L-Carnitine		
				2-Hexenoylcarnitine		
eicosanoids	Leukotriene B4 ethanolamide	Omega-Carboxy-trinor-leukotriene B4	18-Carboxy-dinor-LTE4	Omega-Carboxy-trinor-leukotriene B4	Omega-Carboxy-trinor-leukotriene B4	18-Carboxy-dinor-LTE4

Omega-Carboxy-trinor-leukotriene B4	18-Carboxy-dinor-LTE4	13E-Tetranor-16-carboxy-LTE4	18-Carboxy-dinor-LTE4	18-Carboxy-dinor-LTE4	Leukotriene B4 ethanolamide
18-Carboxy-dinor-LTE4	13E-Tetranor-16-carboxy-LTE4	Omega-Carboxy-trinor-leukotriene B4	13E-Tetranor-16-carboxy-LTE4	13E-Tetranor-16-carboxy-LTE4	67-dihydro-5-oxo-12-epi-LTB4
13E-Tetranor-16-carboxy-LTE4	Leukotriene B4 ethanolamide	6,7-dihydro-12-epi-LTB4	Leukotriene B4 ethanolamide	Leukotriene B4 ethanolamide	5-Oxo-6-trans-leukotriene B4
Leukotriene B4 ethanolamide	5-Oxo-6-trans-leukotriene B4	10,11-dihydro-leukotriene B4	1011-dihydro-12-oxo-LTB4	13,14-Dihydro PGF-1a	1011-dihydro-12-oxo-LTB4
10,11-dihydro-20-dihydroxy-LTB4	Leukotriene B5	12-Keto-tetrahydro-leukotriene B4	12(S)-Leukotriene B4	PGF2a ethanolamide	12(S)-Leukotriene B4
Prostaglandin E2 ethanolamide	12-Keto-leukotriene B4	Prostaglandin E2 ethanolamide	6-trans-12-epi-Leukotriene B4	Prostaglandin E2 ethanolamide	6-trans-12-epi-Leukotriene B4
13,14-Dihydro PGF-1a	PGF2a ethanolamide	13,14-Dihydro PGF-1a	6-trans-Leukotriene B4	17-HETE	6-trans-Leukotriene B4
PGF2a ethanolamide	Prostaglandin E2 ethanolamide	9,10,13-TriHOME	Leukotriene B5	13-HETE	Leukotriene B5
1314-Dihydro PGF-1a	13,14-Dihydro PGF-1a	9,12,13-TriHOME	12-Keto-leukotriene B4	10-HETE	12-Keto-leukotriene B4
Prostaglandin G1	bicyclo-PGE2	5,6-DHET	Leukotriene B4	19(S)-HETE	Leukotriene B4
20-Hydroxy-PGF2a	15d PGD2	11,12-DiHETrE	Omega-Carboxy-trinor-leukotriene B4	5-HETE	13,14-Dihydro PGF-1a
9-HODE	Delta-12-Prostaglandin J2	8,9-DiHETrE	Prostaglandin E2 ethanolamide	11,12-EpETrE	Prostaglandin E2 ethanolamide
12,13-EpOME	Prostaglandin B2	14,15-DiHETrE	1314-Dihydro PGF-1a	9-HETE	Delta-12-Prostaglandin J2
	Prostaglandin A2	17-HETE	Prostaglandin C1	12-HETE	Prostaglandin B2
	Prostaglandin J2	13-HETE	9-Deoxy-delta12-PGD2	12,13-DHOME	Prostaglandin B1
	15-Keto-1314-dihydroprostaglandin A2	10-HETE	Prostaglandin-c2	9,10-DHOME	Prostaglandin A2
	12,13-DHOME	19(S)-HETE	bicyclo-PGE2	11(R)-HETE	Prostaglandin J2
	9,10-DHOME	5-HETE	Delta-12-Prostaglandin J2	16(R)-HETE	Prostaglandin A1
		11,12-EpETrE	Prostaglandin B2	8-HETE	8-iso-PGA1
		9-HETE	Prostaglandin B1	15(S)-HETE	15-Keto-1314-dihydroprostaglandin A2
		12-HETE	Prostaglandin A2		PGF2a ethanolamide
		12,13-DHOME	Prostaglandin J2		5-HPETE
		9,10-DHOME	Prostaglandin A1		8,15-DiHETE
		11(R)-HETE	8-iso-PGA1		17,18-DiHETE
		16(R)-HETE	Leukotriene A4		14,15-DiHETE
		8-HETE	15-Keto-1314-dihydroprostaglandin A2		12,13-DHOME
		15(S)-HETE	1314-Dihydro PGF-1a		9,10-DHOME
		14R,15S-EpETrE	12,20-DiHETE		8(S)-HPETE
			9-HEPE		11(R)-HPETE
			15d PGD2		11H-14,15-EETA
			12-KETE		12(R)-HPETE
			5-HPETE		15(S)-HPETE

				9-HODE		12(S)-HPETE
				8,15-DiHETE		
				5-KETE		
				5,15-DiHETE		
				17,18-EpETE		
				17,18-DiHETE		
				15-KETE		
				14,15-DiHETE		
				12-HEPE		
				5-HEPE		
				15H-11,12-EETA		
				12,13-EpOME		
				8(S)-HPETE		
				11(R)-HPETE		
				11H-14,15-EETA		
				12(R)-HPETE		
				15(S)-HPETE		
				12(S)-HPETE		
steriod hormones	Tetrahydrocorticosterone				17a,21-Dihydroxypregnenolone 11b,21-Dihydroxy-5b-pregnane-3,20-dione 3a,21-Dihydroxy-5b-pregnane-11,20-dione 3b,17a,21-Trihydroxypregnenone 3b,15b,17a-Trihydroxypregnenone	
purines, pyrimidines	Inosine triphosphate	Inosine triphosphate	Inosine triphosphate	Inosine triphosphate	Inosine triphosphate	Inosine triphosphate
	8-Hydroxy-7-methylguanine	Inosine	8-Hydroxy-7-methylguanine	8-Hydroxy-7-methylguanine	N4-Acetylcytidine	N4-Acetylcytidine
	N4-Acetylcytidine	N4-Acetylcytidine	FAPy-adenine	N4-Acetylcytidine	FAPy-adenine	8-Hydroxy-7-methylguanine
	FAPy-adenine	FAPy-adenine	Thymidine 3,5-cyclic monophosphate	FAPy-adenine	5-Methylthioadenosine	FAPy-adenine
	5-Methylthioadenosine	Thymidine 3,5-cyclic monophosphate	5-Methylthioadenosine	Thymidine 3,5-cyclic monophosphate	7-Methylguanosine	5-Methylthioadenosine
	7-Methylguanosine	Cytidine monophosphate	7-Methylguanosine	5-Methylthioadenosine	5-Methylcytosine	7-Methylguanosine
	Cytosine	5-Methylthioadenosine	Cytosine	7-Methylguanosine	Uridine	Cytosine
	Deoxycytidine	7-Methylguanosine	Deoxycytidine	Cytosine	5-Fluorodeoxyuridine monophosphate	Deoxycytidine
	Pseudouridine	Cytosine	Pseudouridine	Deoxycytidine	Adenine	5-Methylcytosine
	Uridine	Deoxycytidine	Uridine	Uridine		Uridine

	Adenosine monophosphate		Deoxyguanosine	5-Fluorodeoxyuridine monophosphate		5-Fluorodeoxyuridine monophosphate
	Adenine		Adenosine	Adenine		S-Adenosylhomocysteine
			5-Fluorodeoxyuridine monophosphate			Adenosine monophosphate
			Adenosine monophosphate			Adenine
other	Arachidonoyl Serinol	Arachidonoyl Serinol	Arachidonoyl Serinol	Arachidonoyl Serinol	Arachidonoyl Serinol	Oleamide
	Oleamide	Oleamide	Oleamide	Oleamide	Oleamide	Creatinine
	NADH	NADH	NADH	NADH	Porphobilinogen	Creatine
	Fucose 1-phosphate	Fucose 1-phosphate	S-Adenosylhomocysteine	Creatinine	Creatine	Taurine
	5-Aminolevulinic acid	S-Adenosylhomocysteine	Creatinine	Taurine	Creatinine	
	Ubiquinone-1	Creatinine		Porphobilinogen		
	L-2-Hydroxyglutaric acid	Creatine		Creatine		
	Taurine					
	S-Adenosylhomocysteine					
	Creatinine					
	Taurine					
	Creatine					

Chapter 6: *In vivo* solid phase microextraction chemical biopsy tool for monitoring doxorubicin residue in human lung tissue during clinical *in vivo* lung perfusion (IVLP)

6.1 Preamble

Chapter 6 of this thesis has been submitted to the journal Angewandte Chemie [EMID:1887f04136457f99 –Manuscript number: 202003084] and is equally co-authored with B. Bojko. Other co-authors include M. Olkowicz, A. Roszkowska, B. Kupcewicz, P. Reck dos Santos, K. Ramadan, S. Keshavjee, T. Waddell, G.A. Gomez-Rios, M. Tascon, K. Gorynski, M. Cypel, J. Pawliszyn. The collaboration was initiated by B. Bojko, J. Pawliszyn, and M. Cypel who were also responsible for the experimental design. Experimental execution, sampling at the hospital for both clinical trials and instrumental analysis for targeted and untargeted work and data processing for targeted and untargeted analysis was completed by the author of this thesis with assistance from G.A. Gomez-Rios, M. Tascon and M. Olkowicz. Statistical analysis was completed by B. Bojko, B. Kupcewicz and the author of this thesis and biochemical interpretation from annotation was conducted by B. Bojko, A. Roszkowska, and Mariola Olkowicz. The final formatted manuscript was equally written by B. Bojko, Khaled Ramadan, A. Roszkowska and the author of this thesis. Please see *Statement of contributions*. The authors would like to thank our collaborators at MilliporeSigma for kindly providing us with the fibers and chromatographic columns employed for this investigation. We would also like to thank Thermo Fisher Scientific for lending us the triple quadrupole mass spectrometer that was used in this work (TSQ Quantiva). Funding: We are grateful to the Canadian Cancer Society for their support in the development of IVLP via innovation grants, as well as its further support in the clinical trial with DOX IVLP as part of the innovation-to-impact grant. We are also grateful to the Canadian Institute of Health Research (CIHR) - Natural Sciences and Engineering Research Council (NSERC) of Canada Collaborative Health Research Projects program for their financial support [grant 355935 entitled "Supervised *in vivo* lung perfusion strategy for treatment of cancer metastases to the lungs. Real-time

monitoring of chemotherapy by on-site analytical platform"] and the Natural Sciences and Engineering Research Council of Canada Industrial Research Chair (IRC) program.

6.2 Introduction

Pulmonary metastases are known to develop in approximately 30% of patients with malignant tumors, most frequently in patients suffering from sarcomas. Although surgical resection is a widely accepted treatment for pulmonary metastases, a 5-year survival rate of about 20% after complete resection remains disappointing.[176] Unfortunately, most patients develop recurrent metastasis, probably as a result of micrometastatic disease present at the time of the initial operation. Most recurrences occur in the lungs themselves, suggesting that the lung is the major reservoir of occult metastatic burden (Figure 6.1). Therefore, a treatment capable of specifically targeting the lung to eradicate micrometastatic disease would be highly beneficial for this patient population. By building upon our experience with ex vivo lung perfusion for repair of donor lungs for transplantation,[125,177] our group recently developed and described a technique for isolated *in vivo* lung perfusion (IVLP) to facilitate localized drug delivery to lungs during surgical resection.[142,143] Based on these pre-clinical studies, a phase I clinical trial (NCT02811523) using doxorubicin (DOX) during IVLP for treatment of lung sarcoma metastases is underway.

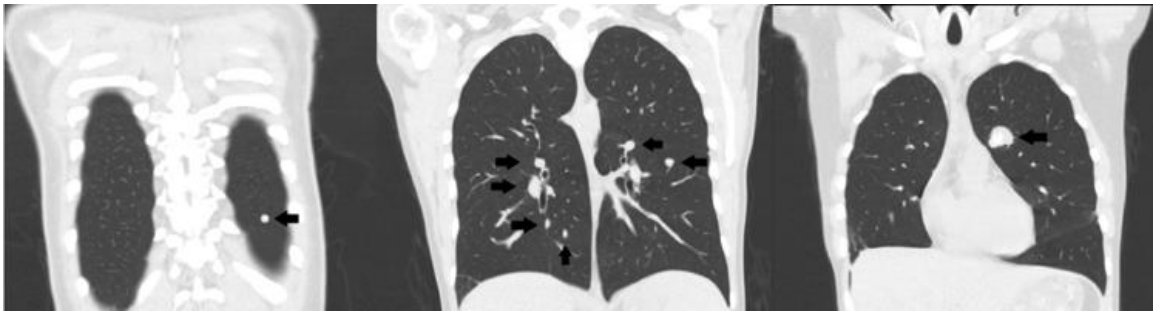

Figure 6.1 Pre-operative lung computed tomography (CT) scan for 1st patient subjected to IVLP showing numerous bilateral pulmonary sarcoma metastases as denoted by arrows

While perfusate and blood analyses can be easily and repeatedly performed throughout the IVLP procedure due to their non-invasive sample collection nature, such methods do not allow for accurate enough

determination of DOX concentration in lung tissue. Direct determination of DOX in different compartments of lung tissue is desired during IVLP, as such an approach can provide precise information about drug level and its biodistribution within particular lung lobes. Traditionally, accurate determination of DOX in lungs requires collection of tissue via tissue biopsy, an invasive process that can only be performed from peripheral locations of the organ at the end of lung perfusion. In addition, traditional analytical methods for tissue determinations require lengthy sample processing and analysis, thus preventing real-time determinations of concentration and biodistribution of DOX in lung tissue over the course of IVLP. The absence of such information during IVLP, in turn, introduces potential for administration of subtherapeutic or toxic tissue levels of DOX. A minimally invasive method capable of monitoring DOX levels in tissue in close to real-time conditions would allow for safe, effective, and accurate administration of DOX in lung during IVLP. Certainly, implementation of such a monitoring tool during IVLP would be of critical therapeutic benefit, as such a measure would optimize treatment while preventing adverse effects associated with toxic levels of DOX in the target organ. Additionally, analysis of other indicators such as small endogenous molecules could reveal individual patient's response to drug toxicity or organ stress[178] by providing insight into ongoing biochemical processes during IVLP. Access to such information would be useful for effective tailoring of this treatment, as it would enable dose adjustments based on measurements of patient response rather than just DOX concentration levels.

Herein, biocompatible solid phase microextraction (Bio-SPME) technology is proposed as a new analytical strategy to assist in real-time measurements of DOX in tissue and perfusate during IVLP. Bio-SPME has already been reported for analysis of tissues.[129,130] This chemical biopsy procedure involves the extraction of small molecules such as xenobiotics and endogenous tissue components from a biological system by directly inserting sharpened microprobe the size of an acupuncture needle (ca. 0.3 mm diameter) into the tissue (Figure 6.2) without removal of any tissue residue.[141,179] The probe consists of a nitinol (Ni/Ti) alloy wire coated with a matrix-compatible extraction phase; in this case, a crosslinked slurry composed of micron-sized sorbent particles suspended in a biocompatible oligomer binder. The crosslinked

polyacrylonitrile oligomer forms a smooth surface characterized by small size pores, which exclusively permit the diffusion of small molecules from tissue to dispersed sorbent particles while preventing the adsorption of tissue components such as proteins, red blood cells, and other endogenous macromolecules onto the surface of the coating. Recovery of these small compounds is obtained via their desorption from the coating into a small amount of organic solvent, which is then subjected to instrumental analysis.

Figure 6.2 Biocompatible solid phase microextraction (Bio-SPME) probe

Quantitative analysis can be performed since Bio-SPME is conveniently amenable to a range of separation and detection techniques, including high-performance liquid chromatography (HPLC) coupled to tandem mass spectrometry (MS/MS) - the standard method for bioanalytical determinations. Qualitative analysis by way of untargeted metabolomics can also be performed via HPLC coupled to high-resolution mass spectrometry (HRMS). SPME has shown great potential in the field of clinical metabolomics due to its extractive capabilities for a broad range of both polar and non-polar small molecules (100 – 1200 Da.).[57,155] The advantage of carrying out a chemical biopsy via SPME in comparison to several other approaches is that Bio-SPME can be used to perform *in vivo* metabolomics.[55,57,62,180] Given its minimally invasive design, non-depletive extraction principle, and biocompatibility, information regarding the metabolites present within the system at a given time can thus be easily obtained without disrupting molecular binding or equilibrium within the system, nor damaging the microprobe itself.[62] In addition, Bio-SPME can be hyphenated to stand-alone mass spectrometer (MS) instruments, resulting in shorter analysis times and closer to real-time *in vivo* monitoring of DOX levels.[62] The herein proposed approach certainly fits within the growing trend of incorporating intraoperative real-time analysis of small molecules in animal and human studies via automated MS-based diagnostic protocols. Devices such as intelligent Knife (iKnife),

MasSpec Pen, and SpiderMass are among modern biocompatible tools that enable easy and fast introduction of extracted analytes to MS instrumentation, thus providing access to relevant information regarding the status of tissue during surgery.[181–183] In line with these surging trends, the development of sampling/sample preparation techniques based on microdialysis (MD) and SPME for such applications has observed increased demand in recent years, as such techniques facilitate reliable *in vivo* measurements of drug concentration and biodistribution within selected organs.[141,184,185]

Here, Bio-SPME is used to monitor DOX and its metabolites, as well as small endogenous molecules, present within the system over the course of IVLP. The current work presents the determination and quantification of DOX in the following settings: (i) an *in vivo* pig model over various drug doses as a proof-of-concept and (ii) an *in vivo* IVLP human clinical trials. The work also demonstrates that the SPME chemical biopsy enriches other low molecular weight compounds, such as potential markers of drug toxicity or organ stress over the course of IVLP.

6.3 Materials and methods

6.3.1 Study design

The main objective of this study was to evaluate the potential of Bio-SPME probes as chemical biopsy to nondestructively extract and analyze the concentration and biodistribution of DOX in lung tissue during IVLP procedure. The experiments were performed on *in vivo* pig model over various drug doses and during *in vivo* IVLP human clinical trial. In addition, we investigated *in vivo* profile of small endogenous molecules in human lung tissue over the course of IVLP-DOX administration. IVLP procedure and Bio-SPME lung sampling were conducted at Toronto General Hospital. Bio-SPME extraction of perfusate samples was performed on-site at Toronto General Hospital and in the analytical laboratory at University of Waterloo. HPLC-MS/MS and HPLC-HRMS analyses were performed in the analytical laboratory at University of Waterloo.

6.3.2 *In vivo* animal study

Two Yorkshire pigs weighing approximately 35 kg were used. The study was approved by the Animal Care Research Committee at Toronto General Research Institute. A porcine left lung IVLP model was used to model delivery of high doses of DOX during IVLP. The IVLP model procedure has been described elsewhere.[176,186] The doses of DOX administered were 150 and 225 mg/m2. SPME sampling was performed from the lower lobe of the left lung before perfusion (t0) and 30, 90, 150, and 210 min after the start of the IVLP procedure, using the protocol described below.

6.3.3 *In vivo* human study

The clinical trial was registered with www.clinicaltrials.gov, and institutional research ethics board approval was obtained. Two individuals were enrolled in clinical study: 22-year old and 66-year-old males with bilateral recurrent pulmonary metastases secondary to osteogenic sarcoma (Figure 6.1). All lung lesions treated with DOX using the IVLP platform could be resected with wedge or segmental resections. Both patients had previous systemic exposure to DOX (<450 mg) and had previously received a bilateral metastasectomy.

The technical details of the procedure have been described elsewhere.[176] Briefly, a clam-shell thoracotomy was performed, and the left pulmonary hilum was dissected. The pulmonary artery and upper and lower pulmonary veins were dissected and subsequently cannulated and attached to the IVLP perfusion system. Lung isolation was performed using vascular clamps, and IVLP was initiated and run for 3 hours. DOX was added to the IVLP perfusion solution at a concentration of 5 and 7μg/mL for the first and second patient, respectively.

For Bio-SPME sampling of lung, three probes (Figure 6.2) were placed in different areas of the lung (upper, middle, and lower sections) at predetermined time points over the course of the surgery. In both cases, the lung was sampled prior to drug administration, hourly during IVLP, and once after reperfusion. Extractions with the use of Bio-SPME probes were carried out for 20 minutes under static conditions. For Bio-SPME

sampling of perfusate, three fibers were used for on-site extraction of collected perfusion fluid. A 20-minute static extraction was performed on these samples as well. For both Bio-SPME sampling cases, the probes were subsequently rinsed manually in water for 5 s, wiped with a Kimwipe, and immediately snap-frozen in dry ice. Additional perfusate samples were also collected and snap-frozen in dry ice until further analysis in the laboratory. Concentrations of DOX in lung and in perfusate were determined in accordance with the recently published and validated SPME-HPLC-MS/MS protocol with some minor modifications. Information regarding the type of probes employed and instrumentation for analysis can also be found in this publication.[125] In addition, the analytical method to identify and quantify DOX key metabolites (doxorubicinol (DOX-ol), doxorubicinone (DOX-one), and doxorubicinolone (DOX-olone)) has been developed.

6.3.4 Statistical analysis

The metabolomics experiments were performed separately for both cases because of the long-time interval between the recruitment of the patients. First dataset was used for selection of important endogenous features, while the second dataset was used for confirmation of the initial findings. In metabolomics experiments, the number of features detected is typically much larger than the number of samples studied. In our study, the first dataset consisted of n = 12 samples and p =138 variables. Selection of variables prior to chemometric analysis was carried out using the LASSO method. LASSO (Least Absolute Shrinkage and Selection Operator) applies a regularization process where it penalizes the coefficients of regression variables, forcing certain coefficients to be set to zero. Thus, LASSO removes variables that are redundant by effectively providing a simpler model that does not contain those coefficients. The number of variables selected using the LASSO method has to be smaller or equal to the number of samples. Moreover, LASSO will often select only a single feature from a set of highly correlated variables.[142] Principal component analysis (PCA) was applied to the selected data after autoscaling (Unit-Variance scaling). PCA analysis employed internal cross-validation using the Leave-one-out-cross-validation (LOOCV) method. The

validation metrics root mean squares errors of calibration (RMSEC) and cross-validation (RMSECV) were calculated.

6.4 Results

6.4.1 Determination and quantification of DOX during IVLP

In vivo animal study. As a proof-of-concept for the sampling method, initial experiments were carried out using pigs as the experimental model. No bleeding or adverse effects were observed in any of the sampled areas of the lung in either pig case (Figure 6.3).

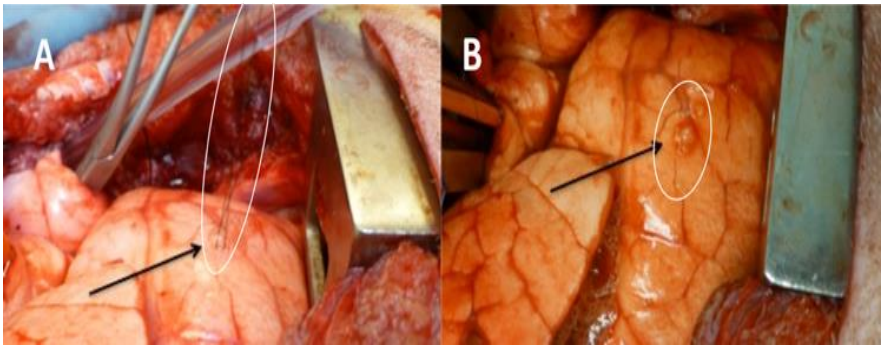

Figure 6.3 *In vivo* sampling of pig lungs during IVLP with doxorubicin. (A): triplicate of Bio-SPME probes during sampling; (B): the same location of lung after removal of SPME probes. *(Reprinted with permission)*[129]

Single Bio-SPME probe from each time point was used to assess lung tissue concentration of DOX. Lung tissue concentrations of DOX were successfully measured during two separate IVLP procedures, where DOX doses of either 150 mg/m2 or 225 mg/m2 were administered (Figure 6.4).

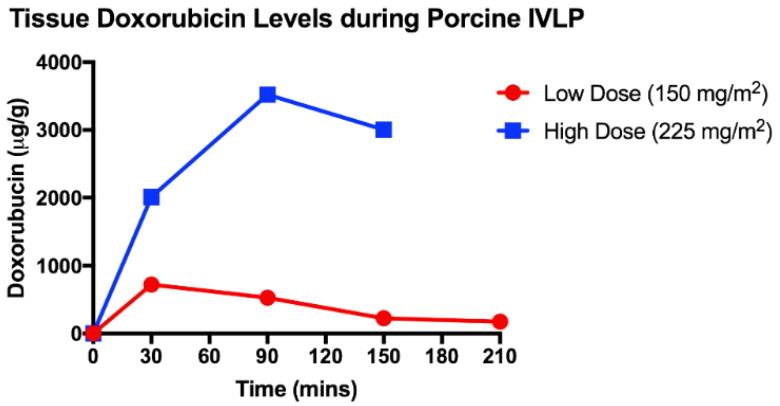

Figure 6.4 Concentration profile of DOX in lower lobe of the lung during IVLP (sampling points: 30, 90, 150, and 210 min). Red circles and blue squares – levels of DOX after administration with 150 and 225 mg/m2, respectively.

As expected, sampling before DOX administration (time zero, pre-IVLP) did not show the presence of the chemotherapeutic agent in lung tissue. Subsequent samplings exhibited a trend of a quick peak of drug followed by steady decline. For the lung perfused with a drug dose of 150 mg/m2, a maximum measured concentration of 723 µg/g DOX was noted at the 30 min mark after IVLP was initiated. For the lung perfused with a dose of 225 mg/m2 DOX, a maximum measured concentration of 3521 µg/g was reached after 90 min of IVLP. In the case of the high dose (225 mg/m2 DOX), the whole procedure ceased at 150 minutes, as the animal did not tolerate the injury caused by the high dose being administered.

In vivo human study. There were no intra-operative complications and use of Bio-SPME probes did not cause lung injury. For the first patient, wedge resection was performed for 6 lesions on the right lung and 4 lesions on the left lung. Total operative time was 7 hours 19 minutes in the case of 22-year-old patient and 6 hours and 47 min in the case of 66-year-old patient. Both patients tolerated the procedure well and did not require ICU admission. Each patient was discharged home on postoperative day 7 (POD7). They had an uneventful post-operative period and returned to regular activity after 1 month. At 6 months, 1st patient's forced expiratory volume in one second (FEV1) decreased from 4.7L (82% predicted) to 2.9L (50% predicted) and his forced vital capacity (FVC) decreased from 5.6L (80% predicted) to 3.4L (48% predicted). The patient developed bilateral lung recurrences after 6 months of follow-up, which have

progressed despite further treatment. He remained alive until 1 year of follow-up. Second patient at 6-month follow-up remained in overall good health.

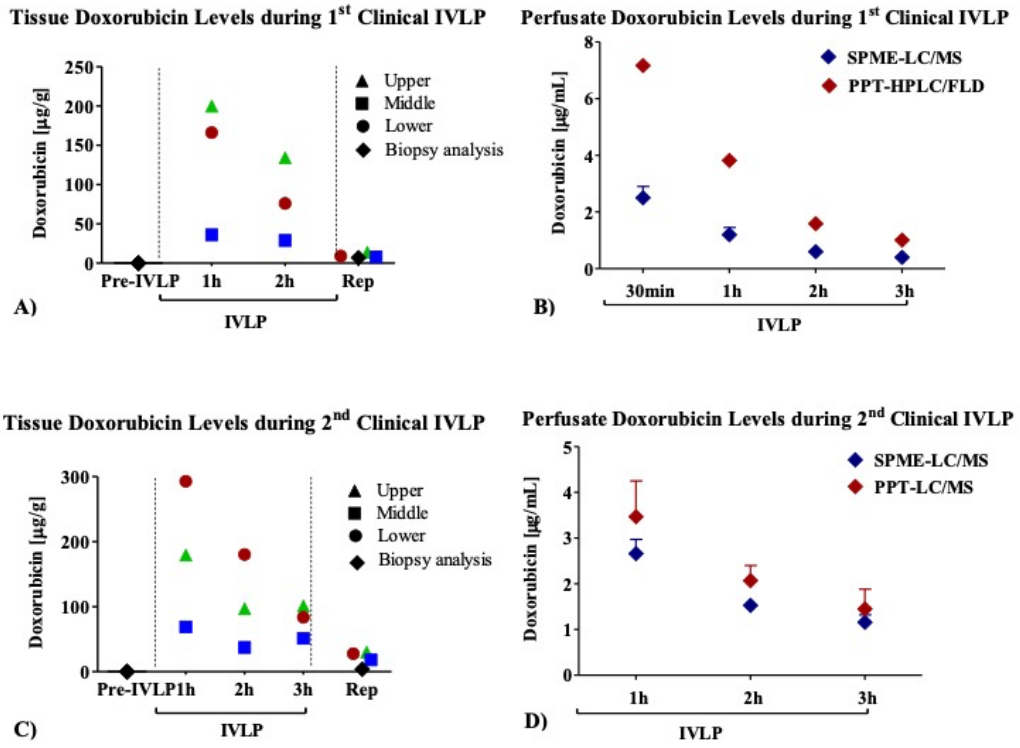

Figure 6.5 Concentration of doxorubicin measured by Bio-SPME-HPLC-MS/MS in lung tissue during first (A) and second (C) clinical IVLP. Time points include 1-hour pre-IVLP, 1, 2, 3 hours during IVLP, and 30 minutes post-IVLP during lung reperfusion. Red, blue, and green dots represent the three locations of the fiber in the lung during sampling. The red circle designates the upper section of the lung, the blue square designates a section between the upper and lower lobes (middle) of the lung, and the green triangle designates the lower section of the lung. Black diamonds show when hospital biopsies were taken. (B, D) Concentration of doxorubicin in perfusate as measured by Bio-SPME-HPLC-MS/MS and the standard approach (hospital assay - PPT-HPLC/FLD or PPT-LC/MS), during human IVLP, represented by the blue and red diamonds, respectively.

For the 22-year old patient, concentrations of DOX in the upper, middle, and lower regions of the perfused lung showed similar trends during IVLP (Figure 6.5A). Expectedly, before perfusion started (pre-IVLP), lung tissue was free of DOX. Maximum lung tissue concentrations of drug measured by Bio-SPME were reached at the first hour of IVLP, and were 200 µg/g, 36 µg/g, and 166 µg/g, for the upper, middle, and

lower sections of the lung, respectively. Lung tissue concentration dropped steadily over the course of IVLP and reached a nadir of 14 µg/g, 8 µg/g, and 9 µg/g for the upper, middle, and lower areas of the lung, respectively, by 30 min post blood reperfusion (after IVLP termination). The hospital assay (current gold standard technique done in tissue biopsies to measure DOX), which consisted of protein precipitation (PPt) followed by HPLC with fluorescence detection (HPLC/FLD), showed a DOX concentration of 7.0 µg/g in the biopsy tissue 30 min post-reperfusion. Further details on the hospital assay employed have been published elsewhere.[187] For the 66-year old patient, the highest tissue concentrations of DOX estimated with Bio-SPME probes were also noticed in the first hour of lung perfusion, and were 179 µg/g, 69 µg/g, and 293 µg/g, for the upper, middle, and lower sections of the lung, respectively (Figure 6.5C). Similarly, to the first human case, lung tissue concentrations of DOX exhibited a decreasing trend throughout the procedure reaching the levels of 30, 18 and 28 µg/g for the upper, middle, and lower areas of the lung, respectively 30 min post blood reperfusion. The hospital assay utilizing collected biopsy samples predictably revealed no drug at the stage of pre-perfusion and its very low content during pulmonary reperfusion (Figure 6.5C).

In addition to *in vivo* tissue measurements of DOX and its metabolites, the drug was also extracted by SPME probes on-site as well as in the analytical laboratory from perfusate samples collected at the same time points used for the *in vivo* lung sampling. For the 1st clinical case, the total drug amount given to the perfusion circuit, was 5.0 µg/mL. Concentration of DOX in the perfusate decreased steadily from the beginning of the IVLP procedure (Figure 6.5B). SPME-HPLC-MS/MS analysis revealed that after 30 minutes, the DOX concentration in the perfusate was 2.4 µg/mL and that over the course of the procedure this decreased to a nadir of 0.3 µg/mL by the end of the perfusion. PPt-HPLC/FLD analysis of perfusate samples performed by the clinical laboratory showed a concentration of 7.2 µg/mL after 30 minutes, and a nadir of 1.0 µg/mL by the end of the perfusion. DOX concentration measurements of frozen perfusate samples analyzed by SPME-HPLC-MS/MS after transport to an off-site location showed no statistically

significant differences from perfusate samples analyzed by SPME in the operating room (p = 0.75) (Table 6.1).

Table 6.1 Concentration of DOX in perfusate collected during 1st clinical IVLP and measured via Bio-SPME-HPLC-MS/MS for samples obtained on site and samples brought back to the laboratory for traditional analysis (denoted as UW).

On-site analysis				In-laboratory analysis			
Sample	Average (µg/mL)	SD	%RSD (n= 3)	Sample	Average (µg/mL)	SD	% RSD (n = 3)
Perf_T1	2.5	0.1	6	Perf_T1_UW	2.4	0.5	20
Perf_T2	1.2	0.05	4	Perf_T2_UW	1.4	0.1	9
Perf_T3	0.6	0.03	5	Perf_T3_UW	0.4	0.06	16
Perf_T4	0.4	0.02	5	Perf_T4_UW	0.3	0.1	45

During 2nd clinical IVLP, the dose of the drug administered into the perfusion circuit was 7 µg/mL and detected concentration of DOX in the perfusate samples in the first hour of the procedure was equal to 2.66 µg/mL. In next hours of IVLP, a further decline in DOX level was observed with the level of 1.16 µg/mL noticed at 3rd hour of perfusion (Figure 6.5D). For the second patient, a similar decreasing trend in the terms of the drug level in perfusate samples over the course of IVLP was also observed with the standard approach employing PPt as a streamlined sample preparation method (Figure 6.5D), however using the same instrumental method and analytical conditions the results received with two different strategies were even more comparable.

Figure 6.5B and Figure 6.5D show direct comparison SPME results with standard assays showing a good agreement between the data. In case of Figure 6.5B the PPt-HPLC/FLD assay was performed by external clinical lab for single samples at each time point, while in Figure 6.5D the PPt-LC/MS assay was performed on triplicate sample, similar as SPME extraction. It should be noted that the estimated precision obtained for SPME (RSD below 5%) are much better compared to PPt/LC/MS (RSD below 15%).

Furthermore, the identification and quantification of key metabolites of DOX, namely doxorubicinol (DOX-ol), doxorubicinone (DOX-one), and doxorubicinolone (DOX-olone) was performed for both clinical cases. However, the results showed that DOX metabolites were present at trace levels in the tested matrices (Figure 6.6). Only DOX-ol formed in the major metabolic route of DOX metabolism was

detectable at visible level, but its content in lung tissue did not exceed 5% of the intact drug, and therefore was considered as insignificant.

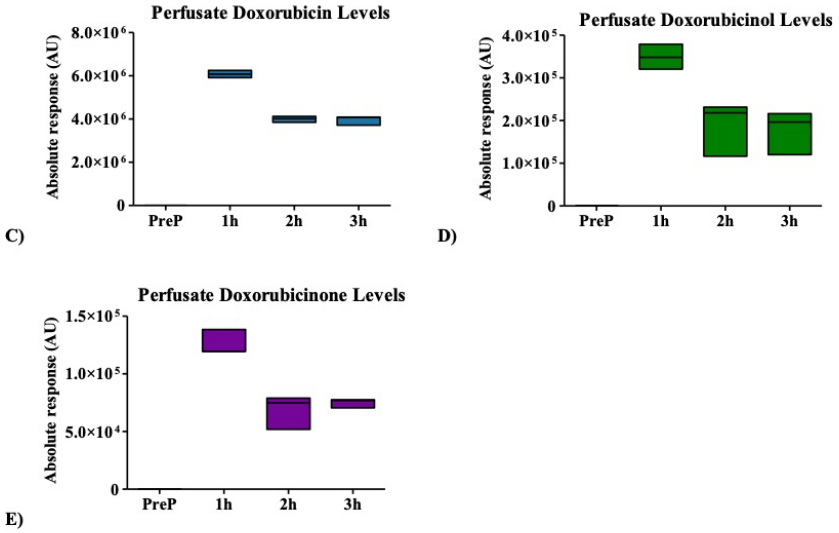

Figure 6.6 Floating bars presenting levels of doxorubicin and its key metabolites (doxorubicinol and doxorubicin aglycone) over the course of IVLP procedure. The detection range together with median values for each compound analyzed in relevant matrixes (lung tissue (A, B) or perfusate samples (C-E), respectively) have been denoted. As indicated above, the intact drug was a predominant one detected in investigated systems with some amounts of metabolites resulting from its biotransformation but contributing no more than 5% to the resultant pool of analyzed compounds.

6.5 Discussion

The current study demonstrates that the developed method based on SPME enables quantitative monitoring of DOX from lung tissue in a safe and minimally invasive manner. Multiple insertions of Bio-SPME chemical biopsy probes did not cause tissue injury during *in vivo* administration in either pig or human lungs. Each patient recovered uneventfully and had no complications from the SPME fiber insertion or the IVLP-DOX administration. Bio-SPME sampling was successfully performed on-site (*in vivo* and *in situ*), but analysis and data processing were still done in the analytical lab. No difference was observed among perfusate results for analyses carried out on-site or in-lab; however, the availability of MS instruments within or near the operating room would offer the possibility of more rapid target drug concentration determinations. A fully on-site setup is feasible since Bio-SPME probes can be directly coupled to a mass

spectrometer (SPME-MS), thereby providing results within seconds.[62,188,189] More recently we have also developed portable fluorometer coupled to laptop designed to be deployed in a surgery room for fast and direct quantification of DOX in the tissue via detection of this compound in the SPME coating (manuscript submitted). Fluorescence readout, however, can only provide the information about DOX concentration, but not about its metabolites or endogenous compounds, hence the information about organ condition in respect to biochemical alterations still requires the application of MS analysis. In both pig and human cases, DOX tissue levels presented similar trends during IVLP, wherein drug concentrations peaked between sixty to ninety minutes after the start of IVLP and subsequently dropped. This is more evident in the clinical trial since all sampled areas of the lung – upper, middle, and lower – exhibited the same pattern. As there were no measured leaks in the IVLP circuit, two potential reasons may explain this observed pattern: a) biotransformation of DOX into metabolites, leading to less intact drug available for extraction (that was rather not supported by our results indicating the formation of negligible amount of metabolites-please see below) or b) diffusion of DOX into cells. Bio-SPME probe extracts only free concentration of compounds, and therefore will not remove DOX bound to the intracellular components. The binding or partitioning of DOX into cells, therefore, decreases its free concentration in the extracellular environment of the lung where the microprobe performs sampling, which is reflected in the trend of decreasing DOX concentration. The results of DOX level obtained by Bio-SPME-HPLC-MS/MS for the lower lobe of the lung after drug washout (9 µg/g for first human case and 28 µg/g for second human case) were comparable to results obtained on tissue biopsies employing the standard assay further confirming the reliability of the approach proposed. Furthermore, the results from this study indicate that perfusion of the lung does not necessarily provide homogenous drug distribution, which may also account for the slight difference between the results provided by each assay, as the samples, although derived from the same lobes, were not obtained from the exact same location. It is important to emphasize that the differences in sample preparation fundamentals between SPME and PPT also contribute to some differences in the results gathered for perfusate samples employing these two methods. Furthermore, Bio-SPME has the added advantage of providing information

about the total as well as free drug concentrations; the latter offering the drug fraction immediately available for tissue binding.[62,190] Despite some differences in absolute measured DOX concentrations between the SPME-HPLC-MS/MS and PPt-HPLC/FLD assays, as seen on Figure 6.5B, there was an identical decreasing trend observed by both techniques, showing reliability and relative agreement of the methods. In addition, although the developed Bio-SPME-LC/MS method also offers a possibility to monitor DOX key metabolites (DOX-ol, DOX-one and DOX-olone), none of them were found at significant level in the lung tissue during DOX administration via IVLP. This finding is in line with generally accepted assumption that intact drug rather than its metabolites is responsible for pharmacological activity and anticancer effects.

6.5.1 Screening of small molecules in lung tissue during IVLP-DOX administration

The same Bio-SPME extracts that were used to perform targeted therapeutic analysis of DOX via HPLC-MS/MS were also used for screening of other low molecular weight compounds via HPLC-HRMS. Figure 6.7. shows the results of principal component analysis (PCA) conducted on samples obtained for the 1st clinical case at different time points for the duration of IVLP.

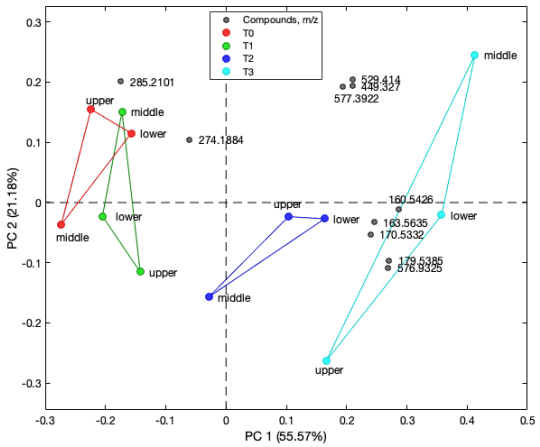

Figure 6.7 Principal component analysis showing separation of the data obtained at subsequent time points for different sections of the lung; red denote baseline sampling, before IVLP; green, blue, and turquoise denote 1 hour and 2 hours after the start of IVLP and 30 minutes after the start of blood reperfusion (RMSEC = 0.462, RMSECV = 0.838), respectively. The biplot reflects the distribution of molecular features (compounds), denoted as grey points, selected with LASSO with respect to subsequent data points.

It is evident that samples collected from each time point group relatively well together, with separation seen as a transitionary pattern from the left to the right part of the plot. It was even more pronounced for 2nd clinical case pointing at a clear discrimination among metabolomic patterns for samples collected before commencing perfusion, during IVLP, and reperfusion (Figure 6.8).

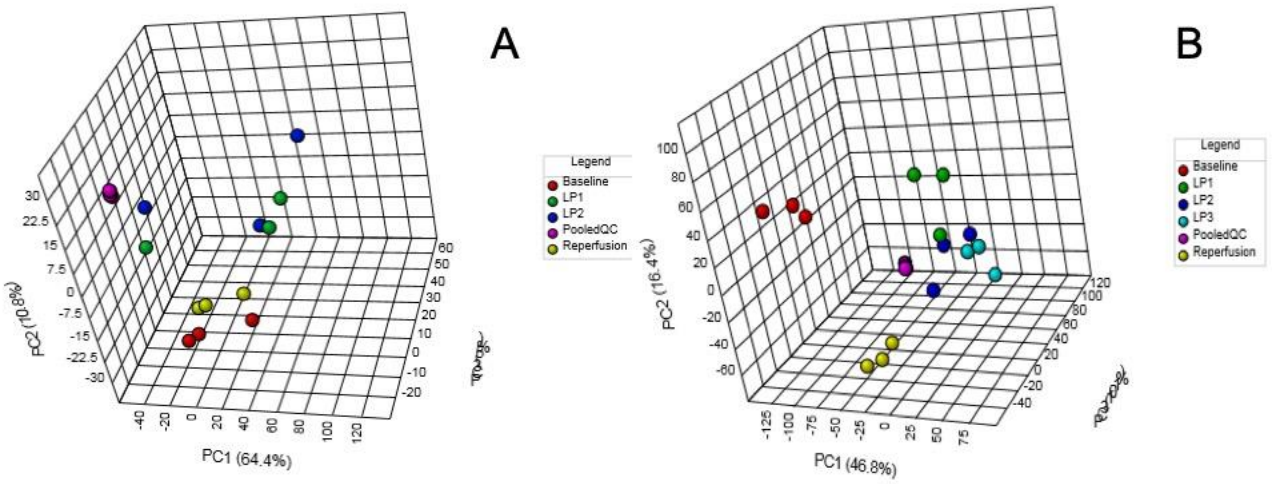

Figure 6.8 3-dimensional PCA score plots comparing LC/MS metabolomic profiles among four (1st clinical case (A))/five (2nd clinical case (B)) conditions corresponding to 4/5 sampling time-points (pre-perfusion, 1st, 2nd and 3rd hour of IVLP, reperfusion). Colored dots represent individual samples collected during sampling of different sections of the lung. Excellent discrimination among studied conditions (pre-perfusion vs. IVLP vs. reperfusion) has been found. Baseline – samples collected at pre-perfusion, LP1 – samples collected at 1st hour of IVLP, LP2 – samples collected at 2nd hour of IVLP, LP3 – samples collected at 3rd hour of IVLP, reperfusion – samples collected 30 min post reperfusion

Introduction of Least Absolute Shrinkage and Selection Operator (LASSO) analysis enabled selection of the compounds of the highest importance in the separation between T0, T1, T2, and T3, or between T0 and T3 only (before IVLP and after reperfusion). It should be emphasized that after the IVLP procedure, lungs were flushed with perfusate not containing DOX (reperfusion) in order to remove any remaining drug from the isolated organ, thereby avoiding systemic side effects. As expected, among the compounds differentiating all four time points were doxorubicin and several other molecules of possible endogenous or exogenous origin. The biplot in Figure 6.7 represents the relationship between the data collected at given time points during IVLP for all three sections of the lung, and masses of importance selected by LASSO.

Additionally, correlation analysis performed between all detected compounds and DOX lung concentration and distribution resulted in a number of metabolites exhibiting statistical significance. Cases, where the statistical significance was observed in at least two lung sections, were subjected to further identification and biological interpretation. The biplot plotted and the list of selected masses for the aforementioned metabolites can be found in Figure 6.9 and Table 6.2, respectively.

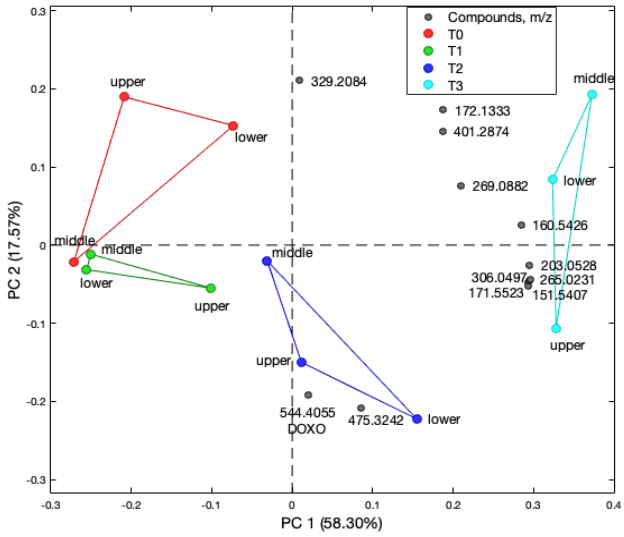

Figure 6.9 The biplot reflecting distribution of the molecular features (compounds) from Table 6.2 with respect to subsequent data points (RMSEC = 0.470, RMSECV = 1.008).

Table 6.2 List of selected masses by Least Absolute Shrinkage and Selection Operator (LASSO) for endogenous low molecular weight compounds. Putative identifications are based on accurate mass vs. database and RT/log(p) relation/correlation.

Compound	m/z	adduct	Δ ppm
Cardiolipin/CL (68:4)	475,3242	M+2H+Na	2
Cardiolipin (70:7)	475,3242	M+3H	4
PG (38:3)	401,2874	M+2H	4
11-Hydroxyandrosterone	329,2084	M+Na	1
5-Androstenetriol	329,2084	M+Na	1
5-Androstene-3b,16a,17a-triol	329,2084	M+Na	1
5-Androstene-3b,16b,17a-triol	329,2084	M+Na	1
Oxandrolone	329,2084	M+Na	1
N-Acetyl-L-isoleucine	329,2084	2M+H-H2O	4
4-Hydroxydodecanedioic acid	329,2084	M+2ACN+H	4
5-hydroxydodecanedioic acid	329,2084	M+2ACN+H	4
2-Hydroxydodecanedioic acid	329,2084	M+2ACN+H	4
6-Hydroxydodecanedioic acid	329,2084	M+2ACN+H	4
3-Hydroxydodecanedioic acid	329,2084	M+2ACN+H	4
3-Methylglutaconyl-CoA	306,0497	M+2H+Na	2
5-carboxy-2-pentenoyl-coa	306,0497	M+2H+Na	2
Cytidine 2'-phosphate	306,0497	M+H-H2O	2
Cytidine monophosphate	306,0497	M+H-H2O	2
Butenylcarnitine	306,0497	M+2K-H	2
Cytidine 2',3'-cyclic phosphate	306,0497	M+H	4

Arabinosylhypoxanthine	269,0882	M+H	1
Inosine	269,0882	M+H	1
Allopurinol riboside	269,0882	M+H	1
Methyl 5-acetoxyhexanoate	265,0231	M+2K-H	3
Nonate	265,0231	M+2K-H	3
Aldehydo-D-Mannose	203,0528	M+Na	1
Keto-D-fructose	203,0528	M+Na	1
Allo-Inositol	203,0528	M+Na	1
Alpha-L-Allose	203,0528	M+Na	1
D-Galactofuranose	203,0528	M+Na	1
Muco-Inositol	203,0528	M+Na	1
Hydroxypropionic acid	203,0528	2M+Na	1
3-Deoxyarabinohexonic acid	203,0528	M+Na	1
Beta-D-Glucose	203,0528	M+Na	1
Glyceraldehyde	203,0528	2M+Na	1
Allose	203,0528	M+Na	1
Alpha-D-Glucose	203,0528	M+Na	1
Beta-D-Galactose	203,0528	M+Na	1
L-Gulopyranose	203,0528	M+Na	1
Inositol	203,0528	M+Na	1
Myo-Inositol	203,0528	M+Na	1
Dihydroxyacetone	203,0528	2M+Na	1
Scyllo-Inositol	203,0528	M+Na	1
L-Lactic acid	203,0528	2M+Na	1
D-Fructose	203,0528	M+Na	1
D-Glucose	203,0528	M+Na	1
D-Galactose	203,0528	M+Na	1
D-Mannose	203,0528	M+Na	1
Fructose	203,0528	M+Na	1
Beta-D-Galactofuranose	203,0528	M+Na	1
Cis-Inositol	203,0528	M+Na	1
Neo-Inositol	203,0528	M+Na	1
Nonanoylcarnitine	172,1333	M+ACN+2H	1
2,6 Dimethylheptanoyl carnitine	172,1333	M+ACN+2H	1
3a,20b-Pregnanediol	172,1333	M+H+Na	4
Pregnanediol	172,1333	M+H+Na	4
5alpha-Pregnane-3alpha,20alpha-diol	172,1333	M+H+Na	4
7a,17-dimethyl-5b-Androstane-3a,17b-diol	172,1333	M+H+Na	4
Glucosamine 6-sulfate	171,5523	M+2ACN+2H	2
N-Sulfo-D-glucosamine	171,5523	M+2ACN+2H	2
5'-Methylthioadenosine	160,5426	M+H+Na	3
Glycerophosphocholine	151,5407	M+2Na	0
Creatine riboside	151,5407	M+H+K	3

Putative identification of the presented features enabled selection of those of important biological significance, namely compounds related to lung toxicity or injury. Among the identified endogenous compounds were 5'-methylthioadenosine (MTA) and creatine riboside (CR). In addition, the Bio-SPME approach was capable of detecting alterations in several lipid classes, including cardiolipins (Table 6.2). MTA and cardiolipins levels were elevated during the IVLP, but not before the perfusion, while creatine riboside was found in the extracts obtained at all time points that might be assigned to an active metabolism of proliferating cancerous cells rather than the activity of chemotherapeutic drug (Figure 6.10).

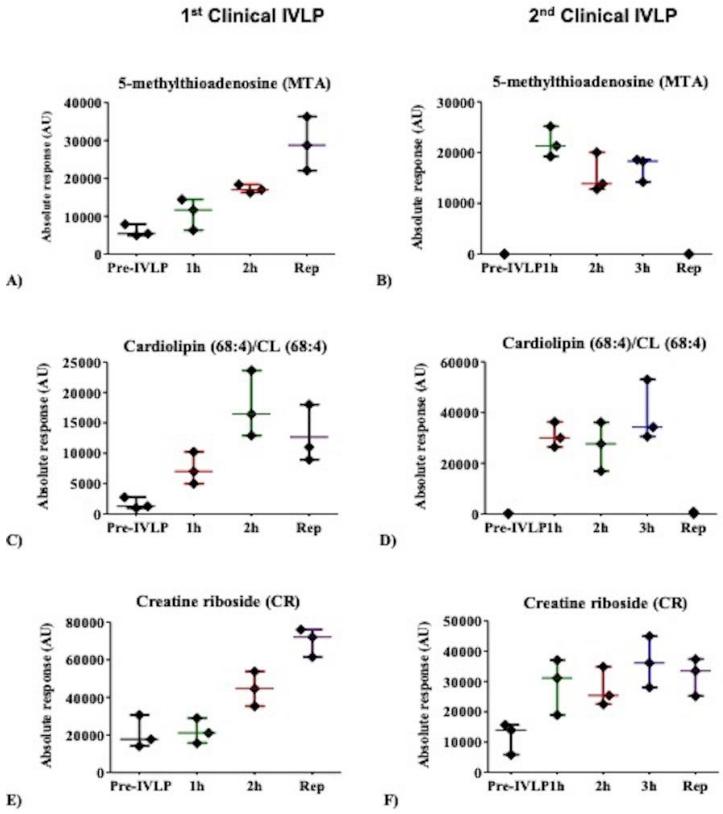

Figure 6.10 Scatter plots showing relative intensities of selected features/metabolites primarily dysregulated upon one-time chemotherapy treatment for an individual patient. Each dot in the scatter plots represents an individual metabolite in each sample.

With the use of an optimized Bio-SPME-LC/MS method, obtained extracts were additionally subjected to screening of other low molecular weight compounds such as metabolites of DOX and

endogenous/exogenous small molecules. As demonstrated in previous studies, SPME is suitable for extraction and monitoring of a broad range of metabolites (from highly hydrophilic to hydrophobic ones) in different biomatrices.[155] SPME has ability to monitor unstable compounds, like oxylipins, which was recently reported in brain.[191] Changes in the profiles of endogenous compounds corresponding to the administration of DOX during IVLP were monitored to verify if the analytical strategy proposed for drug monitoring could also be adopted for screening of known markers of drug activity. As a proof of concept, compounds that showed correlation with DOX activity including 5-methylthioadenosine (MTA), and cardiolipins (CLs), as well as the biomarker of the lung cancer, creatine riboside (CR), were putatively identified in sample extracts. Presence of the metabolites was reported in the first case and further confirmed in the second one. It has been previously reported that MTA exhibits proapoptotic effects on different cancer cells.[192,193] On the other hand, based on a study where DOX was used as a model drug, MTA was proposed to provide mechanisms to evade drug-induced apoptosis in tumor cells.[194] It has been suggested that MTA may have a dual role in the regulation of cellular homeostasis; therefore, further investigation of the relationship between MTA-DOX during IVLP should be performed on a larger cohort of patients/cases. DOX has also been previously shown to exhibit a strong correlation with lipid metabolism. In a rodent model, DOX led to elevated serum triglyceride and blood glucose levels through the downregulation of PPARγ.[195] An in vitro study with parental (MCF-7/S) and DOX-resistant (MCF-7/Dox) human breast cancer cells demonstrated that lipid profile changes can mediate the modulation of membrane fluidity in drug-resistant cells.[196] The authors observed an increase in the levels of several lipids, including cardiolipins, in resistant cells. Interestingly, DOX was already described as a specific probe for transversal distribution of cardiolipin.[197,198] As it can be seen in Figure 6.10 MTA and cardiolipin (68:4) levels were elevated during the IVLP, while creatine riboside was found in the extract obtained at all time points, i.e. it was independent on DOX administration (Figure 6.10). CR is considered a product of high creatine levels and high phosphate flux due to the higher energy demands of rapidly dividing tumor cells.[199] The level of this compound has been found to be significantly higher in the urine of patients with non-small cell lung

cancer (NSCLC) compared to healthy individuals.[200,201] Moreover, it has been previously reported that increased levels of CR are associated with increased tumor size and poor prognosis. Therefore, it has been speculated that this compound may not only be useful as a marker of early detection of lung cancer but also aid in the provision of more accurate prognoses.[202] Based on our finding it can be postulated that MTA, cardiolipins and CR may be promising targets for further study in SPME-based DOX activity evaluation during IVLP. Moreover, as the first attempt at real-time profiling of metabolites in human lung tissue exposed to chemotherapy, this case study provides insights into the correlation between DOX and other endogenous molecules in the living system.

However, the results of metabolite screening, although promising, contain limited data to draw any concluding remarks as the analyses in this case study were carried out in extracts specifically obtained for DOX analysis, and most of the small molecules described in this paper had low sensitivity. Therefore, as a next step, an optimum sample preparation protocol should be implemented to improve recovery of compounds of interest other than DOX. This will facilitate more in-depth study of organ-specific mechanisms as well as the adverse effects of DOX action, as such analyses are usually conducted on a large number of samples to account for biological variability and improve reliability of significant findings.

6.6 Conclusion

In summary, this work presents the first successful clinical use of the *in vivo* Bio-SPME chemical biopsy approach. The sampling/enrichment tool was used to reliably measure drug concentrations in lung tissue during a clinical case of localized DOX delivery. At the same time, a wide range of other molecules were extracted for metabolomic analysis, demonstrating the potential of the technique for real-time monitoring and early indication of lung toxicity and injury during the procedure. Based on these results, Bio-SPME can be used as a tool to assist in the safe and efficacious implementation of IVLP treatment for local chemotherapy by offering temporal and spatial monitoring of the drug concentration in individual patients. The Bio-SPME chemical biopsy tool provides significant advantages as a novel approach for tissue

sampling since it imparts real-time information about both the levels of the administered chemotherapy, as well as its effect and toxicity, as represented by the changing metabolomic landscape in the organ. Bio-SPME also shows potential as a complementary technique to aid in the elucidation of pathways affected or mechanisms of action of targeted therapies.

Chapter 7: Solid phase microextraction coupled to mass spectrometry via a microfluidic open interface for rapid therapeutic drug monitoring

7.1 Preamble

Chapter 7 has already been published in *Analyst* (**2019**, 144(12), 3721-3728) under the title "Solid phase microextraction coupled to mass spectrometry via a microfluidic open interface for rapid therapeutic drug monitoring". This paper was co-authored with M. Tascon, V.R. Acquaro, N. Reyes-Garcés, T. Vasiljevic, G.A. Gomez-Rios, M. Wasowicz and J. Pawliszyn. Please see *Statement of contributions*. No permissions from the journal were necessary to reuse the material in this thesis as per journal instructions – authors do not require permissions requested. The authors would like to thank Dr. Angela Jerath and her team at Toronto General Hospital/University Health Network for the collection of patient plasma samples. We greatly appreciate Dr. Chang Liu (SCIEX) for his initial support in this project, as well as Waters Corporation for providing the HLB particles used to manufacture the SPME fibers herein described. The authors are grateful to SCIEX and the Natural Sciences and Engineering Research Council (NSERC) of Canada for the financial support provided through the Industrial Research Chair program. Finally, we would like to thank the Science Technical Services at the University of Waterloo for aiding in the construction of the microfluidic open interface. V.A.J. thanks FAPESP, process 2016/16180-6 for his scholarship

7.2 Introduction

Tranexamic acid (TXA), classified as an antifibrinolytic agent, is a synthetic lysine analogue that works by inhibiting plasminogen and thus prevents its conversion to plasmin, an enzyme that degrades fibrin in blood clots.[63] This medication is used to stop or reduce bleeding in a wide variety of hemorrhagic conditions.[64] For instance, it is used in a number of high-risk operations such as cardiac surgery, liver transplantation, as well as in emergency rooms to treat cases of hemorrhaging as a result of trauma.[63,64] Its safety profile

provides significant advantages over older generation antifibrinolytic agents such as aprotinin and ecallantide, which have been linked to increased mortality, increased post-operative bleeding, increased blood transfusion requirements, and kidney failure.[64] Although no major risk factors have been reported in relation to the use of TXA in clinical applications, increased incidences of post-operative seizures in cardiac surgical patients have been reported in association with its increased clinical use in high doses.[63,64] A number of investigations directed at reaching the appropriate target concentrations unveiled high inter-patient variability for TXA, in that therapeutic levels varied greatly from patient to patient, often exceeding the target concentrations of both high dose and low dose dosing schedules.[3,64] Recently, Jerath *et al.* carried out a study demonstrating that exceedingly high TXA plasma levels – beyond 100 µg/mL – may be attributed to poor drug clearance from the system as a result of kidney dysfunction or failure.[76] The above investigation was carried out by measuring levels of TXA in the plasma of patients presenting varying stages of kidney damage who were undergoing cardiac surgery with the use of TXA.[203] These findings aided in the development of a new dosing regimen that accommodates patients who suffer from renal insufficiency. In this context, the development of technologies geared at fast and precise point-of-care (POC) analysis play a vital role in further advances in personalized medicine.[204] Such developments are especially critical in cases where the inter-patient variability is high, necessitating accurate regulation of dosage to produce the desired therapeutic effect.

In this context, the direct coupling of solid-phase microextraction (SPME) to ambient mass spectrometry (MS) has emerged as a solution that efficiently integrates the sample preparation step with analysis.[189,205,206] Indeed, several clinical applications reported to date have demonstrated the ability of this platform to both minimize overall time of analysis as well as mass spectrometer contamination.[134,207–209] In this work, a novel recently developed MOI that directly couples SPME to tandem mass spectrometry (MS/MS) in order to measure TXA is presented.[188] This interface allows for efficient analyte transmission into the electrospray ionization (ESI) interface; hence, allowing a dramatic reduction in acquisition time when compared to the traditional liquid chromatography (LC) protocol (time scale on order of seconds by MOI versus time scale

on order of minutes by LC).[210] Furthermore, after extraction, analytes collected onto the SPME devices are eluted for a period of 5 seconds into an open microfluidic desorption chamber which subsequently rapidly introduces the plug of desorbed analytes into the ESI interface and allows for improved sensitivity in comparison to other SPME-MS approaches.[62] In light of the recently reported connection between TXA use and post-operative seizures, and considering the well-documented sizable inter-patient variability of this drug, the currently presented technology was applied for the high-throughput monitoring of TXA in plasma samples taken from patients presenting different stages of renal damage undergoing cardiac surgery. Assessments carried out at various time-points, from five minutes after the bolus was injected, up until 72 hours post-surgery. The technology was also cross-validated against a previously validated thin film solid phase microextraction (TFME) with the use of LC-MS/MS method.[83] The methodology showed turnaround times of 15 minutes per sample for single-injection analysis (i.e. one sample at the time), and less than 30 seconds per sample for high-throughput analysis (i.e. extraction from a 96-well plate). These results demonstrate the capabilities of this technique towards close to real-time analysis of TXA, while evidencing its great potential for therapeutic drug monitoring in a wide range of clinical applications.

7.3 Methods and materials

7.3.1 Chemicals and materials

Tranexamic acid (trans-4-(aminomethyl)cyclohexanecarboxylic acid), the internal standard cis-4-aminocyclohexanecarboxylic acid, LC-MS grade formic acid, HPLC grade acetonitrile and methanol as well as chemicals used to prepare phosphate buffered saline (PBS), namely sodium chloride, potassium chloride, potassium phosphate monobasic, sodium phosphate dibasic were purchased from Sigma-Aldrich (Oakville, ON, Canada). Deionized water was obtained from a Milli-Q Reference A+ water purification system (Fisher Scientific). LC-MS grade water, used to prepare PBS as well as the stock solutions, was purchased from Fisher Scientific (Ottawa, ON, Canada). Human plasma (sodium citrate) was obtained from Lampire Biological Laboratories Inc. (Pipersville, PA, USA). HLB Supel™-Select particles (~ 60 µm) used

for thin-film solid phase microextraction (TFME) were kindly provided by Supelco (Bellefonte, PA, USA), while HLB particles (~ 5 µm) used to fashion Bio-SPME fibres were kindly provided by Waters Corporation (Winslow, UK). Polypropylene 96-well 2 mL deep plates were purchased from Fisher Scientific (ON, Canada).

7.3.2 Human plasma samples

All procedures employed in this study, including the retrieval of samples from patients, were approved by the Research Ethics Boards of the Toronto General Hospital/ University Health Network and the University of Waterloo. Each patient signed an informed consent while recruited to participate in the study. Plasma samples were obtained from patients undergoing elective high or low risk cardiac surgery under cardiopulmonary bypass (CPB). For high risk (HR) cardiac surgery the dose administered was as outlined in the Blood Conservation Using Antifibrinolytics in a Randomized Trial (BART) study[78] whereby 30 mg/kg bolus of TXA infused over a 15 min span post induction of anaesthesia (period 1) followed by an infusion of TXA at a dose of 16 mg/kg·hr (period 2) until the sternotomy was closed with a 2 mg/kg load in the pump prime. For low risk (LR) cardiac surgery, the dose was as per institutional practise at Toronto General Hospital as outlined by Jerath *et al*[203] whereby patients received a bolus dose of 50 mg/kg post induction of anaesthesia. The sampling protocol, which is schematically demonstrated in Figure 7.1, was as outlined in previous research.[83] Blood samples were first collected at baseline and then at 5 min and 10 min during period 1 which was the administration of a bolus dose (single dose of TXA given to the patient by injection into a blood vessel). During period 2, whereby TXA was infused, samples were collected post sternotomy (chest opening), immediately before and after the start of CPB, and at 30 min intervals during CPB for up to four sampling points. Samples were collected again after CPB and prior to chest closing. Finally, in period 3 - the post operation (postop) period - samples were collected at 1 hr, 2 hr, 4 hr, 8 hr, 12 hr, 24 hr, 48 hr, and 72 hr. A total, 114 samples were expected to be collected from 6 patients, with each of the 19 samples obtained, processed in triplicate. However, only 86 samples were obtained from 6 patients undergoing cardiac surgery for reasons undisclosed.

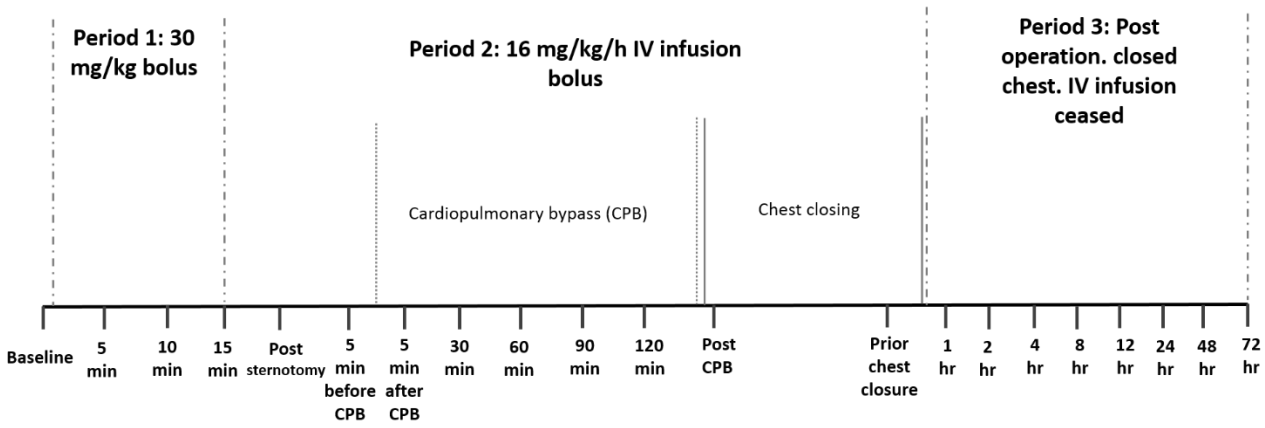

Figure 7.1 Patient blood samples were collected during surgery - which is segmented into 3 periods. First, baseline samples were collected prior to Period 1. Samples were then collected at 5 min and 10 min during Period 1 whereby a 30 mg/kg bolus dose of tranexamic acid is administered over 15 minutes. During period 2 of intravenous infusion of 16 mg/kg/hr, samples were collected post-sternotomy (after chest opening), 5 min before and after the start of cardiopulmonary bypass (CPB), at 30 minutes intervals during CPB for up to 4 sampling points, post CPB and prior to chest closure. During period 3, the post operation period where intravenous infusion was ceased, samples were finally collected at 1 hr, 2 hr, 4 hr, 8 hr, 12 hr, 24 hr, 48 hr and 72 hr.

7.3.3 High throughput analysis with concept-96 unit

The Concept-96 autosampler, shown in Figure 7.2, is a software-operated system that automatically performs each step of the SPME protocol: pre-conditioning, extraction, rinsing, and desorption.[47] The brush format differs slightly using a fiber form factor as opposed to TFME form factor which is presented in Figure 2.2 *section 2.3.6 "Concept-96 for SPME automation"* of Chapter 2. It houses a robotic arm, where either the 96 blades or fibres can be immobilized. These devices are compatible with 96-well plates, which can be stationed in their respective compartments on the unit. The system allows for preparation of up to 96 samples at once. After completing the sample preparation workflow, well plates can be deposited directly into the auto sampler of the LC system.

7.3.4 Sample preparation

All samples, including human plasma samples used to create the matrix-matched external calibration curve, were prepared as follows: 250 µL of sample was placed in a 2 mL well, and diluted with 750 µl of a PBS solution containing the internal standard. The dilution of samples (1:3) was supported for this application

due to the high therapeutic levels of TXA in the samples, as well as negligible binding of TXA to plasma proteins (~ 3%).[54] Extractions from the prepared samples were carried out with TFME in brush format and Bio-SPME fibres; both compatible with the 96-well plate format.

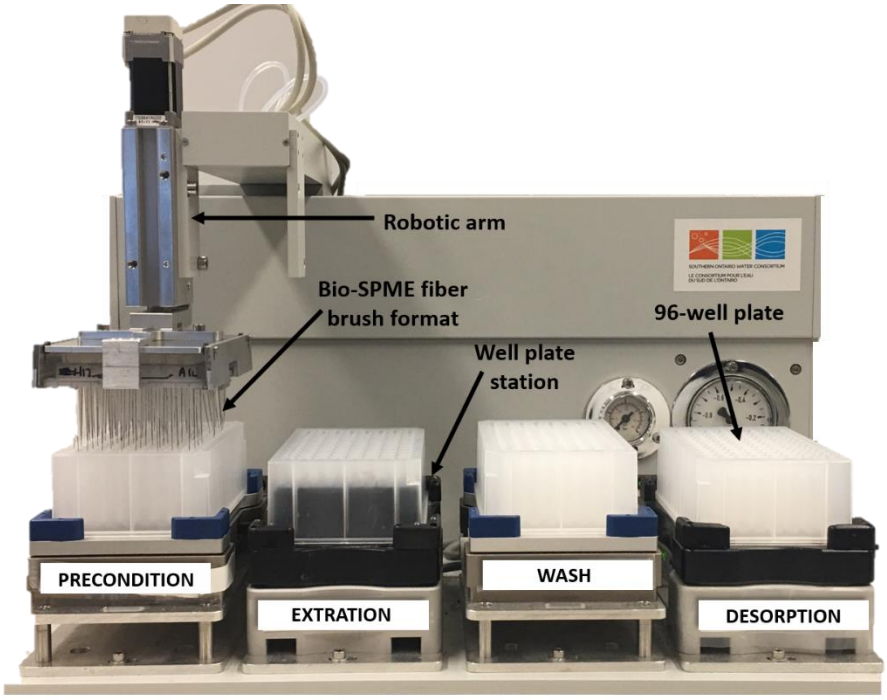

Figure 7.2 The Concept-96 is a software operated system that permits high throughput solid phase microextration (SPME) sample preparation of 96 samples simultaneously. It automatically performs each step of the SPME protocol – preconditioning, extraction, wash and desorption – with the help of a robotic arm that houses the brush format of the SPME configuration to be used (Bio-SPME fibers). This brush format is compatible with 96 well plates which are placed on their respective stations.

7.3.5 Calibration and quality control samples

Stock solutions of tranexamic acid were prepared by dilution of 100 mg/mL initial stock in pure LC-MS grade water. The solutions ranged from 500 µg/mL to 100 000 µg/mL and were stored at 4 ^{0}C in amber vials. A matrix-matched external calibration curve was prepared by adding 10 µL of the respective concentration of stock to 1 mL of human plasma. Samples were then submitted to low agitation for 45 minutes at room temperature to allow for equilibration to occur prior to the sample preparation step. The standard curve was validated at a working concentration of 100 µg/mL, which was prepared using the same

dilution ratio of a separate stock solution of 10 000 µg/mL of TXA. Phosphate buffered saline was prepared by dissolving 1.44 g sodium phosphate, 0.2 g potassium phosphate, 8.0 g sodium chloride, and 0.2 g potassium chloride in 1 L LC-MS grade water and adjusted to pH 7.4. The PBS was then spiked with 2 400 µg/mL of the internal standard cis-4-aminocyclohexanecarboxylic acid.

7.4 Instrumental analysis

7.4.1 SPME-LC-MS/MS

The TFME brush was prepared using a spray protocol developed in-house.[80] The device was coated with 60 µm HLB particles, and characterized by final coating dimensions of 2 cm length and 0.3 mm thickness.[211] Collected patient samples were prepared for analysis in 96-well plates, which were then mounted on their respective stations on the Concept-96. The SPME protocol for the LC-MS/MS method was as follows: pre-conditioning of the coating was carried out in 1.5 mL 50:50 (v/v) methanol/water for 15 min at 1500 rpm; extraction was performed at room temperature (25 ^{0}C) from 1 mL of biological matrix for 5 min at 1500 rpm; a 10 s agitated rinse (1500 rpm) was carried out in 1 mL 90:10 (v/v) water/methanol; and desorption was completed in 1 mL 3:3:4 (v/v/v) acetonitrile/methanol/water for 10 min at 1500 rpm. The desorption plate was then mounted into the autosampler and 10 µL of resultant extracts were withdrawn for LC-MS/MS analysis.

High performance liquid chromatography was performed with an Accela autosampler and pump (San Jose, CA, USA). Mass spectrometric detection was carried out with a triple quadrupole mass spectrometer TSQ Vantage (Thermo Scientific, San Jose, USA). Chromatographic separation was performed on a Discovery HS F5-3 column (10 cm x 2.1 mm, 3 µm) with a corresponding PFP guard column (Supelco, Bellefonte, PA, USA). A previously developed method detailing the conditions of the chromatographic separation and detection of TXA via LC-MS/MS was described elsewhere in detail.[77] Mobile phase A was 100 % water, while mobile phase B was 100 % acetonitrile, each with 0.1% formic acid. The 8-minute gradient chromatographic method had a final flow rate of 300 µL/min, and was carried out as follows: 90 % A from

0-2 minutes, 40 % A from 2-5.5 minutes with a hold at 40% A to 6 minutes, ending with a 2-minute re-equilibration at 90% A. The ESI parameters were: positive ion mode; nitrogen gas set at GS1 = 25, GS2 = 25; collision gas (CAD) =10; curtain gas = 25; heated nebulizer temperature = 450 °C; and electrospray voltage = 5000 V.

7.4.2 Bio-SPME-MOI-MS/MS

Bio-SPME fibres were prepared on a nitinol support in accordance to a dipping method developed in our laboratory.[134] The final dimensions of the fibres were 4 mm coating length and 20 µm of thickness, using 5 µm HLB particles. Parameters for analysis via MOI-MS/MS were as follows: extraction time was 15 min, followed by two 5 s rinsing steps with water, then desorption for 5 seconds at the MOI device, which was directly coupled to the mass spectrometer API 4000 triple quadrupole (AB SCIEX, Concord, Ontario). The operational duty cycle and performance of this interface is described in detail elsewhere.[188,210,212] The LC pump employed for fluid delivery was a 200 Series Perkin Elmer (Santa Clara, CA, USA), while ionization was produced with the use of a TurboIon™ spray source. Conditions required for the desorption step consisted of an equilibrium between the pump flow at (350 $\mu L \cdot min^{-1}$) and the electrospray ionization (ESI) aspiration. Essentially, the MOI device is designed with two sections[188] as shown in the second step of the analytical workflow in Figure 7.3.

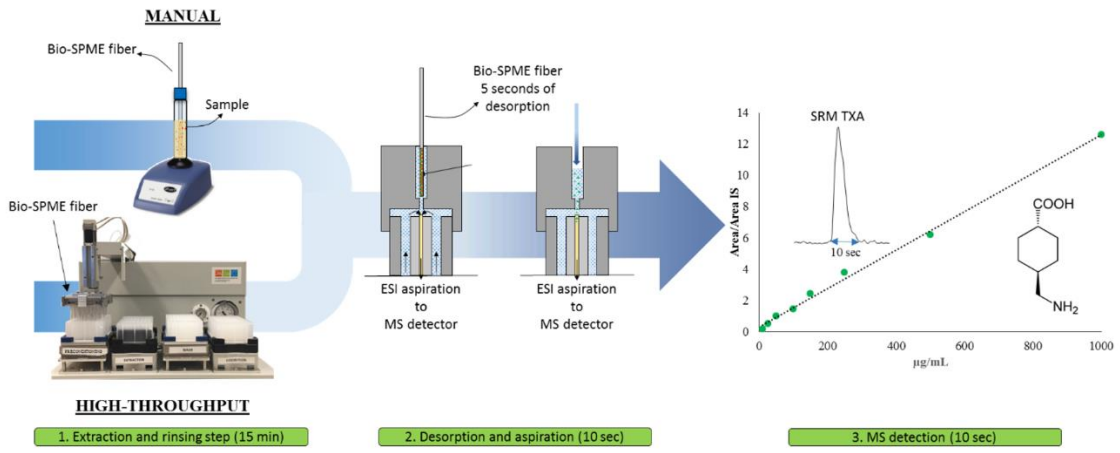

Figure 7.3 The Analytical workflow for Bio-SPME-MOI-MS/MS

The top section, which functions as the SPME desorption chamber, consists of a Teflon cylinder with two holes connected by a channel of a smaller diameter.[188] The connection between the open ambient desorption chamber and the electrospray needle employed in this device was inspired by the design of the open-port interface reported by Van Berkel et al.[188,189,209,210,212] Succinctly, the procedure involves the employment of two co-axial tubes that allow for solvent delivery through the gap formed between these two tubes. Once the solvent reaches the top of the coaxial tubes, it is aspirated towards the MS by means of the Venturi effect produced by the ESI source. ESI parameters were as follows: positive ion mode; nitrogen gas set at GS1 = 90, GS2 = 70; collision gas (CAD) = 6; curtain gas = 25; heated nebulizer temperature = 300 °C; and electrospray voltage = 5000 V. Chromatograms of the typical signals for blank plasma and patient samples are shown in Figure 7.4 and Figure 7.5, respectively. The solvent employed in the MOI-MS/MS system was methanol with 0.1% v/v formic acid. These conditions provided better sensitivity for this direct-to-MS application than acetonitrile or the desorption conditions used for TFME-LC-MS/MS.

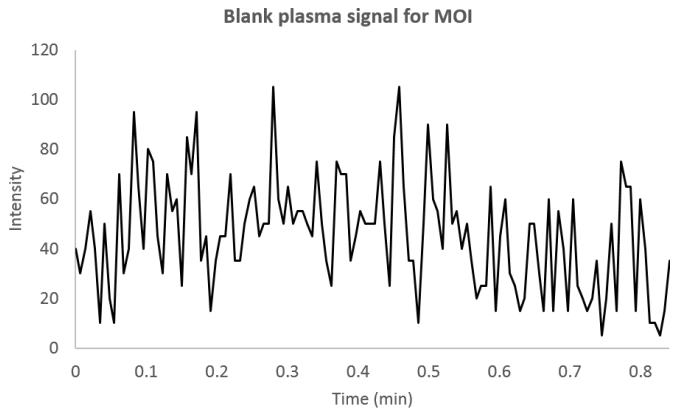

Figure 7.4 The signal for a blank plasma sample prepared with biocompatible solid phase microextraction (Bio-SPME) fibers and analyzed via microfluidic open interface tandem mass spectrometry (MOI-MS/MS).

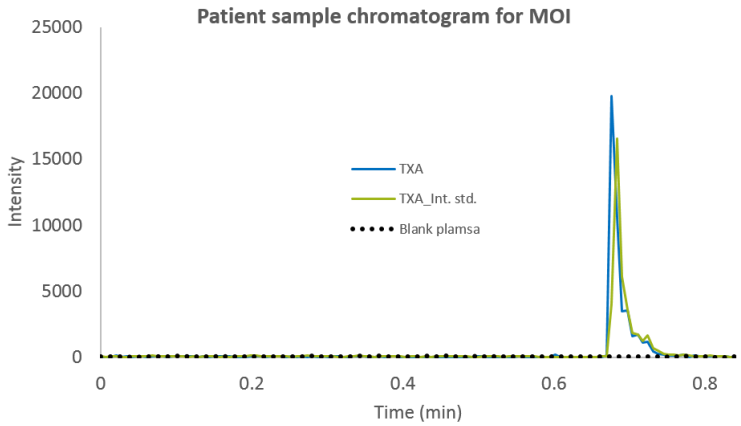

Figure 7.5 The signal for a blank plasma sample superimposed with a signal from patient sample prepared using biocompatible solid phase microextraction (Bio-SPME) fibers and analyzed via microfluidic open interface tandem mass spectrometry (MOI-MS/MS).

7.5 Results and discussion

7.5.1 SPME-MOI as a tool for rapid analysis of clinical samples

Given that tranexamic acid is known to present high inter-patient variability, concentration levels for TXA should be closely monitored in patients over the course of treatment. In this regard, previous studies have

demonstrated the emergence of a two-group stratified trend of TXA plasma concentration for patients receiving the same therapeutic treatment.[64] For the confirmatory high throughput study performed by Jerath *et al*,[203] patients were first categorized based on the type of cardiac surgery endured – low risk (LR) or high risk (HR). Within each group, patients were further categorised by healthy renal function and on the basis of degree of chronic renal dysfunction, stages 1 – 5; stage 1 being normal or increased glomerular filtration rate (GFR) and stage 5 being kidney failure.[203] As the use of TF-SPME technology for monitoring TXA in plasma has already been validated in previous research[54,82,83] against traditional methods such as ultrafiltration (UF) and plasma protein precipitation (PPt) which is routinely used for analysis in clinical applications, the same technology, with a few modifications was employed for this high throughput study.

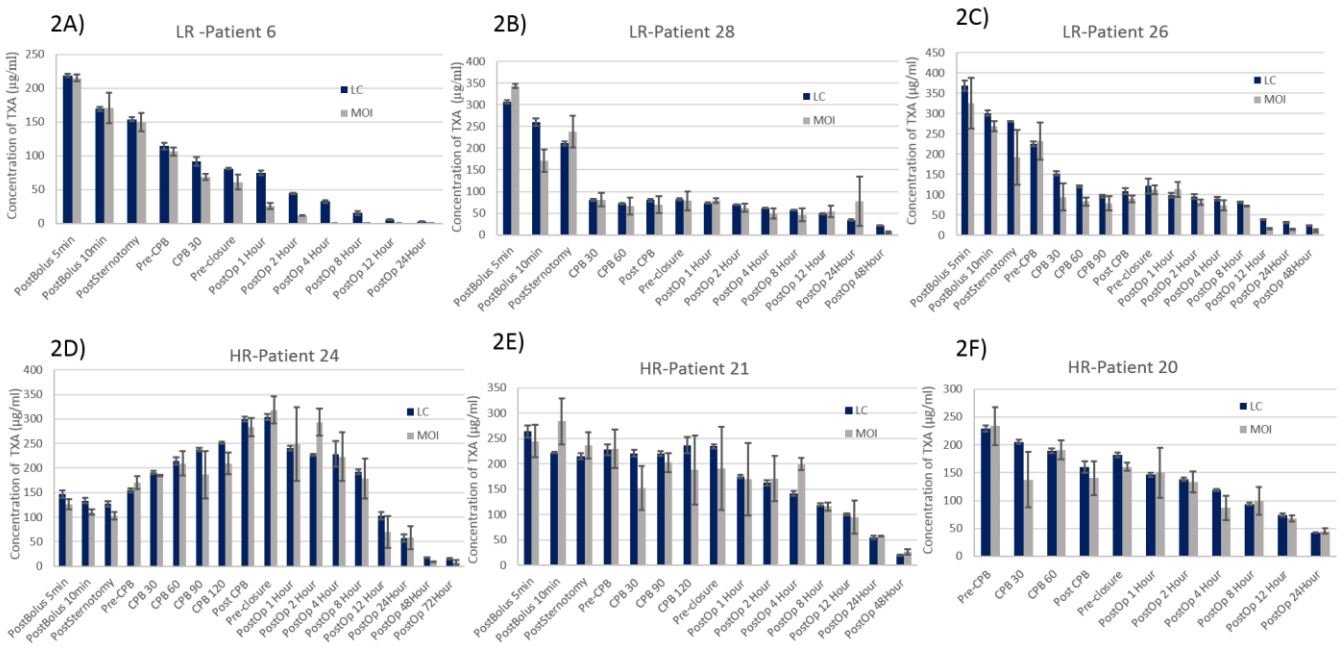

Figure 7.6 Patient profiles of 6 patients from two different risk groups. Figures 2A, 2B and 2C show profiles for patients who underwent low risk cardiac surgery with a dosing schedule as per institutional practice at the Toronto General Hospital. Figures 2D, 2E and 2F show profiles of patients who underwent high risk cardiac surgery with Blood Conservation Using Antifibrinolytics in a Randomized Trial (BART) dosing schedule. Results obtained via SPME-LC-MS/MS is represented by bars in dark blue while results obtained via SPME-MOI-MS/MS are represented by grey bars.

Given that all patients within the same risk category (high risk or low risk) were submitted to the same dosing schedule, the drastic differences observed in patient profiles as seen in Figure 7.6 (for example high

risk patients in Figure 7.6D, Figure 7.6E and Figure 7.6F, patients with more severe chronic renal dysfunction (CRD) experience elevated and persistently high TXA concentrations – Figure 7.6D and Figure 7.6E– in comparison to patients with normal kidney function – Figure 7.6F) endorses not only the need for revision and adjustment of the current TXA dosing schedule for cardiac surgical patients, but also the necessity of rapid sample analysis technology to facilitate POC testing. The former would generally contribute towards improving the recovery of patients post operation, particularly those with renal impairment, while the latter would better navigate clinical practitioners in personalizing treatment peri-operatively. Herein, we explain how Bio-SPME-MOI-MS/MS can be used as an alternative technology for rapid high throughput analyses of clinically relevant samples containing TXA. For instance, Figure 7.3 shows two sample preparation workflows that can be used with this technology. The first approach, the single injection strategy, allows for turnaround times under 15 minutes. The second approach, namely the high throughput workflow, as illustrated in Figure 7.3, allows for simultaneous extraction of TXA from up to 96 plasma samples. Hence, total sample preparation time drops to less than 10 seconds per sample, with total analysis times of approximately 30 seconds per sample given that the operator needs to manually place each Bio-SPME device on the MOI. As such, this method not only offers the selectivity provided by mass spectrometry and the efficient sample clean-up afforded by SPME but also facilitates rapid sample throughput due to semi-automation via the Concept-96. The Bio-SPME-MOI-MS/MS method produced a coefficient of determination (R^2) of 0.997 and a linear dynamic range over more than two orders of magnitude (refer to Figure 7.3), from 25µg/mL – 1000 µg/mL, comparable to the TFME-LC-MS/MS method. However, an LOQ of 25 µg/mL was obtained for the MOI-MS/MS as opposed to the LOQ of 5 µg/mL obtained for LC-MS/MS. These differences reflect the differences observed in recoveries for the target compound, which were dependent on the geometry utilized for analysis, whereby a 1% recovery was experienced for the TFME method in comparison to a 0.1 % recovery for the Bio-SPME method. Nonetheless, the range of concentrations that are expected to be encountered during TXA administration are well above these LOQs, with the target therapeutic level estimated to be 100 µg/mL. The method was

validated in human plasma at a working concentration of 100 µg/mL, with an inter-day precision of 20 %, a corresponding average accuracy of 91 % (n = 15), and an intra-day precision of 20 %, corresponding to an average accuracy of 95 % (n = 5).

As a result, Figure 7.6 shows the relatively close reproducibility of patient profiles by Bio-SPME-MOI-MS/MS in comparison to the trend generated by TFME-LC-MS/MS from both sets of patients undergoing high-risk (HR) or low-risk (LR) cardiac surgical procedures. Each bar plot shows the comparison of MOI (represented by grey bars) vs LC (represented by dark blue bars) for the concentration of tranexamic acid in plasma at each time point over the course of surgery. The profiles generated by Bio-SPME-MOI-MS/MS are very similar to profiles obtained by TFME-LC-MS/MS in that the same trend for a particular individual was observed. For instance, HR-Patient 24 had much higher TXA levels between CPB-30 (30 minutes after the start of cardiopulmonary bypass) and post-op-4hour (4 hours post operation after removal of CPB and cessation of TXA IV infusion) compared to the concentrations prior to Pre-CPB (start of surgery before cardiopulmonary bypass was implemented). In other patients however, such as HR-Patient 20 and HR-Patient 21, although TXA concentrations remain high (greater than 100 µg/mL), there is a more obvious decreasing trend of TXA plasma concentrations over the course of surgery, unlike that seen with HR-Patient 24. All three patients of this risk group belong to stage 4 chronic renal dysfunction. Despite belonging to the same stage and receiving the same dosing schedule, there are clear differences in the profiles between these patients. LR-Patient 26 and LR-Patient 28 experienced a sharp drop in concentration around CPB-30, however the concentration levels essentially plateaued at these lower concentrations with a slight spike at pre-closure and postop 1 hour from LR-Patient 26 until concentrations finally decreased during the post op period around 12 hours and 24 hours for LR-Patient 26 and LR-Patient 28 respectively. However, LR-Patient 6 experienced a much sharper decreasing trend than the other patient counterparts in the same risk group and especially in comparison to those patients in the high-risk group. The concentration plateau seen in LR-Patient 26 and LR-Patient 28 are indicative of increased residence time of TXA in plasma due to poor renal filtration as both patients belong to stage 4 renal dysfunction whereas LR-Patient 6 belongs to

stage 2 renal dysfunction. These results comparing MOI-MS/MS to LC-MS/MS are astounding, especially considering the large difference in time of analysis that exists between the two methods. For instance, approximately 19 continuous hours would be needed to process 96 samples via LC-MS/MS as opposed to the less than 2 hours needed for the manually operated MOI-MS/MS workflow to produce comparable results. Moreover, the proposed method proves robustness, as the samples were run on a blinded basis and completely randomized.

7.5.2 Statistical validation of the MOI methodology

Figure 7.7 and Figure 7.8 demonstrate the results of the statistical validation performed on the data acquired from both methods. The Passing-Bablok regression, shown in Figure 7.7, was constructed in order to statistically cross-validate the SPME-MOI-MS/MS method for monitoring TXA in plasma with the previously validated SPME-LC-MS/MS method.

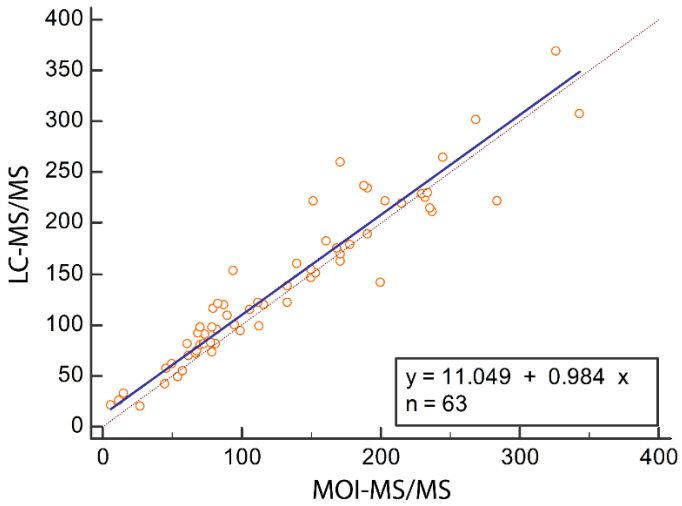

Figure 7.7 Passing-Bablock regression of data obtained from LC-MS/MS vs. MOI-MS/MS.

The Passing-Bablok regression uses an orthogonal regression algorithm which assumes that measurement imprecision is present in both methods under comparison. Six patients, were analysed initially by SPME-LC-MS/MS for the purposes of the high throughput study.[76] Both methods exhibited consistency in signal response over concentration. From the 86 sample pairs that were obtained from measurements with LC vs

MOI from 6 patients, 25 pairs exhibited statistically different results ($p < 0.05$) and were therefore excluded from further analysis. As such, n = 63 pairs were used for further statistical cross validation of the two methods. The results from the regression, which included 63 sampling pairs suggest equal suitability for both methods, with a slope of 0.984 (0.909 to 1.06), and an intercept of 11.049 (1.91 to 16.3). A statistical comparison of the two methods via the Spearman correlation coefficient yielded a value of 0.958 (0.931 to 0.974), further indicating that the methods have a linear relationship and are highly correlated ($p < 0.01$).

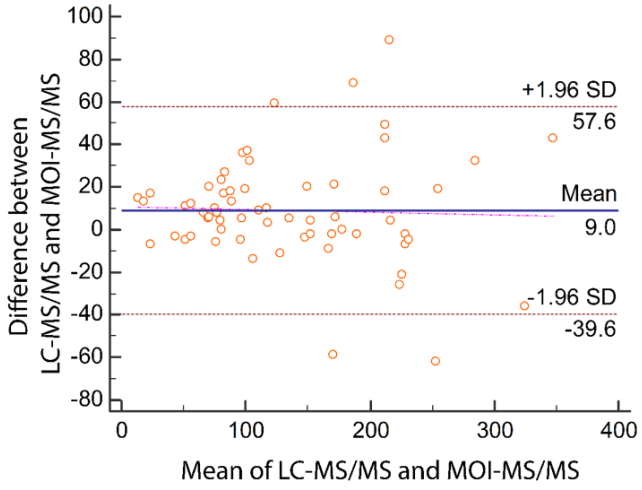

Figure 7.8 Bland-Altman plot of data pairs (n=63) of LC-MS/MS and MOI-MS/MS

Furthermore, to supplement the results of the Passing-Bablok regression, a Bland-Altman plot was constructed. The Bland-Altman plot shown in Figure 7.8 shows that the mean absolute difference in TXA quantification was observed to be 9.0. A value of ±1.96 standard deviation (SD) was used for the limit of agreement values (LOA), thus obtaining an interval from −39.6 (lower agreement limit) to 57.6 (upper agreement limit). The number of data pairs observed to be beyond the LOA value was 5 out of 63, which confirmed a Bland–Altman index of 7.9%. Thus, 92.1 % of the compared pairs were distributed within the acceptable range (within the ±1.96 SD limit). The comparative results presented low discrepancy between both methods, with the majority of the values distributed around the mean (9.0) and completely random,

indicating that no tendency is present in the analysis. Thus, confirming the suitability of Bio-SPME-MOI-MS/MS for the monitoring of TXA in plasma samples.

7.5.3 MS-based POC technologies

The MOI has already demonstrated to have about one order of magnitude more sensitivity than the open port probe interface for Bio-SPME applications for several targeted compounds.[188,189] The main differences were attributed to the small desorption volume employed as well as the static desorption allowing for a very sharp injection plug. Additionally, this technology is complementary to other ambient technologies such as DART and DESI which have been implemented in a number of clinical applications and are largely employed in a wide range of bioanalytical applications including screening of small molecules in biological fluids, 2D imaging of tissues and high throughput screening and drug discovery, respectively.[213–216] However, most of these applications are directed towards the analysis of compounds present in high concentrations where strong matrix effects are not compromising the detectability. When sample preparation for direct-to-MS approaches is taken into account, the most widespread is SPE.[12,217] Rapidfire™ especially, has been demonstrated to be useful for therapeutic drug monitoring of immunosuppressive drugs in whole blood with sample turnaround times of less than 15 s.[12] However, for total analysis time, the number of steps is not fully contemplated including protein precipitation, incubation and centrifugation. Noteworthy, Unlike SPME, in SPE this protocol cannot be skipped in clinical samples such as whole blood or plasma due to the chances of cartridge clogging. Regarding SPME-MS interfaces, Coated blade spray (CBS)[205] is another concept, that has also shown potential for high throughput therapeutic drug monitoring affording sample analysis times of less than 55 s.[208] As a substrate spray method, the entire blade can be exposed to a fluid sample for a predetermined amount of time, thereby conducting an SPME based extraction.[207,208] Alternatively, similar to Paper spray (PS), a spot analysis can be performed wherein a small sample volume can be directly applied to the blade coating surface prior to desorption/ ionization. There are fewer methodologies still, like PS, that are used for quantitative therapeutic drug monitoring and POC analysis.[74,218] Given that SPME fibers can be easily interfaced with the MOI, this technology offers a

unique advantage not only as an alternative approach to the bulk of these strategies but also a complementary technique as it can be used for both quantitative *in vivo* and *ex vivo* analysis.[62,188,189,209] Owing to the SPME device's small diameter (Ø < 250 µm), MOI presents a breakthrough for rapid quantitative and qualitative practices for assessing more complex biological materials such as various tissues/organs that have been subjected to therapy.

7.6 Conclusions

The work herein presented demonstrates that employment of liquid chromatography instrumentation for quantitation of TXA in plasma can be circumvented by directly coupling SPME to mass spectrometry via the developed MOI, thereby dramatically improving sample throughput. In fact, to the best of our knowledge, it is the first time that a SPME-MS approach is validated for a large number of clinical samples demonstrating the feasibility for rapid therapeutic drug monitoring. Since SPME integrates sample preparation and sample clean-up in one step, while being amenable for automation with the 96-concept, a large number of plasma samples from patients can be prepared and subsequently submitted to instrumental analysis within a short period of time, affording total analysis time of less than 30 seconds per sample. The currently presented method achieved a linear dynamic range between 25 µg/mL – 1000 µg/mL, which is comparable to that produced by TFME-LC-MS/MS. This LOQ of 25 µg/mL result is suitable for the range of TXA concentrations expected from such clinical applications; and undoubtedly reproduced the profiles of 6 patients from two different risk groups, with an average accuracy and precision of 95% and 20 %, respectively. It must also be noted that despite Bio-SPME-MOI-MS/MS did not achieve similar precision as found by TFME-LC-MS/MS method, the attained values are nonetheless sufficient and acceptable for a POC or screening methodology. Presumably, one of the main contributing factors behind the observed difference in performance may be attributed to the absence of an autosampler for conducting the analysis since the fibers were introduced manually to the MOI. Uncertainties in the final quantitative data may arise because of variations in the reaction times of placing or removing the fibers into or from the MOI, as well as variations in the amount of time that elapsed for desorption and switching the flow to allow aspiration.

Additionally, the fibers used were prepared in laboratory using a relatively novel dipping strategy developed in house.[134] The use of commercially available fibers can be a source of potential improvement. Furthermore, although use of an internal standard is meant to correct for any possible variations, the internal standard used was not an isotopically labelled standard which may not completely address the system variations. Nevertheless, the Passing-Bablok regression was performed to cross-validate the developed MOI methodology against the LC-MS/MS gold standard. The correlation was slightly lower in the lower concentration range (intercept) due to the differences in LOQ achieved by LC-MS/MS vs MOI-MS/MS respectively. However, the assays agreed reasonably well in the expected TXA concentration range for both methods (slope of the regression line 0.931 to 0.974). Bio-SPME-MOI offers a breakthrough for rapid sample analysis and high sample throughput—requirements for on-site clinical applications such as therapeutic drug monitoring and POC testing. With the necessity for rapid sample analysis afoot, based on the work presented herein and the possibility of mass spectrometers being introduced into clinical settings, this technology can be implemented for real-time analysis of biological samples in hospitals and clinics, providing and easy to use tool for POC-testing, screening, and onsite therapeutic drug monitoring in biofluids and/or tissues either *in vivo* or *ex vivo*.

Chapter 8: Conclusion

The objective of the research was twofold. First, this research sought to demonstrate the potential and range of SPME in the clinical field of personalized medicine, particularly for TDM and metabolomics in a range of complex biological samples. In Chapter 2, a high-throughput TFME method was developed for the TDM of TXA in plasma and urine, which expanded on previous research that focused only on plasma. The results from the work in this chapter were used by clinicians to develop a more comprehensive PK profile in an effort to adjust the dosing schedule for patients with chronic renal dysfunction.[76] In Chapter 3, an SPME method based on a mixture of sorbent phases was used to perform global serum profiling on patients with PsD and PsA. This study resulted in two key observations: 1) PsA disease progression may provide more insight to disease conversion (the development of PsA), and 2) there is an apparent correlation between dysregulated fatty acid enzymes and PsA disease severity, as evidenced by an increase in a number of circulating organic acids. While Chapters 2 and 3 focused on the use of SPME for *ex vivo* analysis of biofluids, Chapters 4, 5, and 6 focused on the use of SPME in more difficult and dynamic clinical settings. Specifically, the work in these chapters demonstrated the proficiency of SPME as an *in vivo* sampling tool for the analysis of lung tissue during ILP systems. Chapter 4 solely focused on tissue metabolomics, using *in vivo* SPME to investigate the changes taking place over the duration of NEVLP. The results of this study showed the capacity of NEVLP as an organ-preservation technique, as the lung exhibited continued metabolic functions, which was evidenced by the tentative presence of both anti-inflammatory and pro-inflammatory metabolites. In contrast, Chapters 5 and 6 illustrate SPME's capabilities for concomitant TDM and pharmacometabolomics. In Chapter 5, an SPME-based method for the *in vivo* quantitation of FOLFOX in porcine lung was developed and applied to real samples collected via *in vivo* SPME fibers during pre-clinical IVLP and IV trials, which was followed by proof-of-concept pharmacometabolomics to assess the changes in the lung during IVLP or IV under chemotherapy. The preliminary results revealed that the metabolic changes in the lung were not only treatment related (as a result of the chemotherapy), but

they were also influenced by the route of administration. For instance, compared to IVLP, the IV route seemed to produce more consistent results related to drug metabolites, specifically for FdUMP, which is the active metabolite of F. In Chapter 6, a previously developed SPME-based method for the quantitation of DOX in tissue was used for monitoring DOX administered to human lungs via clinical IVLP trials, after which, a proof-of-concept pharmacometabolomics followed. Chapter 6 presented the first successful clinical use of *in vivo* SPME, thereby showing its potential for monitoring not only drug concentration and distribution but also monitoring markers of lung toxicity or injury during the procedure. *In vivo* SPME can therefore by effectively implemented for temporal and spatial monitoring of therapeutic drug pharmacokinetics as well as the impact of this therapy specific to an individual.

It is worth mentioning that many of these studies were limited to proof-of-concept metabolomics (i.e., pharmacometabolomics) due to various limitations, such as: availability/schedule of surgeons and students; research culture (e.g., willingness of participating surgeons or students); time limitations; clinical/surgical limitations; unforeseen circumstances, including limited number of patients enrolled in a study; and the interdisciplinary nature of the study. Typically, a much larger cohort and a closer examination of the relationship between the obtained metabolic profile and the clinical parameters/outcomes are required before any results can be confirmed and further implemented into clinical practice. Nevertheless, there is a lot to be learned from the work presented in this thesis. Aside from its evident potential in personalized medicine, this work shows that SPME is a tool that can be used to improve the metabolomic workflow, as it can be deployed on-site for both the *ex vivo* and, more importantly, *in vivo* sampling of fluids and solid matrices. As shown in Chapter 4, both the on-site and *in vivo* approaches are superior for obtaining the true coverage of the metabolome, as snap-freezing, a common sample preservation practice in the metabolomics workflow, can lead to the formation of artefacts that are not representative of the true metabolome under physiological conditions. Furthermore, in Chapter 5, that the metabolome can be drastically affected not only by the chemotherapy administered but by the route of administration (IVLP vs. IV), and while it may be an obvious hypothesis, it is explored and documented in this thesis. Lastly in Chapter 6, while the number

of patients was low (2 cases), they represent the first successful use of *in vivo* SPME for sampling human lung during clinical IVLP trials with DOX, showing the direction and promise of SPME in being used for determining metabolic-related markers correlated to (in the long run) favorable/adverse clinical outcomes.

The second research objective, addressed in Chapter 7, was to show that SPME can be easily used for rapid diagnostics via real-time TDM or point-of-care metabolic analysis for a variety of complex samples. Since point-of-care metabolic analysis poses a number of field-related research challenges (validation of important metabolic markers), this research focused more explicitly on demonstrating real-time TDM, particularly for the monitoring of TXA in the plasma samples from the patients presented in Chapter 1. Finally, the results presented in Chapter 7 statistically prove that SPME coupled to MS via MOI can achieve similar results in substantially less time than the analytical gold standard, LC-MS.

In conclusion the work presented in this thesis satisfies the research objectives, namely, that SPME can be successfully used in the clinical field for TDM, metabolomics, pharmacometabolomics, and point-of-care testing via rapid analysis.

References

1. Palmer, M., Chan, A., Dieckmann, T. & Honek, J. *Biochemical Pharmacology*. (Hoboken, New Jersey : John Wiley & Sons, 1961).

2. Shafer, S. L., Flood, P. & Schwinn, D. Section 3: Anesthetic Pharmacology. in *Millers Anesthesia* (2009).

3. Nicholson, J. K. *et al.* Metabolic phenotyping in clinical and surgical environments. *Nature* **491**, 384–92 (2012).

4. Clarke, N. *'Phenotypings' for pharmacogenomics and personalized medicine - tamoxifen*. (2015).

5. Reynolds, K., Sarangi, S., Bardia, A. & Dizon, D. S. Precision medicine and personalized breast cancer: combination pertuzumab therapy. *Pharmgenomics. Pers. Med.* **7**, 95–105 (2014).

6. Tessari, A., Palmieri, D. & Di Cosimo, S. Overview of diagnostic/targeted treatment combinations in personalized medicine for breast cancer patients. *Pharmgenomics. Pers. Med.* **7**, 1–19 (2013).

7. Roberts, J. A. *et al.* Individualised antibiotic dosing for patients who are critically ill: challenges and potential solutions. *Lancet. Infect. Dis.* **14**, 498–509 (2014).

8. Fabbri, C., Porcelli, S. & Serretti, A. From pharmacogenetics to pharmacogenomics: The way toward the personalization of antidepressant treatment. *Canadian Journal of Psychiatry* vol. 59 62–75 (2014).

9. Hamburg, M. A. & Collins, F. S. The path to personalized medicine. *N. Engl. J. Med.* **363**, 301–4 (2010).

10. Bach, D. M., Straseski, J. A. & Clarke, W. Therapeutic drug monitoring in cancer chemotherapy. *Bioanalysis* vol. 2 863–879 (2010).

11. Phillips, E. J. The pharmacogenetics of antiretroviral therapy. *Curr. Opin. HIV AIDS* **1**, 249–56 (2006).

12. Grote-Koska, D., Czajkowski, S. & Brand, K. Performance of the New RapidFire System for Therapeutic Monitoring of Immunosuppressants. *Ther. Drug Monit.* **37**, 400–404 (2015).

13. Wishart, D. S. Emerging applications of metabolomics in drug discovery and precision medicine. *Nature Reviews Drug Discovery* vol. 15 473–484 (2016).

14. Beger, R. D. *et al.* Metabolomics enables precision medicine: "A White Paper, Community Perspective". *Metabolomics* **12**, 1–15 (2016).

15. Frédérich, M., Pirotte, B., Fillet, M. & De Tullio, P. Metabolomics as a Challenging Approach for Medicinal Chemistry and Personalized Medicine. *Journal of Medicinal Chemistry* vol. 59 8649–8666 (2016).

16. Vuckovic, D. Current trends and challenges in sample preparation for global metabolomics using liquid chromatography-mass spectrometry. *Analytical and Bioanalytical Chemistry* vol. 403 1523–1548 (2012).

17. Yi, L. *et al.* Chemometric methods in data processing of mass spectrometry-based metabolomics: A review. *Anal. Chim. Acta* **914**, 17–34 (2016).

18. Cui, L., Lu, H. & Lee, Y. H. Challenges and emergent solutions for LC-MS/MS based untargeted metabolomics in diseases. *Mass Spectrom. Rev.* **37**, 772–792 (2018).

19. Kohler, I., Verhoeven, A., Derks, R. J. & Giera, M. Analytical pitfalls and challenges in clinical metabolomics. *Bioanalysis* **8**, 1509–1532 (2016).

20. Wishart, D. S. Advances in metabolite identification. *Bioanalysis* vol. 3 1769–1782 (2011).

21. Aszyk, J., Byliński, H., Namieśnik, J. & Kot-Wasik, A. Main strategies, analytical trends and challenges in LC-MS and ambient mass spectrometry–based metabolomics. *TrAC - Trends in Analytical Chemistry* vol. 108 278–295 (2018).

22. Mehta, A. C. Preanalytical considerations in drug assays in clinical pharmacokinetic studies. *Journal of Clinical Pharmacy and Therapeutics* vol. 14 285–295 (1989).

23. Raju, K. S. R., Taneja, I., Singh, S. P. & Wahajuddin. Utility of noninvasive biomatrices in pharmacokinetic studies. *Biomed. Chromatogr.* **27**, 1354–66 (2013).

24. Carnevale, R. *et al.* New insights into the steen solution properties: Breakthrough in antioxidant effects via NOX2 downregulation. *Oxid. Med. Cell. Longev.* **2014**, (2014).

25. Xue, Y.-J. *et al.* Bioanalysis of drug in tissue: current status and challenges. *Bioanalysis* **4**, 2637–53 (2012).

26. Smith, K. M. & Xu, Y. Tissue sample preparation in bioanalytical assays. *Bioanalysis* **4**, 741–749 (2012).

27. Naz, S., Moreira dos Santos, D. C., García, A. & Barbas, C. Analytical protocols based on LC–MS, GC–MS and CE–MS for nontargeted metabolomics of biological tissues. *Bioanalysis* **6**, 1657–1677 (2014).

28. Gika, H. & Theodoridis, G. Sample preparation prior to the LC–MS-based metabolomics/metabonomics of blood-derived samples. *Bioanalysis* **3**, 1647–1661 (2011).

29. Souza-Silva, É. A. *et al.* A critical review of the state of the art of solid-phase microextraction of complex matrices iii. bioanalytical and clinical applications. *TrAC Trends Anal. Chem.* (2015) doi:10.1016/j.trac.2015.04.017.

30. General considerations when dealing with biological fluid samples. in *Sampling and Sample preparation for LC-MS-based Metabonomics/Metabolomics of samples of mammalian origin* 1–19 (Elsevier Publications, 2012).

31. Thevis, M., Thomas, A. & Schänzer, W. Targeting prohibited substances in doping control blood samples by means of chromatographic-mass spectrometric methods. *Anal. Bioanal. Chem.* **405**, 9655–67 (2013).

32. Annesley, T. M. Ion suppression in mass spectrometry. *Clin. Chem.* **49**, 1041–4 (2003).

33. Furey, A. Ion suppression; A critical review on causes, evaluation, prevention and applications. **115**, 104–122.

34. Musteata, F. M. Monitoring free drug concentrations: challenges. *Bioanalysis* **3**, 1753–68 (2011).

35. Nilsson, L. B. The bioanalytical challenge of determining unbound concentration and protein binding for drugs. *Bioanalysis* **5**, 3033–50 (2013).

36. Stephenson, F. H. Centrifugation. in *Calculations for Molecular Biology and Biotechnology* 413–421 (Elsevier, 2010). doi:10.1016/B978-0-12-375690-9.00012-7.

37. Luque-Garcia, J. L. & Neubert, T. A. Sample preparation for serum/plasma profiling and biomarker identification by mass spectrometry. *Journal of Chromatography A* vol. 1153 259–276 (2007).

38. Oh, J.-H. & Lee, Y.-J. Sample preparation for liquid chromatographic analysis of phytochemicals in biological fluids. *Phytochem. Anal.* **25**, 314–30 (2014).

39. Murugan, S., Pravallika, N., Sirisha, P. & K, C. A review on bioanalytical method development and validation using LC_MS/MS. *J. Chem. Pharm. Sci.* **6**, 41–45 (2013).

40. Sharma, A., Jaiswal, S., Shukla, M. & Lal, J. Dried blood spots: concepts, present status, and future perspectives in bioanalysis. *Drug Test. Anal.* **6**, 399–414 (2014).

41. Pawliszyn, J. & Lord, H. *Handbook of sample preparation*. (Hoboken, N.J. : Wiley, 2010).

42. Pawliszyn, J. *Handbook of solid phase microextraction*. (Chemical Industry Press, 2009).

43. Shippenberg, T. S. & Thompson, A. C. Overview of microdialysis. *Curr. Protoc. Neurosci.* **Chapter 7**, Unit7.1 (2001).

44. Hammarlund-Udenaes, M. Microdialysis as an Important Technique in Systems Pharmacology—a Historical and Methodological Review. *AAPS J.* **19**, 1294–1303 (2017).

45. Zeitlinger, M., Müller, M. & Joukhadar, C. Lung microdialysis - A powerful tool for the determination of exogenous and endogenous compounds in the lower respiratory tract (mini-review). *AAPS Journal* vol. 7 E600 (2005).

46. Mazzeo, A. T. *et al.* Feasibility of lung microdialysis to assess metabolism during clinical ex vivo lung perfusion. *J. Hear. Lung Transplant.* **38**, 267–276 (2019).

47. Vuckovic, D. High-throughput solid-phase microextraction in multi-well-plate format. *TrAC Trends Anal. Chem.* **45**, 136–153 (2013).

48. Musteata, M. L., Musteata, F. M. & Pawliszyn, J. Biocompatible solid-phase microextraction coatings based on polyacrylonitrile and solid-phase extraction phases. *Anal. Chem.* **79**, 6903–11 (2007).

49. Szultka, M. Pharmacokinetic study of amoxicillin in human plasma by solid-phase microextraction followed by high-performance liquid chromatography–triple quadrupole mass spectrometry. **28**, 255–264.

50. Vuckovic, D. *et al.* In vivo solid-phase microextraction for single rodent pharmacokinetics studies of carbamazepine and carbamazepine-10,11-epoxide in mice. *J. Chromatogr. A* **1218**, 3367–75 (2011).

51. Zhang, X., Es-haghi, A., Musteata, F. M., Ouyang, G. & Pawliszyn, J. Quantitative in vivo microsampling for pharmacokinetic studies based on an integrated solid-phase microextraction system. *Anal. Chem.* **79**, 4507–13 (2007).

52. Reyes-Garcés, N., Bojko, B. & Pawliszyn, J. High throughput quantification of prohibited substances in plasma using thin film solid phase microextraction. *J. Chromatogr. A* **1374**, 40–9 (2014).

53. Boyacı, E., Gorynski, K., Rodriguez-Lafuente, A., Bojko, B. & Pawliszyn, J. Introduction of solid-

phase microextraction as a high-throughput sample preparation tool in laboratory analysis of prohibited substances. *Anal. Chim. Acta* **809**, 69–81 (2014).

54. Bojko, B. *et al.* Determination of tranexamic acid concentration by solid phase microextraction and liquid chromatography-tandem mass spectrometry: first step to in vivo analysis. *J. Chromatogr. B. Analyt. Technol. Biomed. Life Sci.* **879**, 3781–7 (2011).

55. Bojko, B. & Pawliszyn, J. *In vivo* and *ex vivo* SPME: a low invasive sampling and sample preparation tool in clinical bioanalysis. *Bioanalysis* **6**, 1227–1239 (2014).

56. Bojko, B. *et al.* Solid phase microextraction fills the gap in tissue sampling protocols. *Anal. Chim. Acta* **803**, 75–81 (2013).

57. Vuckovic, D. & Pawliszyn, J. Systematic Evaluation of Solid-Phase Microextraction Coatings for Untargeted Metabolomic Profiling of Biological Fluids by Liquid Chromatography-Mass Spectrometry. | *Anal. Chem* **83**, 1944–1954 (2011).

58. *A guide to effective method development in bioanalysis*. *Waters Corporation* (2008).

59. van Dongen, W. D. & Niessen, W. M. A. LC-MS systems for quantitative bioanalysis. *Bioanalysis* **4**, 2391–9 (2012).

60. Chandana, N., Harithapavani, K., Deepa Ramani, N. & Maduri, J. A review on liquid chromatography - Tandem mass spectroscopy. *Journal of Chemical and Pharmaceutical Sciences* vol. 6 210–217 (2013).

61. Lu, X. *et al.* LC-MS-based metabonomics analysis. *Journal of Chromatography B: Analytical Technologies in the Biomedical and Life Sciences* vol. 866 64–76 (2008).

62. Reyes-Garcés, N. *et al.* Advances in Solid Phase Microextraction and Perspective on Future Directions. *Anal. Chem.* **90**, 302–360 (2018).

63. Lecker, I. *et al.* Tranexamic acid-associated seizures: Causes and treatment. *Annals of Neurology* vol. 79 18–26 (2016).

64. Koster, A., Faraoni, D. & Levy, J. H. Antifibrinolytic Therapy for Cardiac Surgery: An Update. *Anesthesiology* **123**, 214–221 (2015).

65. Abou-Diwan, C. *et al.* Plasma and cerebral spinal fluid tranexamic acid quantitation in cardiopulmonary bypass patients. *J. Chromatogr. B Anal. Technol. Biomed. Life Sci.* **879**, 553–556 (2011).

66. Yang, Q. J., Jerath, A., Bies, R. R., Wąsowicz, M. & Pang, K. S. Pharmacokinetic modeling of tranexamic acid for patients undergoing cardiac surgery with normal renal function and model simulations for patients with renal impairment. *Biopharm. Drug Dispos.* **36**, 294–307 (2015).

67. Grassin Delyle, S. *et al.* A validated assay for the quantitative analysis of tranexamic acid in human serum by liquid chromatography coupled with electrospray ionization mass spectrometry. *Clin Chim Acta* **411**, 438–443 (2010).

68. Fabresse, N. *et al.* LC–MS/MS determination of tranexamic acid in human plasma after phospholipid clean-up. *J. Pharm. Biomed. Anal.* **141**, 149–156 (2017).

69. Liao, F. Y., Lin, Y. C., Chen, Y. L. & Feng, C. H. Determination of tranexamic acid in various matrices using microwave-assisted derivatization followed by dispersive liquid-liquid microextraction. *J. Chromatogr. A* **1377**, 35–45 (2015).

70. Pilbrant, A., Schannong, M. & Vessman, J. Pharmacokinetics and bioavailability of tranexamic acid. *Eur. J. Clin. Pharmacol.* **20**, 65–72 (1981).

71. Grassin-Delyle, S. *et al.* Population pharmacokinetics of tranexamic acid in adults undergoing cardiac surgery with cardiopulmonary bypass. *Br. J. Anaesth.* **111**, 916–24 (2013).

72. Hadad, G. M., El-Gindy, A. & Mahmoud, W. M. M. Optimization and Validation of an HPLC-UV Method for Determination of Tranexamic Acid in a Dosage Form and in Human Urine. *Chromatographia* **66**, 311–317 (2007).

73. Lin, F. M. *et al.* An ionizable chromophoric reagent for the analysis of primary amine-containing drugs by capillary electrophoresis. *Electrophoresis* **26**, 621–626 (2005).

74. Ferreira, C. R. *et al.* Ambient Ionization Mass Spectrometry for Point-of- Care Diagnostics and Other Clinical Measurements. *Clin. Chem.* **62**, 99–110 (2016).

75. Fedick, P. W., Bain, R. M., Miao, S., Pirlo, V. & Cooks, G. R. State-of-the-art mass spectrometry for point-of-care and other applications: A hands-on intensive short course for undergraduate students. *Int. J. Mass Spectrom.* **417**, 22–28 (2017).

76. Jerath, A. *et al.* Tranexamic Acid Dosing for Cardiac Surgical Patients With Chronic Renal Dysfunction. *Anesth. Analg.* **127**, 1323–1332 (2018).

77. Gorynski, K. *et al.* Development of SPME method for concomitant sample preparation of rocuronium bromide and tranexamic acid in plasma. *J. Pharm. Biomed. Anal.* **92**, 183–92 (2014).

78. Fergusson, D. A. *et al.* A Comparison of Aprotinin and Lysine Analogues in High-Risk Cardiac Surgery. *N. Engl. J. Med.* **358**, 2319–2331 (2008).

79. Looby, N. T. *et al.* Solid phase microextraction coupled to mass spectrometry: Via a microfluidic open interface for rapid therapeutic drug monitoring. *Analyst* **144**, 3721–3728 (2019).

80. Mirnaghi, F. S., Chen, Y., Sidisky, L. M. & Pawliszyn, J. Optimization of the coating procedure for a high-throughput 96-blade solid phase microextraction system coupled with LC-MS/MS for analysis of complex samples. *Anal. Chem.* **83**, 6018–25 (2011).

81. Reyes-Garcés, N., Bojko, B., Hein, D. & Pawliszyn, J. Solid Phase Microextraction Devices Prepared on Plastic Support as Potential Single-Use Samplers for Bioanalytical Applications. *Anal. Chem.* **87**, 9722–9730 (2015).

82. Wąsowicz, M. *et al.* Use of a novel technique, solid phase microextraction, to measure tranexamic acid in patients undergoing cardiac surgery. *Can. J. Anaesth.* **59**, 14–20 (2012).

83. Bojko, B. *et al.* Therapeutic monitoring of tranexamic acid concentration: high-throughput analysis with solid-phase microextraction. *Ther. Drug Monit.* **34**, 31–7 (2012).

84. Santasania, C. T., Trinh, A. & Sarker, M. Supel-Select HLB SPE for Pharmaceutical Analysis | Sigma-Aldrich. *Reporter US* Volume 27.3 https://www.sigmaaldrich.com/technical-documents/articles/reporter-us/supel-select-hlb-spe.html.

85. Chemicalize - Instant Cheminformatics Solutions. https://chemicalize.com/#/calculation.

86. DrugBank: Tranexamic Acid (DB00302). http://www.drugbank.ca/drugs/DB00302.

87. B. K. Matuszewski, *, M. L. Constanzer, and & Chavez-Eng, C. M. Strategies for the Assessment of Matrix Effect in Quantitative Bioanalytical Methods Based on HPLC−MS/MS. (2003)

doi:10.1021/AC020361S.

88. Rachakonda, T. D., Schupp, C. W. & Armstrong, A. W. Psoriasis prevalence among adults in the United States. *J. Am. Acad. Dermatol.* **70**, 512–516 (2014).

89. Petronic-Rosic, V. & Basko-Plluska, J. Psoriasis: epidemiology, natural history, and differential diagnosis. *Psoriasis Targets Ther.* **2**, 67 (2012).

90. Lowes, M. A., Bowcock, A. M. & Krueger, J. G. Pathogenesis and therapy of psoriasis. *Nat. 2007 4457130* (2007).

91. Alinaghi, F. *et al.* Prevalence of psoriatic arthritis in patients with psoriasis: A systematic review and meta-analysis of observational and clinical studies. *Journal of the American Academy of Dermatology* vol. 80 251-265.e19 (2019).

92. Gladman, D. D., Antoni, C., Mease, P., Clegg, D. O. & Nash, P. Psoriatic arthritis: epidemiology, clinical features, course, and outcome. *Ann. Rheum. Dis.* **64 Suppl 2**, ii14-7 (2005).

93. Haroon, M., Gallagher, P. & FitzGerald, O. Diagnostic delay of more than 6 months contributes to poor radiographic and functional outcome in psoriatic arthritis. *Ann. Rheum. Dis.* **74**, 1045–1050 (2015).

94. Abji, F., Pollock, R. A., Liang, K., Chandran, V. & Gladman, D. D. Brief Report: CXCL10 Is a Possible Biomarker for the Development of Psoriatic Arthritis Among Patients With Psoriasis. *Arthritis Rheumatol.* **68**, 2911–2916 (2016).

95. Eder, L. *et al.* The Incidence and Risk Factors for Psoriatic Arthritis in Patients With Psoriasis: A Prospective Cohort Study. *Arthritis Rheumatol.* **68**, 915–923 (2016).

96. Eder, L. *et al.* The Development of Psoriatic Arthritis in Patients With Psoriasis Is Preceded by a Period of Nonspecific Musculoskeletal Symptoms: A Prospective Cohort Study. *Arthritis Rheumatol.* **69**, 622–629 (2017).

97. Jiang, S., Hinchliffe, T. E. & Wu, T. Biomarkers of An Autoimmune Skin Disease—Psoriasis. *Genomics. Proteomics Bioinformatics* **13**, 224–233 (2015).

98. Yan, D. *et al.* The metabolomics of psoriatic disease. *Psoriasis Targets Ther.* **Volume 7**, 1–15 (2017).

99. Li, L. *et al.* Untargeted serum metabonomics study of psoriasis vulgaris based on ultra-performance liquid chromatography coupled to mass spectrometry. *Oncotarget* **8**, (2017).

100. Kamleh, M. A. *et al.* LC–MS Metabolomics of Psoriasis Patients Reveals Disease Severity-Dependent Increases in Circulating Amino Acids That Are Ameliorated by Anti-TNFα Treatment. *J. Proteome Res.* **14**, 557–566 (2015).

101. Armstrong, A. W. *et al.* Metabolomics in psoriatic disease: pilot study reveals metabolite differences in psoriasis and psoriatic arthritis. *F1000Research* **3**, 248 (2014).

102. Yan, J. Identifying biomarkers in human psoriasis: revealed by a systems metabolomics approach. *Br. J. Dermatol.* **176**, 555–557 (2017).

103. Ottas, A., Fishman, D., Okas, T.-L., Kingo, K. & Soomets, U. The metabolic analysis of psoriasis identifies the associated metabolites while providing computational models for the monitoring of the disease. *Arch. Dermatol. Res.* **309**, 519–528 (2017).

104. Bojko, B. *et al.* Solid-phase microextraction in metabolomics. *TrAC Trends Anal. Chem.* **61**, 168–180 (2014).

105. Gladman, D. D. & Chandran, V. Observational cohort studies: Lessons learnt from the University of Toronto Psoriatic arthritis program. *Rheumatology* vol. 50 25–31 (2011).

106. Chambers, M. C. *et al.* A cross-platform toolkit for mass spectrometry and proteomics. *Nat. Biotechnol.* **30**, 918–920 (2012).

107. Smith, C. A., Want, E. J., O'Maille, G., Abagyan, R. & Siuzdak, G. XCMS: Processing Mass Spectrometry Data for Metabolite Profiling Using Nonlinear Peak Alignment, Matching, and Identification. *Anal. Chem.* **78**, 779–787 (2006).

108. Roszkowska, A. *et al.* Tissue storage affects lipidome profiling in comparison to in vivo microsampling approach. *Sci. Rep.* **8**, (2018).

109. Libiseller, G. *et al.* IPO: a tool for automated optimization of XCMS parameters. *BMC Bioinformatics* **16**, 118 (2015).

110. Uppal, K., Walker, D. I. & Jones, D. P. xMSannotator: An R Package for Network-Based Annotation of High-Resolution Metabolomics Data. *Anal. Chem.* **89**, 1063–1067 (2017).

111. Wishart, D. S. *et al.* HMDB: the Human Metabolome Database. *Nucleic Acids Res.* **35**, D521–D526 (2007).

112. Chong, J. *et al.* MetaboAnalyst 4.0: towards more transparent and integrative metabolomics analysis. *Nucleic Acids Res.* **46**, W486–W494 (2018).

113. Huan, T. *et al.* Systems biology guided by XCMS Online metabolomics. *Nat. Methods* **14**, 461–462 (2017).

114. Smith, C. A. *et al.* METLIN. *Ther. Drug Monit.* **27**, 747–751 (2005).

115. Matsumoto, M., Kuhara, T., Inoue, Y., Shinka, T. & Matsumoto, I. Abnormal fatty acid metabolism in patients in hopantenate therapy during clinical episodes. *J. Chromatogr.* **562**, 139–45 (1991).

116. Okajima, K. *et al.* Clinical and Biochemical Findings of a Patient with Thanatophoric Dysplasia Type I: Additional Finding of Dicarboxylic Aciduria. *Cleft Palate-Craniofacial J.* **39**, 246–248 (2002).

117. Bergoffen, J., Kaplan, P., Hale, D. E., Bennett, M. J. & Berry, G. T. Marked elevation of urinary 3-hydroxydecanedioic acid in a malnourished infant with glycogen storage disease, mimicking long-chain L-3-hydroxyacyl-CoA dehydrogenase deficiency. *J. Inherit. Metab. Dis.* **16**, 851–6 (1993).

118. Muth, A. *et al.* Simultaneous enantioselective analysis of chiral urinary metabolites in patients with Zellweger syndrome. *J. Chromatogr. B. Analyt. Technol. Biomed. Life Sci.* **792**, 269–77 (2003).

119. Roman, M. A., Nair, S., Tsui, S., Dunning, J. & Parmar, J. S. Ex vivo lung perfusion: A comprehensive review of the development and exploration of future trends. *Transplantation* vol. 96 509–518 (2013).

120. Hsin, M. K. *et al.* Metabolic Profile of Ex Vivo Lung Perfusate Yields Biomarkers for Lung Transplant Outcomes. *Ann. Surg.* **267**, 196–197 (2018).

121. Nakajima, D., Cypel, M. & Keshavjee, S. Ex vivo organ repair (drug and gene delivery). in *Technological Advances in Organ Transplantation* 235–259 (Springer International Publishing,

2018). doi:10.1007/978-3-319-62142-5_10.

122. Cypel, M. *et al.* Normothermic Ex Vivo perfusion prevents lung injury compared to extended cold preservation for transplantation. *Am. J. Transplant.* **9**, 2262–2269 (2009).

123. Cypel, M. *et al.* Technique for Prolonged Normothermic Ex Vivo Lung Perfusion. *J. Hear. Lung Transplant.* **27**, 1319–1325 (2008).

124. Galasso, M. *et al.* Inactivating hepatitis C virus in donor lungs using light therapies during normothermic ex vivo lung perfusion. *Nat. Commun.* **10**, (2019).

125. Cypel, M. *et al.* NOrmothermic ex vivo lung perfusion in clinical lung transplantation. *N. Engl. J. Med.* **364**, 1431–1440 (2011).

126. Kan, M., Shumyatcher, M. & Himes, B. E. Using omics approaches to understand pulmonary diseases. *Respiratory Research* vol. 18 (2017).

127. Yang, I. V. & Schwartz, D. A. Epigenetic control of gene expression in the lung. *American Journal of Respiratory and Critical Care Medicine* vol. 183 1295–1301 (2011).

128. Fiehn, O. Metabolomics – the link between genotypes and phenotypes. *Plant Mol. Biol.* **48**, 155–171 (2002).

129. Cudjoe, E., Bojko, B., Togunde, P. & Pawliszyn, J. In vivo solid-phase microextraction for tissue bioanalysis. *Bioanalysis* **4**, 2605–19 (2012).

130. Bojko, B. *et al.* Low invasive in vivo tissue sampling for monitoring biomarkers and drugs during surgery. *Lab. Investig.* **94**, 586–594 (2014).

131. Cudjoe, E., Bojko, B., de Lannoy, I., Saldivia, V. & Pawliszyn, J. Solid-Phase Microextraction: A Complementary In Vivo Sampling Method to Microdialysis. *Angew. Chemie Int. Ed.* **52**, 12124–12126 (2013).

132. Reyes-Garcés, N. *et al.* In Vivo Brain Sampling Using a Microextraction Probe Reveals Metabolic Changes in Rodents after Deep Brain Stimulation. *Anal. Chem.* **91**, 9875–9884 (2019).

133. Reyes-Garcés, N. & Gionfriddo, E. Recent developments and applications of solid phase microextraction as a sample preparation approach for mass-spectrometry-based metabolomics and lipidomics. *TrAC - Trends in Analytical Chemistry* vol. 113 172–181 (2019).

134. Gómez-Ríos, G. A. *et al.* Quantitative analysis of biofluid spots by coated blade spray mass spectrometry, a new approach to rapid screening. *Sci. Rep.* DOI: 10.1038/s41598-017-16494-z (2017) doi:10.1038/s41598-017-16494-z.

135. Yu, M., Olkowicz, M. & Pawliszyn, J. Structure/reaction directed analysis for LC-MS based untargeted analysis. *Anal. Chim. Acta* **1050**, 16–24 (2019).

136. Miller, E., Morel, A., Saso, L. & Saluk, J. Isoprostanes and neuroprostanes as biomarkers of oxidative stress in neurodegenerative diseases. *Oxidative Medicine and Cellular Longevity* vol. 2014 (2014).

137. Gladine, C. *et al.* Neuroprostanes, produced by free-radical mediated peroxidation of DHA, inhibit the inflammatory response of human macrophages. *Free Radic. Biol. Med.* **75**, S15 (2014).

138. Murata, T. *et al.* Anti-inflammatory role of PGD2 in acute lung inflammation and therapeutic application of its signal enhancement. *Proc. Natl. Acad. Sci. U. S. A.* **110**, 5205–5210 (2013).

139. Napylov, A. *et al.* In Vivo Solid-Phase Microextraction for Sampling of Oxylipins in Brain of Awake, Moving Rats. *Angew. Chemie - Int. Ed.* **59**, 2392–2398 (2020).

140. Ariel, A. & Serhan, C. N. Resolvins and protectins in the termination program of acute inflammation. *Trends in Immunology* vol. 28 176–183 (2007).

141. Vuckovic, D. *et al.* In vivo solid-phase microextraction: Capturing the elusive portion of metabolome. *Angew. Chemie - Int. Ed.* **50**, 5344–5348 (2011).

142. Reck, P. *et al.* Modified in vivo lung perfusion allows for prolonged perfusion without acute lung injury. *J. Thorac. Cardiovasc. Surg.* **147**, 774–782 (2014).

143. Reck dos Santos, P. *et al.* Modified In Vivo Lung Perfusion for Local Chemotherapy: A Preclinical Study With Doxorubicin. *Ann. Thorac. Surg.* **101**, 2132–2140 (2016).

144. Fischel, J. L. *et al.* Impact of the oxaliplatin-5 fluorouracil-folinic acid combination on respective intracellular determinants of drug activity. *Br. J. Cancer* **86**, 1162–8 (2002).

145. Wilson, P. M., Danenberg, P. V, Johnston, P. G., Lenz, H.-J. & Ladner, R. D. Standing the test of time: targeting thymidylate biosynthesis in cancer therapy. *Nat. Rev. Clin. Oncol.* **11**, 282–98 (2014).

146. Danenberg, P. V. *et al.* Folates as adjuvants to anticancer agents: Chemical rationale and mechanism of action. *Crit. Rev. Oncol. Hematol.* **106**, 118–131 (2016).

147. Goirand, F. *et al.* How can we best monitor 5-FU administration to maximize benefit to risk ratio? *Expert Opinion on Drug Metabolism and Toxicology* vol. 14 1303–1313 (2018).

148. Miura, K. *et al.* 5-FU metabolism in cancer and orally-administrable 5-FU drugs. *Cancers* vol. 2 1717–1730 (2010).

149. Di Francesco, A. M., Ruggiero, A. & Riccardi, R. Cellular and molecular aspects of drugs of the future: Oxaliplatin. *Cellular and Molecular Life Sciences* vol. 59 1914–1927 (2002).

150. Alcindor, T. & Beauger, N. Oxaliplatin: A review in the era of molecularly targeted therapy. *Curr. Oncol.* **18**, 18–25 (2011).

151. Graham, M. A. *et al.* Clinical pharmacokinetics of oxaliplatin: A critical review. *Clinical Cancer Research* vol. 6 1205–1218 (2000).

152. Saif, M. W., Choma, A., Salamone, S. J. & Chu, E. Pharmacokinetically guided dose adjustment of 5-fluorouracil: a rational approach to improving therapeutic outcomes. *J. Natl. Cancer Inst.* **101**, 1543–52 (2009).

153. Rattner, J. & Bathe, O. Monitoring for Response to Antineoplastic Drugs: The Potential of a Metabolomic Approach. *Metabolites* **7**, 60 (2017).

154. Eckhart, A. D., Beebe, K. & Milburn, M. Metabolomics as a Key Integrator for "Omic" Advancement of Personalized Medicine and Future Therapies. *Clin. Transl. Sci.* **5**, 285–288 (2012).

155. Vuckovic, D., Zhang, X., Cudjoe, E. & Pawliszyn, J. Solid-phase microextraction in bioanalysis: New devices and directions. *J. Chromatogr. A* **1217**, 4041–4060 (2010).

156. Deng, J., Yang, Y., Wang, X. & Luan, T. Strategies for coupling solid-phase microextraction with mass spectrometry. *TrAC Trends Anal. Chem.* **55**, 55–67 (2014).

157. Swindle, M. M. *Swine in the laboratory : surgery, anesthesia, imaging, and experimental techniques*. (CRC Press, 2007).

158. Lendor, S. *et al.* Solid Phase Microextraction-Based Miniaturized Probe and Protocol for Extraction of Neurotransmitters from Brains in Vivo. *Anal. Chem.* **91**, 4896–4905 (2019).

159. Lendor, S., Gómez-Ríos, G. A., Boyacı, E., Vander Heide, H. & Pawliszyn, J. Space-Resolved Tissue Analysis by Solid-Phase Microextraction Coupled to High-Resolution Mass Spectrometry via Desorption Electrospray Ionization. *Anal. Chem.* **91**, 10141–10148 (2019).

160. Roszkowska, A. *et al.* Equilibrium ex vivo calibration of homogenized tissue for in vivo SPME quantitation of doxorubicin in lung tissue. *Talanta* **183**, 304–310 (2018).

161. Wishart, D. S. *et al.* DrugBank 5.0: a major update to the DrugBank database for 2018. *Nucleic Acids Res.* **46**, D1074–D1082 (2018).

162. Breda, M. & Barattè, S. A review of analytical methods for the determination of 5-fluorouracil in biological matrices. *Anal. Bioanal. Chem.* **397**, 1191–201 (2010).

163. Ito, H. *et al.* A full validated hydrophilic interaction liquid chromatography-tandem mass spectrometric method for the quantification of oxaliplatin in human plasma ultrafiltrates. *J. Pharm. Biomed. Anal.* **71**, 99–103 (2012).

164. REMAUD, G., BOISDRONCELLE, M., MOREL, A. & GAMELIN, A. Sensitive MS/MS–liquid chromatography assay for simultaneous determination of tegafur, 5-fluorouracil and 5-fluorodihydrouracil in plasma. *J. Chromatogr. B* **824**, 153–160 (2005).

165. Carli, D. *et al.* Simultaneous quantification of 5-FU, 5-FUrd, 5-FdUrd, 5-FdUMP, dUMP and TMP in cultured cell models by LC-MS/MS. *J. Chromatogr. B. Analyt. Technol. Biomed. Life Sci.* **877**, 2937–44 (2009).

166. Tsume, Y., Provoda, C. J. & Amidon, G. L. The achievement of mass balance by simultaneous quantification of floxuridine prodrug, floxuridine, 5-fluorouracil, 5-dihydrouracil, α-fluoro-β-ureidopropionate, α-fluoro-β-alanine using LC-MS. *J. Chromatogr. B. Analyt. Technol. Biomed. Life Sci.* **879**, 915–20 (2011).

167. Büchel, B. *et al.* LC-MS/MS method for simultaneous analysis of uracil, 5,6-dihydrouracil, 5-fluorouracil and 5-fluoro-5,6-dihydrouracil in human plasma for therapeutic drug monitoring and toxicity prediction in cancer patients. *Biomed. Chromatogr.* **27**, 7–16 (2013).

168. Chavani, O., Jensen, B. P., Strother, R. M., Florkowski, C. M. & George, P. M. Development, validation and application of a novel liquid chromatography tandem mass spectrometry assay measuring uracil, 5,6-dihydrouracil, 5-fluorouracil, 5,6-dihydro-5-fluorouracil, α-fluoro-β-ureidopropionic acid and α-fluoro-β-alanine in human plasma. *J. Pharm. Biomed. Anal.* **142**, 125–135 (2017).

169. Chen, P. *et al.* A LC-MS/MS method for the analysis of intracellular nucleoside triphosphate levels. *Pharm. Res.* **26**, 1504–1515 (2009).

170. Patring, J. D. M., Johansson, M. S., Yazynina, E. & Jastrebova, J. A. Evaluation of impact of different antioxidants on stability of dietary folates during food sample preparation and storage of extracts prior to analysis. *Anal. Chim. Acta* **553**, 36–42 (2005).

171. Sanmartín-Suárez, C., Soto-Otero, R., Sánchez-Sellero, I. & Méndez-Álvarez, E. Antioxidant properties of dimethyl sulfoxide and its viability as a solvent in the evaluation of neuroprotective

antioxidants. *J. Pharmacol. Toxicol. Methods* **63**, 209–215 (2011).

172. Priest, D. G., Schmitz, J. C., Bunni, M. A. & stuart, R. K. Pharmacokinetics of Leucovorin Metabolites in Human Plasma as a Function of Dose Administrated Orally and Intravenously. *JNCI J. Natl. Cancer Inst.* **83**, 1806–1812 (1991).

173. JA, S., D, S. & WT, W. Pharmacokinetics of the diastereoisomers of leucovorin after intravenous and oral administration to normal subjects. *Cancer Res.* **44**, 3114–3119 (1984).

174. De Brouwer, V., Zhang, G.-F., Storozhenko, S., Van Der Straeten, D. & Lambert, W. E. pH stability of individual folates during critical sample preparation steps in prevision of the analysis of plant folates. *Phytochem. Anal.* **18**, 496–508 (2007).

175. Wigle, T. J., Tsvetkova, E. V., Welch, S. A. & Kim, R. B. DPYD and fluorouracil-based chemotherapy: Mini review and case report. *Pharmaceutics* vol. 11 (2019).

176. Pastorino, U., McCormack, P. & Ginsberg, R. A new staging proposal for pulmonary metastases: Results of analysis of 5206 cases of resected pulmonary metastases. *Chest Surg. Clin. N. Am.* **8**, 197 (1998).

177. Cypel, M. *et al.* Functional repair of human donor lungs by IL-10 gene therapy. *Sci. Transl. Med.* **1**, 4ra9 (2009).

178. Everett, J. R. From metabonomics to pharmacometabonomics: The role of metabolic profiling in personalized medicine. *Frontiers in Pharmacology* vol. 7 (2016).

179. Ouyang, G., Vuckovic, D. & Pawliszyn, J. Nondestructive sampling of living systems using in vivo solid-phase microextraction. *Chemical Reviews* vol. 111 2784–2814 (2011).

180. Huq, M., Tascon, M., Nazdrajic, E., Roszkowska, A. & Pawliszyn, J. Measurement of Free Drug Concentration from Biological Tissue by Solid-Phase Microextraction: In Silico and Experimental Study. *Anal. Chem.* **91**, 7719–7728 (2019).

181. St John, E. R. *et al.* Rapid evaporative ionisation mass spectrometry of electrosurgical vapours for the identification of breast pathology: Towards an intelligent knife for breast cancer surgery. *Breast Cancer Res.* **19**, 59 (2017).

182. Zhang, J. *et al.* Nondestructive tissue analysis for ex vivo and in vivo cancer diagnosis using a handheld mass spectrometry system. *Sci. Transl. Med.* **9**, (2017).

183. Saudemont, P. *et al.* Real-Time Molecular Diagnosis of Tumors Using Water-Assisted Laser Desorption/Ionization Mass Spectrometry Technology. *Cancer Cell* **34**, 840-851.e4 (2018).

184. Rodvold, K. A., Hope, W. W. & Boyd, S. E. Considerations for effect site pharmacokinetics to estimate drug exposure: concentrations of antibiotics in the lung. *Current Opinion in Pharmacology* vol. 36 114–123 (2017).

185. Ouyang, G., Vuckovic, D. & Pawliszyn, J. Nondestructive sampling of living systems using in vivo solid-phase microextraction. *Chemical Reviews* vol. 111 2784–2814 (2011).

186. Cypel, M. *et al.* Functional repair of human donor lungs by IL-10 gene therapy. *Sci. Transl. Med.* **1**, 4ra9 (2009).

187. Kümmerle, A. *et al.* A validated assay for measuring doxorubicin in biological fluids and tissues in an isolated lung perfusion model: matrix effect and heparin interference strongly influence doxorubicin measurements. *J. Pharm. Biomed. Anal.* **33**, 475–494 (2003).

188. Tascon, M., Alam, M. N., Gómez-Ríos, G. A. & Pawliszyn, J. Development of a Microfluidic Open Interface with Flow Isolated Desorption Volume for the Direct Coupling of SPME Devices to Mass Spectrometry. *Anal. Chem.* **90**, 2631–2638 (2018).

189. Gomez-ríos, G. A. *et al.* Open Port Probe Sampling Interface for the Direct Coupling of Biocompatible Solid-Phase Microextraction to Atmospheric Pressure Ionization Mass Spectrometry. *Anal. Chem.* **89**, 3805–3809 (2017).

190. Huq, M., Tascon, M., Nazdrajic, E., Roszkowska, A. & Pawliszyn, J. Measurement of Free Drug Concentration from Biological Tissue by Solid-Phase Microextraction: In Silico and Experimental Study. *Anal. Chem.* **91**, 7719–7728 (2019).

191. Napylov, A. *et al.* In Vivo Solid-Phase Microextraction for Sampling of Oxylipins in Brain of Awake, Moving Rats. *Angew. Chemie - Int. Ed.* **59**, 2392–2398 (2020).

192. Li, T. W. H. *et al.* S-adenosylmethionine and methylthioadenosine inhibit cellular FLICE inhibitory protein expression and induce apoptosis in colon cancer cells. *Mol. Pharmacol.* **76**, 192–200 (2009).

193. Iraburu, M. *et al.* S-adenosylmethionine and methylthioadenosine are antiapoptotic in cultured rat hepatocytes but proapoptotic in human hepatoma cells. *Hepatology* **35**, 274–280 (2002).

194. Bigaud, E. & Corrales, F. J. Methylthioadenosine (MTA) regulates liver cells proteome and methylproteome: Implications in liver biology and disease. *Mol. Cell. Proteomics* **15**, 1498–1510 (2016).

195. Arunachalam, S., Tirupathi Pichiah, P. B. & Achiraman, S. Doxorubicin treatment inhibits PPARγ and may induce lipotoxicity by mimicking a type 2 diabetes-like condition in rodent models. *FEBS Lett.* **587**, 105–110 (2013).

196. Todor, I. N., Lukyanova, N. Y. & Chekhun, V. F. The lipid content of cisplatin- and doxorubicin-resistant MCF-7 human breast cancer cells. *Exp. Oncol.* **34**, 97–100 (2012).

197. Cheneval, D., Muller, M., Toni, R., Ruetz, S. & Carafoli, E. Adriamycin as a probe for the transversal distribution of cardiolipin in the inner mitochondrial membrane. *J. Biol. Chem.* **260**, 13003–13007 (1985).

198. Parker, M. A., King, V. & Howard, K. P. Nuclear magnetic resonance study of doxorubicin binding to cardiolipin containing magnetically oriented phospholipid bilayers. *Biochim. Biophys. Acta* **1514**, 206–16 (2001).

199. Bamji-Stocke, S., van Berkel, V., Miller, D. M. & Frieboes, H. B. A review of metabolism-associated biomarkers in lung cancer diagnosis and treatment. *Metabolomics* vol. 14 1–16 (2018).

200. Mathé, E. A. *et al.* Noninvasive urinary metabolomic profiling identifies diagnostic and prognostic markers in lung cancer. *Cancer Res.* **74**, 3259–3270 (2014).

201. Haznadar, M. *et al.* Urinary metabolite risk biomarkers of lung cancer: A prospective cohort study. *Cancer Epidemiol. Biomarkers Prev.* **25**, 978–986 (2016).

202. Mathé, E. A. *et al.* Noninvasive urinary metabolomic profiling identifies diagnostic and prognostic markers in lung cancer. *Cancer Res.* **74**, 3259–3270 (2014).

203. Jerath, A; Yang, QJ; Pang, S; Looby, N; Reyes-Garces, N; Vasiljevic, T; Bojko, B; Pawliyszyn, J; Beattie, WS; Yau, T. W. M. Tranexamic acid dosing for cardiac surgical patients with chronic renal dysfunction: a new dosing regimen. *Anesth. Analg.* manuscript accepted (2017).

204. La Marca, G. Mass spectrometry in clinical chemistry: the case of newborn screening. *J. Pharm. Biomed. Anal.* **101**, 174–182 (2014).

205. Gómez-Ríos, G. A. & Pawliszyn, J. Development of coated blade spray ionization mass spectrometry for the quantitation of target analytes present in complex matrices. *Angew. Chem. Int. Ed. Engl.* **53**, 14503–7 (2014).

206. Gómez-Ríos, G. A. & Pawliszyn, J. Solid phase microextraction (SPME)-transmission mode (TM) pushes down detection limits in direct analysis in real time (DART). *Chem. Commun.* **50**, 12937–12940 (2014).

207. Tascon, M. *et al.* Ultra-fast quantitation of voriconazole in human plasma by coated blade spray mass spectrometry. *J. Pharm. Biomed. Anal.* **144**, 106–111 (2017).

208. Tascon, M. *et al.* High-Throughput Screening and Quantitation of Target Compounds in Biofluids by Coated Blade Spray-Mass Spectrometry. *Anal. Chem.* **89**, 8421–8428 (2017).

209. Liu, C. *et al.* Fast quantitation of opioid isomers in human plasma by differential mobility spectrometry/mass spectrometry via SPME/open-port probe sampling interface. *Anal. Chim. Acta* **991**, 89–94 (2017).

210. Van Berkel, G. J. & Kertesz, V. An open port sampling interface for liquid introduction atmospheric pressure ionization mass spectrometry. *Rapid Commun. Mass Spectrom.* **29**, 1749–1756 (2015).

211. Mirnaghi, F. S. & Pawliszyn, J. Development of coatings for automated 96-blade solid phase microextraction-liquid chromatography-tandem mass spectrometry system, capable of extracting a wide polarity range of analytes from biological fluids. *J. Chromatogr. A* **1261**, 91–8 (2012).

212. Van Berkel, G. J. *et al.* Combined Falling Drop/Open Port Sampling Interface System for Automated Flow Injection Mass Spectrometry. *Anal. Chem.* **89**, 12578–12586 (2017).

213. Gross, J. H. Direct analysis in real time—a critical review on DART-MS. *Anal. Bioanal. Chem.* **406**, 63–80 (2014).

214. Jarmusch, A. K. *et al.* Lipid and metabolite profiles of human brain tumors by desorption electrospray ionization-MS. *Proc. Natl. Acad. Sci. U. S. A.* **113**, 1486–91 (2016).

215. Pirro, V. *et al.* Intraoperative assessment of tumor margins during glioma resection by desorption electrospray ionization-mass spectrometry. *Proc. Natl. Acad. Sci. U. S. A.* **114**, 6700–6705 (2017).

216. Neifeld, J. R. *et al.* Ultrafast Screening of Synthetic Cannabinoids and Synthetic Cathinones in Urine by RapidFire-Tandem Mass Spectrometry. *J. Anal. Toxicol.* **40**, 379–387 (2016).

217. Razavi, M. *et al.* High-Throughput SISCAPA Quantitation of Peptides from Human Plasma Digests by Ultrafast, Liquid Chromatography-Free Mass Spectrometry. *J. Proteome Res.* **11**, 5642–5649 (2012).

218. Lin, C.-H., Liao, W.-C., Chen, H.-K. & Kuo, T.-Y. Paper spray-MS for bioanalysis. *Bioanalysis* **6**, 199–208 (2014).